UNRAVELING THE ROLE OF SNARE INTERACTIONS IN NEUROTRANSMITTER RELEASE

APPROVED BY SUPERVISORY COMMITTEE

Ege Kavalali, Ph.D., Committee Chair

Jose Rizo-Rey, Ph.D., Advisor

Michael Rosen, Ph.D.

Hongtao Yu, Ph.D.

To my parents, Tiansheng Chen and Lingling Zhao

UNRAVELING THE ROLE OF SNARE INTERACTIONS IN NEUROTRANSMITTER RELEASE

by

XIAOCHENG CHEN

DISSERTATION

Presented to the Faculty of the Graduate School of Biomedical Sciences

The University of Texas Southwestern Medical Center at Dallas

In Partial Fulfillment of the Requirements

For the Degree of

DOCTOR OF PHILOSOPHY

The University of Texas Southwestern Medical Center at Dallas

Dallas, Texas

March, 2005

ACKNOWLEDGEMENTS

First, I would like to thank my mentor, Dr. Jose Rizo-Rey, who gave me enormous help and support during the past four years. He is the person who helped me to join the DCMB program in UT Southwestern Medical Center, enlightened me with NMR technology and provided me an excellent laboratory to learn, to work and to grow up. He is one of the best teachers that I have ever met. His passion for science, his enthusiasm for new ideas and his rigorous scientific attitude had a profound impact on me. In addition, he is also an easy-going person. He never places himself in a "BOSS" position; on the contrary, he always talks and acts like a friend, which makes even the toughest project much easier. Without him, it would be impossible for me to succeed.

I also give my thanks to all the people in Jose's laboratory, who are always so generous in helping each other. It is really a great pleasure to work with them. Dr. Evguenii Kovrigin, a former postdoc, was the person that initially worked on the complexin project. His initial contribution was very important for the later structural analysis. Dr. Jun Lu, another post doctoral fellow in the laboratory, gave me much help as I just arrived at Dallas. Dr. Irina Dulubova provided all kinds of help and support in the laboratory. Demet Arac is always like a sister for me. We had great times in working together, discussing together and traveling together. Tara Murphy, Minghua Wen and Iryna Huryeva provided excellent technical assistance.

I thank my dissertation committee members, Dr. Ege Kavalali, Dr. Michael Rosen, and Dr. Hongtao Yu for their insightful criticism and important suggestions. I thank Dr. Diana Tomchick and Dr. Mischa Machius for helping me solve the crystal structure of the complexin/SNARE complex. I also thank Dr. Thomas Südhof for providing many constructive and useful suggestions.

I would like to thank my parents, my sister and my grandma for their love and encouragement. Their understanding and support during all the time is like the wind underneath my wings that enable me to fly for my goals without any concern. Finally, I would like to thank my husband, Tzu-Ming Wang, for his love and support through the journey of conducting research and writing up this dissertation.

UNRAVELING THE ROLE OF SNARE INTERACTIONS IN NEUROTRANSMITTER RELEASE

Publication No. _____

Xiaocheng Chen (Ph.D.)

The University of Texas Southwestern Medical Center at Dallas, 2005

Jose Rizo-Rey (Ph.D.)

The release of neurotransmitters by Ca^{2+}-triggered synaptic vesicle exocytosis is tightly controlled by an intricate protein machinery. Essential components of this machinery are the synaptic vesicle protein synaptobrevin and the plasma membrane proteins syntaxin 1 and SNAP-25, which are collectively known as SNAREs and form a tight complex (the core complex). The assembly of the core complex may mediate membrane fusion.

Complexin is a highly conserved cytoplasmic protein that binds tightly to the SNARE complex. Analysis of the interaction between complexin and the SNARE complex showed that complexin binds to the groove between the synaptobrevin and syntaxin helices, and the

binding stabilizes the syntaxin/synaptobrevin interface. These results led to a model whereby complexin stabilizes the fully assembled SNARE complex, which is critical for the fast Ca^{2+}-triggered neurotransmitter release.

The N-terminal domain of syntaxin 1 folds back and forms a 'closed' conformation, which interacts with munc18-1, an essential protein in the neurotransmitter release. It has been proposed that the binding of munc18-1 might change the closed conformation. To test this model, I solved the solution structure of the N-terminal domain within the closed conformation of syntaxin 1 and structure comparisons showed that the N-terminal domain adopts the same conformation whether it is isolated, bound to Munc18-1, or within the closed conformation.

Analysis of the Ca^{2+}-binding properties of the core complex revealed that it contains several low affinity Ca^{2+} binding sites and most of them are nonspecific for Ca^{2+}. A SNAP-25 mutation that causes a change in the Ca^{2+}-dependence of secretion in chromaffin cells has no effect on the SNARE/synaptotagmin 1 interactions, but has a conspicuous effect on core complex assembly. Thus, the SNAREs are unlikely to directly act as Ca^{2+} sensors, but SNARE complex assembly is tightly coupled to Ca^{2+} sensing in neurotransmitter release.

To directly test SNARE function, I reconstituted v- and t-SNAREs into separate liposomes and carefully characterized the proteoliposomes containing v- and t-SNAREs. Fusion between the v- and t-SNARE proteoliposomes was then monitored with a lipid mixing assay. Interestingly, little fusion was observed. The results suggest that the SNAREs alone are not sufficient to mediate membrane fusion.

TABLE OF CONTENTS

PRIOR PUBLICATIONS

Chen X, Tomchick DR, Kovrigin E, Arac D, Machius M, Südhof TC, and Rizo J (2002) Three-dimensional structure of the complexin/SNARE complex. *Neuron,* **33,** 397-409.

Yamaguchi T, Dulubova I, Min SW, Chen X, Rizo J, and Südhof TC (2002) Sly1 binds to Golgi and ER syntaxins via a conserved N-terminal peptide motif. *Dev Cell,* **2,** 295-305.

Chandra S, Chen X, Rizo J, Jahn R, and Südhof TC (2003) A broken alpha -helix in folded alpha -Synuclein. *J Biol Chem,* **278,** 15313-15318.

Matos MF, Mukherjee K, Chen XC, Rizo J, and Südhof TC (2003) Evidence for SNARE zippering during Ca2+-triggered exocytosis in PC12 cells. *Neuropharmacology*, **45,** 777-786.

Chen X, Tang J, Südhof TC, and Rizo J (2005) Are Neuronal SNARE proteins Ca^{2+} sensors? *J Mol Biol*, **347**, 145-58.

LIST OF FIGURES

LIST OF TABLES

LIST OF DEFINITIONS

1D, 2D, 3D	one, two and three-dimensional
BCA	bicinchoninic acid
BoNT	botulinum neurotoxin
BSA	bovine serum albumin
CCD	charged coupled device
CD	circular dichroism
C.elegans	*Caenorhabditis elegans*
CF	carboxyfluorescein
CMC	critical micellar concentration
CNS	crystallography and NMR system
Cpx26-83	Rat complexin I (26-83)
CPXI	complexin I
CPXII	complexin II
CSA	chemical shift anisotropy
DD	dipole-dipole interaction
DLS	Dynamic light scattering
d_{min}	high resolution limit (Å)
DOPS	1,2-dioleoyl phosphatidylserine
DTT	dithiothreitol
E.coil	*Eschericheria coli*

EDTA	ethylene diamine tetraacetic acid
EGTA	ethylene glycol-bis (β-aminoethyl ether)-tetraacetic acid
EPR	electron paramagnetic resonance
FPLC	fast performance liquid chromatography
FRET	fluorescence resonance energy transfer
GST	glutathione-S-transferase
H/D exchange	hydrogen-deuterium exchange
HEPES	N-(2-hydroxyethyl) piperizine-N'2-ethanesulphonic acid
HSQC	heteronuclear single quantum coherence
IPTG	isopropyl β-D-thiogalactopyranoside
K_D	dissociation-constant
KDa	kilodalton
LB	luria broth
LDCV	large dense-core vesicles
LMV	large multilamellar vesicles
LUV	large unilamellar vesicles
NBD-DPPE	N-(7-nitro-2,1,3-benzoxadiazole-4-yl)-1,2-dipalmitoyl-PE
Ni-NTA	nickel-nitrilotriacetic acid
NMR	nuclear magnetic resonance
NOE	nuclear Overhauser effect
NOESY	nuclear Overhauser effect spectroscopy

NSF	N-ethylmaleimide-sensitive factor
SNAPs	soluble NSF attachment proteins
OD	optical density
OG	octyl-β-D-glucopyranoside
PAGE	polyacrylamide gel electrophoresis
PBS	phosphate buffered saline
PC	phosphatidylcholine
PCR	polymerase chain reaction
PE	phosphatidylethanolamine
POPC	1-palmitoyl, 2-oleoyl phosphatidylcholine
ppm	part per million
PS	phosphatidylserine
R_{eff}	effective detergent to lipid molar ratio
rhodamine-DPPE	N-(lissamine rhodamine B sulfonyl) 1,2-dipalmitoyl-PE
rmsd	root mean square deviation (Å)
R_{sat}	effective ratio at the onset solubilization of liposomes
R_{sol}	effective ratio at the total solubilization of liposomes
SDS	sodium dodecylsulfate
SMR	the strongest methyl resonance
SNAP	soluble NSF attachment protein
SNAP-25	synaptosome-associated protein of 25 kDa
SNARE	SNAP receptor

SNC	the C-terminal SNARE motif of SNAP-25
SNN	the N-terminal SNARE motif of SNAP-25
Syb2	rat synaptobrevin 2 (29-93)
Syx	Rat syntaxin 1A (188-259)
SyxH3	His-tagged rat syntaxin 1A (183-288)
SyxS	rat syntaxin 1A (191-253)
TCA	trichloroacetic acid
TeNT	tetanus neurotoxin
TOCSY	total correlation spectroscopy
TRIS	tris (hydroxymethyl) aminomethane
TROSY	transverse-relaxation optimized spectroscopy
t-SNARE	target membrane SNARE
UV	ultra-violet
VAMP	vesicle-associated membrane protein
v-SNARE	vesicle SNARE
WR	working reagent

CHAPTER 1 GENERAL INTRODUCTION

1.1 Neurons and Membrane Trafficking in the Nerve Terminal

The human brain contains about 10^{11} neurons. Each neuron forms thousands of connections with other neurons to communicate information with each other. To transmit information, neurons adopt unique structural features with four distinct regions: the cell body, the dendrites, the axon, and the axon terminals (Lodish, 2000; Figure 1.1). The cell body contains the nucleus and is the place of synthesis of virtually all neuronal proteins and membranes. The axon is specialized for the conduction of a particular type of electric signal, called an action potential. The axon terminals form synapses with the dendrites or the cell bodies of other neurons. Synapses are the junctions where neurons pass signals to other cells. The electric signal transmits quickly along the axon and reaches the axon terminals, where vesicles filled with neurotransmitter are docked. The action potential triggers fusion of vesicles with the plasma membrane and release of neurotransmitters, which are chemical signals. The dendrites are specialized to receive chemical signals from the axon termini of other neurons.

Numerous membrane trafficking events are involved to maintain the function of a neuron, such as, replenishment of the components at the nerve terminal and the recycling of synaptic vesicles (Figure 1.2). Among all these processes, the most intriguing event is the secretion of neurotransmitter by exocytosis of synaptic vesicles in response to an action

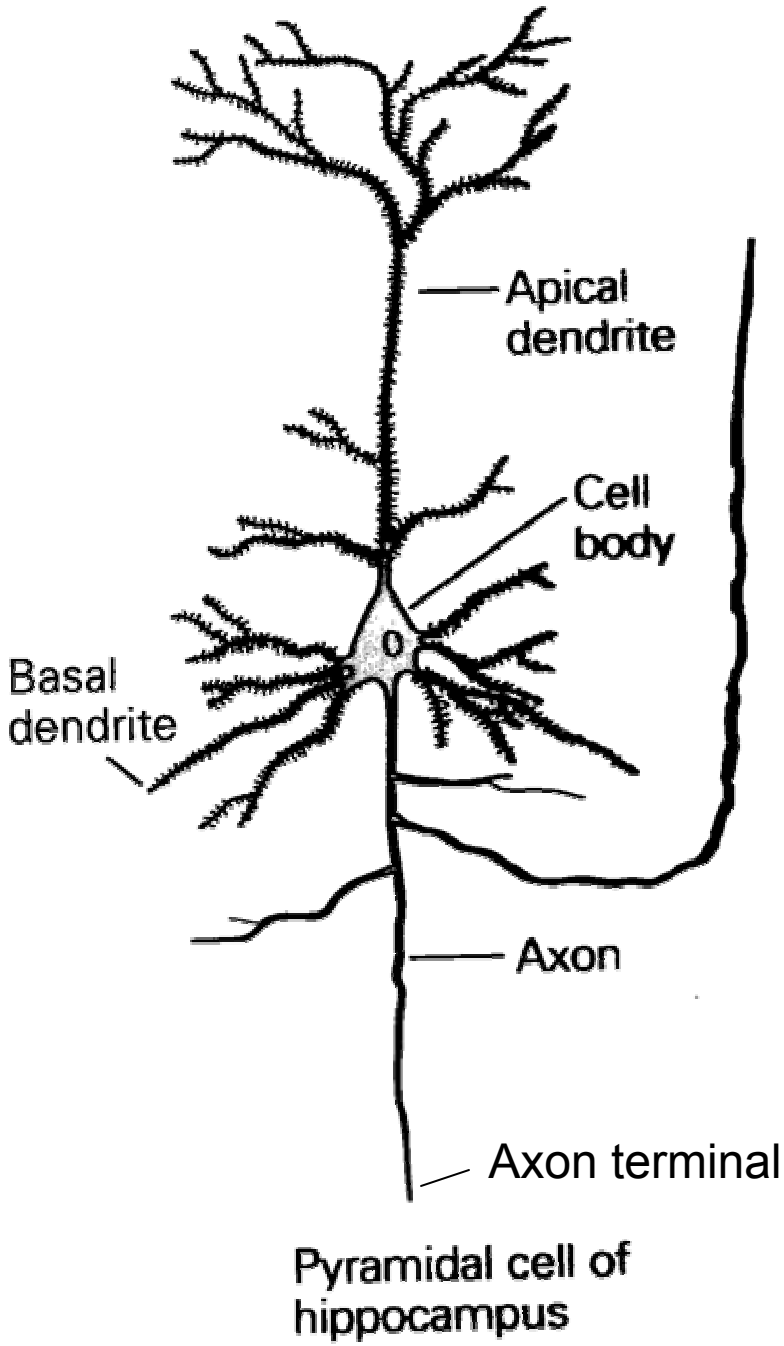

Figure 1.1 Mophology of a typical mammalian neuron (pyramidal cell of the hippocampus). There are four distinct regions: the cell body, the dendrites, the axon and the axon terminal (Lodish, 2000).

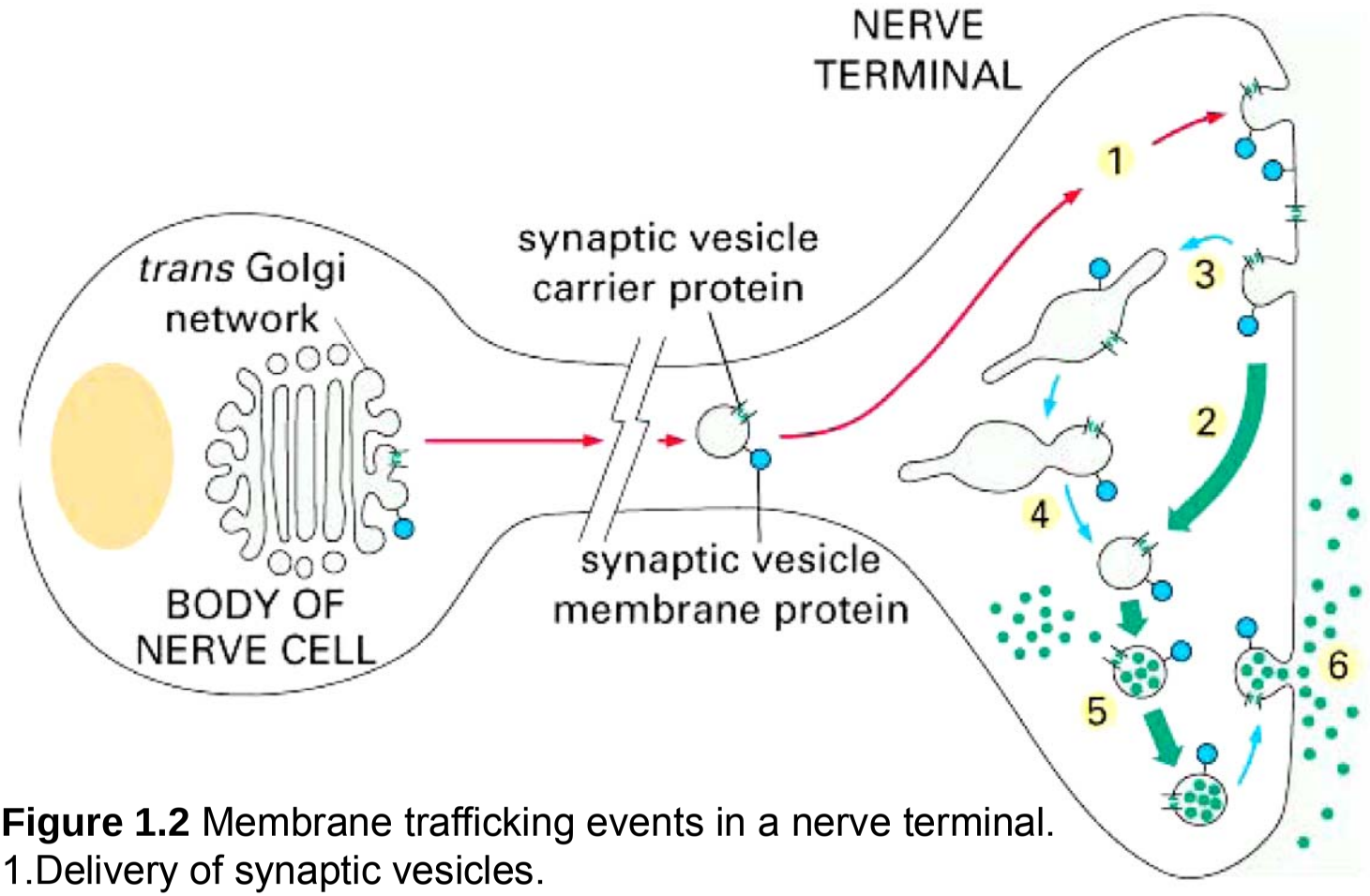

Figure 1.2 Membrane trafficking events in a nerve terminal.
1.Delivery of synaptic vesicles.
2.Endocytosis of synaptic vesicles.
3.Endocytosis of synaptic vesicles and delivery to endosome.
4.Budding of synaptic vesicles from endosome.
5.Loading of neurotransmitter into synaptic vesicles.
6.Secretion of neurotransmitter by exocytosis.

potential. This event is characterized by its extremely fast speed and tight regulation by Ca^{2+}. My research projects during the last four years were aimed at understanding the molecular mechanism of neurotransmitter release by studying the structure and function of the proteins that are crucial for this process.

1.2 Synaptic Vesicle Cycle

To support fast and repeated rounds of release, synaptic vesicles undergo a trafficking cycle. The synaptic vesicle cycle can be roughly divided into five steps: targeting, docking, priming, fusion and endocytosis (Südhof, 1995; Figure 1.3). Briefly, the vesicles loaded with neurotransmitters are targeted to the presynaptic terminals and docked on the active zone, the specialized region where vesicle fusion and transmitter release occur. Then, the docked vesicles undergo a very important priming step, which makes the vesicles ready for Ca^{2+} triggering. Once Ca^{2+} enters the presynaptic terminal, a subset of the primed vesicles will fuse with plasma membrane and release neurotransmitters into the synaptic cleft in less than 0.5msec (Sabatini and Regehr, 1999). The fused synaptic vesicles are retrieved back for recycling.

1.3 Membrane Fusion

Synaptic vesicle exocytosis is basically a membrane fusion process. Membrane fusion does not occur spontaneously. In an aqueous environment, a thin layer of water separates the

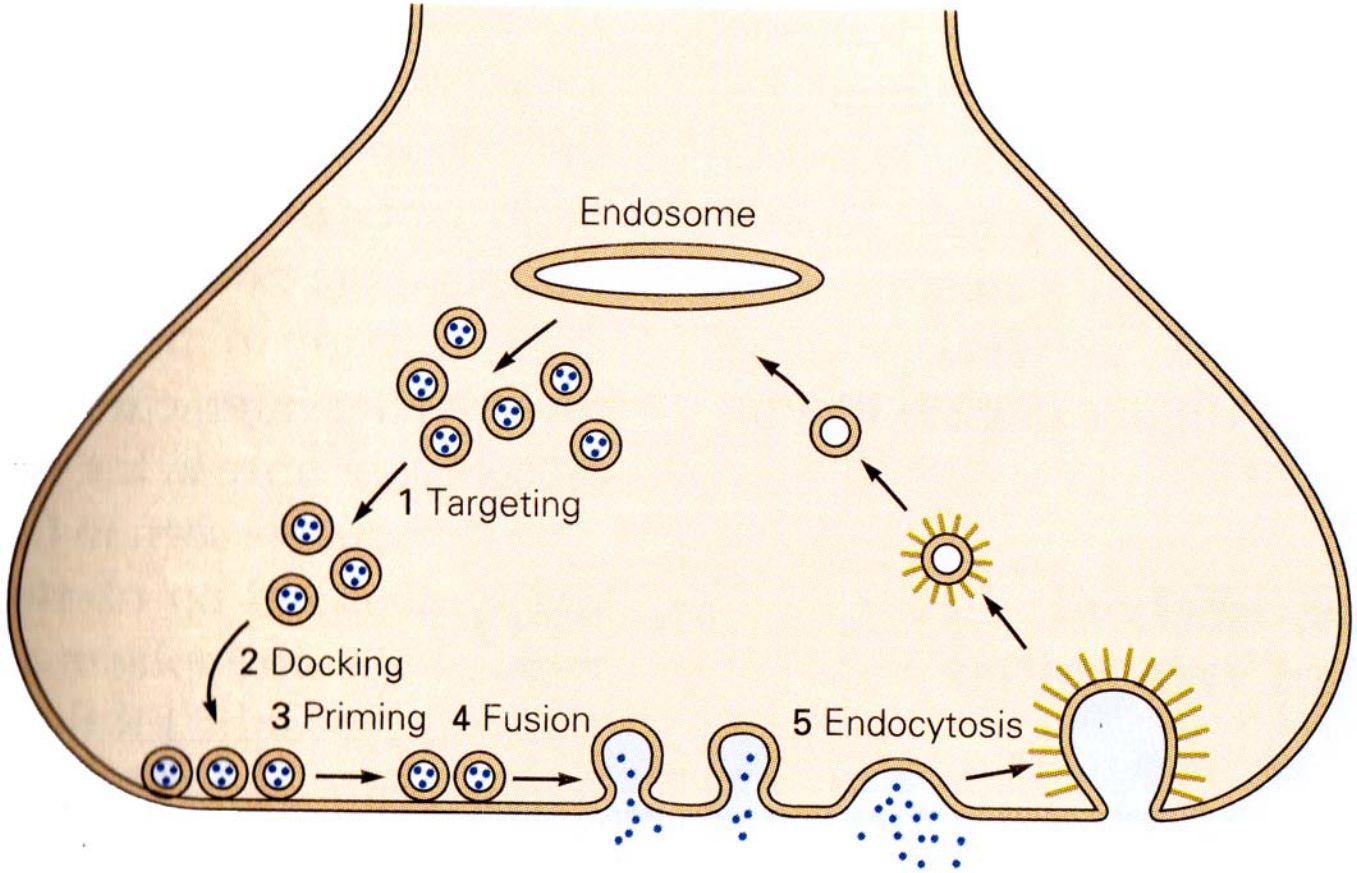

Figure 1.3 Synaptic vesicle recycling pathway involves five distinct steps: targeting, docking, priming, fusion and endocytosis. Small circles represent synaptic vesicles. Little dark dots stand for neurotransmitters. Clathrin mediated endocytosis is shown. Gray bars around synaptic vesicles represent clathrin molecules.

membranes before fusion. Forces that act on the membrane bilayers are Van der Waals attraction, electrostatic repulsion of charged lipids and hydration repulsion. Phospholipid membranes need to get closer than 3nm for fusion to occur (Helm and Israelachvili, 1993). At such a short distance, the repulsive forces between two opposing membranes are very strong. Membranes fusion requires some kind of defects in lipid bilayers to expose hydrophobic interiors and allow lipid mixing. The defects can be caused by membrane proteins or special lipid compositions.

1.3.1 Formation of the Fusion Pore

Two extreme views about the formation of the fusion pore have been proposed, namely the proteinaceous view and the lipidic view. In the first view (Almers and Tse, 1990; Lindau and Almers, 1995), proteins play a leading function. According to this view, a protein oligomer penetrates two opposing phospholipid membranes and forms an open channel between two compartments. Lipid molecules then enter the fusion pore to cover the newly exposed amphiphilic surfaces. In the other view, lipids play a more active role in opening the fusion pore, while proteins mainly act as an enzyme, to lower the activation energy for fusion (Monck *et al.*, 1995). This second model assumes that the fusion pore is composed of lipids and that membrane fusion must follow the physical laws determining lipidic phases. The mechanism of opening fusion pore is still under debate. However, it is clear that both protein and lipid play important roles in membrane fusion.

1.3.2 Stalk Model of Membrane Fusion

Currently, the most favored theoretical model of membrane fusion is the stalk model (Markin *et al.*, 1984). According to this model, fusion occurs via formation of discrete intermediates. The first intermediate is a stalk, also called a semitoroidal structure, in which the proximal monolayers of the two opposing lipid bilayers are connected by a stalk (Figure 1.4b). Once the stalk has formed, the distal monolayers are pulled toward each other, forming a dimple. This transition stage is also referred to as the hemifusion stage (Figure 1.4c). After contact between the two distal monolayers has been established, relaxation of the energy from the void spaces will result in the opening of fusion pore (Figure 1.4d). This model is supported by theoretical calculations and the stalk intermediate has been shown to exist in several independent studies (Chernomordik, 1996; Lee and Lentz, 1997; Basanez *et al.*, 1998).

1.4 Properties of the Lipids

As the major components of the cell membrane, lipids undoubtedly play an essential role in membrane fusion. All the lipids in the cell membrane are amphipathic, that is, they have a hydrophilic end and a hydrophobic hydrocarbon end. The most abundant membrane lipids are the phospholipids, which usually have one hydrophilic head group and two hydrophobic hydrocarbon tails. The hydrophobic tails generally consist of fatty acids, which vary in shape and length.

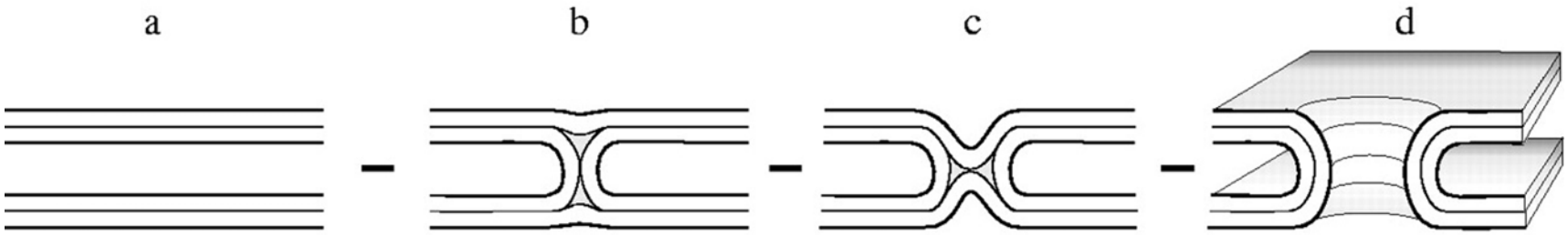

Figure 1.4 Intermediates in membrane fusion. Thick lines represent hydrophilic surfaces of lipid membranes, and thin lines represent the interface between the two leaflets of the bilayer. (a) Two membranes are separated; (b) fusion stalk (the proximal but not the distal leaflets are continuous; void spaces are shown in gray); (c) transbilayer contact; (d) opening of the fusion pore (Jahn and Sudhof, 1999).

In water, lipids tend to aggregate to bury the hydrophobic tail and expose their hydrophilic head to minimize the free energy. The different shape and length of the hydrophobic tails can change the packing of the lipids and affect the membrane curvature (Zimmerberg *et al.*, 1993). The most common phospholipids, such as phosphatidylcholine and phosphatidylserine, have a cylinder shape (Figure 1.5c); they can spontaneously form bilayers, with the hydrophobic tails sandwiched between the hydrophilic head groups (Figure 1.5d). Those lipid molecules with a large head group and small hydrocarbon tails have a shape of inverted cone (Figure 1.5a). Typical examples are detergents and lysophospholipids. They tend to form spherical micelles and favor the positive curvature of the membrane (Figure 1.5b). On the contrary, there are also some cone-shaped lipids, for instance, phosphatidylethanolamine and cholesterol, containing big fatty acid tails and a small head group (Figure 1.5e). This type of lipids prefers a negative membrane curvature (Figure 1.5f). Therefore, the asymmetric presence of certain lipid molecules in one of the leaflets of a lipid bilayer may destabilize the bilayer structure and favor the non-bilayer intermediate structure, i.e. the stalk, and consequently facilitate the fusion process (Israelachvili *et al.*, 1980; Chernomordik *et al.*, 1995).

1.5 Proteins that are Essential for Synaptic Vesicle Exocytosis

Extensive studies have led to the identification of numerous proteins that are involved in neurotransmitter release (Südhof, 1995; Augustine *et al.*, 1996; Jahn and Südhof, 1999; Lin and Scheller, 2000). The major players for synaptic vesicle fusion include N-ethylmaleimide-

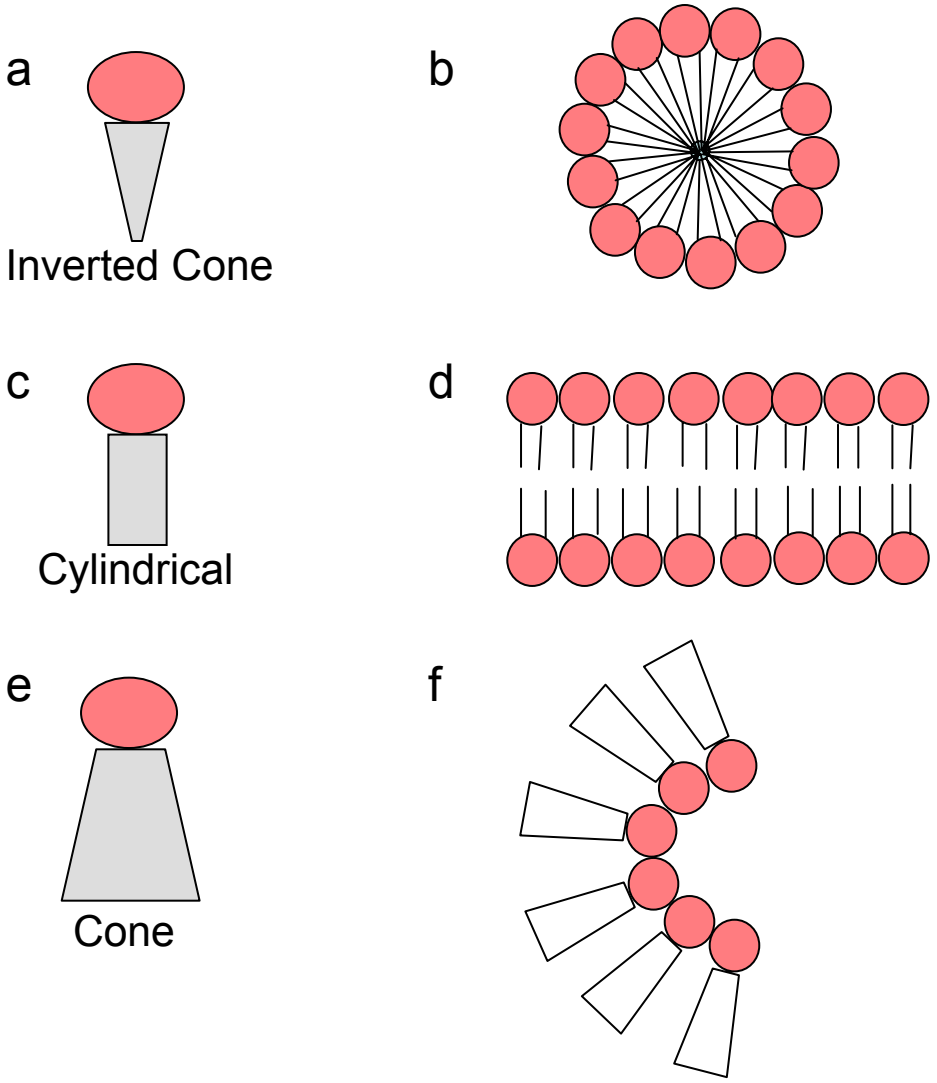

Figure 1.5 Molecular shapes and polymorphic phases exhibited by lipids and detergents in water. Red circles represent polar head groups of lipids. Lipids with a shape of inverted cone (a) tend to form micellar structures (b). The cylindrical lipids (c) spontaneously form lipid bilayers (d). The cone shaped lipids (e) favor negative membrane curvature (f).

sensitive factor (NSF), soluble NSF attachment proteins (SNAPs), SNAP receptors (SNAREs), munc18-1, and Rab 3. Homologues of these proteins have been found in different organisms ranging from yeast to human, suggesting that synaptic vesicle fusion shares a common mechanism with many other types of intracellular vesicular traffic (Bennett and Scheller, 1993; Ferro-Novick and Jahn, 1994). In addition, proteins such as munc13-1, synaptotagmin 1 and the complexins are crucial for Ca^{2+}-triggered exocytosis, but not for the constitutive membrane fusion events (Sollner, 2003). Thus, these proteins are specialized for the tight spatial and temporal regulation of neurotransmitter release. Below I discuss the proteins that I have been working with and the proteins that are closely related with my research projects.

1.5.1 SNAREs

SNAREs represent a large evolutionarily conserved protein family that is involved in all steps of the secretory and endocytic pathway. The best-characterized SNAREs are those function in neuronal exocytosis, which include synaptobrevin (VAMP), syntaxin 1 and synapse-associated protein of 25 kDa (SNAP-25). Synaptobrevin is associated with the vesicle membrane and is generally called v-SNARE, whereas syntaxin 1 and SNAP-25 are anchored on the target membrane, and are designated as t-SNAREs. Their essential role in synaptic vesicle exocytosis was demonstrated by the finding that clostridial neurotoxins inhibit neurotransmitter release by selective and specific proteolysis of synaptobrevin, syntaxin 1 or SNAP-25 (Schiavo *et al.*, 1992; Link *et al.*, 1992; Blasi *et al.*, 1993a; Blasi *et al.*, 1993b). The functional importance of the SNAREs was also shown by the observation

that the SNAREs interact with NSF and SNAPs, which are necessary for intracellular fusion (Sollner *et al.*, 1993b). In addition, synaptobrevin, syntaxin 1 and SNAP-25 were found to form a tight complex, which is disassembled by the ATPase activity of NSF (Sollner *et al.*, 1993a). Based on these results, Rothman and colleagues proposed a general model, also called 'the SNARE hypothesis', to explain the function of the SNAREs in membrane fusion. This model proposed that the recognition and interaction between SNAREs on vesicle and target membrane provides specificity for vesicle targeting and docking (Sollner *et al.*, 1993b; Rothman, 1994).

However, cleavage of the SNAREs by clostridial neurotoxins inhibits the synaptic vesicle fusion, but has no effects on vesicle docking (Südhof *et al.*, 1993), suggesting that the SNAREs are more likely to act downstream of vesicle docking, perhaps even function in the fusion step. To understand how the SNAREs participate in membrane fusion, extensive biochemical and structural studies were performed and many important aspects of the SNAREs were revealed (Fasshauer *et al.*, 1998a; Fasshauer *et al.*, 1998b; Pelham, 1999; Jahn *et al.*, 1999; Lin *et al.*, 2000). Syntaxin 1 and synaptobrevin each possess one SNARE motif, adjacent to their C-terminal transmembrane regions (Figure 1.6b and 1.6d). SNAP-25 contains two SNARE motifs (the N-terminal and the C-terminal SNARE motifs designated as SNN and SNC respectively) which are joined by a long loop. Four cysteine residues in the loop are palmitoylated, which attaches SNAP-25 on the membrane (Figure 1.6e). The SNARE motifs of these three proteins assemble into a highly stable four-helix bundle, named 'core complex' or SNARE complex (Figure 1.6c), which is proteolysis and SDS resistant,

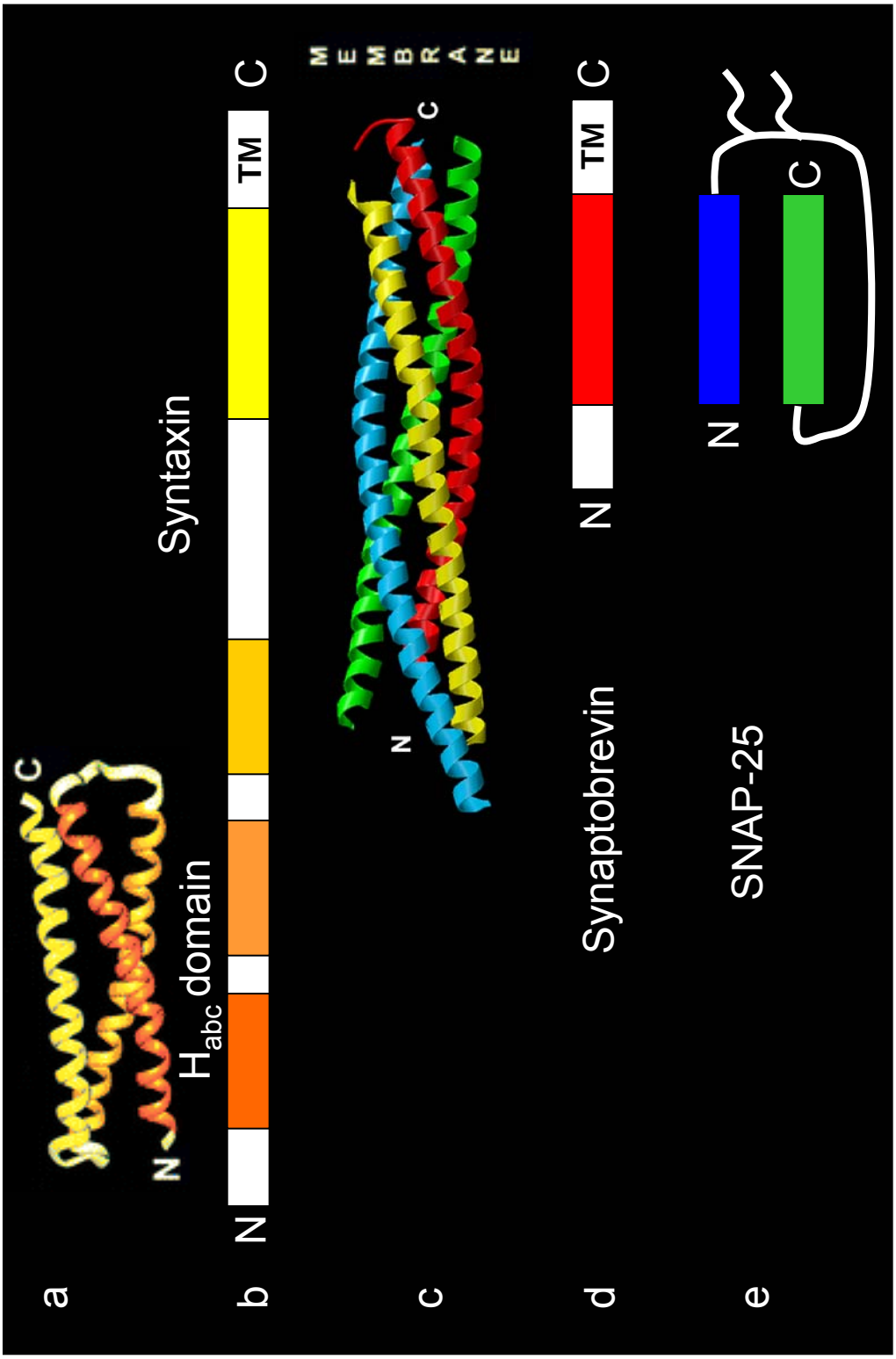
a
b
c
d
e
Syntaxin
N
C
TM
H_{abc} domain
MEMBRANE
N
C
Synaptobrevin
N
TM
C
SNAP-25
N
C

Figure 1.6

Figure 1.6 Summary of known structural information of the neuronal SNARE proteins. (a) Ribbon diagram of the structure of the syntaxin 1 N-terminal H_{abc} domain (Fernandez *et al.*, 1998). (b,d,e) The domain structures of syntaxin, synaptobrevin and SNAP-25. The SNARE motifs are color coded as follows: syntaxin 1 (b), yellow; synaptobrevin (d), red; SNAP-25 amino terminus (e), blue; and SNAP-25 carboxyl terminus (e), green. The long curve line in (e) represents the loop connecting the two SNARE motifs and the short curve lines represent the palmitoylation sites. (c) Ribbon diagram of the structure of the core complex (Sutton *et al.*, 1998). Four SNARE motifs align in parallel fashion with the C-terminal ends close to the membranes (Jahn and Südhof, 1999).

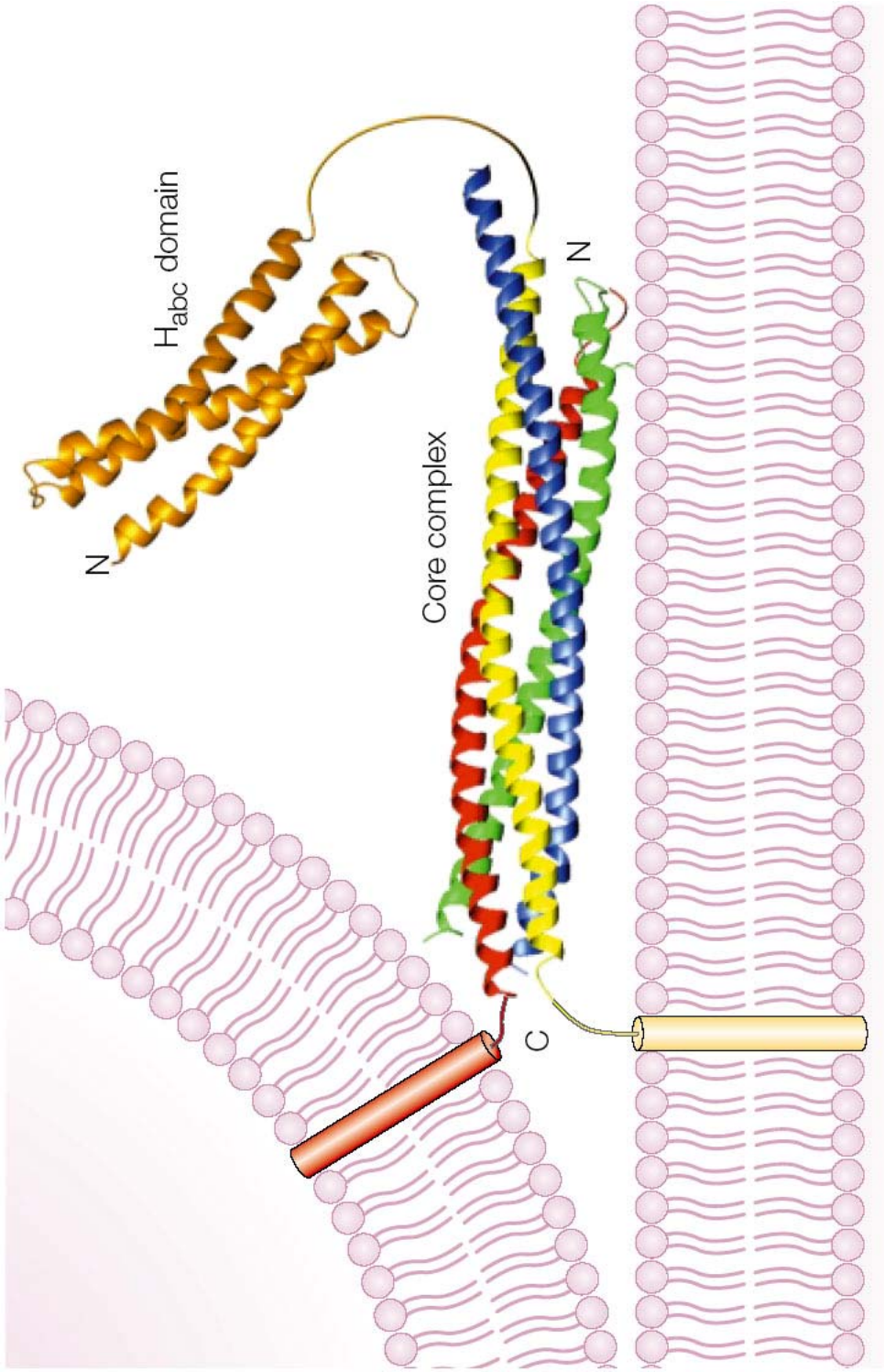

Figure 1.7

Figure 1.7 Hypothetical model of the neuronal SNARE complex as it brings two membranes to close proximity. The ribbon diagrams include the crystal structure of the core complex and the NMR structure of the N-terminal H_{abc} domain of syntaxin. The SNARE motifs are colored as in Figure 1.6. The H_{abc} domain is colored in orange. The cylinders inside the lipid bilayers represent the transmembrane regions of syntaxin 1 and synaptobrevin. The curved lines stand for the linker regions (Rizo and Südhof, 2002).

and only denatures above 90^{o}C (Hayashi *et al.*, 1994; Fasshauer *et al.*, 1998a; Poirier *et al.*, 1998a). Electron microscopy studies showed that syntaxin 1 and synaptobrevin are aligned in parallel within the core complex (Hanson *et al.*, 1997). This parallel arrangement was further confirmed by spin labeling electron paramagnetic resonance (EPR) spectroscopy studies (Poirier *et al.*, 1998b) and fluorescence resonance energy transfer (FRET) experiments (Lin and Scheller, 1997). Consistent with these results, the crystal structure of the neuronal SNARE complex revealed a highly twisted parallel four-helix bundle (Sutton *et al.*, 1998). Since the SNARE motifs of synaptobrevin and syntaxin 1 are adjacent to their transmembrane regions, the parallel structure arrangement led to the proposal that formation of the core complex could bring the synaptic vesicle and plasma membranes into close proximity and might facilitate or execute fusion (Figure 1.7). However, there is still considerable debate as to whether the core complex alone is sufficient to mediate membrane fusion and how the assembly and disassembly cycle is related to the actual membrane fusion event (Weber *et al.*, 1998; Hu *et al.*, 2002; Rizo and Südhof, 2002; Kweon *et al.*, 2003; Rizo, 2003; Chen *et al.*, 2004).

1.5.2 Special Features of Syntaxin 1

Among the neuronal SNAREs, syntaxin 1 is particularly interesting. Circular dichroism spectroscopy showed that the isolated synaptobrevin and SNAP-25 are largely unstructured, whereas syntaxin 1 exhibits significant α-helicity (Fasshauer *et al.*, 1997a; Fasshauer *et al.*, 1997b). Previous study in our laboratory showed that syntaxin has a conserved N-terminal domain, known as H_{abc}, which forms an antiparallel three-helix bundle (Fernandez *et al.*,

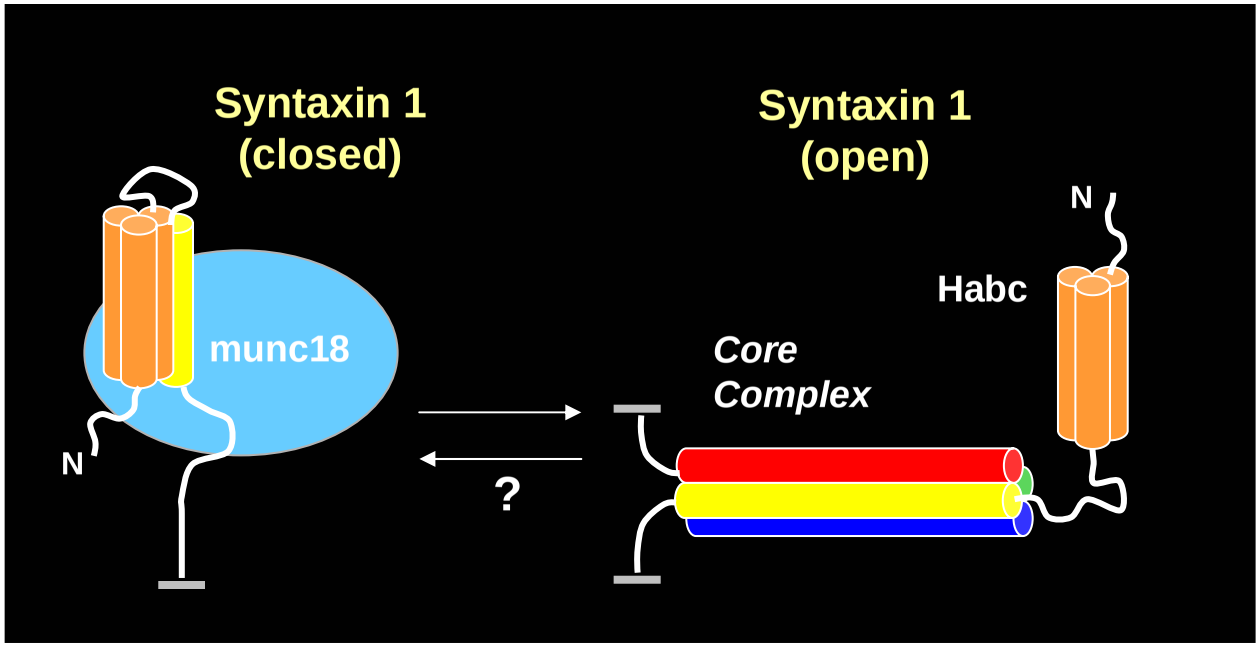

Figure 1.8 Models of the closed and open conformations of syntaxin 1. The cylinders represent a-helices and the curved lines represent unstructured linkers. The horizontal grey bars stand for membranes. The closed conformation (left) is pictured as a four helix bundle, where three helices of the Habc domain (orange) fold on to part of the syntaxin SNARE motif region (yellow). Munc18 (cyan ellipse) binds to the closed syntaxin 1. The right side shows the open conformation of syntaxin 1 in complex with synaptobrevin and SNAP-25. The color coding is the same as in Figure 1.6.

1998; Figure 1.6a and 1.6b). This N-terminal domain has been shown to interact with a variety of proteins that are important for neurotransmitter release, such as synaptotagmin and munc13-1 (Shao *et al.*, 1997; Betz *et al.*, 1997; Wu *et al.*, 1999; Matos *et al.*, 2000). The H_{abc} domain folds back and binds to the syntaxin SNARE motif (H3 motif), forming a 'closed' conformation that is incompatible with the formation of the core complex (Dulubova *et al.*, 1999). Thus, the 'closed' syntaxin 1 needs to be opened before the other SNARE proteins can interact with the syntaxin SNARE motif and assemble the core complex (Figure 1.8). It has been suggested that conformational changes in syntaxin, resulting from protein-protein interactions mediate neurotransmitter release. On the other hand, the 'closed' conformation is important for the interaction between syntaxin 1 with munc18-1, an essential protein in the neurotransmitter release (Dulubova *et al.*, 1999; Misura *et al.*, 2000). A double mutant L165A, E166A of syntaxin 1, which is constitutively open, abolishes the binding with munc18-1 (Dulubova *et al.*, 1999).

1.5.3 SM proteins

Just like SNAREs, SM proteins are also required in all types of intracellular membrane traffic events. The first SM protein, named UNC-18, was identified in *C.elegans*, (Brenner, 1974). Munc18-1 (also referred to as n-Sec1 or rb-Sec1), the mammalian homologue of UNC-18, was identified through its tight interaction with syntaxin 1 (Hata *et al.*, 1993; Garcia *et al.*, 1994; Pevsner *et al.*, 1994). The absolute requirement for munc18-1 in synaptic vesicle fusion has been shown by the total silence of the neurons lacking munc18-1, as monitored with electrophysiological measurements (Verhage *et al.*, 2000). Studies of the

munc18-1 homologue in Drosophila, ROP, yielded several lines of intriguing results (Wu *et al.*, 1998; Wu *et al.*, 2001). Overexpression of either ROP or syntaxin (the Drosophila homologue of syntaxin 1) alone caused a decrease in neurotransmitter release. However, when syntaxin and ROP were overexpressed simultaneously, the release defects were suppressed. In addition, expression of syntaxin mutants that decreased ROP binding displayed increased neurotransmitter release. Altogether, these studies suggest that both syntaxin and munc18-1 have essential, but distinct functions, which might be mutually inhibited by the interaction between munc18-1 and syntaxin. Thus, it is crucial to keep both syntaxin and munc18-1 inactive, or in an 'off' state when neurons are at rest. However, at some point such an 'off' state needs to be turned 'on'; or in other words, munc18-1 should be released only at the right place and right moment, and at the same time the closed conformation of syntaxin 1 needs to be opened to form the core complex. The mechanism of this transition is still a mystery. The crystal structure of the munc18-1-syntaxin 1 complex revealed extensive association between munc18-1 and syntaxin 1 (Figure 1.9a). The contact area covers both the N-terminal domain and the SNAREs motif region of syntaxin 1 (Misura *et al.*, 2000), which explains the tight interaction found by biochemical methods and the inability to form the core complex when syntaxin 1 is bound by munc18-1 (Dulubova *et al.*, 1999). Together with the observation that syntaxin 1 is incapable of forming SNARE complexes when bound to munc18-1, the structure of the munc18-1-syntaxin 1 complex suggests that munc18-1 might potentially function through regulating the conformational changes of syntaxin 1, and therefore facilitate the formation of the core complex (Misura *et al.*, 2000). Such a model assumes that the structure of the isolated syntaxin 1 is different from

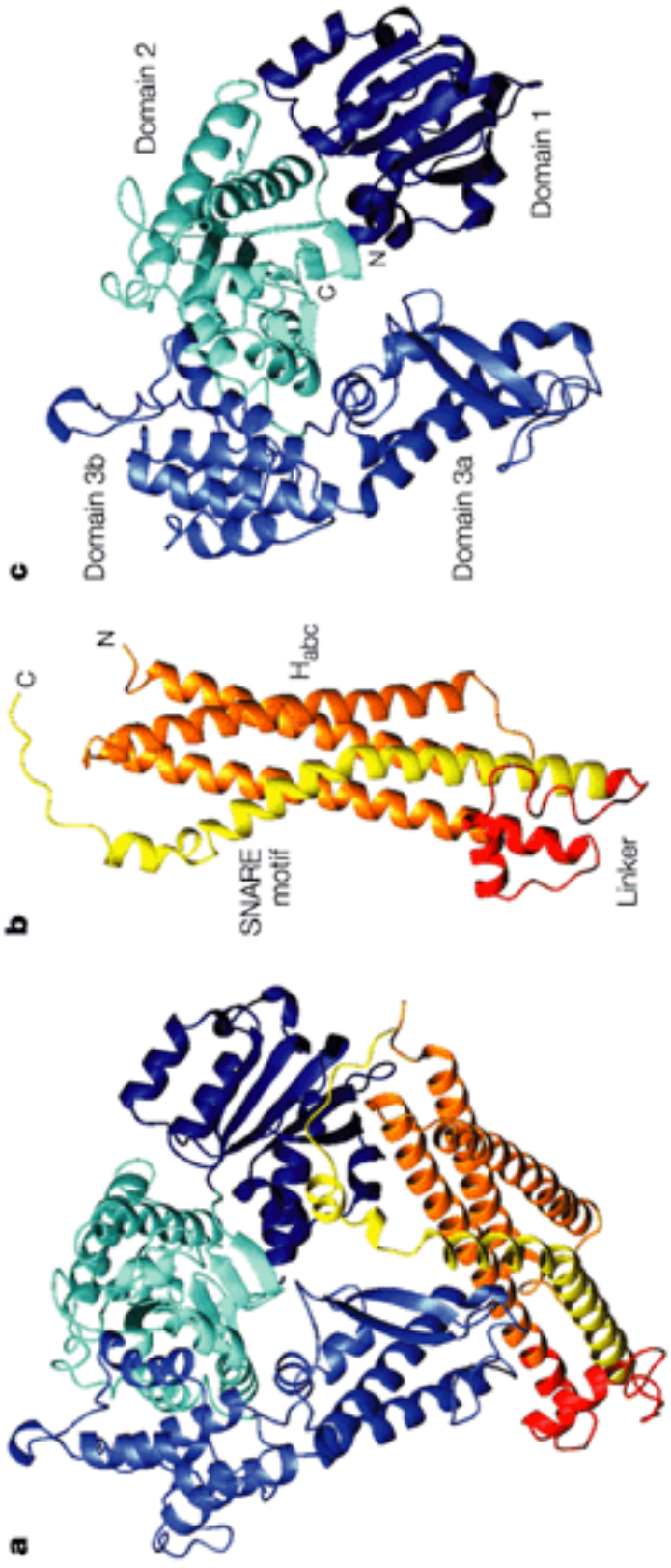
a
b
C
N
H_{abc}
SNARE
motif
Linker
c
Domain 2
Domain 1
C
N
Domain 3b
Domain 3a

Figure 1.9

Figure 1.9 Ribbon diagrams of the structure of the munc18/syntaxin 1 complex. (a) Structure of the complex showing the extensive contact between syntaxin 1(orange and yellow helices) and munc18 (blue). (b) Structure of syntaxin 1 in the complex. The syntaxin SNARE motif (yellow) forms an α-helix. The N-terminus of the SNARE motif binds to a groove of the H_{abc} domain (orange), while the C-terminus departs and forms an irregular, partially helical structure. (c) Structure of munc18 in the complex. Its different domains are colored in different shades of blue (Rizo and Südhof, 2002).

that of the munc18-1-bound syntaxin 1 (Figure1.9b). The most direct way to test this model is to compare the two structures. Since the structure of the isolated syntaxin 1 is not available, I have tried to obtain the solution structure of the minimal fragment of the 'closed' syntaxin 1 (residues 26-230), containing the N-terminal domain, the linker region and half of the SNARE motif (Dulubova *et al.*, 1999). Unfortunately, I was only able to solve the structure of the N-terminal domain (residues 26-140) within the closed syntaxin 1, whereas the data for the rest region are poor, presumably because of some dynamic processes. However, the current results suggest that the N-terminal domain of syntaxin 1 adopts the same conformation whether it is alone, bound to munc18-1, or in the 'closed' conformation (see details in chapter 4). Thus, it is unlikely that munc18-1 binding alters the closed conformation of isolated syntaxin 1.

The binding mode between syntaxin 1 and munc18-1 is an exception among their homologues governing membrane traffic in different cellular compartments. A recent systematic study from our laboratory showed that the syntaxin homologues, Sed5p, Tlg2p and Ufe1p from yeast, as well as syntaxin 5, 16 and 18 from vertebrates, have a short evolutionarily conserved N-terminal peptide, upstream of the autonomously folded N-terminal domain. The small peptide, rather than the whole 'closed' syntaxin, binds to the corresponding SM proteins (Yamaguchi *et al.*, 2002; Dulubova *et al.*, 2003). This observation suggests that the SM protein potentially could interact with syntaxin independent of core complex formation, which might represent a general mechanism in at least a subset of intracellular membrane fusion events. Given the diversity of the interactions between SM

proteins and the SNARE proteins in different membrane trafficking systems, as well as the universal requirement of SM proteins in all types of intracellular membrane fusion reactions, SM proteins must have a more general and essential function.

Studies of mouse chromaffin cells lacking munc18-1 suggested a role for munc18-1 in docking of large dense-core vesicles (LDCV) to the plasma membrane (Voets *et al.*, 2001). However, docking was unaltered in brain synapses of munc18-1 knockout mice, suggesting that the most important function of munc18-1 is downstream of docking (Verhage *et al.*, 2000). Furthermore, Sec1, the SM protein involved in the yeast secretory pathway, binds to the assembled SNARE complexes (Carr *et al.*, 1999). A mutagenesis study of Sec1 showed that a Sec1 mutant that blocked >95% of cell secretion has a much minor effect on the formation of the core complex (Grote *et al.*, 2000). This observation suggests a role for Sec1 after SNARE complex assembly. The actual function of SM proteins is still under debate. Clearly, it is crucial to understand the function of SM proteins before we can explain all these intriguing data and gain further insight into the mechanism of neurotransmitter release.

1.5.4 Complexins

Complexins are highly charged proteins of 134 amino acids. There are two closely related isoforms, complexin I and complexin II (abbreviated as CPXI and CPXII). Complexins are neuron specific proteins and largely co-localize with syntaxin and SNAP-25. Complexins were identified through their tight interaction with the core complex (McMahon *et al.*, 1995; Takahashi *et al.*, 1995; Ishizuka *et al.*, 1995). The previous nuclear magnetic resonance

(NMR) spectroscopy studies from our laboratory revealed that isolated complexins lack a tertiary structure but have a central helical region that can specifically bind to the core complex (Pabst *et al.*, 2000). The functional importance of complexins has been demonstrated by the lethal phenotype observed in the CPX I/II double knockout mice (Reim *et al.*, 2001). Interestingly, in the CPXI/II double knockout mice, neurotransmitter release by hypertonic sucrose treatment is normal, while the efficiency of the Ca^{2+} triggered neurotransmitter release is decreased dramatically (Reim *et al.*, 2001). In addition, complexins have been found to be involved in several neurological disorders, such as schizophrenia, bipolar disorder and Huntington disease (Eastwood and Harrison, 2000; Morton and Edwardson, 2001; Edwardson *et al.*, 2003). Thus, understanding the function of complexins will not only help to elucidate the regulation mechanisms of neurotransmitter release, but also provide clues on the pathology of some human diseases.

It has been suggested that complexin induces oligomerization of SNARE complexes by reshuffling the two SNARE motifs of SNAP-25 into separate SNARE complexes (Tokumaru *et al.*, 2001). However, such a model is incompatible with the molecular properties of the complexin-SNARE interaction and no oligomerization of SNARE complex was observed in the separate studies of the complexin/SNARE interactions by other researchers (Pabst *et al.*, 2000; Pabst *et al.*, 2002). Moreover, the linkage of the two SNARE motifs of SNAP-25, which is supposed to be critical to mediate SNARE complex oligomerization in the presence of complexin, is not required for exocytosis in PC12 cells

(Chen *et al.*, 2001). Thus, rigorous biochemical and biophysical studies are imperative to understand the function of complexin.

The selective decrease in the efficiency of fast Ca^{2+}-triggered release observed in the complexin double knockout mice suggests that complexin functions in a late step of exocytosis, close to Ca^{2+} triggering (Reim *et al.*, 2001). However, it is difficult to correlate the complexin function with the Ca^{2+} independent interaction between complexin and the core complex (Pabst *et al.*, 2000). To gain further insight into the mechanism of the complexin function, I studied the interaction between CPXI and the SNARE complex using a combination of NMR spectroscopy and X-ray crystallography (see details in chapter 3). The three dimensional structure of the complexin/SNARE complex revealed that complexin binds in an antiparallel fashion to the groove between synaptobrevin and syntaxin helices with an α-helical conformation. Complexin binding does not change the conformation of the core complex; instead, the deuterium exchange experiments by NMR spectroscopy showed that complexin binding stabilizes the core complex. Altogether, these results suggest a working model that complexin specifically binds to and stabilizes the fully assembled SNARE complexes, which are committed to the fast Ca^{2+}-triggered neurotransmitter release (Chen *et al.*, 2002).

1.5.5 Synaptotagmin I

Synaptotagmin I is a synaptic vesicle protein, containing a short transmembrane region (domain II) and two C_2-domains (domain IV and VI; Perin *et al.*, 1990; Perin *et al.*, 1991a;

Perin *et al.*, 1991b). Both C_2-domains can bind Ca^{2+} with low intrinsic Ca^{2+} affinities and their Ca^{2+} binding regions exhibit striking similarities (Sutton *et al.*, 1995; Shao *et al.*, 1996; Shao *et al.*, 1998; Ubach *et al.*, 1998; Fernandez *et al.*, 2001; Ubach *et al.*, 2001), indicating that there may be a cooperative function of these two domains (Figure 1.10). Given its Ca^{2+} binding characteristics, synaptotagmin I is believed to be the major calcium sensor in fast neurotransmitter release (Brose *et al.*, 1992; Geppert *et al.*, 1994; Bennett, 1999; Fernandez-Chacon *et al.*, 2001). Direct evidence was provided by genetic studies in C. elegans, drosophila and mice, where mutant synaptotagmins caused severe impairment of the fast Ca^{2+} dependent synaptic transmission, whereas the slow asynchronous component of neurotransmitter release was normal (Nonet *et al.*, 1993; Littleton *et al.*, 1993; Geppert *et al.*, 1994). This idea is further supported by the good correlation between the Ca^{2+} affinity of synaptotagmin I and the Ca^{2+} sensitivity of neurotransmitter release (Fernandez-Chacon *et al.*, 2001). Although these functional studies convincingly showed that synaptotagmin I plays a role in fast Ca^{2+}-triggered synaptic transmission, the mechanism of action of the synaptotagmin I is still unclear. It has been shown that both C_2-domains can bind phospholipids in a Ca^{2+} dependent manner (Davletov and Südhof, 1993; Fernandez *et al.*, 2001). Multiple studies have also reported Ca^{2+}-dependent and Ca^{2+}-independent interactions of synaptotagmin I with SNARE proteins (Südhof and Rizo, 1996; Südhof, 2002; Chapman, 2002). There has been a long-term debate about which interaction plays a primary role in the function of synaptotagmin I, and whether these interactions can occur simultaneously or compete with each other. An elegant study performed by Rizo and colleagues showed that phospholipids compete with the neuronal core complex for Ca^{2+}-dependent binding to

a

b

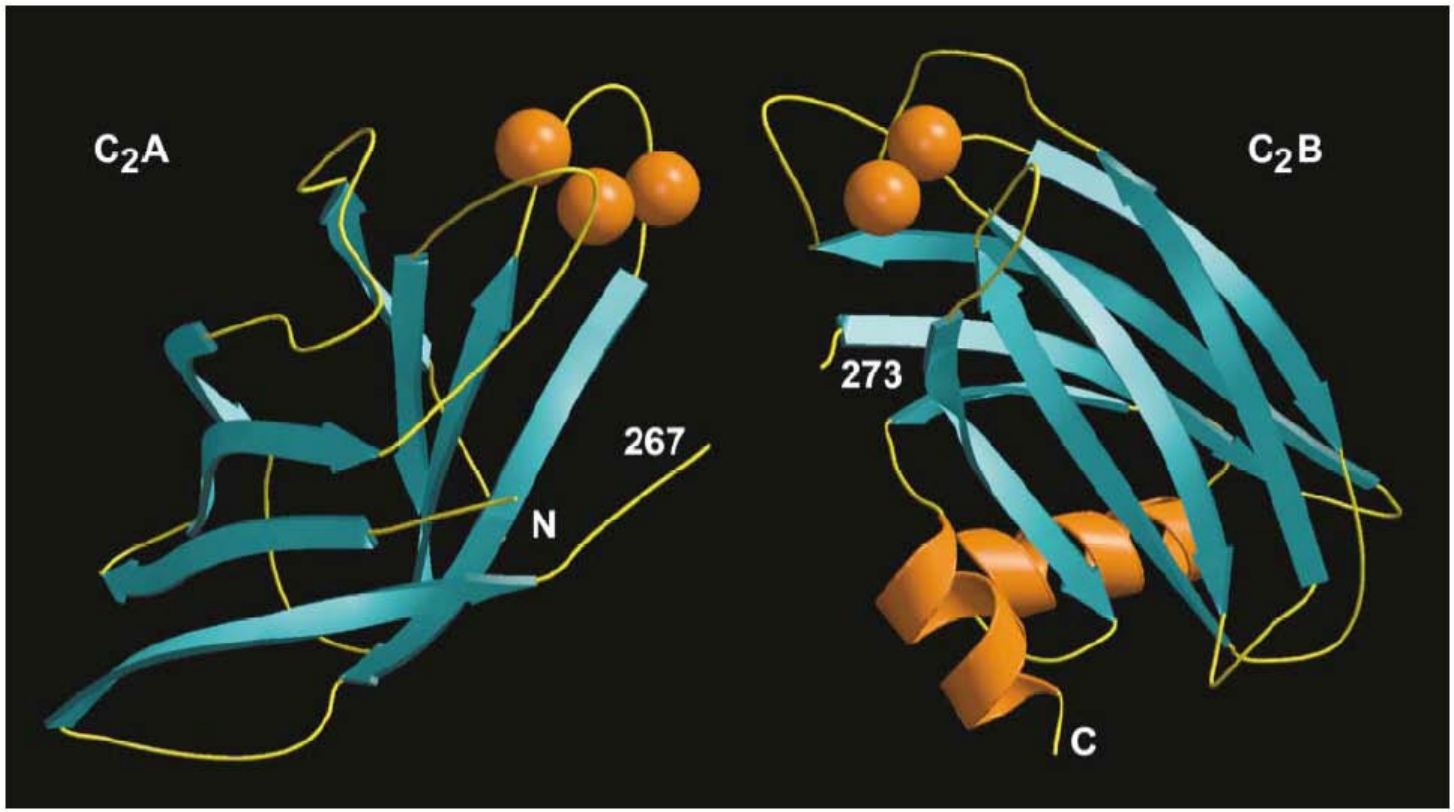

Figure 1.10

Figure 1.10 Summary of known structural information of synaptotagmin 1. (a) The domain structure of synaptotagmin 1. C_2A and C_2B domains are colored in red and TM stands for transmembrane region. The residue numbers of the domain boundaries are labeled above the domain structure. (b) Ribbon diagrams of the C_2A and C_2B domains of synaptotagmin 1. Strands are colored in cyan, and helices are colored in orange. The orange spheres represent the Ca^{2+} ions. The two C_2-domains are oriented with their Ca^{2+} binding sites in close proximity. The orientation has been chosen to illustrate the potential cooperative function of the C_2 domains of synaptotagmin 1 (Fernandez *et al.*, 2001).

synaptotagmin I (Arac *et al.*, 2003). This result is consistent with the observations that Ca^{2+}-dependent phospholipid binding probably underlies the function of synaptotagmin 1 in triggering neurotransmitter release (Fernandez-Chacon *et al.*, 2001; Shin *et al.*, 2002; Mackler *et al.*, 2002).

Twelve additional synaptotagmins have been discovered and many of them are co-expressed with synaptotagmin I in the brain (Südhof, 2002). All synaptotagmins share the same Ca^{2+} cooperativity and Ca^{2+}-dependent phospholipid binding but have distinct Ca^{2+} binding properties. It has been proposed that synaptotagmins perform complementary functions in Ca^{2+}-triggered exocytosis and the combination and relative abundance of various synaptotagmins could contribute to shaping the characteristic Ca^{2+} responses of synapses (Südhof, 2002). On the other hand, some evidence has suggested that neuronal SNAREs might also function as Ca^{2+} sensors in Ca^{2+}-triggered exocytosis. This notion has been recently reinforced by the observation that the Ca^{2+}-cooperativity of secretion decreased in chromaffin cells overexpressing a mutant SNAP-25 bearing a double residue substitution (E170A/Q177A; Sorensen *et al.*, 2002). To clarify whether the neuronal SNAREs play a role as Ca^{2+} sensor in neurotransmitter release, I have studied the Ca^{2+} binding properties of the core complex using NMR spectroscopy (see details in chapter 5). The results showed that the core complex contains several low affinity Ca^{2+} binding sites and most of them are not specific for Ca^{2+}. In addition, GST pull-down assays showed that the mutant SNAP-25 has no effect on either the Ca^{2+}-dependent or the Ca^{2+}-independent interactions between SNAREs and synaptotagmin I. Instead, I found that the SNAP-25 mutant has a conspicuous

effect on the kinetics and efficiency of core complex assembly. In summary, these results suggest that the SNAREs do not act as Ca^{2+} sensors, but core complex assembly is tightly coupled to Ca^{2+} sensing in neurotransmitter release.

1.6 Approaches to Study the Mechanism of Neurotransmitter Release

Insights into the mechanism of neurotransmitter release are mainly gained from three areas of investigation: (1) Discovery of new proteins that are important for synaptic transmission with genetic and biochemical techniques (2) Study of protein-protein and protein-lipid interactions with biochemical and biophysical methods (3) reconstitution of membrane fusion in a cell free system, which bridges the gap between physiological observations and molecular analysis results.

As discussed in previous sections, numerous proteins have been identified and significant progress has been made towards understanding both the structure and function of the important proteins in neurotransmitter release. Now it is the time to put together all these information and directly test function of individual protein with a reconstitution assay. Reconstitution of membrane proteins is a method to re-incorporate purified proteins into phospholipid vesicles and study properties of the membrane proteins in a condition that mimics their native environment. This approach, circumventing the complexity of the native membranes and the interference from other membrane constituents, has been proved to be a very useful tool for elucidating functional and structural aspects of individual membrane

proteins (Rigaud *et al.*, 1995; Rigaud and Levy, 2003). Several attempts to analyze the function of SNAREs in membrane fusion with reconstitution methods have been reported (Rizo, 2003), but different reconstitution experiments yielded completely different results. Some reconstitution assays showed that SNAREs are sufficient to mediate fusion (Weber *et al.*, 1998; Parlati *et al.*, 1999; Schuette *et al.*, 2004), whereas SNAREs failed to mediated fusion in other reconstitution systems (Hu *et al.*, 2002; Kweon *et al.*, 2003; Chen *et al.*, 2004). Thus, a reliable reconstitution system is in dire need to clarify the confusion and finally address whether SNARE can mediate membrane fusion.

To this end, I reconstituted SNAREs with a well-studied reconstitution procedure, which has been successfully used to reconstitute several prototypic energy-transducing membrane proteins (Paternostre *et al.*, 1988; Rigaud *et al.*, 1988; Richard *et al.*, 1990; Levy *et al.*, 1990a; Levy *et al.*, 1990b; Levy *et al.*, 1990c; Levy *et al.*, 1992; Yu *et al.*, 1993; Hao *et al.*, 1994). The proteoliposomes containing t-SNAREs and v-SNAREs were carefully characterized to ensure the proper incorporation of SNAREs and minimize artificial fusion (see details in chapter 6). Fusion between t-SNARE proteoliposomes and v-SNARE proteoliposomes was then monitored with a standard lipid mixing assay (Struck *et al.*, 1981). Little fusion was observed between t-SNARE liposomes and v-SNARE liposomes after two hours at 37^{o}C, suggesting that the SNAREs alone are not sufficient to mediate membrane fusion (see details in chapter 6).

CHAPTER 2 RESONANCE ASSIGNMENTS OF THE CORE COMPLEX INVOLVED IN SYNAPTIC VESICLE FUSION

2.1 Introduction

As discussed in the first chapter, the SNAREs play a central role in neurotransmitter release. However, whether the SNARE complex assembly precedes or causes membrane fusion is still under debate and how the SNAREs cooperate with other important players to achieve the high speed and tight regulation of the fusion process is still unclear. To unravel these mechanisms, it is critical to understand the dynamics and energetics of the SNARE complex formation, as well as interactions between the core complex and the other molecules that are involved in neurotransmitter release.

Nuclear magnetic resonance (NMR) is a powerful analytical technique to study molecular dynamics, energetics and interactions. NMR measures the response of nuclear spins to an applied sequence of radio-frequency pulses in a large homogeneous magnetic field (Wüthrich, 1986). The signal decays exponentially with a characteristic time constant, the transverse relaxation time, T_2, which is tightly associated with molecular size and molecular motion (Figure 2.1a and 2.1b). The core complex in this study contains the minimal sequences of syntaxin, synaptobrevin and SNAP-25 involved in the SNARE complex (Sutton *et al.*, 1998), with the exception that the syntaxin fragment was truncated at residue 253. The molecular weight of the core complex is about 32 KDa, which is the upper

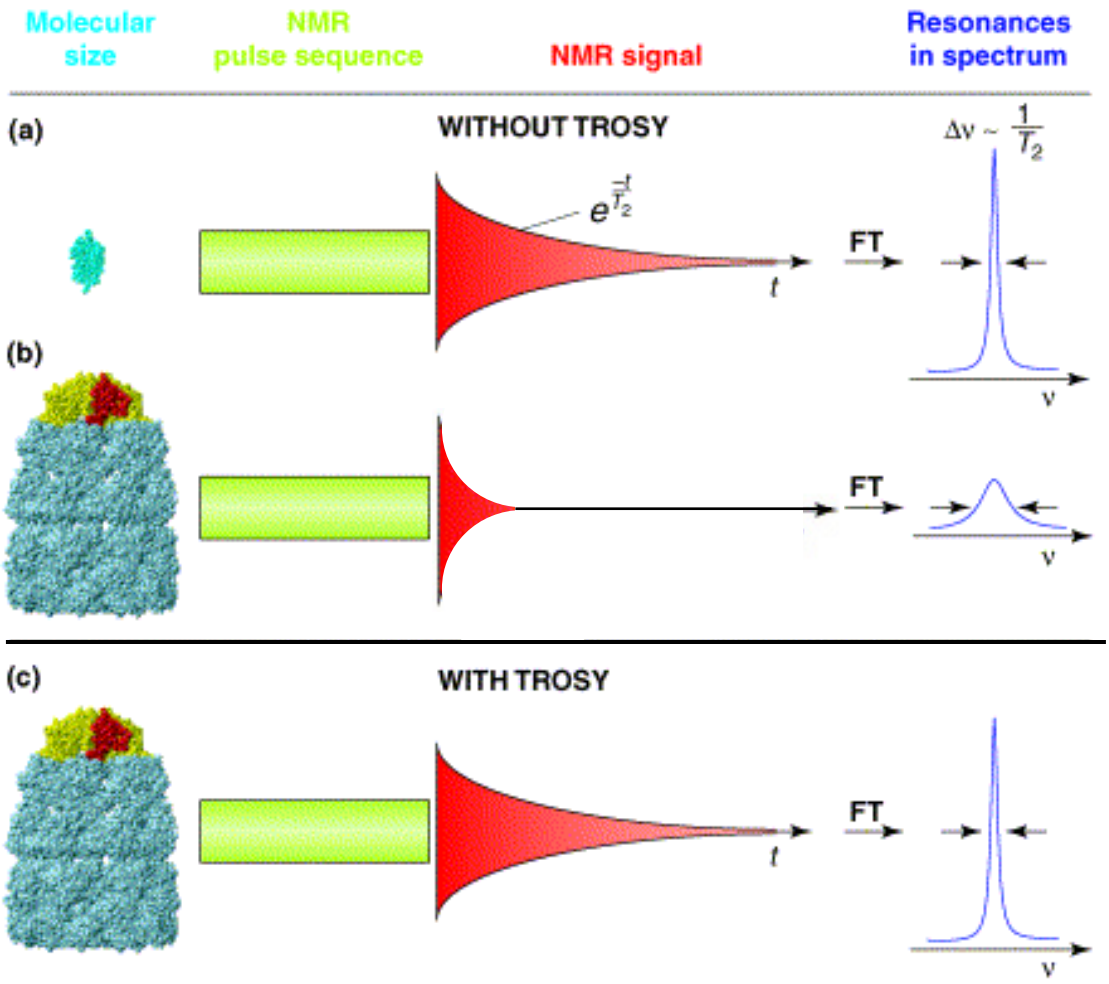

Figure 2.1 NMR spectroscopy with small and large molecules in solution. (a) Small molecules tumble fast in solution, resulting in slow relaxation of the NMR signals and long transverse relaxation time (T_2). The NMR spectrum after Fourier transformation (FT) reveals sharp NMR peaks with narrow line widths ($\Delta\nu$). (b) Large molecules tumble slowly in solution, so the NMR signals relax faster. This results in weaker signals and broader lines. (c) TROSY-based NMR substantially reduces the transverse relaxation of large molecules, and subsequently improves the spectral resolution and sensitivity (Fernandez and wider, 2003).

limit for conventional NMR spectroscopy (Clore and Gronenborn, 1994). In addition, the core complex assumes an elongated cylindrical structure, which leads to an even slower tumbling rate and shorter relaxation time than expected for its molecular mass. The NMR experiments of such a large molecule suffering from the fast relaxation of the NMR signal usually yield poor spectra with broadened resonance lines and low sensitivity (Figure 2.1a and 2.1b).

To overcome these difficulties, I took advantage of the recent development of transverse-relaxation optimized spectroscopy (TROSY) (Pervushin *et al.*, 1997; Fernandez and Wider, 2003). There are two main relaxation mechanisms for diamagnetic macromolecules: one depends on the dipole-dipole interaction (DD) and the other depends on the chemical shift anisotropy (CSA). The two mechanisms interfere with each other, and in certain situations they can cancel each other. The ^{1}H nuclei of amide groups have a scalar coupling with the corresponding ^{15}N nucleus, and the NMR signals split into two components. Each component has different line widths because of the relaxation interference (Figure 2.2b). Conventional NMR experiments combine the two components by a technique called ‘decoupling’, at the expense of averaging the relaxation rates (Figure 2.2a). However, the TROSY–based NMR technique exclusively selects the component with slow relaxation rate and eliminates the fast relaxing component (Figure 2.2c). At first glance, the TROSY technique seems to waste half of the signal, but in the case of large molecules, slower relaxation readily compensates for the loss of signal and improves the spectral sensitivity substantially (compare Figure 2.1b and 2.1c; Pervushin *et al.*, 1997). The residual line width

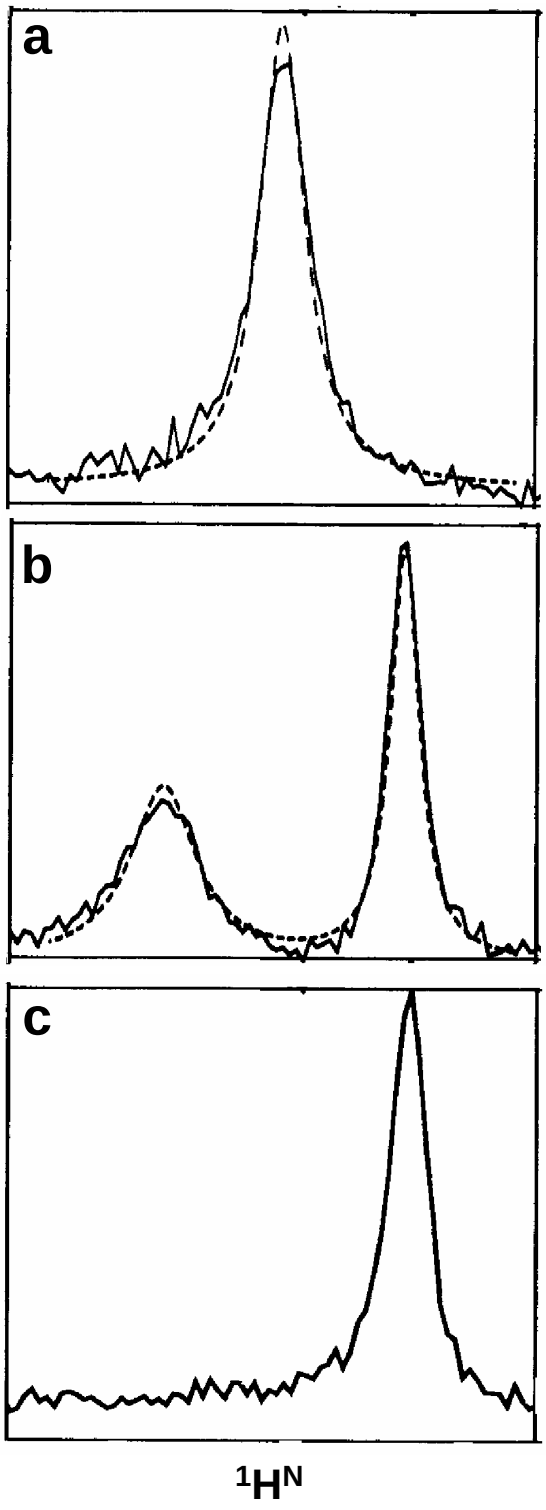

Figure 2.2 Impact of TROSY on NMR signals of an amide proton. NMR signals of an amide proton with (a) traditional NMR technique, (b) without “decoupling” of the scalar coupling between ^1H nuclei and ^{15}N nuclei, (c) with TROSY technique, which selectively keeps the NMR signal with slow relaxation rate.

in Figure 2.2c is almost entirely due to DD interactions with remote hydrogen atoms in the protein, and can thus be efficiently suppressed by deuterium labeling (Grzesiek and Bax, 1993; Yamazaki *et al.*, 1994a; Yamazaki *et al.*, 1994b; Farmer and Venters, 1995; Nietlispach *et al.*, 1996). In addition, The DD interaction is independent of the static magnetic field, whereas the CSA increases with higher magnetic fields. Thus, the TROSY effect can be further optimized by selecting the appropriate magnetic field strength.

With TROSY-based NMR techniques in combination with perdeuteration, I was able to acquire high quality NMR spectra of the core complex at 600 MHz. As a first step towards any NMR studies of the core complex, I assigned the backbone resonances of the core complex using two types of information, through bond connectivities (from triple resonance experiments) and through space connectivities (from nuclear Overhauser effect experiments).

2.2 Material and Methods

2.2.1 Recombinant Protein Preparation

DNA constructs encoding GST fusion proteins of the SNARE motifs of rat synaptobrevin 2 (residues 29-93, hereafter abbreviated Syb2), rat syntaxin 1A (191-253, abbreviated SyxS) and human SNAP-25 (residues 11-82 and 141-203, both containing an additional TRP residue at the C terminus to facilitate detection; abbreviated SNN and SNC respectively) were prepared using custom-designed primers and standard PCR cloning techniques, and subcloned into the pGEX-KT expression vector by Kovrigin E., a former postdoctoral fellow

in our laboratory. Each plasmid was transformed into *Escherichia coli* BL21(DE3) cells for protein expression. Glycerol stocks (8% glycerol) of the transformed cells were kept at -80^{o}C.

For a routine one liter bacteria culture, 50 ml LB media was inoculated with a single colony from an agar/ampicillin plate and incubated in a shaker at 250 rpm overnight at 37^{o}C. The next day, proper amount of culture (usually 10-20 ml) was transferred to 1liter LB media to make sure that the starting OD_{600} is around 0.1. All media contained 50 ug/ml ampicillin. The flask was incubated at 37^{o}C and shaken at 250 rpm till OD_{600} reached 0.6-0.8, then the temperature was lowered to 25^{o}C and 0.4 mM IPTG (isopropyl β-D-thiogalactopyranoside, from Sigma) was added to induce protein expression for 17-18 hours. The cells were harvested by centrifugation at 4000 rpm for 30 min in swing buckets with a rotor JS 4.2 (Model J6-MI centrifuge, Beckman Instruments) and resuspended into 35ml PBS buffer (10mM Phosphate, 2.7mM KCl and 137mM NaCl, pH7.4) containing 2 mM EDTA, 5 mM EGTA, 0.5 mM ABESF and 10 *u*l/ml sigma inhibitor cocktail (Sigma). The cell suspension was frozen with liquid nitrogen and stored in -80^{o}C for further protein purification.

Whenever isotope labeling was necessary, M9 minimal media were used instead of LB media. 1 liter M9 media contains: 6.8 g Na_2HPO_4, 3.0 g KH_2PO_4, 0.5 g NaCl, 1.0 g NH_4Cl, 2.0 mM $MgSO_4$, 100 *u*M $CaCl_2$, and 4.0 g D-(+)-glucose. Uniform ^{15}N labeling was achieved by using M9 minimal media prepared with $^{15}NH_4Cl$ instead of the normal NH_4Cl. Uniform ^{13}C labeling was achieved by replacing unlabeled glucose with $^{13}C_6$-D-glucose, and 3.0 g $^{13}C_6$-D-glucose was used instead of 4.0 g because of the high cost of the $^{13}C_6$-glucose.

Perdeuteration was achieved by growing bacteria using D_2O as the solvent. A combination of these labeling schemes yielded double or triple isotope labeled proteins (i.e. ^{2}H, ^{15}N labeled proteins or ^{2}H, ^{15}N, ^{13}C labeled proteins).

The frozen cells from 1 liter culture were thawed and passed through a high pressure homogenizer (Model EmulsiFlex-C5, Avestin Inc.) for 3 to 4 times. The cell debris was spun down by centrifugation at 18,000 rpm for 30 min in a JA-20 rotor with the Beckman centrifuge (model J2-21). The supernatant was filtered with 0.45 *u*M syringe filter (Nalgene) and mixed with 1.0-1.5 ml slurry of the cleaned glutathione Sepharose 4B (Amersham Pharmacia Biotech.) at 4°C overnight. GST fusion proteins were bound tightly to the glutathione beads, whereas unbound proteins and non-specifically bound proteins were removed by washing sequentially with 20 ml PBS (1% triton X-100), 20 ml PBS (1M NaCl) and 20 ml PBS for three to five times. In the cases of the purification of Syb2 and SNN, a benzonase (0.25 units/*u*l) treatment was used to remove DNA followed by extensively washing with PBS. The resin was then washed with 3 ml thrombin cleavage buffer (50 mM Tris, pH 8.0, 200 mM NaCl and 2.5mM $CaCl_2$) for three times. A treatment with 5-7 units/ml thrombin (from bovine plasma, sigma) at room temperature was followed to remove the GST tag and release the proteins with N-terminal extra two residues (GS) from the construct. The proteins were eluted with corresponding elution buffers (table 2.1) and further purified by gel filtration through a Superdex-75 Hiload 16/60 column (Amersham Pharmacia Biotech.). The purity of the preparation was assessed by SDS-PAGE and Coomassie blue staining. The typical yield according to the UV_{280nm} measurement was 3-5 mg per liter of culture.

	Elution buffer
Syb2	20 mM Sodium Phosphate buffer pH7.4, 200 mM Sodium Chloride
SyxS	50 mM Tris buffer pH8.0, 150 mM Sodium Chloride
SNN	20 mM Sodium Phosphate buffer pH8.0, 150 mM Sodium Chloride
SNC	20 mM Sodium Phosphate buffer pH7.4, 200 mM Sodium Chloride

Table 2.1 Elution buffer for each SNARE motif

2.2.2 NMR Sample Preparation

NMR signals of large molecules with molecular masses greater than 20 KDa are highly overlapped. Taking advantage that the core complex (32 KDa) was assembled with four individually expressed and purified SNARE fragments, I prepared four NMR samples with only one SNARE motif ^{2}H, ^{15}N and ^{13}C labeled in each sample (table 2.2). Thus, I was able to observe one SNARE motif at one time in NMR experiments, which decreased the number of the observable resonance fourfold and dramatically relieved the signal-overlap problem. In sample 1 and sample 2, the SNARE motifs that are neighboring to the triple labeled SNARE motifs, according to the crystal structure of the core complex (Sutton *et al.*, 1998), were deuterium labeled to reduce the DD relaxation and improve the spectral sensitivity (table 2.2).

	Syb2	SyxS	SNN	SNC
Sample 1	^{2}H, ^{15}N, ^{13}C	^{2}H	--	^{2}H
Sample 2	^{2}H	^{2}H, ^{15}N, ^{13}C	^{2}H	--
Sample 3	--	--	^{2}H, ^{15}N, ^{13}C	--
Sample 4	--	--	--	^{2}H, ^{15}N, ^{13}C

Table 2.2 Isotope labeling scheme for the NMR samples.

The high stability of the core complex enabled facile preparation by simply mixing the purified isotope labeled SNARE motif with 1.2 equivalents of each of the other three purified unlabeled SNARE motifs, followed by an overnight incubation at 4^{o}C. The formed core complex is SDS-resistant, thus the formation of the core complex was checked with SDS-PAGE. The small amount of unassembled fragments was removed by extensive concentration/dilution with a Millipore concentrator (10 KDa cutoff). The final concentration of the core complexes was about 300 *u*M according to UV_{280}, and the buffer condition for NMR experiments was 20 mM Tris pH 7.4 and 250 mM NaCl.

2.2.3 NMR Spectroscopy

All NMR experiments were performed at 32^{o}C on Varian INOVA600 spectrometers. For each sample, I acquired and analyzed one-dimensional (1D) spectra, TROSY-based heteronuclear single quantum coherence (HSQC) spectra, three-dimensional (3D) TROSY-based HNCA and HN(CO)CA spectra and ^{1}H-^{15}N nuclear Overhauser effect spectroscopy-HSQC (NOESY-HSQC) spectra. The acquisition time for each 3D experiment was about 3 days. Minimal spectral widths in the nitrogen dimension were used to increase the spectral

resolution during the same total acquisition time (table 2.3). All NMR were processed with the program NMRPipe (Delaglio *et al.*, 1995) and analyzed with the program NMRView (Johnson and Blevins, 1994).

NMR samples	Syb2 m2cc	SyxS m2cc	SNN m2cc	SNC m2cc
^{15}N Spectral width (Hz)	1250.0	1027.0	1348.8	1045.0

Table 2.3 Spectral widths in nitrogen dimension for each NMR sample. 'M2cc' stands for the mini-minimal core complex. The syntaxin, synaptobrevin and SNAP-25 fragments correspond to the minimal sequences involved in the SNARE complex (Sutton *et al.*, 1998), and in addition, the syntaxin fragment is C-terminally truncated at residue 253. The NMR samples are named based on the ^{15}N and ^{13}C labeled SNARE motif in each sample. For instance, the sample Syb2 m2cc is the mini-minimal core complex containing ^{2}H, ^{15}N and ^{13}C labeled Syb2.

2.2.4 Thermal Denaturation

Thermal denaturation curves were recorded on an Aviv model 62DS spectropolarimeter using a 1 mm path length cell monitoring the CD absorption at 222 nm. The core complex sample for thermal denaturation was about 3 *u*M in 20 mM sodium phosphate buffer (pH7.5) containing 150mM NaCl. The fraction of unfolded protein at each temperature was calculated by using the formula $(I_{obs} - I_f)/(I_u - I_f)$, where I_{obs} is the observed signal intensity, and I_u and I_f are the signal intensities of the unfolded and folded states, respectively. I_u and I_f

as a function of temperature were calculated by extrapolation of the linear regions at the extremes of the unfolding curves.

2.3 Results

2.3.1 Purification of the SNARE Motifs and Assembly of the Core Complex

The top panels of Figure 2.3 show the gel filtration profiles of the SNARE motifs through the Superdex-75 Hiload 16/60 column (Amersham Pharmacia Biotech.). SyxS eluted with an apparent molecular weight of 30 KDa (Figure 2.3a), which is consistent with the observation that the SNARE motif of syntaxin forms homotetramers in solution (Misura *et al.*, 2001b). The SNARE motifs of SNAP25 and synaptobrevin also eluted earlier than globular proteins with similar molecular weight (Figure 2.3b, 2.3c and 2.3d), because they do not have tertiary structure (Fasshauer *et al.*, 1997b).

The SNARE motifs of syntaxin, synaptobrevin and SNAP25 that I prepared correspond to the minimal sequences involved in the SNARE complex (Sutton *et al.*, 1998) except that the syntaxin SNARE motif was truncated at residue 253. The deletion of five residues at the C terminus of the syntaxin SNARE motif dramatically reduces the aggregation of the SNARE complex (Margittai *et al.*, 2001) and facilitates the NMR study of the core complex. In addition, the truncation does not affect the assembly and stability of the core complex. Stoichiometric amounts of the SNARE motifs assembled almost quantitatively into a SDS-resistant complex (Figure 2.3E) and thermal melting experiments monitored by

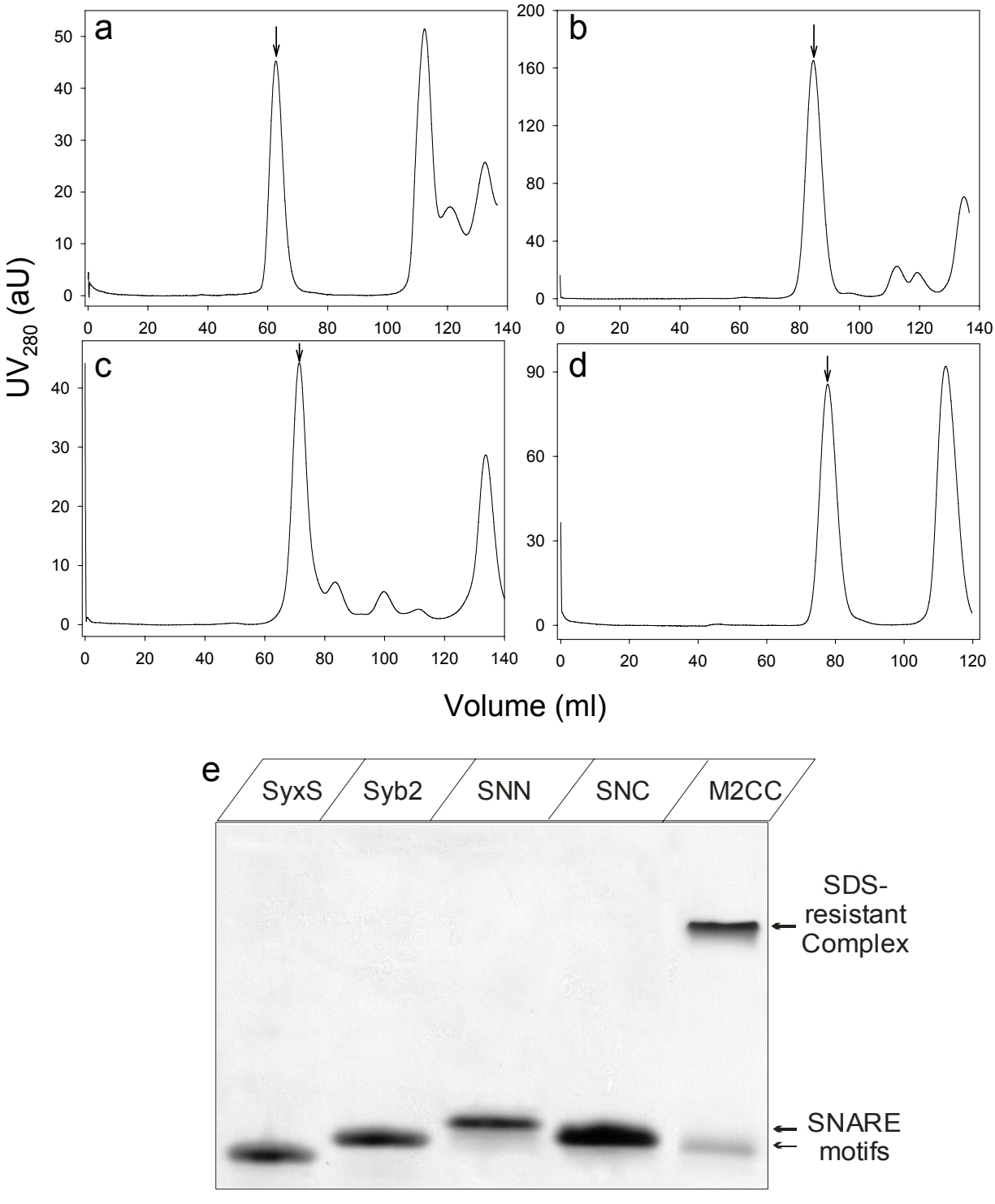
a
b
c
d
UV280 (aU)
Volume (ml)
e
SyxS
Syb2
SNN
SNC
M2CC
SDS-resistant Complex
SNARE motifs

Figure 2.3

Figure 2.3 Purification of the SNARE motifs. Elution profiles of (a) SyxS, (b) Syb2, (c) SNN, (d) SNC through a Superdex-75 column. The peaks indicated with arrows were the corresponding SNARE proteins. The peaks on the right side are the protein inhibitors added before sample injection. (e) The purified SNAREs and the assembled core complex were analyzed by SDS-PAGE followed by Coomassie blue staining.

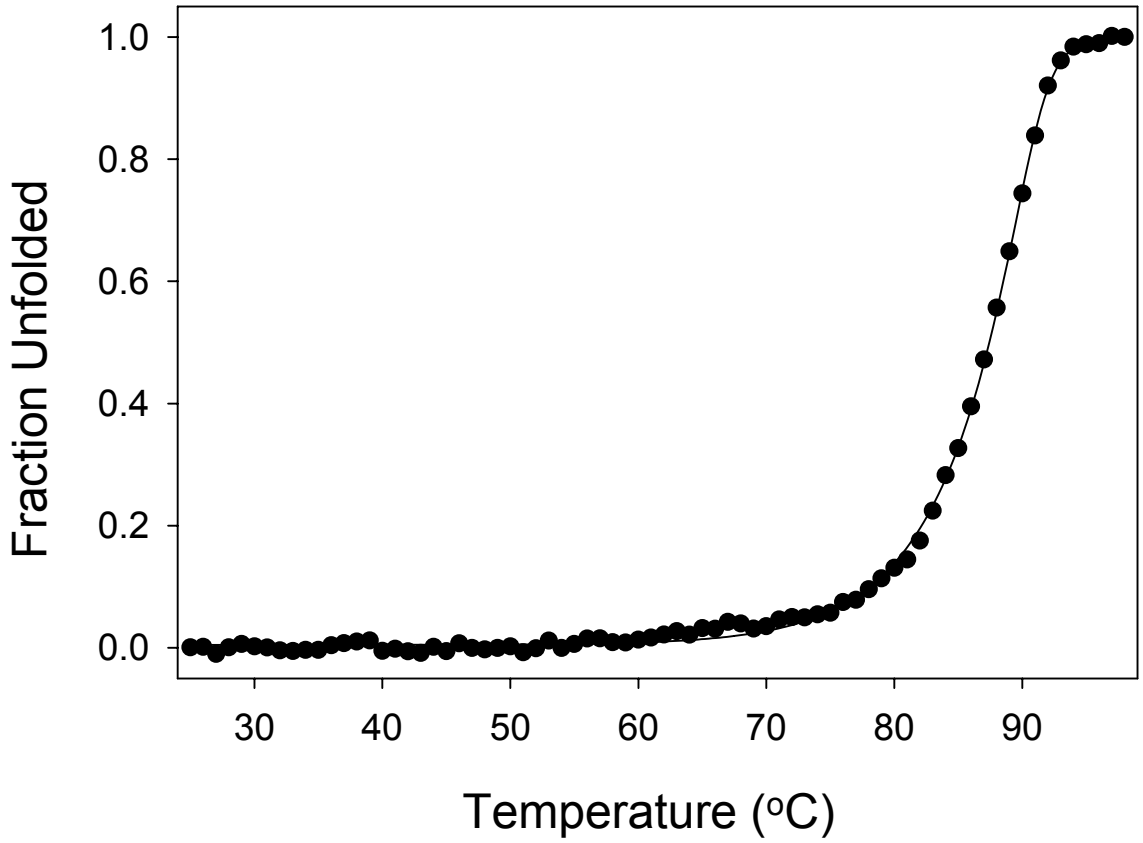

Figure 2.4 Thermal denaturation curve of the core complex. Denaturation as a function of temperature was monitored by the decrease in the CD absorbance at 222 nm. The curves were normalized after subtracting the linear temperature dependence of the absorbance of the assembled and disassembled states derived from the extremes of the denaturation curves.

circular dichroism showed that this complex denatures at about 90 ^{o}C (Figure 2.4), similar to the non-truncated minimal SNARE complex (Fasshauer *et al.*, 2002).

2.3.2 One Dimensional NMR

Figure 2.5 is a typical 1D ^{1}H NMR spectrum of the core complex. The intensity and line-shape of the methyl group in 1D spectrum is very informative. The intensity of the strongest methyl resonance (SMR) of the core complex is observed at 0.8-0.9, and its intensity usually increases linearly with the concentration of the sample (Arac *et al.*, 2003). However, if the sample aggregates, the line width of the methyl group will increase and the intensity of the SMR will decrease with molecular mass. Thus, 1D NMR spectroscopy was used to verify the concentration of the core complex and I also compared the line widths of the well-isolated methyl resonances (indicated by arrows in Figure 2.5), as well as the quality of the TROSY-HSQC spectra of the samples containing different amount of the core complex to characterize the aggregation state of the core complex. According to these studies, the maximum concentration that the core complex can reach without causing aggregation is about 300 *u*M. Thus, the core complex samples with a concentration of 300 *u*M were used for the two-dimensional and three-dimensional experiments.

2.3.3 Backbone Assignments of the SNARE Motifs in the Core Complex

The assignments were obtained mainly by using three-dimensional (3D) TROSY-based HNCA and HN(CO)CA experiments. The HNCA experiment correlates the amide H(*i*) and N(*i*) frequencies with both the intra-residues Cα(*i*) and the sequential Cα(*i*-1) due to the

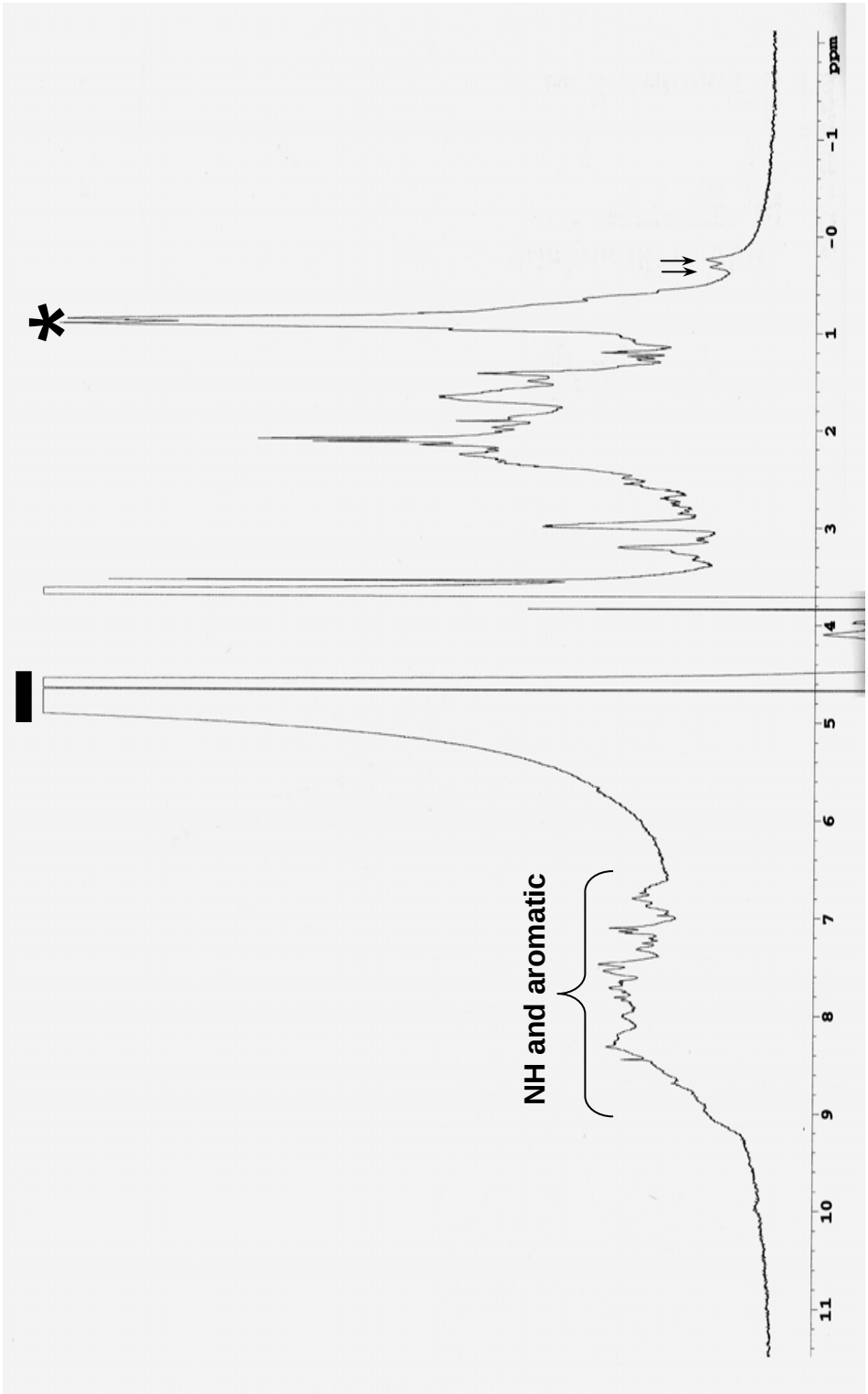

Figure 2.5

Figure 2.5 1D NMR spectrum of the core complex. The spectrum was acquired using a 300 *u*M sample at pH 7.5 and 32 ^{o}C with 250 mM $NaCl_2$. The signals under bracket are mainly from amide and aromatic protons. The peak indicated by an asterisk is the strongest methyl resonance (SMR) signal. The intensity of the SMR was used to estimate the protein concentration. The arrows indicate two well-isolated methyl resonances, whose line widths indicate the aggregation state of the core complex sample. The tall peak in the middle of the spectrum indicated by a black bar is the water signal after incomplete water suppression.

similar sizes of the one bond J_{NCa} coupling constant (-11 Hz) and the two bond J_{NCa} coupling constant (7 Hz), whereas the HN(CO)CA experiment provides only inter-residue connectivity, that is, the correlation of the amide H(*i*) and N(*i*) frequencies with the Cα(*i*-1) via the carbonyl resonance (Figure 2.6). Therefore, backbone assignments were generally obtained from the Cα to Cα(*i*-1) connections. Sequential HN/HN nuclear Overhauser effect (NOE) connectivities were used to confirm the assignments and resolve ambiguities. Traditional ^{1}H-^{15}N NOESY-HSQC experiment was applied here because little improvement was observed in the TROSY-based NOE experiment. Examples of the assignment procedure with strips from HNCA, HN(CO)CA and NOESY are shown in Figure 2.7. The assignments of the NH cross-peaks in ^{1}H-^{15}N TROSY-HSQC spectra of the Syb2, SyxS, SNN and SNC SNARE motifs within the core complex are shown in Figure 2.8. The backbone resonance assignments for the SNARE complex have been deposited in the BioMagResBank under accession number 6235.

HNCA

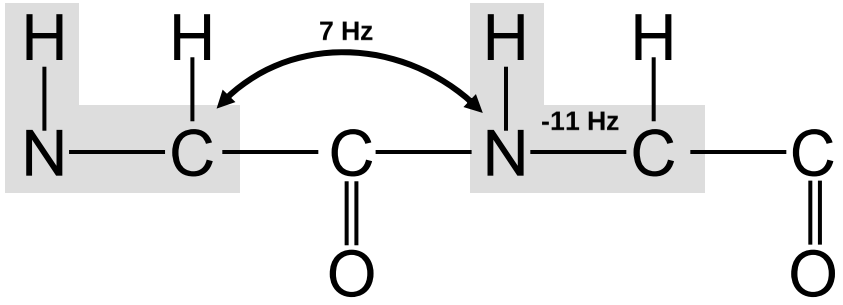

HNCOCA

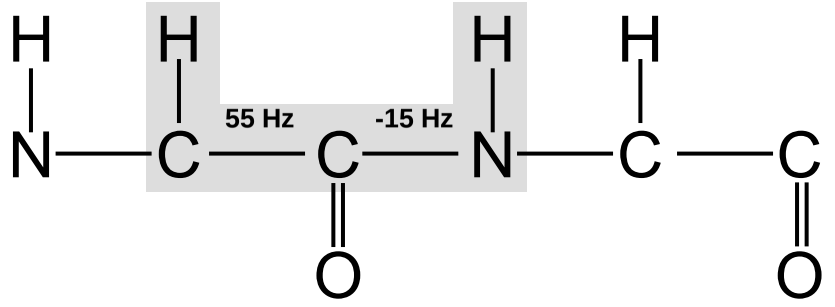

Figure 2.6 Schemes of HNCA and HNCOCA experiments. The nuclei correlated in each experiment are highlighted in grey and the coupling constants are indicated.

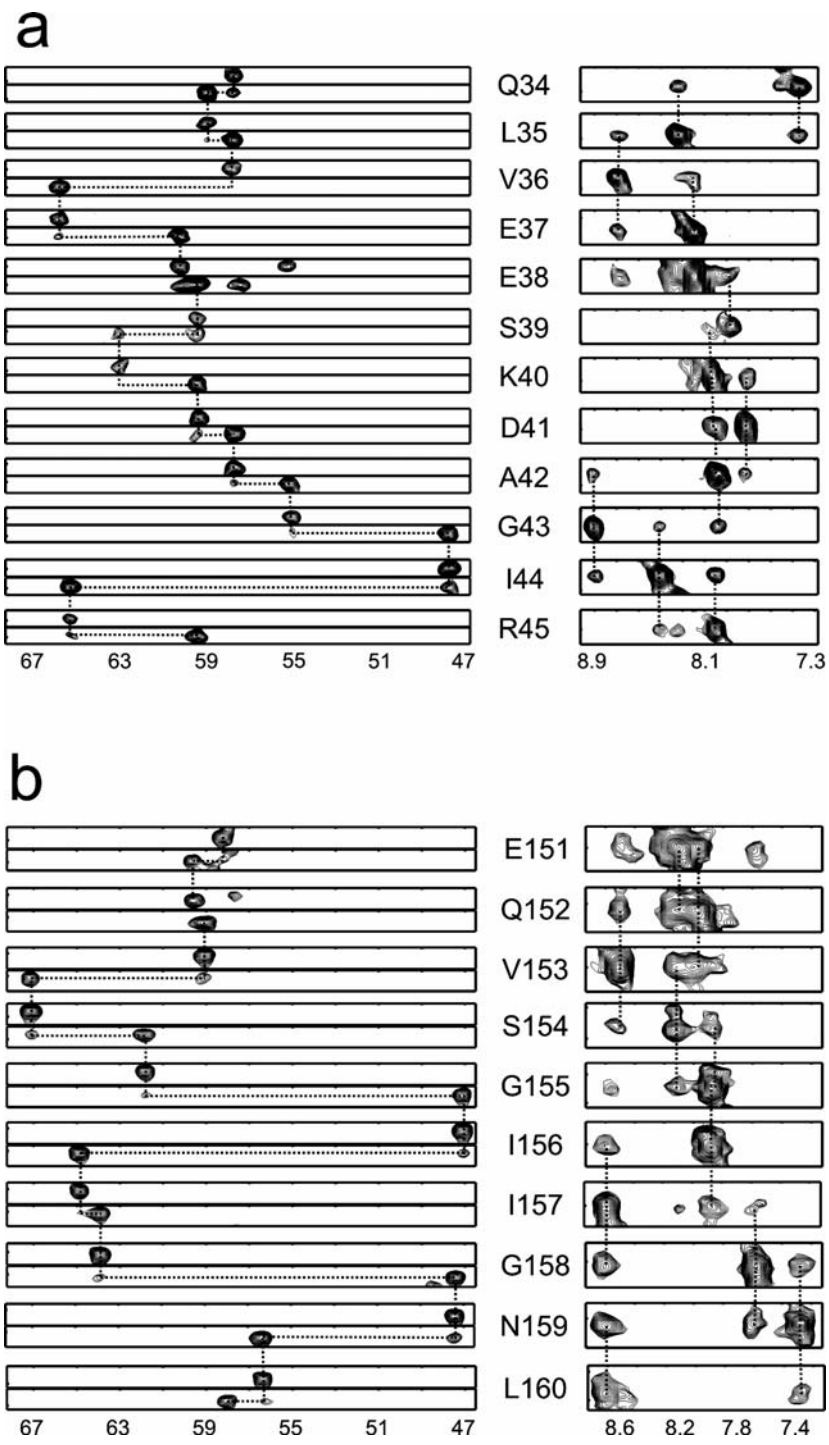
a
Q34
L35
V36
E37
E38
S39
K40
D41
A42
G43
I44
R45
67
63
59
55
51
47
8.9
8.1
7.3
b
E151
Q152
V153
S154
G155
I156
I157
G158
N159
L160
67
63
59
55
51
47
8.6
8.2
7.8
7.4

Figure 2.7

Figure 2.7 Strip plots illustrating the sequential assignments of the SNARE motifs within the core complex. The strips correspond to residues Gln34 to Arg45 of the SNN SNARE motif (a) and residues Glu151 to Leu160 of the SNC SNARE motif (b). For each residue, the left panel shows the TROSY-HNCOCA (top) and TROSY-HNCA (bottom) spectra, and the right panel shows the ^{1}H-^{15}N NOESY-HSQC spectrum. The sequential backbone assignments are indicated by dashed lines.

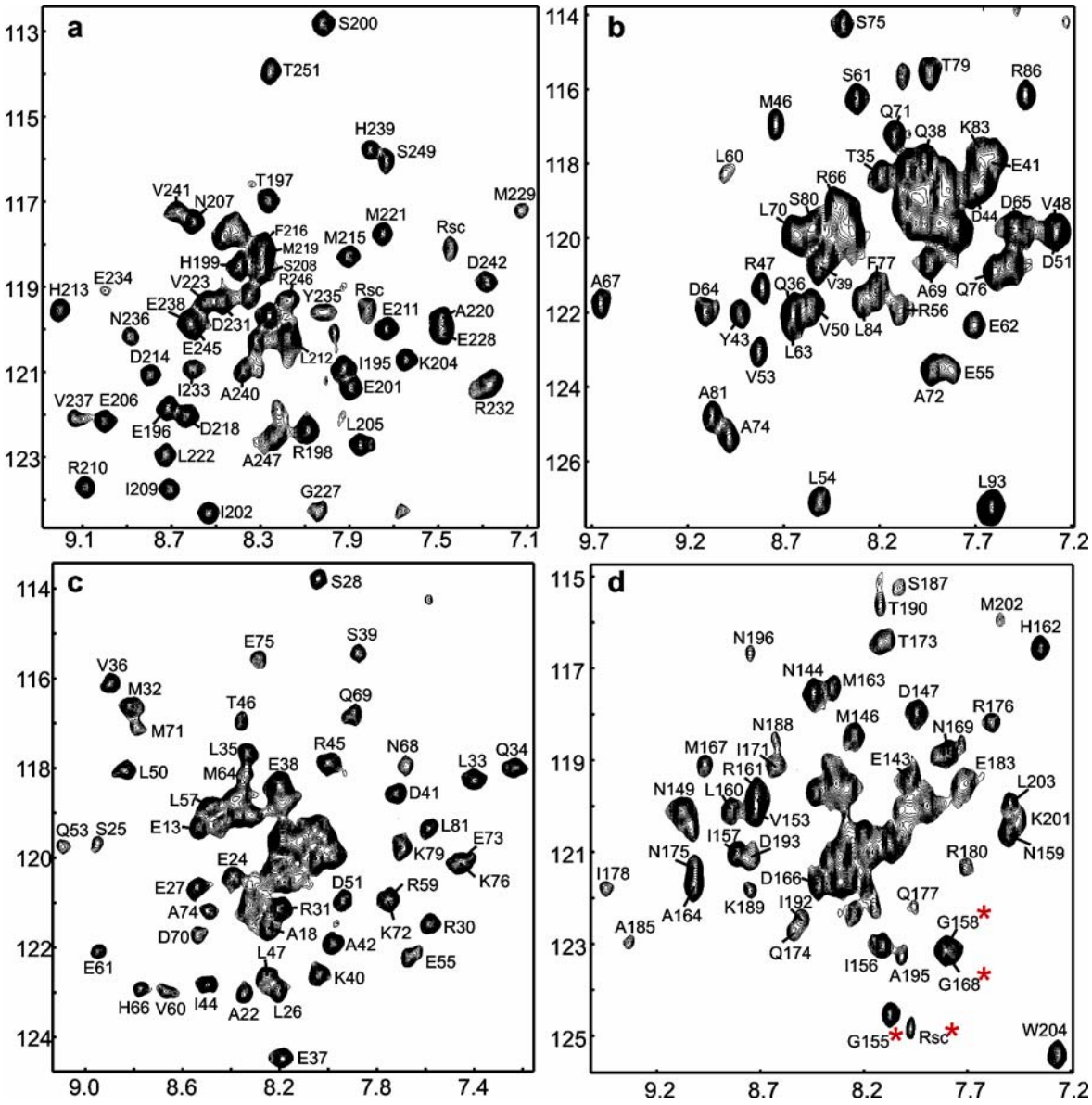
a
S200
T251
H239
S249
T197
V241
N207
M229
M221
F216
M219
M215
Rsc
H199
S208
D242
R246
H213
E234
V223
Y235
Rsc
E238
E211
A220
N236
D231
E228
E245
D214
L212
I195
K204
I233
A240
E201
V237
E206
R232
E196
D218
L205
L222
A247
R198
R210
I209
G227
I202
b
S75
T79
R86
S61
M46
Q71
Q38
K83
L60
T35
E41
R66
S80
L70
D65
V48
D44
R47
F77
D51
A67
D64
Q36
V39
A69
Q76
Y43
V50
L84
R56
E62
L63
V53
E55
A81
A72
A74
L54
L93
c
S28
E75
S39
V36
M32
T46
Q69
M71
L35
R45
N68
Q34
L50
M64
E38
L33
D41
L57
E13
L81
Q53
S25
E73
K79
E24
K76
E27
D51
R59
A74
R31
A18
K72
R30
D70
A42
E55
L47
E61
K40
H66
V60
I44
A22
L26
E37
d
S187
T190
M202
H162
N196
T173
N144
M163
D147
R176
M146
N169
N188
M167
I171
R161
E143
E183
N149
L160
L203
V153
K201
I157
D193
N175
R180
N159
I178
D166
Q177
K189
I192
A164
A185
G158
Q174
I156
A195
G168
G155
Rsc
W204

Figure 2.8

Figure 2.8 Assignment of the backbone resonances of the SNARE motifs in the core complex. Expansions of ^{1}H-^{15}N TROSY-HSQC spectra of the SNARE complex with the SyxS(a), Syb2(b), SNN(c) and SNC (d) SNARE motifs ^{2}H, ^{15}N-labeled, illustrating the assignments of selected cross-peaks, are shown. Arginine sidechain NH groups are indicated by 'Rsc'. Cross-peaks that are folded in the ^{15}N dimension are indicated by an asterisk (*).

CHAPTER 3 STRUCTURAL AND FUNCTIONAL ANALYSIS OF THE INTERACTION BETWEEN COMPLEXIN I AND THE SNARE COMPLEX

3.1 Introduction

The high speed and tight regulation of exocytosis are critical for neural function and rely on a cascade of protein-protein interactions (Südhof, 1995). Particularly interesting among these interactions are those involving the SNAREs and the core complex. The neuronal SNAREs include the synaptic vesicle protein synaptobrevin/VAMP, and the synaptic plasma membrane proteins syntaxin 1 and SNAP-25 (synaptosome-associated protein of 25 kDa). These proteins are characterized by sequences called SNARE motifs and form a highly stable complex, called the SNARE complex or the core complex (Sollner *et al.*, 1993a). Formation of the core complex brings the synaptic vesicle and plasma membranes together and has been proposed to cause membrane fusion (Hanson et al., 1997).

However, it is still under debate when assembly of the SNARE complex happens in the multi-step events that lead to Ca^{2+} triggered neurotransmitter release and how this process is regulated. To gain further insights, additional proteins that interact with the SNARE complex need to be studied. Complexins are evolutionarily conserved proteins that specifically bind to the core complex with a central helical region and may regulate the function of the core complex (McMahon *et al.*, 1995; Pabst *et al.*, 2000). Neurotransmitter release by the hypertonic sucrose treatment is normal in the CPXI and CPXII double

knockout mice, while the efficiency of the Ca^{2+} triggered neurotransmitter release decreased dramatically (Reim et al., 2001). This result implies that the complexins function at a late stage of exocytosis, perhaps close to the Ca^{2+} triggering step. On the other hand, the biochemical studies showed that the interaction between complexins and the core complex is Ca^{2+} independent (McMahon *et al.*, 1995; Pabst *et al.*, 2000).

To understand the molecular basis for these intriguing observations and unravel the function of complexin, I carried out a detailed structural and functional study of the interaction between complexin and the core complex using a combination of NMR spectroscopy and X-ray crystallography. Our results show that complexin binds in an antiparallel, α-helical conformation to the groove between the synaptobrevin and syntaxin SNARE motifs of the core complex. The binding does not cause any overall conformational change in the core complex except some slight sidechain re-orientations. Interestingly, the deuterium-exchange experiments suggested that complexin binding stabilizes the interface between the synaptobrevin and syntaxin SNARE motifs in the core complex. Since synaptobrevin resides in the synaptic vesicle membrane, whereas syntaxin is on the plasma membrane, this interface bears the strong repulsive forces of the two closely apposed membranes. Therefore, complexin may function as glue that seals the interface between the synaptobrevin and the syntaxin of the core complex to ensure efficient Ca^{2+}-triggered neurotransmitter release.

3.2 Material and Methods

3.2.1 Recombinant Protein Preparation

Rat complexin I (26-83) (abbreviated as Cpx26-83) was subcloned into the expression vector pGEX-KT for expression as a GST fusion protein by Kovrigin E., a former postdoctoral fellow in our laboratory. The plasmid was transformed into *Escherichia coli* BL21 (DE3) cells for protein expression. Glycerol stock (8% glycerol) of the transformed cells was kept in -80^{o}C.

The expression and purification procedures for Cpx26-83 were similar to those for the SNARE motifs as described in chapter 2, except that the Cpx26-83 after the cleavage of GST was eluted with 20 mM sodium acetate buffer (pH4.5), and the eluted Cpx26-83 was further purified by ion exchange chromatography (Figure 3.1a). Briefly, a linear gradient of salt (0 to 500 mM NaCl) was used to elute Cpx26-83 from the Source S column (Amersham Pharmacia Biotech.). Cpx26-83 eluted at 300 mM salt and the purity of the preparation was assessed by SDS-PAGE and Coomassie blue staining (Figure 3.1b).

For control experiments, a plasmid containing syntaxin 1A (188-259) (abbreviated Syx), was expressed and purified with exactly the same methods as those for purification of SyxS (see chapter 2).

3.2.2 Complexin/SNARE Complex Preparation

Assembly of the SNARE core complex followed the same procedure as described in the previous chapter. The complexin/SNARE complex was prepared by addition of 1.2

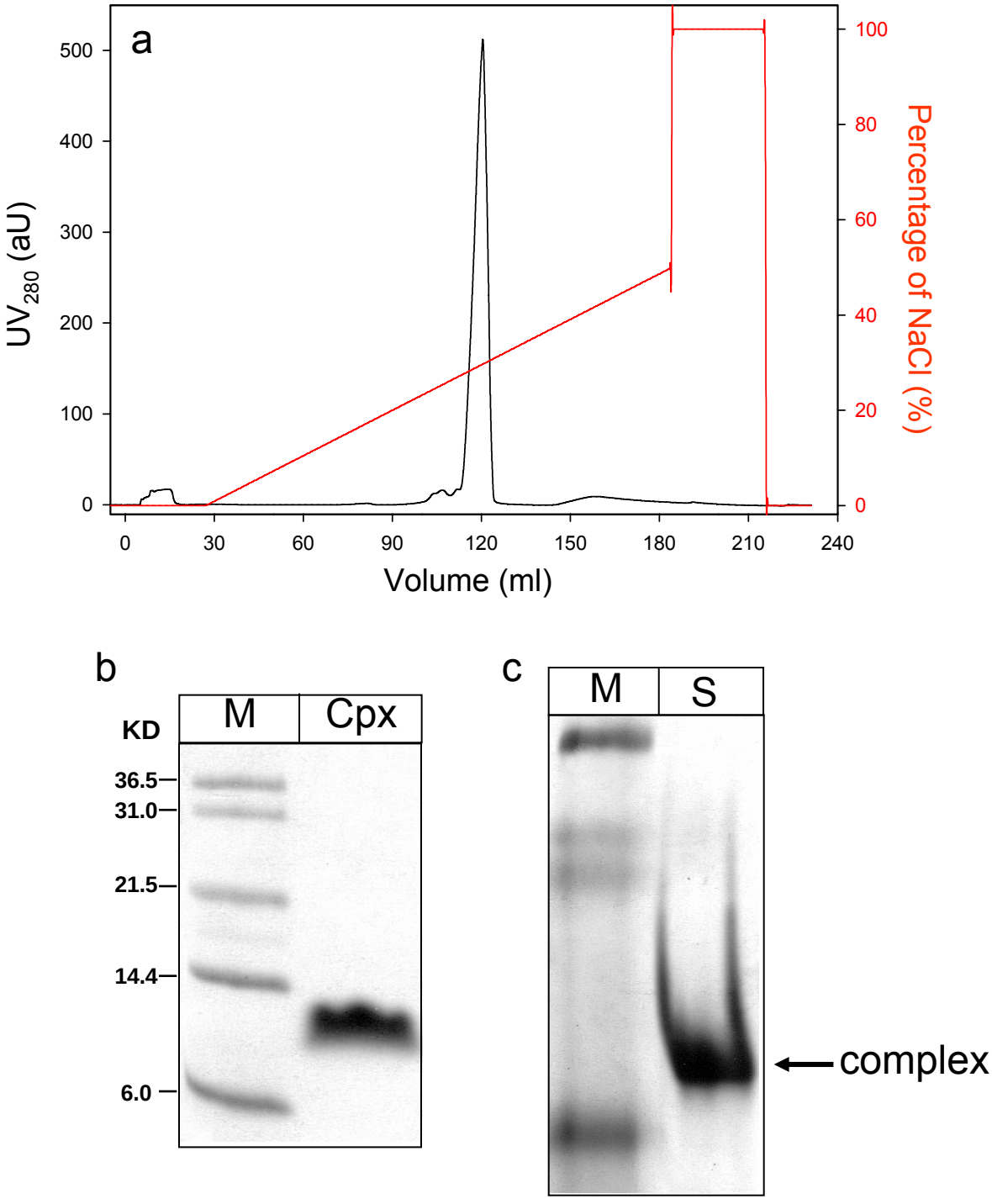
a
UV280 (aU)
Percentage of NaCl (%)
Volume (ml)
0
100
200
300
400
500
20
40
60
80
100
0
30
60
90
120
150
180
210
240
b
KD
M
Cpx
36.5
31.0
21.5
14.4
6.0
c
M
S
complex

Figure 3.1

Figure 3.1 Purification of Cpx26-83 and assembly of the complexin/SNARE complex. (a) Elution profiles of Cpx26-83 through a Source S column. (b) SDS-PAGE of the purified Cpx26-83. (c) Native gel of the assembled complexin/SNARE complex. M represents the molecular weight marker lane, and S represents the sample lane.

equivalents of Cpx26-83 to preassembled SNARE complex and incubated for 2 hours at 4^{o}C. An extensive concentration/dilution step with Millipore concentrator (10 KDa cutoff) was used to remove the small amount of unassembled fragments and at the same time change the sample buffer to final conditions. The purity of the complex was checked by native gel (Figure 3.1c).

3.2.3 NMR Spectroscopy

Samples for ^{1}H-^{15}N TROSY-HSQC spectra contained 100 *u*M SNARE complexes or 100 *u*M complexin/SNARE complexes in 20 mM Tris (pH7.4) buffer with 150 mM NaCl. The concentrations of samples for resonance assignments of Cpx26-83, SyxS and Syb2 in the complexin/SNARE complexes were between 170 and 300 *u*M and the buffer contained 20 mM Tris (pH7.4) and 250 mM NaCl. The core complex samples with or without complexin for hydrogen-deuterium (H/D) exchange experiments contained 100 *u*M complexes with ^{2}H, ^{15}N labeled Syb2. The samples were then diluted quickly into 20mM Tris (pH7.4) buffer with 150mM NaCl in D_2O solvent and concentrated immediately with Millipore concentrator (10 KDa cutoff). All NMR experiments were performed on Varian INOVA500 or INOVA600 at 32^{o}C, except that H/D exchange experiments were performed at 30^{o}C. The backbone assignments of the complexin/SNARE complexes were obtained with essentially the same methods as described in chapter 2.

3.2.4 Complexin/SNARE Complex Crystallization

The complexin/SNARE complex was concentrated to 10 mg/ml in 20 mM Tris buffer (pH7.5), and 130 mM NaCl and stored in small aliquots at -80 ^{o}C. The crystallographic studies of the complexin/SNARE complex were performed in collaboration with Dr. Tomchick and Dr. Machius of the Structural Biology Laboratory in UT Southwestern Medical Center. Crystals of the complex were obtained by vapor diffusion technique. Briefly, a hanging drop containing protein, stabilizing buffers, precipitant and crystallization aids, is allowed to equilibrate in a closed system with a much larger reservoir which contains the same chemicals but the protein. Because the salt concentration in the reservoir is higher than that in the hanging drop, water evaporates from the drop and consequently the protein concentration increases gradually, which leads to the formation of protein crystals in certain buffer conditions. Initial crystals were obtained with 30% (v/v) iso-propanol, 100 mM Hepes (pH7.5) and 200 mM Magnesium chloride in the reservoir solution. The crystallization conditions were further optimized to 35% (v/v) iso-propanol, 100 mM Hepes (pH7.5) and 200 mM Magnesium chloride, where tiny trigonal bipyramidal crystals grew spontaneously at 4^{o}C after overnight pre-incubation at room temperature. Streak seeding was used to increase the size of the crystals. In streak seeding experiments, a whisker was used to gently touch a crystal. Crystal seeds attached to the whisker and were quickly transferred to equilibrated drops containing 27% (v/v) iso-propanol, 100 mM Hepes (pH7.5) and 200 mM Magnesium chloride in the reservoir. Enough seeds remained on the whisker to seed 6 drops. Diffraction quality crystals were obtained after incubation at 4^{o}C (Figure 3.2). Crystals were transferred to fresh reservoir solution at 4^{o}C containing 20% glycerol as cryoprotectant and flash cooled in liquid propane, then stored in liquid nitrogen until used for data collection.

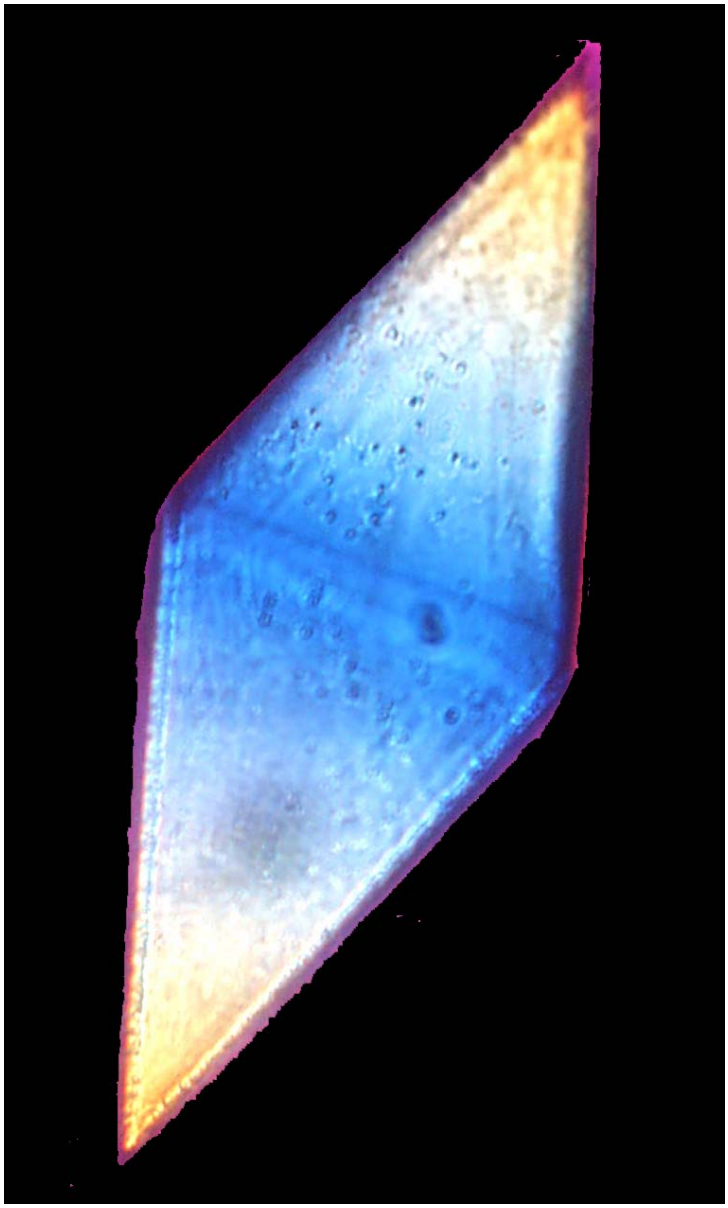

Figure 3.2 Crystallization of the complexin/SNARE complex. Trigonal bipyramidal crystals were obtained by streak seeding in the equilibrated hanging drop containing 27% (v/v) iso-propanol, 100mM Hepes (pH7.5) and 200 mM Magnesium chloride.

3.2.5 Data Collection

Dr. Tomchick helped me to collect and process the diffraction data. The initial diffraction data were collected to a Bragg spacing (d_{min}) of 3.4 Å with a 20 *u*m single crystal at 110K using an R axis IV imaging plate system (MSC, Houston, TX) mounted on a Rigaku RU-200 rotating anode (CuKα) (Rigaku, Japan) operated at 100 mA and 50 kV. These data were used for the initial structure solution. Subsequently, a complete data set was collected to a d_{min} of 2.5 Å from a 200 *u*m single crystal, obtained by streak seeding at 100K at the Structural Biology Center 19-1D beamline of the Advanced Photon Source with the use of the SBC 2 CCD detector (Naday et al., 1998). This crystal displayed anisotropic diffraction and exhibited the symmetry of space group $P2_12_12_1$ with unit cell parameters of a=40.49 Å, b=60.42 Å, and c=159.79 Å. There was one complex per asymmetric unit. All data were processed and scaled in the HKL2000 program suit (Otwinowski and Minor, 1997). Intensities were converted to structure factor amplitudes and placed on an approximate absolute scale by the program TRUNCATE from the CCP4 package (French and Wilson, 1978; Bailey, 1994). The Wilson B value calculated for the observed data between a d_{min} of 4.0 and 2.5 Å was 53 $Å^2$. Data collection and processing statistics are summarized in Table 3.1.

3.2.6 Crystallographic Structure Solution and Refinement

The crystal structure of the complexin/SNARE complex was solved via molecular replacement using the program AMORE (Navaza, 1994). Initial model coordinates were obtained by modifying the coordinates of the SNARE complex (PDB code 1sfc; Sutton et al.,

1998) to remove the extra residues that were not included in my constructs. A single solution of the rotation and translation function was obtained by searching between a d_{min} of 8.0 and 4.0 Å, and the final correlation coefficient was 0.39. Rigid-body refinement of the coordinates from this solution versus data between a d_{min} of 20.0 and 3.4 Å was conducted in the program package CNS 1.0 (Brunger *et al.*, 1998) with a random 5% subset of all data set aside for an R_{free} factor calculation. The resulting electron density map was examined with the program O (Jones et al., 1991). Extra density was observed at the C-terminal end of the core complex assuming a clearly α-helical conformation, but the side chain density was too weak to determine the correct orientation of the complexin helix. Subsequent rigid body refinement of the coordinates versus the synchrotron data between a d_{min} of 20.0 and 2.5 Å yielded interpretable electron density for the complexin helix in terms of orientation and sequence.

3.3 Results

3.3.1 NMR Analysis of the Complexin/SNARE Complex

The ^{1}H-^{15}N TROSY-based HSQC experiment is a powerful method to study protein-protein interactions. Similar as the ^{1}H-^{15}N HSQC experiment, each cross-peak in a ^{1}H-^{15}N TROSY-based HSQC spectrum corresponds to one NH group for each nonproline residue in a ^{2}H, ^{15}N labeled protein. The binding of an unlabeled component changes the chemical environment of the NH groups that are near the binding sites of the labeled protein, leading to alterations in their chemical shifts. In addition, the binding interaction can also cause exchange

broadening, which results in decreased cross-peak intensities. Unless the interaction causes overall conformational change of the labeled protein, changes in the ^{1}H-^{15}N TROSY-HSQC spectrum, together with the assignment information of the isotopically labeled protein, can be used to map the binding site.

Previous NMR studies in our laboratory showed that the full-length complexin I is largely unfolded, except for a central helical region (Pabst *et al.*, 2000). This helical region spans approximately from residue 29 to residue 86, of which the N-terminal half (residues 29-64) formed a stable α-helix, whereas the C-terminal half (residues 65-86) had a lower tendency to form α-helix. When the full-length complexin binds to the unlabeled core complex, several HSQC cross-peaks of the complexin broaden beyond detection due to the formation of a larger complex. According to the assignments of full-length complexin, the disappeared cross-peaks correspond to the residues at the central α-helical region, indicating that the central α-helical region is responsible for interaction with the core complex. Consistently, deletion mutagenesis also showed that complexin binds to the core complex through its central region (Pabst *et al.*, 2000). Therefore, my research project was focused on the structural and functional studies of the interaction between the central peptide (Cpx26-83) and the SNARE complex.

The ^{1}H-^{15}N HSQC spectrum of ^{2}H-^{15}N labeled Cpx26-83 exhibited poor dispersion in the ^{1}H dimension (black contours in Figure 3.3a), suggesting that the complexin fragment, similar to its full-length version, does not have any tertiary structure. Upon adding the

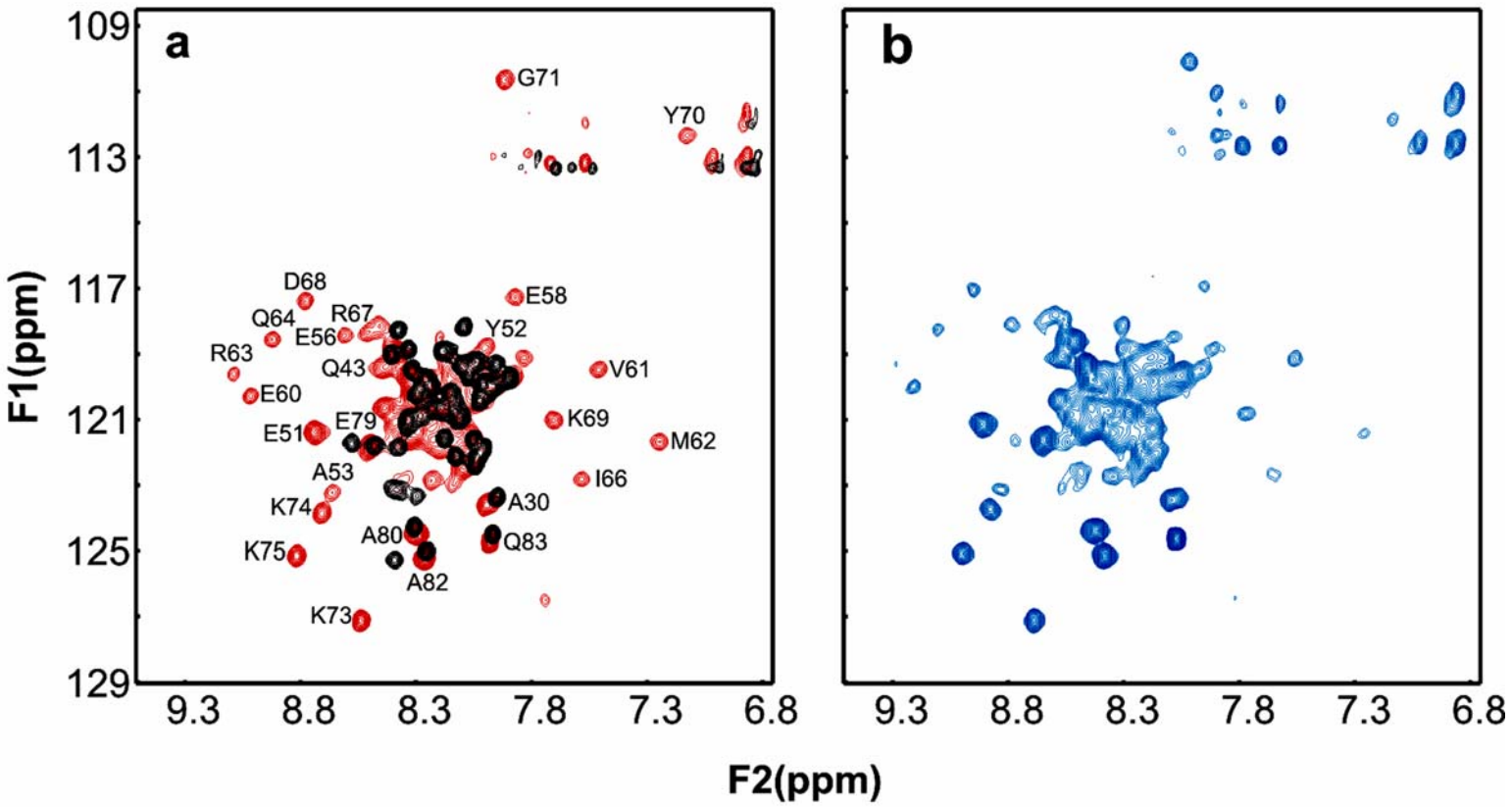

Figure 3.3 Cpx26-83 binding to the SNARE complex analyzed by ^{1}H-^{15}N TROSY-HSQC spectra. (a) ^{1}H-^{15}N TROSY-HSQC spectra of the isolated ^{2}H, ^{15}N-labeled Cpx26-83 (black contours) and the ^{2}H, ^{15}N-labeled Cpx26-83 bound to the unlabeled m2cc (red contours). The assignments of the well-resolved backbone cross-peaks from the bound form are showed. (b) ^{1}H-^{15}N TROSY-HSQC spectra of ^{2}H, ^{15}N-labeled Cpx26-83 bound to the minimal unlabeled SNARE complex.

unlabeled core complex, a striking dispersion of a subset of the cross-peaks was observed and the dispersed cross-peaks were generally broader compared with the cross-peaks in the HSQC spectrum of the isolated Cpx26-83 (red contours in Figure 3.3a). The observation of cross-peak dispersion and broadening is indicative of the formation of quaternary contacts between a specific region of Cpx26-83 and the core complex.

As discussed in the previous chapter, the syntaxin fragment in my NMR studies of the core complex was truncated at residue 253 to lessen the aggregation of the SNARE complex. To test weather this truncation affects the interaction between Cpx26-83 and the SNARE complex, I also prepared a SNARE complex with the full syntaxin SNARE motif (Syx). The HSQC spectrum of ^{2}H-^{15}N Cpx26-83 bound to this intact SNARE complex is practically superimposable with the spectrum of the Cpx26-83 bound to the minimal core complex (Figure 3.3b). In addition, a more severe cross-peak broadening was observed due to the aggregation of the non-truncated SNARE complex. Therefore, the C-terminal truncation of the syntaxin SNARE motif does not affect complexin binding to the SNARE complex.

To investigate which residues of complexin were involved in the binding interaction, I assigned most of the backbone resonances of Cpx26-83 bound to the core complex with a similar procedure to that described in chapter 2. Briefly, the assignments were obtained primarily from correlation of Cα(i-1) cross-peaks in HNCOCA spectra to Cα(i) cross-peaks in HNCA spectra and sequential NH/NH NOEs were used to verify the assignments. The assignments of the well-dispersed cross-peaks are labeled in Figure 3.3a. The dispersed and

broadened cross-peaks mainly correspond to residues 50-70 of complexin, which constitutes the region directly involved in binding to the core complex. Significant downfield chemical shifts of the Cα carbons were observed, indicating that Cpx26-83 bound to the core complex with a helical conformation. The comparison of the amide and Cα carbons chemical shifts of Cpx26-83 bound to the SNARE complex with those observed in isolated complexin (Pabst *et al.*, 2000) showed that the largest changes due to the interaction are in the binding region (residues 50-70; Figure 3.4a and 3.4b). However, additional amide chemical shift changes and downfield chemical shifts of Cα carbons were also observed beyond the binding region. It has been shown that the N-terminal half of the central region of the isolated complexin (residues 29-64) can form a stable helix, whereas the C-terminal half (residues 65-86) contain a substantial but lower population of α-helix (Pabst *et al.*, 2000). The widespread chemical shift changes upon binding to the core complex can be explained by the stabilization of the α-helical conformation in the binding region of the Cpx26-83 and the subsequent propagation of the α-helical conformation beyond the binding region. Interestingly, the N-terminal 16 residues of Cpx26-83 had remarkably similar chemical shifts before and after binding to the core complex (Figure 3.4a and 3.4b). Thus, the N-terminal 16 residues are not involved in direct interaction with the core complex.

To map the binding region in the core complex, I prepared four SNARE complex samples. In each sample, only one of the four SNARE motifs was ^{2}H-^{15}N labeled. The effects of Cpx26-83 on each SNARE motif in the core complex were monitored individually by ^{1}H-^{15}N TROSY-HSQC experiments. Figure 3.5 shows the ^{1}H-^{15}N TROSY-HSQC spectra of

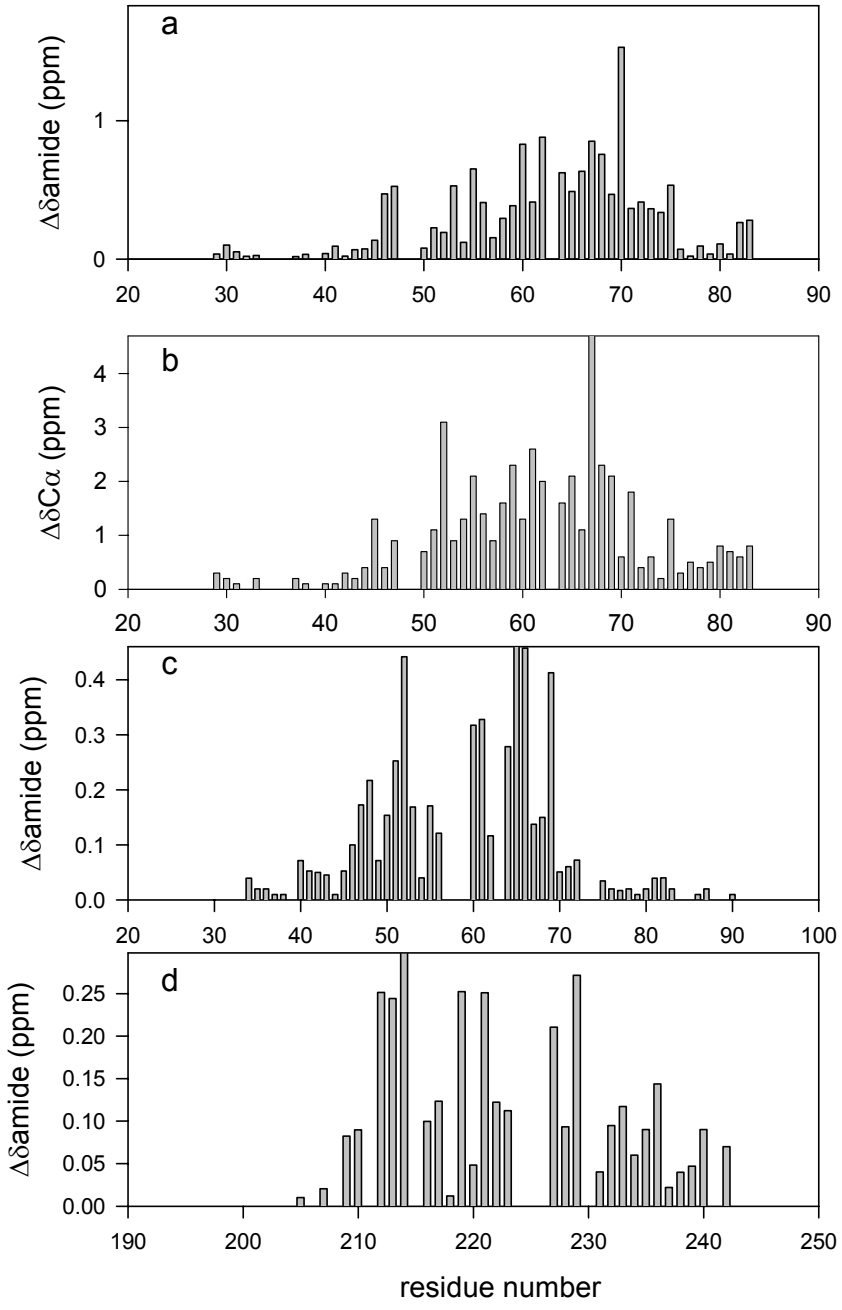
a
Δδamide (ppm)
b
ΔδCα (ppm)
c
Δδamide (ppm)
d
Δδamide (ppm)
residue number

Figure 3.4

Figure 3.4 Chemical shift changes caused by the complexin/SNARE complex interaction. (a) Amide chemical shift differences between the isolated Cpx26-83 and the Cpx26-83 bound to m2cc. (b) Cα chemical shift changes of the Cpx26-83 upon binding to the core complex. (c and d) Amide chemical shift changes of the synaptobrevin (c) and syntaxin (d) SNARE motifs within the SNARE complex due to the complexin binding. Amide chemical shift changes were calculated as $\Delta\delta=([\Delta\delta HN]^2+[0.17\times\Delta\delta N]^2)^{1/2}$, where $\Delta\delta HN$ and $\Delta\delta N$ are the amide ^{1}H and ^{15}N chemical shift changes, respectively.

each SNARE Motif of the core complex in the absence (black contours) and presence of complexin (red contours). Lots of cross-peak movements were observed in the spectra of SyxS and Syb2 in the core complex (Figure 3.5a and 3.5b), whereas only slightly perturbations were observed for the SNAP-25 SNARE motifs (Figure 3.5c and 3.5d). Thus, the NMR studies, consistent with previous mutagenesis studies (Pabst *et al.*, 2000), suggested that complexin binds to the interface between syntaxin and synaptobrevin in the core complex.

Then, I assigned most of the backbone resonances of the syntaxin and synaptobrevin SNARE motifs in the complexin/SNARE complex using essentially the same methodology as described in chapter 2. Comparison with the backbone assignments of the SNARE motifs of syntaxin and synaptobrevin in the SNARE complex revealed the complexin-induced changes. The major cross-peak movements are indicated by blue arrows in Figure 3.5a and 3.5b. A detailed and quantitative comparison of the amide chemical shifts of the SyxS and Syb2 SNARE motifs in the absence and presence of Cpx26-83 showed that the largest differences were located in the middle regions of both SNARE motifs (Figure 3.4c and 3.4d) with a similar length as the binding region in complexin. However, there is no big change of the Cα carbon chemical shifts of the SyxS or Syb2 SNARE motifs upon complexin binding, indicating that the interaction did not induce large conformational changes in the four helix bundle structure of the core complex. In summary, NMR analysis showed that complexin bound to the central region of the groove between syntaxin and synaptobrevin with a helical

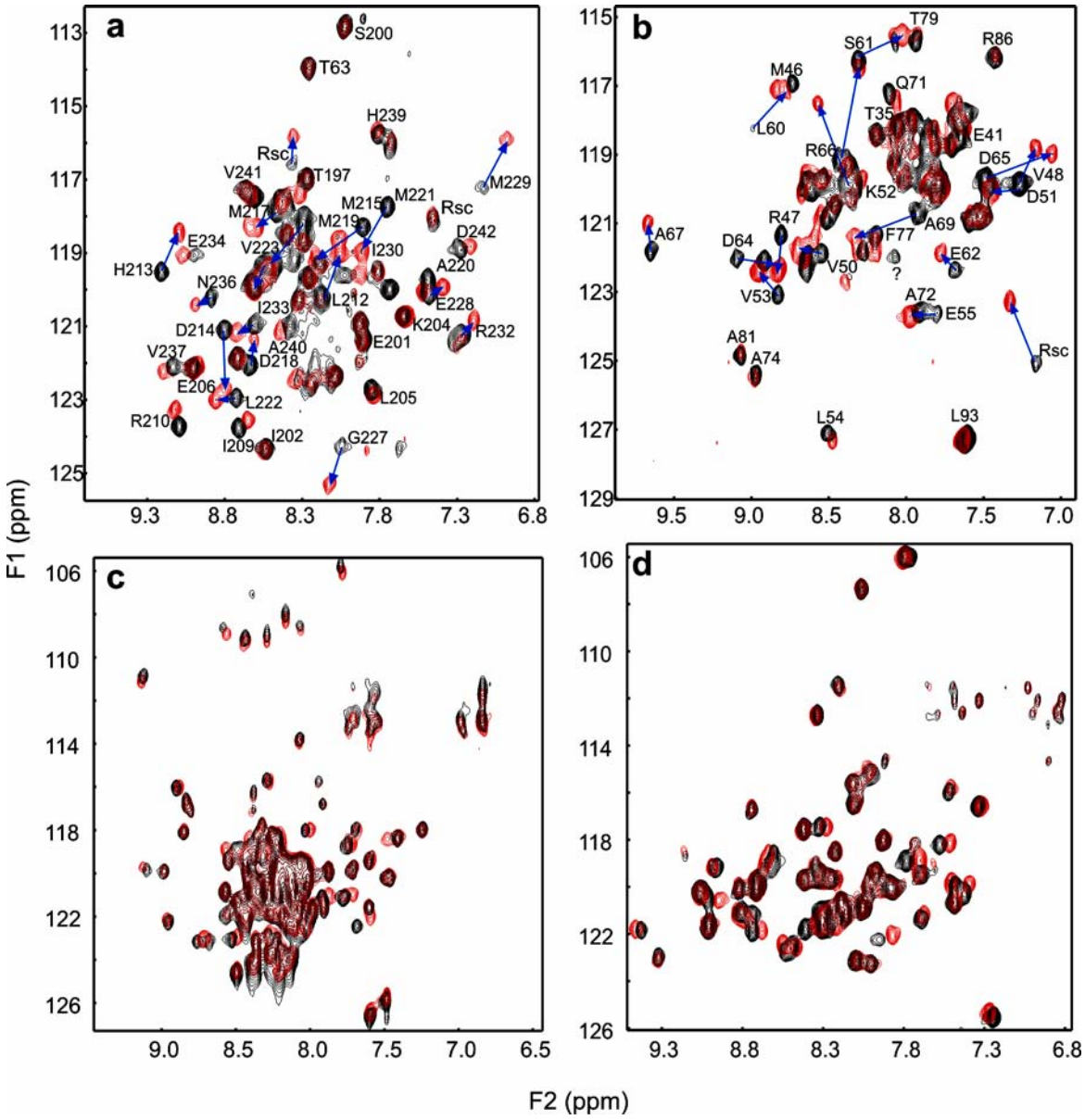
a
b
c
d
F1 (ppm)
F2 (ppm)
S200
T63
H239
Rsc
V241
T197
M229
M217
M215
M221
Rsc
M219
D242
E234
V223
I230
H213
A220
N236
I233
L212
E228
D214
K204
R232
A240
E201
V237
D218
E206
L205
L222
R210
I209
I202
G227
T79
S61
R86
M46
Q71
L60
T35
E41
R66
D65
V48
K52
D51
R47
A69
A67
F77
D64
E62
V50
V53
A72
E55
A81
A74
Rsc
L54
L93

Figure 3.5

Figure 3.5 Changes in the ^{1}H-^{15}N TROSY-HSQC spectra of the SNARE complex induced by Cpx26-83 binding. ^{1}H-^{15}N TROSY-HSQC spectra of the SNARE complex with SyxS (a), Syb2 (b), SNN (c) and SNC (d) ^{2}H, ^{15}N-labeled in the absence (black contours) and presence (red contours) of Cpx26-83 are shown. For SyxS (a) and Syb2 (b), the assignments of the well resolved cross-peaks are labeled, and the arrows illustrate the cross-peak shifts caused by Cpx26-83 binding.

conformation and the binding interaction did not cause major conformational changes in the core complex.

3.3.2 Crystallization of the Complexin/SNARE Complex

The NMR studies yielded an overall picture of the binding interaction between complexin and the core complex. However, a high resolution structure of the complexin/SNARE complex would still be desirable to provide a detailed illustration of the binding site. Since the Cpx26-83/SNARE complex behaved very well in the NMR tube, I went on to crystallize the complex. Luckily, tiny trigonal bipyramidal crystals grew spontaneously in my first crystallization attempt in 35% (v/v) iso-propanol, 100 mM Hepes (pH7.5) and 200 mM Magnesium chloride. Diffraction quality crystals were obtained by streak seeding in the equilibrated hanging drop containing 27% (v/v) iso-propanol, 100 mM Hepes (pH7.5) and 200 mM Magnesium chloride. The crystal diffracted to 2.5 Å resolution in a synchrotron beamline. Unlike the isolated SNARE complex, which crystallizes as a heterotrimer (Sutton *et al.*, 1998), the crystal of the complexin/SNARE complex was of space group $P2_12_12_1$ with one complex in each asymmetric unit, consistent with the observation that C-terminal truncation of the syntaxin SNARE motif reduced the aggregation tendency of the SNARE complex (Margittai et al., 2001). The crystal structure of the complexin/SNARE complex was solved by molecular replacement using an isolated neuronal SNARE complex as a search model and refined to a d_{min} of 2.5 Å. A section of the electron density map is shown in Figure 3.6, and the structural statistics are summarized in table 3.1.

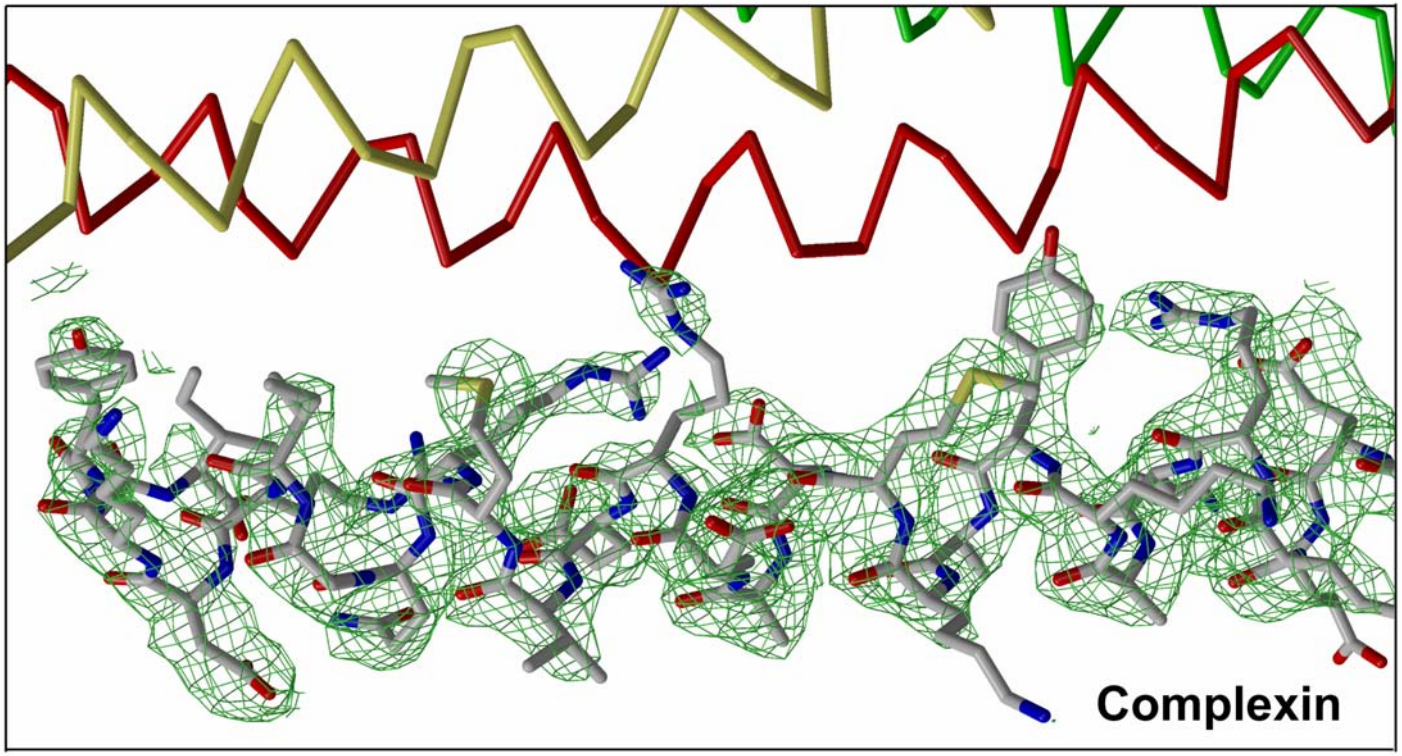

Figure 3.6 Electron density map of the complexin/SNARE complex. The complexin portion of the electron density from a composite omit map for the complexin/SNARE complex is shown; contours are drawn at 1.0× the r.m.s. lever of the map. The final refined coordinates for complexin and Ca traces of the SNAREs are superimposed. The SNARE motifs are color coded as follows: SyxS, yellow; Syb2, red; SNN, blue; and SNC, green. The complexin is colored with the CPK coloring scheme.

Table 3.1 Statistics of Data Collection and Refinement

Space group	$P2_12_12_1$
Cell dimensions	a = 40.49 Å, b = 60.42 Å, c = 159.79 Å
Number of measurements	78,881
Number of independent reflections	14,111
Data range	32.2–2.50 Å
R_{merge}:	
Overall	4.6%
Last shell (2.59–2.50 Å)	16.9%
Data completeness:	
Overall	99.6%
Last shell	99.4%
I/(σ)I:	
Overall	27.8
Last shell	6.6
Number of reflections used in refinement	13,041 (32.23–2.50 Å)
Number of non-H protein atoms	2,496
Number of water molecules, Mg^{2+}	116, 2
R_{work}	23.7%
R_{free}	30.3%
Rmsd in bond lengths	0.010 Å
Rmsd in bond angles	1.2°
Mean B value (Å^2):	
SNARE (all/main chain/side chain)	62.4/60.2/64.5
Complexin (all/main chain/side chain)	83.0/82.4/83.5
Complexin residues 48–70 (all/main chain/side chain)	70.3/70.8/69.9
Water molecules, Mg^{2+}:	65.5, 68.9
Cross-validated σ_A-coordinate error	0.47 Å
Missing residues	synaptobrevin: Gly27, Leu9 syntaxin: Lys191, Thr251-Lys253 snap-25 (1): Gly9, Trp82 complexin: Lys26-Ala31, Lys73-Gln83

3.3.3 Crystal Structure of the Complexin/SNARE Complex

The crystal structure of the complexin/SNARE complex revealed a picture of five helixes, among which four SNARE motifs remain highly twisted forming a four helix bundle and the fifth helix, Cpx26-83, bound to the middle region of the groove between syntaxin and synaptobrevin in an anti-parallel fashion (Figure 3.7a). Very little structural change occurred in the core complex due to the complexin binding. The backbone structure of the SNARE motifs within the complexin/SNARE complex superimposed well with those of the isolated SNARE complex (Figure 3.7b). The rms deviations between our structure and the three different complexes in the asymmetric unit of the crystals of the isolated SNARE complex range from 0.84 to 0.96 Å for 259 equivalent Cα carbons (Syb 28-92, SyxS 192-250, SNN 11-81, SNC 141-204) and are comparable to the corresponding rms deviations among the three independent structures in the SNARE complex heterotrimer (0.53-0.92 Å).

Contrary to the parallel arrangement of four SNARE motifs, the complexin helix was oriented in an antiparallel fashion with respect to the SNARE complex (Figure 3.7a). Only residues 32-72 of Cpx26-83 were observable in the crystal structure, indicating that the rest of the complexin fragment is highly mobile. This result is consistent with the previous NMR studies, where sharp resonances were observed for the 11 C-terminal residues of Cpx26-83 (Figure 3.3a). Residues 48-70 of complexin, the same region identified by our NMR studies, binds to the central part of the groove between the syntaxin and synaptobrevin helices, and the binding buries 1,666 $Å^2$ of solvent accessible surface area between complexin and the SNARE complex (Figure 3.7c and 3.7d). The binding sequences of syntaxin (residues 214-

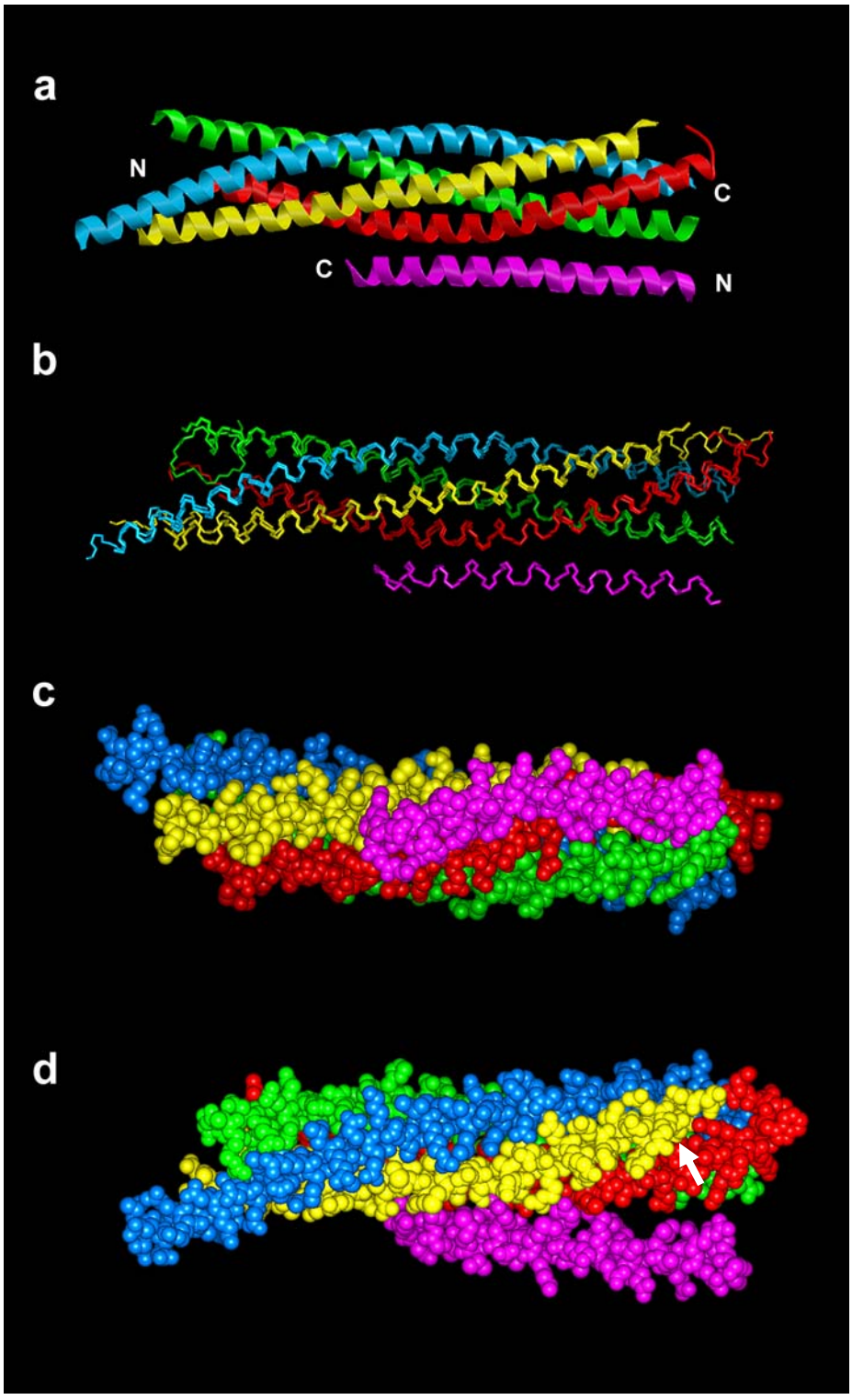

Figure 3.7

Figure 3.7 Structure of the complexin/SNARE complex. (a) Ribbon diagram of the complexin/SNARE complex. The color coding is as follows: SyxS, yellow; Syb2, red; SNN, blue; SNC, green; Cpx26-83, pink. (b) Superposition of the structures of the isolated SNARE complex (Sutton et al., 1998) and the complexin/SNARE complex shows that minimal structural changes are caused by complexin binding. (c) Space filling model of the complexin/SNARE complex illustrates how the C-terminal end of the complexin helix (pink) binds to the center of the groove between the synaptobrevin (red) and syntaxin (yellow) SNARE motifs. (d) The same space filling model shown in (c), but rotated approximately 90^{o} around the horizontal axis, shows that N-terminal end of the complexin helix has no direct interaction with the SNARE complex. The white arrow indicates the position of F77 from synaptobrevin. Figure prepared with the programs InsightII (MSI) and Molscript (Kraulis, 1991).

232) and synaptobrevin (residues 47-68) correlate well with the regions having the largest chemical shift changes upon complexin binding as observed by NMR spectroscopy. However, NMR studies showed that the complexin binding induces additional changes at the C-terminus of the syntaxin SNARE motif beyond the binding region (Figure 3.4d). The extra changes in the syntaxin SNARE motif most likely arise from the local abundance of the aromatic side chains (Y235, H239 and Y243), which are close to the complexin binding region (Figure 3.8 bottom panel). The slight re-orientation of aromatic rings, due to the perturbation from the complexin binding, can induce strong shifts in the resonances of neighboring nuclei. However, it is not meaningful to compare these aromatic rings in our structure with those in the structure of the isolated SNARE complex, since these aromatic side chains are involved in crystal contacts between the three different SNARE complexes within the asymmetric unit (Sutton *et al.*, 1998).

Complexin binding involves an intricate network of hydrophobic, hydrogen bonding and ionic interactions. A summary of the most important interactions that mediate binding of complexin to the SNARE complex is shown in Figure 3.8. Two tyrosine residues (Y52 and Y70) and three arginine residues (R48, R59 and R63) of complexin are critical for binding to the SNARE complex. Y52 forms a hydrogen bond with D64 from synaptobrevin, and Y70 hydrogen-bonds with D218 from syntaxin, which in turn forms a salt bridge with K69 from complexin. Three arginine residues of complexin form numerous salt bridges with three aspartate residues (D57, D65 and D68) from synaptobrevin. In addition, R59 from complexin also hydrogen bonds with S225 from syntaxin. The two tyrosine (Y52 and Y70) and three

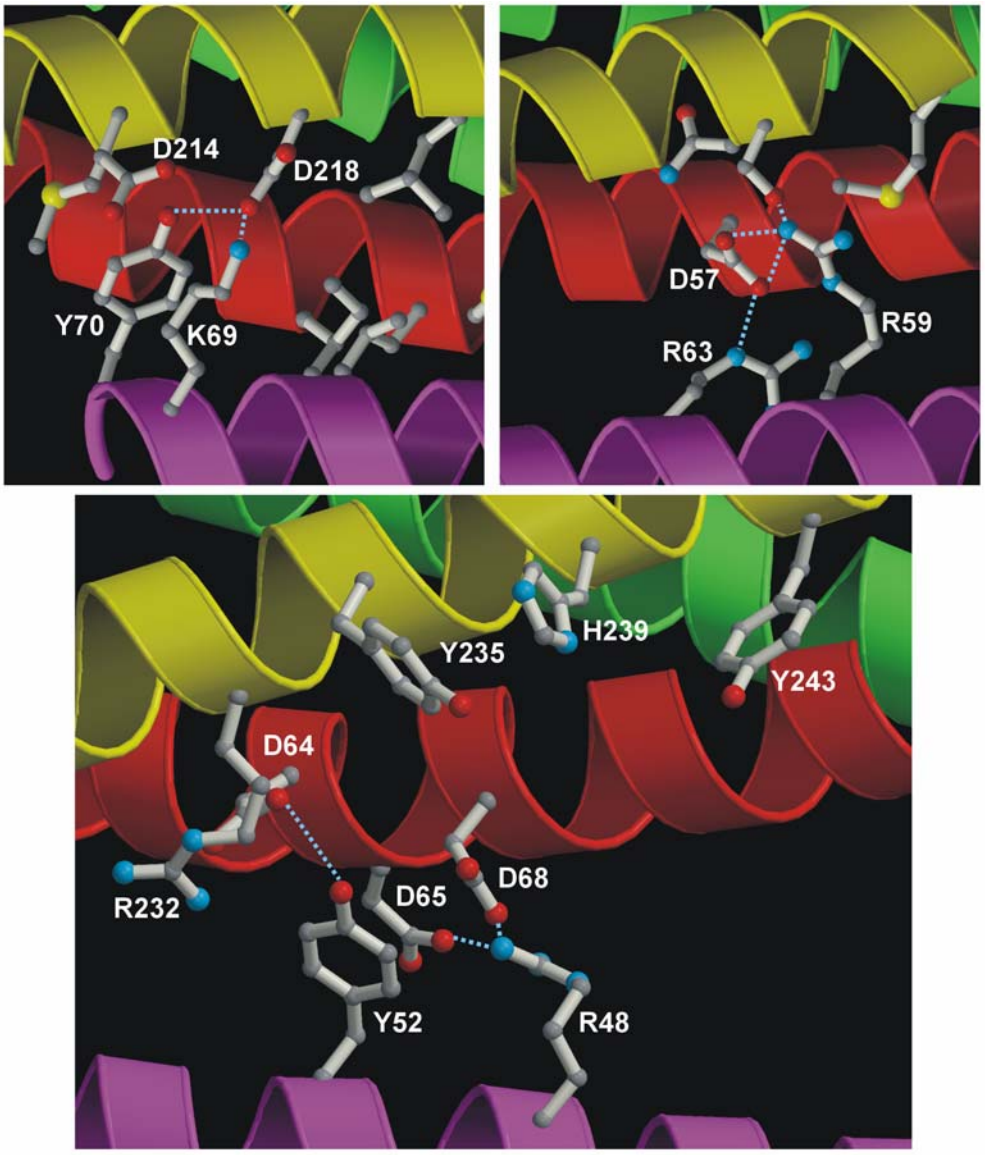
D214
D218
Y70
K69
D57
R59
R63
Y235
H239
Y243
D64
R232
D65
D68
Y52
R48

Figure 3.8

Figure 3.8 Three different close-ups summarizing some of the interactions between complexin and the SNARE complex. All proteins are colored the same as in Figure 3.7. Sidechains are displayed as stick-and ball models. Oxygen atoms are in red and nitrogen atoms are in blue. Dotted lines illustrate the hydrogen bonding and ionic interactions. The bottom panel illustrates the three stacked aromatic residues of syntaxin (Y235, H239, and Y243) located near the complexin/SNARE interface. Figure prepared with the program Molscript (Kraulis, 1991).

arginine residues (R48, R59 and R63), together with additional hydrophobic residues from complexin (M62 and I66), V50 and L54 from synaptobrevin, and M215, L222 and M229 from syntaxin, make extensive hydrophobic contacts at the binding site.

A striking feature of the complexin fragment bound to the SNARE complex is the isolated N-terminal helix, which does not make any contacts with the SNARE complex and there are no lattice contacts in the crystal that could influence the conformation of the "hanging" helix either (Figure 3.7d). The presence of iso-propanol in the crystallization condition raises the question of whether the observed conformation in the crystals is also valid in solution, since iso-propanol, an organic solvent, may induce the helical conformation or disrupt interactions between this region of complexin and the SNARE complex. However, the unusual ability of the N-terminal part of Cpx26-83 to form stable α-helical conformation by itself has been observed in solution NMR studies (Pabst *et al.*, 2000). Moreover, the above NMR studies also showed that no change was observed for the N-terminal 16 residues of Cpx26-83 after its binding to the core complex, indicating that this part of the complexin doesn't directly contact with the SNARE complex (Figure 3.4a and 3.4b). Therefore, the excellent agreement between the NMR results and the complexin binding mode observed in X-ray crystallographic studies validates the structure.

3.3.4 Complexin Binding Stabilizes the SNARE Complex

Because synaptobrevin is located in the synaptic vesicle membrane, whereas syntaxin resides on the plasma membrane, the formation of the core complex brings the two membranes in

close proximity. Thus, the interface between synaptobrevin and syntaxin bears the strong repulsive force of the two membranes during the fusion process. The structural analysis showed that complexin binds to the groove between syntaxin and synaptobrevin, without further changes of the overall conformation of the core complex. One question arises naturally: could complexin act as a tape to seal the interface between syntaxin and synaptobrevin and therefore stabilize the SNARE complex? It is very difficult to test this hypothesis because without the presence of membranes, the core complex in solution is extremely stable, i.e. the SNARE complex is SDS resistant (Hayashi et al., 1994) and can only be denatured at very high temperatures (above 90^{o}C; see chapter 2 and (Fasshauer *et al.*, 1997b)) or in saturating concentrations of urea or guanidinium chloride. These harsh treatments disrupt the binding between complexin and the core complex before they have any measurable effect on the core complex. To overcome these difficulties, I used hydrogen-deuterium (H/D) exchange experiments monitored by ^{1}H-^{15}N TROSY-HSQC spectra to detect the effects of complexin on the local flexibility of the core complex under non-denaturing conditions (Kim et al., 1993; Englander and Hiller, 2001). The H/D exchange experiment essentially measures how fast certain nitrogen-bound protons exchange with deuterium, leading to disappearance of the corresponding cross-peak in ^{1}H-^{15}N TROSY-HSQC spectra. Structural factors have big effects on the H/D exchange rates. For instance, the exchange rates drop dramatically if amide protons are hydrogen-bonded, since the hydrogen bond must break before exchange can occur. Solvent exclusion also retards exchange, since solvent must be accessible to NH group in order for exchange to occur. The protection factors, calculated as the ratios between the observed deuterium exchange rates

and those expected for the same sequence in a random coil (Bai et al., 1993), reflect the protection levels due to formation of secondary or tertiary structure. Therefore, the H/D exchange experiment provides a sensitive tool to probe different degree of protection along individual helices within the assembled SNARE complex. Particularly interesting is the protection pattern of the synaptobrevin helix, because its interaction with syntaxin/SNAP-25 complex, which is believed to be preassembled at the plasma membrane (Nicholson *et al.*, 1998; Fiebig *et al.*, 1999; May *et al.*, 1999; Xiao *et al.*, 2001; Misura *et al.*, 2001a), is likely to be the final step of the core complex assembly. Based on these arguments, I studied the H/D exchange rates of synaptobrevin amide protons within the SNARE complex in the absence and presence of complexin.

To monitor the H/D exchange rate, I placed a core complex sample where only the synaptobrevin SNARE motif is ^{2}H, ^{15}N labeled into D2O buffer. Due to the unusual stability of the SNARE complex, high protection factors were expected for at least some of the amide protons of synaptobrevin. Thus, the H/D exchange experiments were performed under conditions that favor fast amide exchange (pH7.5, 30^{o}C; see Bai et al., 1993). A series of ^{1}H-^{15}N TROSY-HSQC spectra were taken at different time points. Because amide protons exchanged gradually with deuterium from the solvent, the corresponding cross-peaks in HSQC spectra disappeared progressively with time. Figures 3.9a and 3.9b show the ^{1}H-^{15}N TROSY-HSQC spectra obtained after 7 days of deuterium exchange in the absence and presence of complexin, respectively. The residues whose amide protons survived from exchange are labeled in the spectra and summarized in Figure 3.9c. The amount of cross-

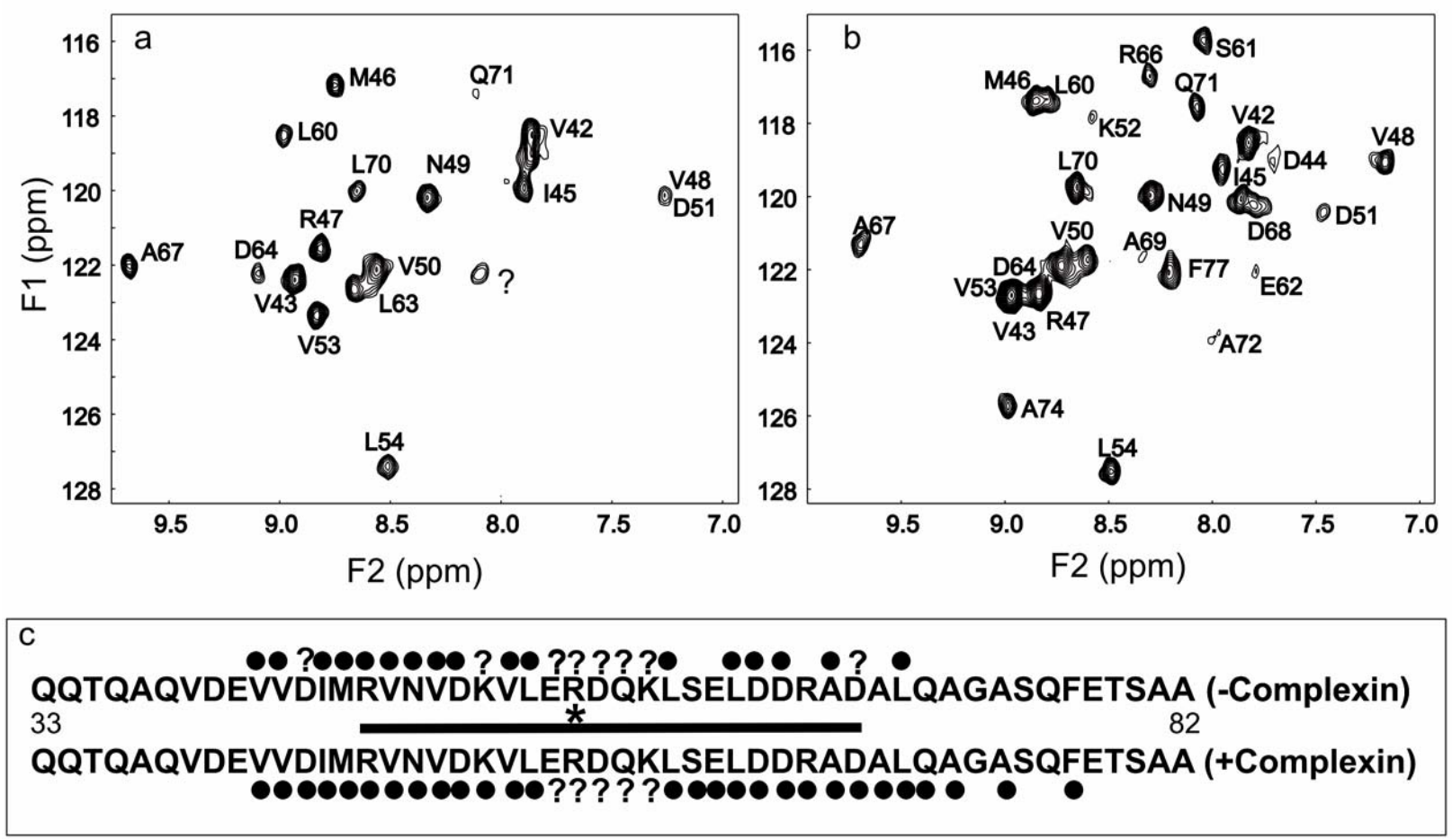
a
b
F1 (ppm)
F2 (ppm)
F2 (ppm)
M46
Q71
L60
V42
L70
N49
I45
V48
D51
R47
A67
D64
V50
V43
L63
V53
L54
R66
S61
K52
D44
D68
A69
F77
E62
V53
A72
A74
c
QQTQAQVDEVVDIMRVNVDKVLERDQKLSELDDRADALQAGASQFETSAA (-Complexin)
33
82
QQTQAQVDEVVDIMRVNVDKVLERDQKLSELDDRADALQAGASQFETSAA (+Complexin)

Figure 3.9

Figure 3.9 Complexin stabilizes the synaptobrevin/syntaxin interface. (a) ^{1}H-^{15}N TROSY-HSQC spectra of the SNARE complex with only Syb2 ^{2}H, ^{15}N-labeled after 7 days at 30^{o}C in D_2O (pD 7.5). (b) ^{1}H-^{15}N TROSY-HSQC spectra of the complexin/SNARE complex with only Syb2 ^{2}H, ^{15}N-labeled after 7 days at 30^{o}C in D_2O (pD 7.5). The assignments of the cross-peaks are labeled. (c) Summary of the protection against deuterium exchange of the amide protons from synaptobrevin within the SNARE complex in the absence (top) and the presence (bottom) of Cpx26-83. Bullets indicate residues whose amide protons remain observable after 7 days of deuterium exchange. Question marks indicate residues that were not assigned or cannot be monitored due to cross-peak overlap. The bar indicates the region that has direct interactions with complexin. The star indicates Arg56, which is the residue involved in the zero layer of the SNARE complex.

peaks observed after seven days is remarkable given the experimental conditions (pH7.5 at 30^{o}C). The protection factors estimated for these amide protons are approximately 10^{7} or larger. Since there is a substantial amount of solvent-accessible surface area along the whole synaptobrevin helix even after complexin binding, such high protection factors indicate the extraordinary resistance to local unfolding.

The H/D exchange experiments of the isolated SNARE complex showed that the N and C termini of synaptobrevin of the isolated SNARE complex are, as expected, least protected because local unfolding could easily start from each end of the complex, whereas the central region, encompassing residues 42 to 70 of synaptobrevin, had different degrees of protection from deuterium exchange on each side of the polar layer residue (R56). The N-terminal half of the central region (residues 42-54) is highly protected, indicating that this region of synaptobrevin forms very stable contacts with the rest of the SNARE complex. As suggested by a “zipping model”, the assembly of the SNARE complex starts from the N terminus and “zippering up” towards the C-terminus (Geppert and Südhof, 1998; Fiebig *et al.*, 1999; Xu *et al.*, 1999; Matos *et al.*, 2003). Therefore, the stable interaction at the N-terminus of the SNARE motifs might be important for the assembly of the core complex. The protection pattern of the C-terminal part (residues 60-70) is fragmented, which may be due to the local unfolding events originating from the polar layer region, where very broad resonances are observed in NMR spectra as described in the previous chapter.

Upon addition of complexin, more residues at the central region of synaptobrevin are protected and strong protection was observed on both sides of the polar layer. Since the complexin fragment covers the central region of the groove between synaptobrevin and syntaxin in the SNARE complex, the increased protection should be partly attributed to the presence of complexin, which blocks the solvent accessibility and slows down the local unfolding in this region. However, additional C-terminal residues beyond the binding region were protected, and the protection even extended to residue F77, which is very close to C-terminal end of the SNARE complex (see white arrow in Figure 3.7). This observation suggested that the C-terminal regions of the synaptobrevin and the syntaxin/SNAP-25 complex form tight contacts that are partially disrupted by the local unfolding process originating from the polar layer. Complexin binding slows down the local motions at the polar layer and facilitates the formation of tight contacts between SNARE motifs at the C-terminal end.

3.3.5 The Model of Complexin Function

Extensive studies have shown that the SNARE proteins assemble into a highly stable ternary complex and the energy released from the formation of the core complex may be used to overcome the repulsive force between the two opposing membranes and may lead to fusion (Sollner *et al.*, 1993a; Hayashi *et al.*, 1994; Hanson *et al.*, 1997). To better understand the function of the SNAREs and the core complex, we studied the interaction between complexin and the SNARE complex. Earlier biochemical and genetic studies showed that complexin binds specifically to the SNARE complex and is essential for normal Ca^{2+}-dependent

neurotransmitter release (McMahon et al., 1995; Pabst *et al.*, 2000; Reim *et al.*, 2001). Here, NMR analyses and X-ray crystallographic studies of the complexin/SNARE complex yield a consistent picture where complexin binds to the groove between syntaxin and synaptobrevin of the SNARE complex. The H/D exchange experiments showed that complexin binding slows down the local unfolding process of the core complex and stabilizes the interface between syntaxin and synaptobrevin.

Full length complexin has 134 residues, among which only 23 residues (residues 48-70) are involved in direct interaction with the core complex. Thus, does this interaction count, at least partially, for the major function of the complexin? The answer to this question directly relates to the validity of any model proposed to explain the complexin function. According to the crystal structure of the complexin/SNARE complex, residues K69 and Y70 of complexin play important roles in the binding to the core complex. Indeed, a recent study by Rosenmund and colleagues in Göttingen, showed that a mutant CPXI (K69A/Y70A) completely abolished the binding to the core complex. Interestingly, overexpression of CPXI (K69A/Y70A) in CPXI/II double deletion mutant hippocampal neurons failed to rescue the CPXI and CPXII double knockout phenotype, while overexpression of the wildtype CPXI successfully rescued the CPXI/II double knockout phenotype (unpublished data from Mansour et al.). Therefore, the major function of complexin is most likely associated with binding to the core complex.

It has been suggested that the SNARE complex might assemble in different steps (Geppert *et al.*, 1998; Fiebig *et al.*, 1999; Xu *et al.*, 1999; Matos *et al.*, 2003). The H/D exchange experiments showed that the N-terminal half of the SNARE complex is extremely stable (Figure 3.9c), and hence, it is possible that N-terminal half can initially assembled while the C-terminal half remains unengaged because of repulsion forces between the membranes. It is easy to envision that once in a while the C-terminal half of the core complex might zip up transiently to form a fully assembled core complex, which is capable to mediate constitutive fusion. However, the fully assembled core complex is metastable and can reverse back to the half assembled core complex. Based on this simplified two-state model of the assembly of the SNARE complex, together with the above structural and functional results of the complexin/SNARE complex, a tentative model to explain the function of the complexin can be proposed (Figure 3.10). This model assumes that there are two interchangeable priming stages that prepare the docked synaptic vesicles ready for fusion. The first priming stage involves the half assembled core complex and the second stage involves formation of the fully assembled core complex. Hypertonic sucrose treatment can trigger synaptic vesicles in both stages to release, whereas only those synaptic vesicles in the second priming stage with the fully assembled SNARE complex are ready for fast Ca^{2+}-triggered release. Complexins specifically bind to the fully assembled SNARE complex and stabilize the second stage. Therefore, this model explains the observation that deletion of complexin causes a selective decrease in fast Ca^{2+}-dependent neurotransmitter release, while leaving the hypertonic sucrose treatment intact. Of course, this model still needs to be tested in future studies and alternative models of complexin function can also be proposed.

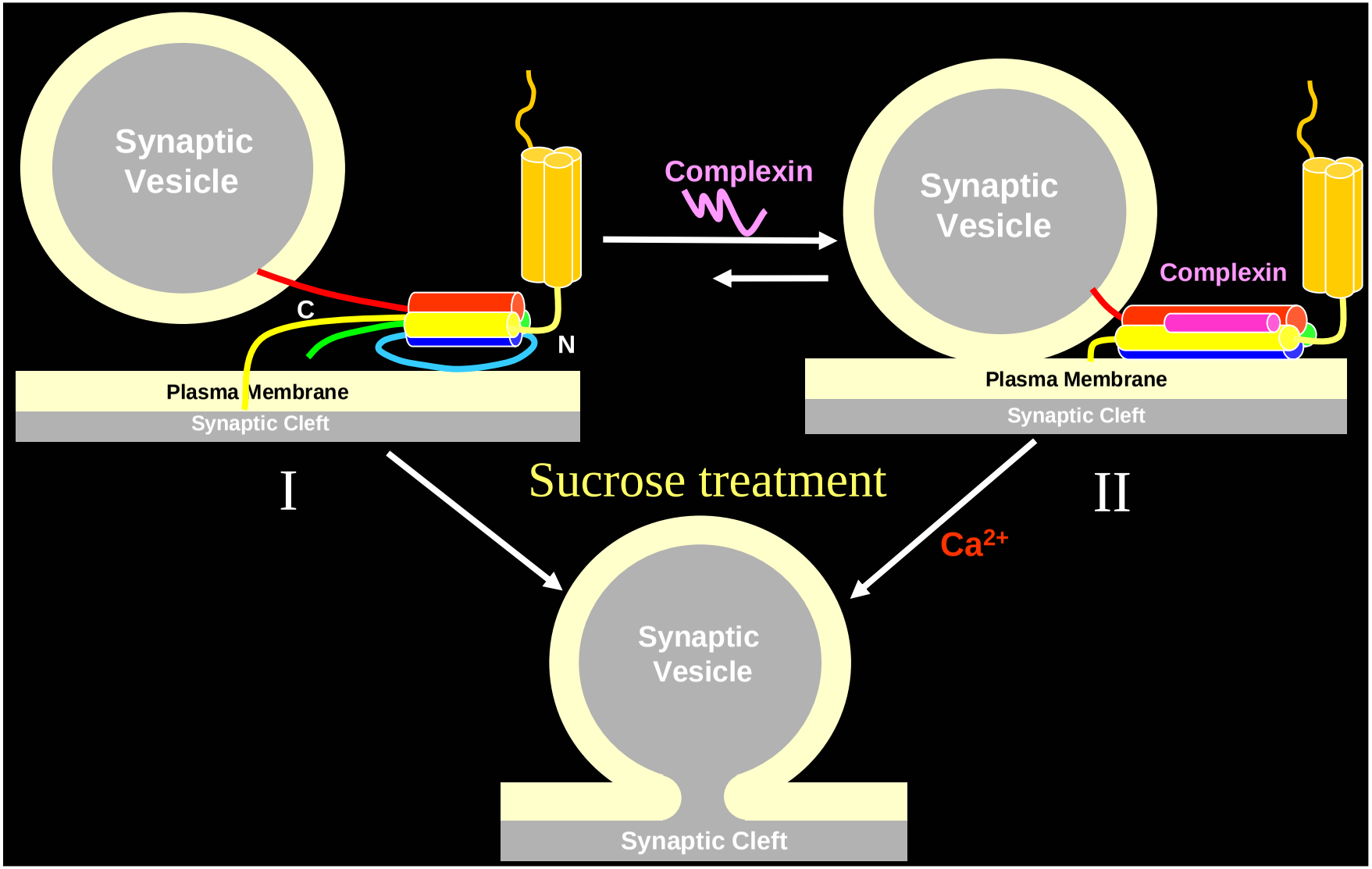
Synaptic Vesicle
C
N
Plasma Membrane
Synaptic Cleft
Complexin
Synaptic Vesicle
Complexin
Plasma Membrane
Synaptic Cleft
I
Sucrose treatment
II
Ca2+
Synaptic Vesicle
Synaptic Cleft

Figure 3.10

Figure 3.10 Model for the function of complexin in neurotransmitter release. This model proposed that there are two stages in the synaptic vesicle priming step. The first stage involves a partially assembled core complex, while stage II involves a fully assembled core complex, which complexin binds to and stabilizes. Hypertonic sucrose treatment can cause synaptic vesicles in both priming stages to fuse, whereas only those vesicles in stage II can undergo Ca^{2+} triggered fast neurotransmitter release. The color coding for each protein is the same as in Figure 3.7, except for the N-terminal domain of syntaxin (orange three helix bundle), which is not present in the structure of the complexin/SNARE complex.

3.3.6 Other Potential Functions of Complexin

There are more than a hundred residues flanking the core complex binding region (residues 48-70) in complexin. The function of these extra residues is still under investigation. Initial NMR studies in our laboratory showed that the region encompassing residues 29-64 of the isolated complexin forms a stable helical conformation (Pabst *et al.*, 2000). Since the binding region of complexin (residues 48-70) also assumes a helical conformation upon binding to the core complex, could this pre-formed N-terminal short helix facilitate the binding of complexin to the core complex?

To test this hypothesis, I performed a mutagenesis study in collaboration with Dr. Rosenmund's group in Göttingen. The residue L41 is in the middle of the helix region of the isolated complexin and the mutation of Leu41 to Pro will terminate the helical conformation. Thus, I tested the interaction between Cpx26-83 L41P and the core complex by NMR spectroscopy. The ^{1}H-^{15}N HSQC spectra of the isolated Cpx26-83 (L41P) exhibit extensive changes with respect to that of the wildtype complexin fragment (Figure 3.11b). This result suggests that the mutation has a strong effect on the conformation of the isolated peptide, as expected from the prediction that the L41P mutation would disrupt the helical conformation. Upon adding unlabeled core complex, the HSQC spectra changes dramatically, indicating that the mutant Cpx26-83 retains the ability to bind to the core complex (Figure 3.11a). The spectrum of the mutant complexin/SNARE complex has a very similar cross-peak dispersion pattern as observed in the spectrum of the wild type complex, suggesting an analogous binding mode with similar binding region (residues 48-70, see Figure 3.11c). The cross-

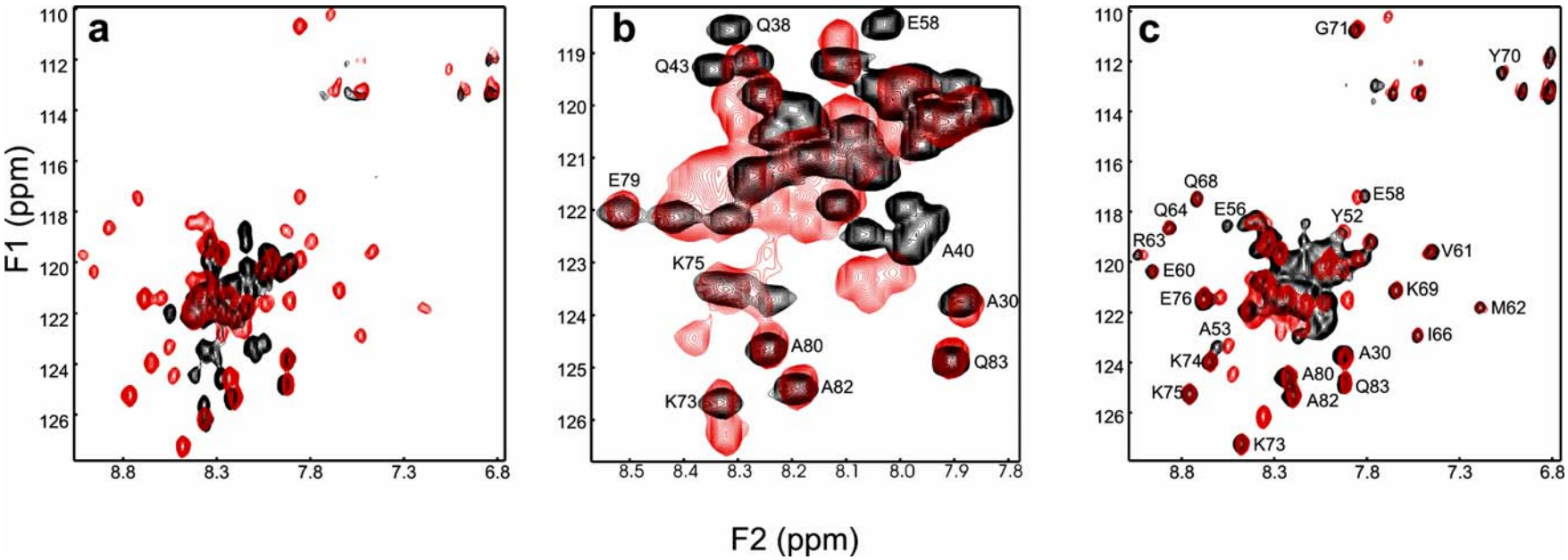

Figure 3.11 Cpx26-83 (L41P) binding to the SNARE complex analyzed by ^{1}H-^{15}N TROSY-HSQC spectra. (a) ^{1}H-^{15}N TROSY-HSQC spectra of Cpx26-83 L41P in isolation (black contours) or bound to the SNARE complex (red contours). (b) ^{1}H-^{15}N TROSY-HSQC spectra of Cpx26-83 wild type (black contours) and Cpx26-83 (L41P) (red contours). Tentative assignments of some well resolved cross-peaks are shown. (c) ^{1}H-^{15}N TROSY-HSQC spectra of Cpx26-83 wild type (black contours) and Cpx26-83 (L41P) (red contours) bound to the SNARE complex. The assignments of the well resolved cross-peaks of the wild type Cpx26-83 bound to the SNARE complex are shown.

peaks from residue 60 to the C-terminus of the Cpx26-83 (L41P) in the mutant complexin/SNARE complex (red contours in Figure 3.11c) are superimposible with those of the wild type Cpx26-83 in the complex (black contours in Figure 3.11c). The cross-peaks from residues 48-59 of the mutant Cpx26-83 shift slightly compared to those from the same residues of the wildtype complex, indicating that the binding of the first ten residues might be slightly perturbed by the point mutation. The cross-peaks from the N-terminal residues (preceding residue 48) are strongly perturbed, as expected from the disruption of the helix in this region. Consistent with the NMR analysis, the biochemical and electrophysiological studies of CPXI L41P carried out by Mansour et al. also showed that CPXI L41P is able to bind to the core complex and the mutant complexin rescues the complexin double knockout phenotype with a similar efficiency as the wild type protein (unpublished data). This result suggested that the helix region in the isolated complexin does not play a role in the major function of complexin.

On the other hand, this mutant CPXI L41P does have an interesting phenotype in the electrophysiological tests with longer high frequency stimulation. Briefly, neurons over-expressing CPXI L41P showed an increase in asynchronous release, while the synchronous charge is similar to that of wild type neurons (unpublished data). One potential model to explain this phenotype is based on the idea that the difference between the synchronous and asynchronous release is simply that the synchronous mode has a fully assembled core complex, while the asynchronous mode involves a partially assembled core complex. Preparing vesicles ready to release in the synchronous mode takes longer time than the

formation of the vesicles that can release in the asynchronous mode. There is equilibrium between the two types of vesicles. Complexin binding shifts the equilibrium towards the synchronous release mode; however, this shift takes some time to develop. CPXI L41P might have defects in shifting the equilibrium in the sense that it slows down the conversion from asynchronous vesicles to synchronous vesicles. Therefore, an increase in asynchronous release was observed during longer high frequency stimulation, because CPXI L41P failed to shift the equilibrium between synchronous and asynchronous release efficiently during high vesicle turnover. Clearly, there are alternative explanations and many more investigation need to be done before we can reach a final conclusion about complexin function.

CHAPTER 4 THREE DIMENSIONAL STRUCTURE OF THE H_{ABC} DOMAIN WITHIN THE CLOSED CONFORMATION OF SYNTAXIN 1

4.1 Introduction

Syntaxin 1 contains an N-terminal domain, the H_{abc} domain, which can fold back and bind to the syntaxin SNARE motif, forming a closed conformation (Dulubova *et al.*, 1999). The closed conformation is incompatible with the formation of the core complex. In other words, the closed conformation of syntaxin 1 needs to be opened to expose its SNARE motif and assemble the core complex with other SNAREs. Munc18-1 specifically binds to the syntaxin 1 closed conformation. A double residue substitution (L165A/E166A) in the linker region between the H_{abc} domain and the syntaxin SNARE motif disrupts the closed conformation of syntaxin 1 and abolishes its interaction with munc18-1 (Dulubova *et al.*, 1999). The crystal structure of the munc18-1-syntaxin 1a complex revealed that munc18-1 wraps around the syntaxin 1 closed conformation with extensive contacts, leading to the proposal that munc18-1 might provide a platform for the assembly of the core complex (Misura *et al.*, 2000). This model implies that the binding of munc18-1 to the isolated syntaxin 1 might change the closed conformation of syntaxin 1 to facilitate the formation of the core complex. Indeed, the crystal structure of the isolated Sso1 (Munson *et al.*, 2000), a syntaxin homologue on the yeast plasma membrane, exhibits significant difference from the syntaxin 1 structure in the munc18-1-syntaxin 1a complex (Misura *et al.*, 2000). On the other hand, minor changes were observed between the crystal structure of the isolated squid munc18-1 (Bracher *et al.*, 2000)

and that of the rat munc18-1 in the complex with syntaxin (Misura *et al.*, 2000). To reconcile the discrepancy, it is necessary to directly compare the structure of the isolated syntaxin 1 and the structure of the syntaxin 1 bound to munc18-1. Since the structure of the isolated syntaxin 1 is not available, I tried to solve the solution structure of the minimal fragment of the closed conformation of syntaxin 1 (residues 26-230), containing the N-terminal domain, the linker region and half of the SNARE motif (Dulubova *et al.*, 1999).

In this chapter, I report the solution structure of the N-terminal domain (residues 26-140) within the closed conformation of syntaxin 1. The result showed that the N-terminal domain of syntaxin 1 adopts the same conformation whether it is alone, bound to Munc18-1, or in the closed conformation.

4.2 Material and Methods

4.2.1 NMR Spectroscopy

The DNA construct expressing the syntaxin 1 (26-230) fragment and all protein samples for NMR studies were prepared by Dr. Josep Ubach, a previous postdoctoral fellow in the laboratory. All NMR experiments were performed on Varian INOVA500 or INOVA600 spectrometers. Resonance assignments, NOEs, $^{3}J_{HN\alpha}$ coupling constants, and amide protection data for structure determination, were obtained from a series of single, double and triple resonance experiments (Clore *et al.*, 1994; Clore and Gronenborn, 1998; Gardner and Kay, 1998) acquired on fully protonated, partially deuterated or fully deuterated samples.

Briefly, the backbone and C_β resonance assignments were mainly obtained by using HNCA, HN(CO)CA, HN(CA)CB and HN(COCA)CB spectra acquired on a ^{2}H, ^{15}N, ^{13}C-labeled sample, together with 3D ^{1}H, ^{15}N-NOESY-HSQC, 3D-(^{1}H, ^{15}N, ^{15}N) correlated-HSQC-NOESY-HSQC acquired on a ^{2}H, ^{15}N-labeled sample. Hα assignments were obtained by analyzing HNHA (Kuboniwa *et al.*, 1994) and ^{1}H, ^{15}N-TOCSY-HSQC spectra acquired on a ^{15}N-labeled sample. (H)C(CO)NH-TOCSY and H(C)(CO)NH-TOCSY spectra of a 50% perdeuterated sample, as well as the ^{1}H-^{15}N-NOESY-HSQC and ^{1}H-^{13}C-NOESY-HSQC spectra acquired on fully protonated samples, were used to assign aliphatic sidechain resonances. NH_2 groups in Asn and Gln were assigned using ^{1}H, ^{15}N-NOESY-HSQC spectrum. In addition, 2D homonuclear DQF-COSY, NOESY and TOCSY data, together with 3D ^{1}H, ^{15}N-NOESY-HSQC and ^{1}H-^{13}C-NOESY-HSQC spectra were used to obtain the aromatic assignments. Stereospecific assignments of Val and Leu methyl groups were obtained from high resolution ^{1}H-^{13}C HSQC spectrum of a 10% ^{13}C-labeled sample. Nuclear Overhauser effects for structure determination were measured from 2D NOESY, and 3D ^{1}H-^{15}N-NOESY-HSQC and 3D ^{1}H-^{13}C NOESY-HSQC experiments. Protection of amide protons from the solvent was measured from the intensities of exchange cross-peaks with the water resonance in ^{1}H-^{15}N-NOESY-HSQC and ^{1}H-^{15}N-TOCSY-HSQC experiments. HNHA spectrum was used to measure $^{3}J_{HN\alpha}$ coupling constants. All data were processed with the program NmrPipe (Delaglio *et al.*, 1995) and analyzed with the program NMRview (Johnson *et al.*, 1994).

4.2.2 Structure Calculations.

NOE cross-peak intensities were classified as strong, medium, weak and very weak, and assigned to restraints of 1.8–2.8, 1.8–3.5, 1.8–5.0 and 1.8–6.0 Å, respectively, with appropriate pseudo-atom corrections. A separate classification was used for NOEs involving methyl groups to account for their stronger intensities. Backbone torsion angles were derived from chemical shift analysis using TALOS (Cornilescu *et al.*, 1999). Restraints were set at 1.5× the standard deviation yielded by TALOS (22.5° minimum). For hydrogen bonds, H–O distances were restrained to 1.7–2.5 Å and N–O distances to 2.7–3.5 Å. Structures were calculated using torsion angle simulated annealing with CNS (Brunger *et al.*, 1998). A total of 100 structures were calculated with the final set of restraints, and the 10 structures with the lowest NOE energy were selected.

4.3 Results

4.3.1 Resonance Assignments

Most of the cross-peaks in the ^{1}H-^{15}N HSQC spectra of syntaxin 1 (26-230) exhibited medium line widths, as expected for a 23 KDa protein, suggesting that syntaxin 1 (26-230) is a folded domain (Figure 4.1). However, cross-peak crowding was observed in the middle of the HSQC spectrum (Figure 4.1). The poor chemical dispersion is most likely due to the high percentage of α helix and the scarcity of aromatic residues, as also observed in the HSQC spectrum of N_{syx}, syntaxin 1A (27-146) (Fernandez *et al.*, 1998). A subset of the cross-peaks exhibited strong line broadening, suggesting that certain region of the syntaxin 1 closed

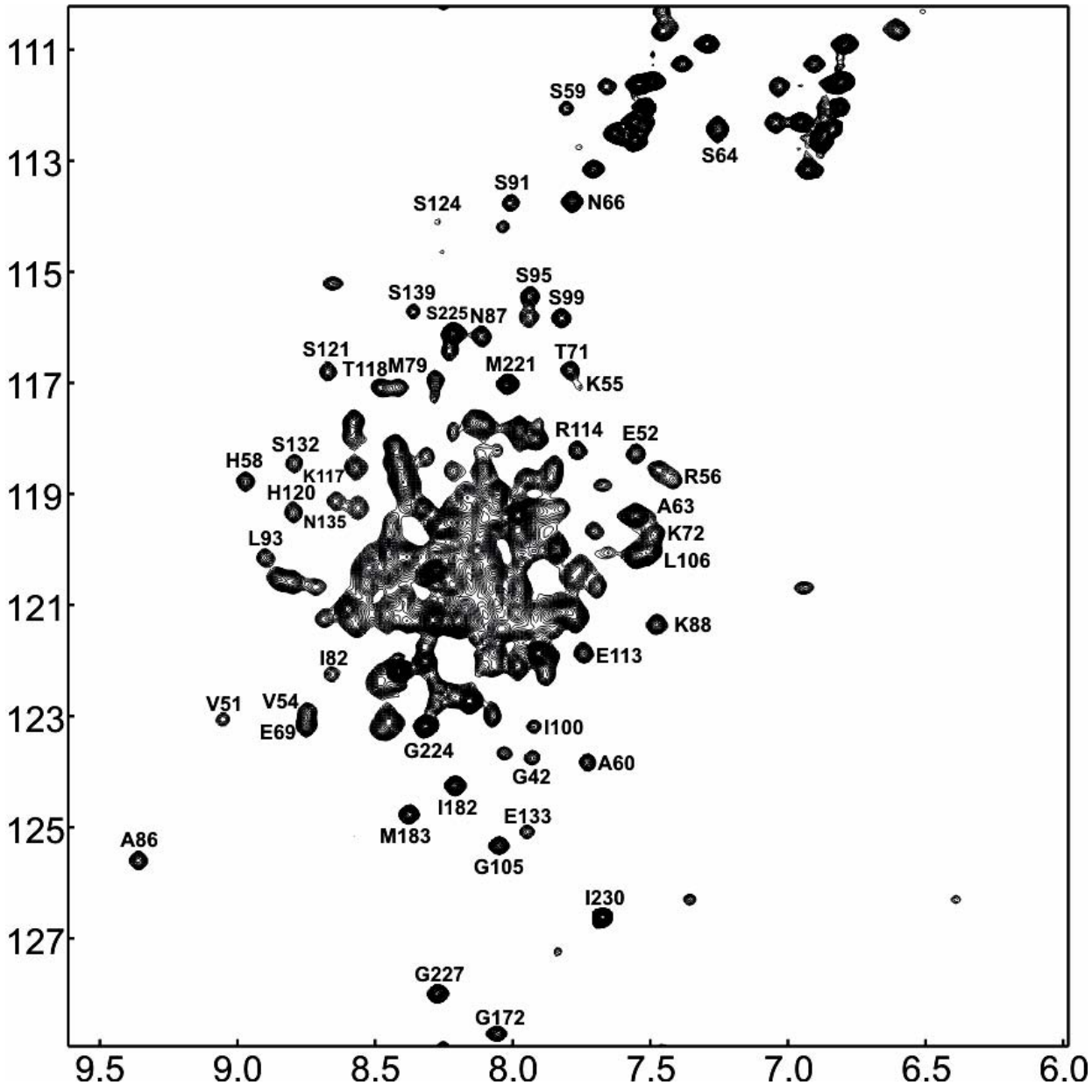

Figure 4.1 ^{1}H-^{15}N HSQC spectrum of syntaxin 1 (26-230). The assignments of the well-resolved cross peaks are shown.

conformation undergoes a slow chemical exchange process. This exchange process also resulted in broadening of the corresponding cross-peaks in the triple resonance and NOESY spectra, and thus hindered the full structure determination of the closed conformation of syntaxin 1.

Backbone assignments were mainly based on analysis of 3D ^{1}H, ^{15}N-NOESY-HSQC and 3D-(^{1}H, ^{15}N, ^{15}N) correlated-HSQC-NOESY-HSQC spectra, as well as a series of triple resonance spectra, including HNCA, HN(CO)CA, HN(CA)CB and HN(COCA)CB spectra. So far, I have already assigned the backbone of the entire N-terminal domain, part of the linker region (residues 171-182) and some of the SNARE motif region (residues 219-230) (Table 4.1). The assignments of the well-dispersed NH cross-peaks in the ^{1}H-^{15}N HSQC spectra of the closed syntaxin 1 are shown in Figure 4.1. The differences between the observed C_α chemical shifts and those expected for a random coil revealed downfield shifts in three regions (residues 26-62, 69-104, and 111-141) of the N-terminal domain (Figure 4.2), suggesting that the N-terminal domain within the closed conformation of syntaxin 1 adopts a similar three-helix structure as the isolated H_{abc} domain (Fernandez *et al.*, 1998). The C_α chemical shifts of the assigned residues in the linker region and the SNARE motif region also exhibited downfield shifts comparing to the random coil chemical shift values (Figure 4.2), indicating that these residues populate α-helical conformations (Wishart and Sykes, 1994).

4.3.2 Structure of the H_{abc} domain within the closed conformation of syntaxin 1

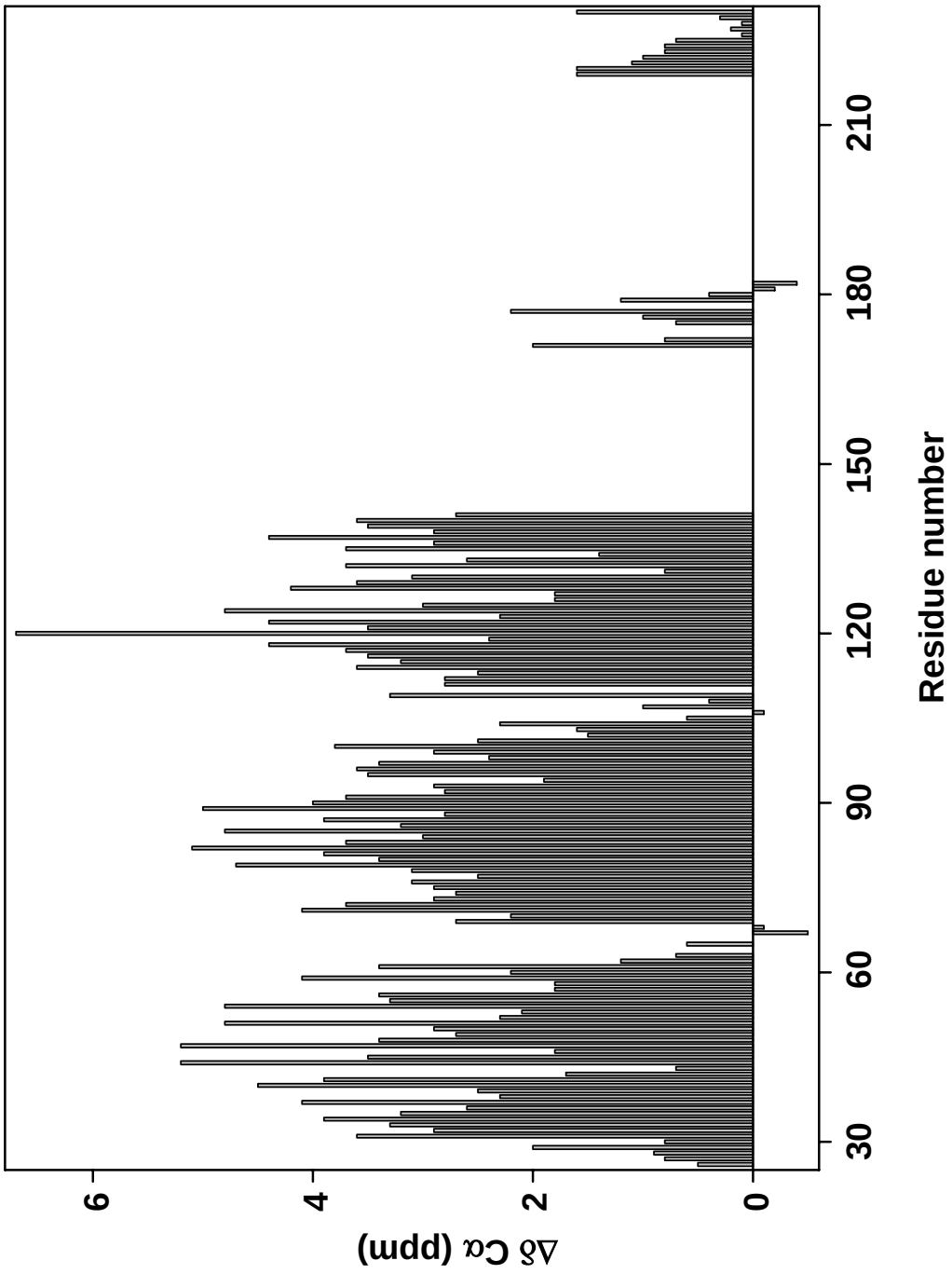

Figure 4.2

Figure 4.2 The H_{abc} domain within the closed syntaxin 1 is a three-helical domain. The differences ($\Delta\delta C\alpha$) between the observed $C\alpha$ chemical shifts and those expected for a random coil (Wishart and Sykes, 1994) are plotted as a function of residue number. Positive deviations indicate α helices. The residues that could not be assigned are left blank.

Structure calculations of the N-terminal domain of the closed syntaxin 1 were performed by simulated annealing using the structure of the isolated N-terminal domain of syntaxin 1 as initial model. A total of 1861 experimental NMR restraints were used to generate the final structures. A superposition of 10 structures with the fewest violations from the restraints is shown in Figure 4.3a. Ribbon diagrams of a representative structure in two different orientations are shown in Figure 4.3b and 4.3c.

The structure of the H_{abc} domain within the closed conformation of syntaxin 1 consists of an up-and-down three-helix bundle conformation, which resembles that of the isolated N-terminal domain (Fernandez *et al.*, 1998; Lerman *et al.*, 2000). A superposition of the current structure with the crystal structure of the isolated Habc domain (Lerman *et al.*, 2000) yields an r.m.s. deviation of 1.8 Å for 113 equivalent Cα carbons (Figure 4.4a). In addition, comparison of the structure of the H_{abc} domain within the syntaxin 1 closed conformation and that within the munc18-1-syntaxin complex showed that the two structures are also remarkably similar with an r.m.s. deviation 1.7 Å for 112 equivalent Cα carbons (Figure 4.4b). These results suggest that the H_{abc} domain of syntaxin 1 assumes the same conformation no matter whether it is isolated (Fernandez *et al.*, 1998; Lerman *et al.*, 2000), in the closed conformation, or within the munc18-1-syntaxin complex (Misura *et al.*, 2000). In addition, available data for the assigned residues in the linker region and the SNARE motif region of syntaxin 1 fit with the structure of syntaxin 1 observed in the munc18-1-syntaxin 1 complex. Thus, it is unlikely that munc18-1 binding causes conformation changes of the closed conformation of syntaxin 1. Indeed, a separate NMR study in our laboratory showed

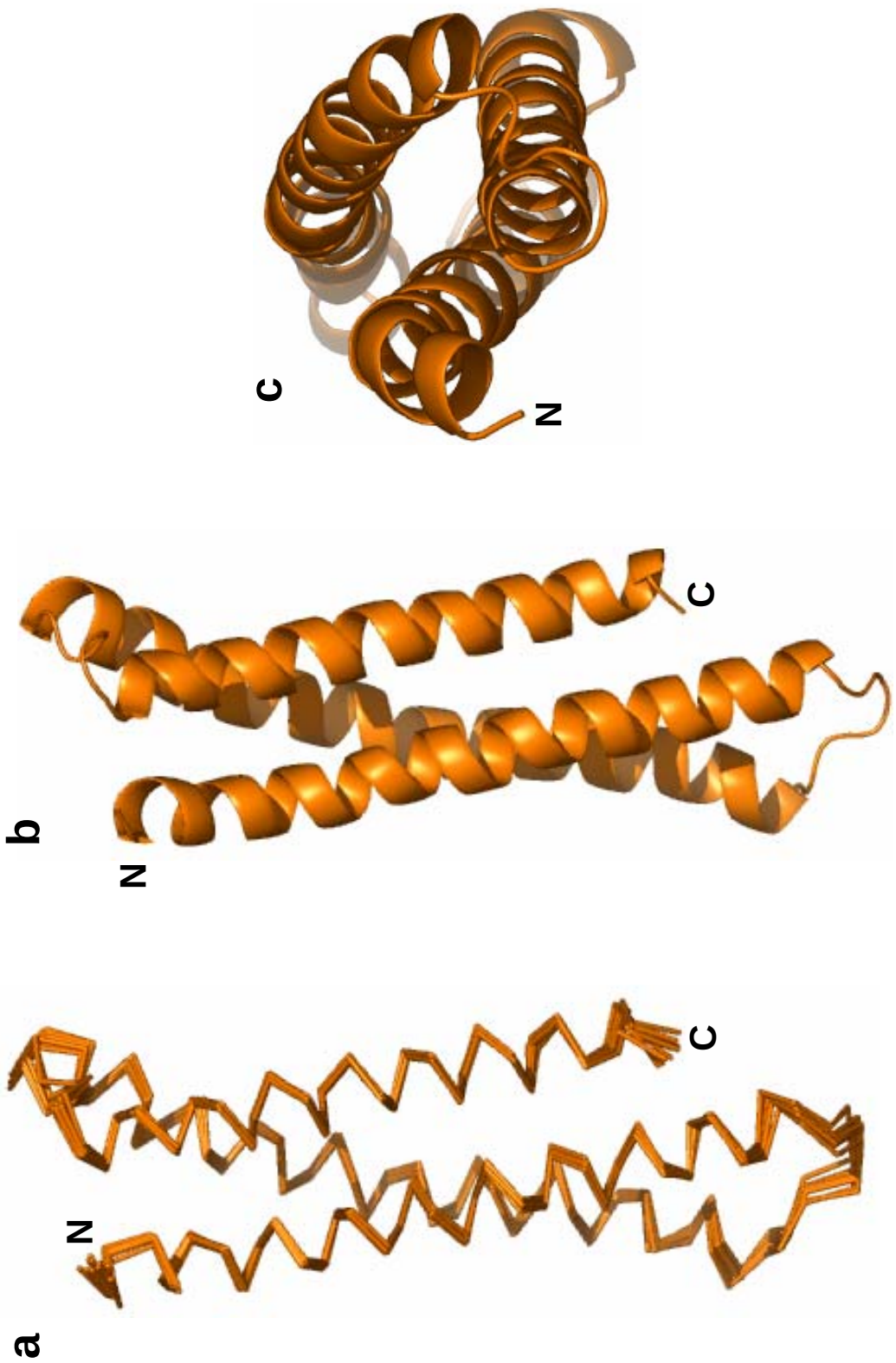

Figure 4.3

Figure 4.3 Structure of the H_{abc} domain within the closed syntaxin 1. (a) Backbone superposition of the 10 structures of the H_{abc} domain with fewest violations from the NMR restraints. (b and c) Ribbon diagrams of a representative structure of the H_{abc} domain within the closed syntaxin 1 in two different orientations. The orientation in (c) results from a 90^{o} rotation of the structure (b) around its horizontal axis. The positions of the N and C termini are indicated. The ribbon diagrams were generated with the program PyMOL.

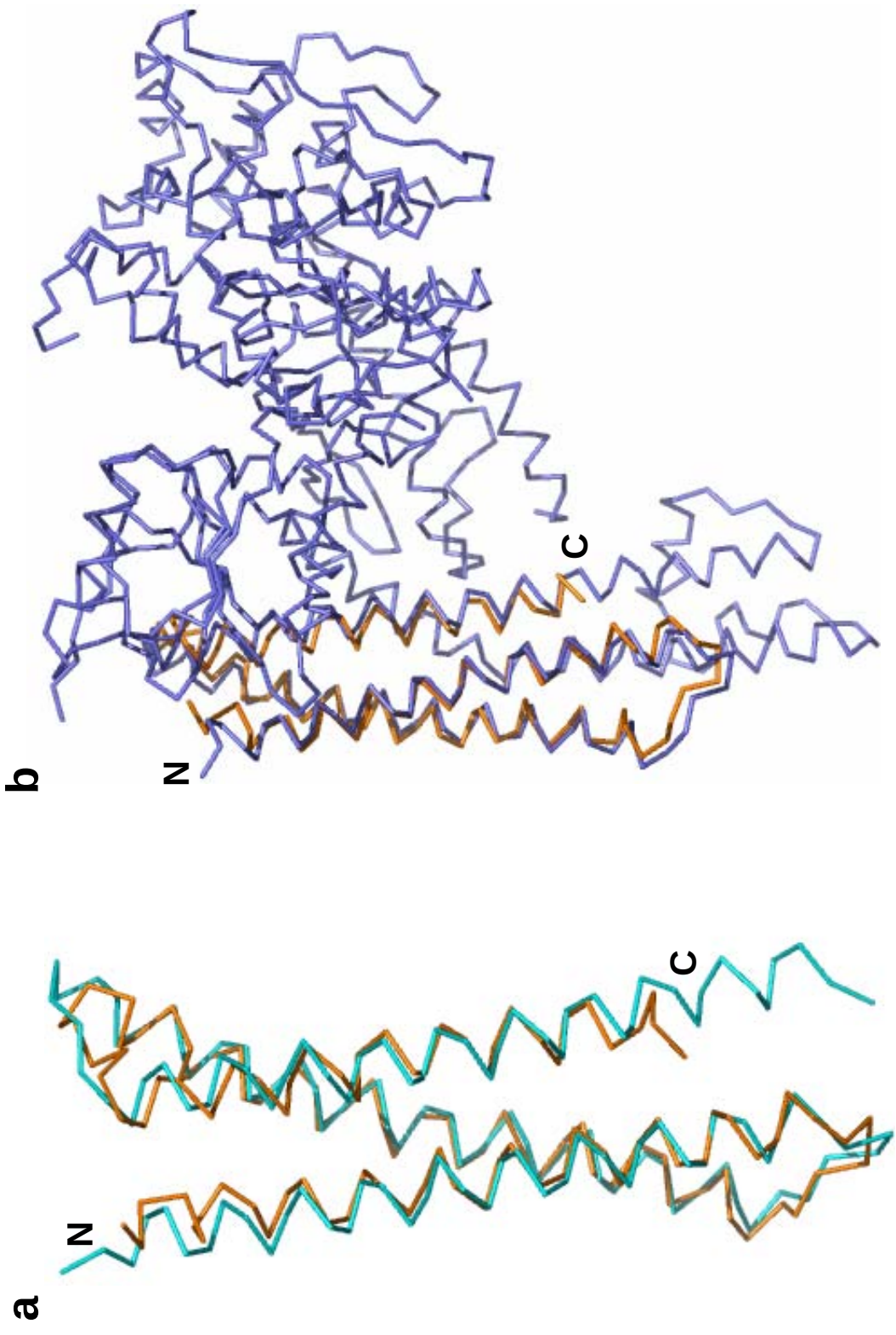

Figure 4.4

Figure 4.4 Comparison of the structures of the H_{abc} domain in isolation (Fernandez *et al.*, 1998), in the closed syntaxin and within the munc18-syntaxin complex (Misura *et al.*, 2000). (a) Superposition of the structure of the isolated H_{abc} domain (cyan) and the H_{abc} domain in the closed syntaxin (orange). (b) Superposition of the structure of the H_{abc} domain within the munc18-syntaxin complex (blue) and the H_{abc} domain in the closed syntaxin (orange). The positions of the N and C termini are indicated. The ribbon diagrams were generated with the program PyMOL.

that the ^{1}H-^{15}N TROSY-HSQC spectrum of the munc18-1-syntaxin complex with ^{2}H, ^{15}N-labeled syntaxin 1 revealed no shifts for cross-peaks from the syntaxin residues that are involved in formation of the closed conformation of syntaxin 1 but do not directly contact munc18-1, also suggesting that munc18-1 binding does not alter substantially the closed conformation of syntaxin 1 (our unpublished data). Of course, the definitive answer will come from further structure determination of the full closed syntaxin 1.

Table 4.1 ^{1}H, ^{15}N, ^{13}C chemical shifts of the H_{abc} domain in the closed conformation of syntaxin 1

26	arg	26.CA	26.CB														
		56.5	29.9														
27	asp	27.N	27.HN	27.CA	27.HA	27.CB	27.HB2	27.HB1									
		121.1	8.27	54.7	4.56	41	2.73	2.66									
28	arg	28.N	28.HN	28.CA	28.HA	28.CB	28.HB2	28.CG	28.HG2	28.CD	28.HD2						
		121.1	8.28	56.9	4.3	29.7	1.83	26.5	1.56	40.8	3.21						
29	phe	29.N	29.HN	29.CA	29.HA	29.CB	29.HB2	29.HD1									
		119.7	8.11	59.9	4.41	38.5	3.17	7.23									
30	met	30.N	30.HN	30.CA	30.HA	30.CB	30.HB2	30.CG	30.HG2	30.HG1							
		119.2	8.31	56	4.53	30.6	2.12	32.6	2.69	2.53							
31	asp	31.N	31.HN	31.CA	31.HA	31.CB	31.HB2	31.HB1									
		120.9	8.17	57.5	4.58	40.2	2.82	2.76									
32	glu	32.N	32.HN	32.CA	32.HA	32.CB	32.HB2	32.CG	32.HG2	32.HG1							
		120.2	8.3	59.2	4.07	28.9	2.08	36.5	2.42	2.25							
33	phe	33.N	33.HN	33.CA	33.HA	33.CB	33.HB2	33.HD1									
		121.5	8.04	61.2	4.18	38.4	3.05	6.84									
34	phe	34.N	34.HN	34.CA	34.HA	34.CB	34.HB2	34.HB1	34.HD1								
		117.4	8.55	61.8	4.05	37.4	3.26	3.12	7.46								
35	glu	35.N	35.HN	35.CA	35.HA	35.CB	35.HB2	35.HB1	35.CG	35.HG2	35.HG1						
		120.8	7.99	59.5	4.07	28.9	2.08	2.17	36.1	2.24	2.46						
36	gln	36.N	36.HN	36.CA	36.HA	36.CB	36.HB2	36.CG	36.HG2	36.HG1	36.HE21	36.HE22					
		120.3	7.78	58.6	4.1	28.2	1.93	34.1	2.51	2.34	7.28	6.78					
37	val	37.N	37.HN	37.CA	37.HA	37.CB	37.HB	37.CG2	37.HG21	37.CG1	37.HG11						
		119.4	8.09	66.3	3.26	31.1	2.08	20.7	0.85	22.6	0.31						
38	glu	38.N	38.HN	38.CA	38.HA	38.CB	38.HB2	38.CG	38.HG2								
		118.4	7.85	58.6	4.01	28.7	2.03	35.6	2.29								
39	glu	39.N	39.HN	39.CA	39.HA	39.CB	39.HB2	39.CG	39.HG2	39.HG1							
		121.1	7.76	58.8	3.74	29.5	1.99	36.5	2.01	1.68							
40	ile	40.N	40.HN	40.CA	40.HA	40.CB	40.HB	40.CG1	40.HG12	40.HG11	40.CD1	40.HD11	40.CG2	40.HG21			
		118.7	8.14	65.7	3.5	37.2	1.87	29.5	2	0.71	14.7	0.72	19.2	0.93			
41	arg	41.N	41.HN	41.CA	41.HA	41.CB	41.HB2	41.HB1	41.CG	41.HG2	41.HG1	41.CD	41.HD2				
		120.3	8.76	59.9	3.7	29.5	1.85	1.92	27.2	1.67	1.57	42.6	3.18				
42	gly	42.N	42.HN	42.CA	42.HA2												
		123.6	7.91	46.7	3.87												
43	phe	43.N	43.HN	43.CA	43.CB	43.HB2	43.HD1										
		121.8	7.86	58.6	38.4	2.91	7.06										
44	ile	44.N	44.HN	44.CA	44.HA	44.CB	44.HB	44.CD1	44.HD11	44.CG2	44.HG21						
		120.3	8.53	66.4	3.65	37.4	2.05	15.3	0.94	18.3	1.04						
45	asp	45.N	45.HN	45.CA	45.CB	45.HB2	45.HB1										
		119.9	8.36	57.4	39.7	2.83	2.68										
46	lys	46.N	46.HN	46.CA	46.HA	46.CB	46.HB2	46.HB1	46.CG	46.HG2	46.CD	46.HD2	46.CE	46.HE2			
		121.9	7.97	58.2	4.19	31.3	2.2	2.09	24.3	1.54	28.2	1.76	41.9	3			
47	ile	47.N	47.HN	47.CA	47.HA	47.CB	47.HB	47.CD1	47.HD11	47.CG2	47.HG21						

Table 4.1 ^{1}H, ^{15}N, ^{13}C chemical shifts of the H_{abc} domain in the closed conformation of syntaxin 1

		119.9	8.29	66.4	3.52	37.6	2.19	13.8	0.97	18.7	0.84						
48	ala	48.N	48.HN	48.CA	48.HA	48.CB	48.HB1										
		120.8	8.44	55.6	3.92	17.7	1.62										
49	glu	49.N	49.HN	49.CA	49.HA	49.CB	49.HB2	49.HB1	49.CG	49.HG2	49.HG1						
		119.3	8.22	59	4.09	29.3	2.16	2.24	35.9	2.45	2.28						
50	asn	50.N	50.HN	50.CA	50.CB	50.HB2											
		120	8.49	55.6	37.8	3											
51	val	51.N	51.HN	51.CA	51.HA	51.CB	51.HB	51.CG2	51.HG21	51.CG1	51.HG11						
		122.9	9.05	67	3.37	30.6	2.38	23.7	0.98	20.9	0.33						
52	glu	52.N	52.HN	52.CA	52.HA	52.CB	52.HB2	52.HB1	52.CG	52.HG2	52.HG1						
		118	7.53	58.6	4	29.1	2.17	2.27	35.7	2.42	2.28						
53	glu	53.N	53.HN	53.CA	53.HA	53.CB	53.HB2	53.HB1	53.CG	53.HG2	53.HG1						
		120	7.72	58.4	4.1	28.9	2.16	2.23	35.7	2.42	2.27						
54	val	54.N	54.HN	54.CA	54.HA	54.CB	54.HB	54.CG2	54.HG21	54.CG1	54.HG11						
		122.7	8.71	67	3.06	30.1	2.4	24.4	0.93	20.9	0.33						
55	lys	55.N	55.HN	55.CA	55.HA	55.CB	55.HB2	55.HB1	55.CG	55.HG2	55.CD	55.HD2	55.CE	55.HE2			
		116.8	7.75	59.7	3.83	32.6	2.06	1.87	26.1	1.57	30.2	1.72	41.9	3			
56	arg	56.N	56.HN	56.CA	56.HA	56.CB	56.HB2	56.HB1	56.CG	56.HG2	56.HG1	56.CD	56.HD2	56.HD1			
		118.4	7.4	59.4	4.11	29.9	2.09	1.88	28.5	1.61	1.89	43.2	3.2	3.3			
57	lys	57.N	57.HN	57.CA	57.CB												
		121.1	8.36	58.2	31.3												
58	his	58.N	58.HN	58.CA	58.HA	58.CB	58.HB2	58.HB1	58.HE2								
		118.4	8.97	57.3	4.01	31.5	3.26	2.74	5.68								
59	ser	59.N	59.HN	59.CA	59.HA	59.CB	59.HB2	59.HB1									
		111.8	7.8	62.2	4.03	62.9	2.08	1.92									
60	ala	60.N	60.HN	60.CA	60.HA	60.CB	60.HB1										
		123.6	7.73	54.4	4.21	18.1	1.59										
61	ile	61.N	61.HN	61.CA	61.HA	61.CB	61.HB	61.CG1	61.HG12	61.HG11	61.CD1	61.HD11	61.CG2	61.HG21			
		120.5	8.7	64.6	3.79	38.2	2.08	30.6	1.91	0.92	14.7	0.82	17.7	1.02			
62	leu	62.N	62.HN	62.CA	62.HA	62.CB	62.HB2	62.CD1	62.HD11	62.CD2	62.HD21						
		119.5	8.16	56.2	4.15	41.5	1.94	26.5	0.98	22.4	0.81						
63	ala	63.N	63.HN	63.CA	63.HA	63.CB	63.HB1										
		119.6	7.49	52.9	4.24	18.9	1.53										
65	pro	65.CA	65.HA	65.CB	65.HB2	65.CG	65.HG2	65.CD	65.HD2								
		63.6	4.42	31.8	2.28	26.7	1.99	50.3	3.85								
67	pro	67.CA	67.HA	67.CB	67.HB2	67.HB1	67.CG	67.HG2	67.HG1	67.CD	67.HD2						
		62.5	4.4	32	2.4	1.82	27.4	2.19	2	49.7	3.68						
68	asp	68.N	68.HN	68.CA	68.HA	68.CB	68.HB2										
		122	8.42	53.8	4.56	41.7	2.81										
69	glu	69.N	69.HN	69.CA	69.HA	69.CB	69.HB2	69.CG	69.HG2								
		123	8.74	59	3.94	29.3	2.01	35.9	2.4								
70	lys	70.N	70.HN	70.CA	70.HA	70.CB	70.HB2	70.CG	70.HG2	70.HG1	70.CD	70.HD2	70.HD1	70.CE	70.HE2	70.HE1	
		119.9	8.42	58.6	4.13	31.3	1.89	24.3	1.46	1.41	28.4	1.74	1.66	41.9	2.99	2.8	

Table 4.1 ^{1}H, ^{15}N, ^{13}C chemical shifts of the H_{abc} domain in the closed conformation of syntaxin 1

71	thr	71.N	71.HN	71.CA	71.HA	71.CB	71.HB	71.CG2	71.HG21								
		116.5	7.79	66.1	3.99	67.4	4.04	22.6	1.28								
72	lys	72.N	72.HN	72.CA	72.HA	72.CB	72.HB2	72.CG	72.HG2	72.HG1	72.CD	72.HD2	72.HD1	72.CE	72.HE2	72.HE1	
		119.6	7.48	60.1	3.9	31.6	1.97	25	1.61	1.39	29.3	1.65	1.7	41.2	2.93	2.82	
73	glu	73.N	73.HN	73.CA	73.HA	73.CB	73.HB2	73.HB1	73.CG	73.HG2	73.HG1						
		121	8.23	59.2	4.08	29.3	2.24	2.16	35.9	2.26	2.46						
74	glu	74.N	74.HN	74.CA	74.HA	74.CB	74.HB2	74.HB1	74.CG	74.HG2	74.HG1						
		120	8.51	59	4.08	29.1	2.24	2.16	35.9	2.45	2.26						
75	leu	75.N	75.HN	75.CA	75.HA	75.CB	75.HB2	75.CD1	75.HD11								
		120	8.1	57.9	4.09	41.2	1.39	26.5	1.04								
76	glu	76.N	76.HN	76.CA	76.HA	76.CB	76.HB2	76.HB1	76.CG	76.HG2	76.HG1						
		119.5	7.98	59.4	4.06	28.7	2.17	2.24	36.1	2.45	2.26						
77	glu	77.N	77.HN	77.CA	77.HA	77.CB	77.HB2	77.CG	77.HG2	77.HG1							
		120.3	8.21	58.8	4.09	28.9	2.16	35.7	2.46	2.28							
78	leu	78.N	78.HN	78.CA	78.HA	78.CB	78.HB2	78.CG	78.HG	78.CD1	78.HD11	78.CD2	78.HD21				
		121.3	8.02	58.1	4.05	42.8	2.05	27.1	1.77	25.6	0.81	23.9	0.91				
79	met	79.N	79.HN	79.CA	79.HA	79.CB	79.HB2	79.HB1	79.CG	79.HG2	79.HG1						
		116.8	8.39	59.9	3.91	32.4	1.97	1.86	31.1	2.77	2.86						
80	ser	80.N	80.HN	80.CA	80.HA	80.CB	80.HB2										
		116.7	8.26	61.5	4.31	62.2	4.08										
81	asp	81.N	81.HN	81.CA	81.HA	81.CB	81.HB2	81.HB1									
		123	8.42	57.8	4.46	41	2.82	2.65									
82	ile	82.N	82.HN	82.CA	82.HA	82.CB	82.HB	82.CG1	82.HG12	82.HG11	82.CD1	82.HD11	82.CG2	82.HG21			
		122.1	8.64	66.3	3.52	37.6	1.73	30.7	1.84	0.73	13.8	0.33	16.4	0.37			
83	lys	83.N	83.HN	83.CA	83.HA	83.CB	83.HB2	83.CG	83.HG2	83.HG1	83.CD	83.HD2					
		119.3	7.71	60.1	3.9	31.8	2.03	24.8	1.53	1.38	29.3	1.69					
84	lys	84.N	84.HN	84.CA	84.HA	84.CB	84.HB2	84.HB1	84.CG	84.HG2	84.HG1	84.CD	84.HD2	84.CE	84.HE2		
		118.3	8.39	59.4	4.05	32.4	1.97	1.87	25.2	1.63	1.42	29.3	1.69	41.5	2.94		
85	thr	85.N	85.HN	85.CA	85.HA	85.CB	85.HB	85.CG2	85.HG21								
		117.8	8.57	66.8	3.54	67.2	4.04	22.4	1.15								
86	ala	86.N	86.HN	86.CA	86.HA	86.CB	86.HB1										
		125.3	9.35	55.4	4.09	17.9	1.72										
87	asn	87.N	87.HN	87.CA	87.HA	87.CB	87.HB2	87.HB1									
		116	8.09	56.6	4.52	38.3	2.92	2.8									
88	lys	88.N	88.HN	88.CA	88.HA	88.CB	88.HB2	88.HB1	88.CG	88.HG2	88.HG1	88.CD	88.HD2	88.HD1	88.CE	88.HE2	88.HE1
		121.1	7.46	59.2	4.06	31.8	1.69	1.56	24.6	1.47	1.16	29.3	1.39	1.2	41.2	2.71	2.43
89	val	89.N	89.HN	89.CA	89.HA	89.CB	89.HB	89.CG2	89.HG21	89.CG1	89.HG11						
		119.2	8.23	67.2	3.21	30.9	1.72	25.2	1.02	20.5	0.05						
90	arg	90.N	90.HN	90.CA	90.CB												
		118	8.41	60	29.4												
91	ser	91.N	91.HN	91.CA	91.CB	91.HB2											
		113.6	7.98	61.8	62.7	4.03											
92	lys	92.N	92.HN	92.CA	92.HA	92.CB	92.HB2	92.CG	92.HG2	92.HG1	92.CD	92.HD2	92.CE	92.HE2			

Table 4.1 ^{1}H, ^{15}N, ^{13}C chemical shifts of the H_{abc} domain in the closed conformation of syntaxin 1

		122.7	8.25	59.2	4.08	31.9	1.89	24.8	1.57	1.46	28.9	1.69	41.5	2.95			
93	leu	93.N	93.HN	93.CA	93.HA	93.CB	93.HB2	93.CD1	93.HD11	93.CD2	93.HD21						
		119.7	8.88	57.9	4.14	40.8	1.49	22.9	0.78	26.1	0.6						
94	lys	94.N	94.HN	94.CA	94.HA	94.CB	94.HB2	94.CG	94.HG2	94.CD	94.HD2	94.CE	94.HE2				
		120.3	8.22	58.3	4.21	30.7	2.03	24.3	1.55	28	1.76	41.5	2.95				
95	ser	95.N	95.HN	95.CA	95.HA	95.CB	95.HB2										
		115.2	7.92	61.6	4.34	62.2	4.08										
96	ile	96.N	96.HN	96.CA	96.HA	96.CB	96.HB	96.CG1	96.HG12	96.HG11	96.CD1	96.HD11	96.CG2	96.HG21			
		121.9	7.86	64.8	3.93	38	2.16	28.5	1.97	1.29	13.4	0.75	17.5	1.08			
97	glu	97.N	97.HN	97.CA	97.HA	97.CB	97.HB2	97.CG	97.HG2								
		122.7	8.43	59.7	4.15	29.3	2.01	35.7	2.4								
98	gln	98.N	98.HN	98.CA	98.HA	98.CB	98.HB2	98.HB1	98.CG	98.HG2	98.HG1	98.HE21	98.HE22				
		117.8	8.41	58.4	4.12	28.2	2.13	2.25	34.1	2.57	2.42	7.53	6.8				
99	ser	99.N	99.HN	99.CA	99.HA	99.CB	99.HB2										
		115.6	7.8	61	4.32	62.3	4.08										
100	ile	100.N	100.HN	100.CA	100.HA	100.CB	100.HB	100.CG1	100.HG12	100.HG11	100.CD1	100.HD11	100.CG2	100.HG21			
		123	7.9	65	3.56	37.6	1.9	29.1	1.75	0.7	14.2	0.63	17.4	0.82			
101	glu	101.N	101.HN	101.CA	101.HA	101.CB	101.HB2	101.CG	101.HG2	101.HG1							
		119.2	8.03	58.8	4.07	29.3	2.09	35.9	2.4	2.23							
102	gln	102.N	102.HN	102.CA	102.HA	102.CB	102.HB2	102.CG	102.HG2	102.HG1	102.HE21	102.HE22					
		117.7	7.95	57.5	4.11	28.4	2.17	33.7	2.5	2.4	7.47	6.79					
103	glu	103.N	103.HN	103.CA	103.HA	103.CB	103.HB2	103.HB1	103.CG	103.HG2							
		119.7	7.83	57.9	4.1	29.3	2.05	2.16	36.3	2.24							
104	glu	104.N	104.HN	104.CA	104.HA	104.CB	104.HB2	104.HB1	104.CG	104.HG2	104.HG1						
		120.8	8.58	58.6	4	29.5	2.1	2.01	36.7	2.36	2.23						
105	gly	105.N	105.HN	105.CA	105.HA2												
		125	8.03	45.6	3.9												
106	leu	106.N	106.HN	106.CA	106.HA	106.CB	106.HB2	106.HB1	106.CG	106.HG	106.CD1	106.HD11	106.CD2	106.HD21			
		120	7.53	54.9	4.35	42.3	1.73	1.55	26.5	1.7	22.6	0.85	25	0.89			
107	asn	107.N	107.HN	107.CA	107.HA	107.CB	107.HB2	107.HB1	107.HD21	107.HD22							
		116.2	8.2	53.7	4.61	37.6	2.75	2.96	6.86	7.61							
108	arg	108.N	108.HN	108.CA	108.CB												
		119.3	8.08	56.4	30.2												
109	ser	109.N	109.HN	109.CA	109.CB												
		115.2	8.32	61.4	63.6												
111	ala	111.CA	111.CB														
		55	17.9														
112	asp	112.N	112.HN	112.CA	112.HA	112.CB	112.HB2	112.HB1									
		117.5	8.08	56.7	4.46	40.4	2.81	2.65									
113	leu	113.N	113.HN	113.CA	113.HA	113.CB	113.HB2	113.HB1	113.CD1	113.HD11	113.CD2	113.HD21					
		121.7	7.72	57.5	3.91	41.2	1.78	1.65	24.4	0.93	25.2	0.9					
114	arg	114.N	114.HN	114.CA	114.HA	114.CB	114.HB2	114.CG	114.HG2	114.HG1	114.CD	114.HD2					
		117.8	7.74	59.6	4.02	29.3	1.99	27.4	1.78	1.66	43	3.24					

Table 4.1 ^{1}H, ^{15}N, ^{13}C chemical shifts of the H_{abc} domain in the closed conformation of syntaxin 1

115	ile	115.N	115.HN	115.CA	115.HA	115.CB	115.HB	115.CG1	115.HG12	115.HG11	115.CD1	115.HD11	115.CG2	115.HG21			
		120.8	7.77	64.4	3.89	37.6	2.06	28.9	1.31	1.82	12.9	1.02	17.5	1.11			
116	arg	116.N	116.HN	116.CA	116.HA	116.CB	116.HB2	116.HB1	116.CG	116.HG2	116.CD	116.HD2	116.HD1				
		119	7.78	59.5	3.84	30	1.13	0.93	26.7	1.31	43.6	2.46	2.62				
117	lys	117.N	117.HN	117.CA	117.HA	117.CB	117.HB2	117.HB1	117.CG	117.HG2	117.HG1						
		118.3	8.55	60.1	4.03	32.4	2.04	1.86	25.9	1.66	1.53						
118	thr	118.HN	118.CA	118.HA	118.CB	118.HB	118.CG2	118.HG21									
		8.46	66.4	4.11	68.3	4.42	21.3	1.32									
119	gln	119.N	119.HN	119.CA	119.HA	119.CB	119.HB2	119.HB1	119.CG	119.HG2	119.HG1	119.HE21	119.HE22				
		121.1	8.56	58.4	4.22	27.8	2.3	2.37	33.7	2.85	2.46	7.37	6.94				
120	his	120.N	120.HN	120.CA	120.HA	120.CB	120.HB2	120.HB1									
		119	8.76	62.2	3.97	31.3	3.36	3.14									
121	ser	121.N	121.HN	121.CA	121.HA	121.CB	121.HB2	121.HB1									
		116.5	8.66	61.6	4.19	62.5	4.16	4.21									
122	thr	122.N	122.HN	122.CA	122.HA	122.CB	122.HB	122.CG2	122.HG21								
		118.4	8.38	66.4	3.98	68.5	4.32	21.1	1.28								
123	leu	123.N	123.HN	123.CA	123.HA	123.CB	123.HB2	123.HB1	123.CG	123.HG	123.CD1	123.HD11	123.CD2	123.HD21			
		121.4	8.3	57.3	3.99	42.8	1.92	1.86	26.3	1.98	25.9	0.86	22.2	0.82			
124	ser	124.N	124.HN	124.CA	124.HA												
		114.3	8.25	62.9	4.03												
125	arg	125.N	125.HN	125.CA	125.HA	125.CB	125.HB2	125.CG	125.HG2	125.HG1	125.CD	125.HD2					
		120.3	8.06	59	4.05	29.3	1.99	27.4	1.78	1.66	42.9	3.23					
126	lys	126.N	126.HN	126.CA	126.HA	126.CB	126.HB2	126.CG	126.HG2	126.CD	126.HD2	126.HD1	126.CE	126.HE2			
		119.5	7.95	58.2	4.21	31.6	2.04	24.8	1.62	28.2	1.78	1.66	42.5	2.88			
127	phe	127.N	127.HN	127.CA	127.CB	127.HD1											
		118.9	8.55	59.7	38.6	7.15											
128	val	128.N	128.HN	128.CA	128.HA	128.CB	128.HB	128.CG2	128.HG21	128.CG1	128.HG11						
		118.6	8.37	66.4	3.27	31.1	2.23	23.5	1.13	21.1	0.96						
129	glu	129.N	129.HN	129.CA	129.HA	129.CB	129.HB2	129.CG	129.HG2								
		121.9	8.47	59.9	4.01	29.3	2.16	36.1	2.25								
130	val	130.N	130.HN	130.CA	130.HA	130.CB	130.HB	130.CG2	130.HG21	130.CG1	130.HG11						
		119.9	8.22	65.3	4.04	31.5	2.18	22.6	1.18	21.1	1.09						
131	met	131.N	131.HN	131.CA	131.CB												
		118.3	8.19	56	28.5												
132	ser	132.N	132.HN	132.CA	132.HA	132.CB	132.HB2										
		118.3	8.78	61.8	4.25	62	3.98										
133	glu	133.N	133.HN	133.CA	133.HA	133.CB	133.HB2	133.CG	133.HG2	133.HG1							
		124.7	7.93	58.9	4.33	28.4	2.26	35.2	2.4	2.24							
134	tyr	134.N	134.HN	134.CA	134.HA	134.CB	134.HB2	134.HB1	134.HD1								
		122.1	8.46	59.4	4.44	36.9	3.41	3.24	7.05								
135	asn	135.N	135.HN	135.CA	135.HA	135.CB	135.HB2	135.HB1									
		118.9	8.65	56.4	4.13	38.4	2.97	2.75									
136	ala	136.N	136.HN	136.CA	136.HA	136.CB	136.HB1										

Table 4.1 ^{1}H, ^{15}N, ^{13}C chemical shifts of the H_{abc} domain in the closed conformation of syntaxin 1

		123	8.43	55.1	4.16	17.7	1.58										
137	thr	137.N	137.HN	137.CA	137.HA	137.CB	137.HB	137.CG2	137.HG21								
		117	8.26	66.4	4.22	68.2	4.56	21.3	1.42								
138	gln	138.N	138.HN	138.CA	138.CB												
		120.8	8.14	58.9	28.8												
139	ser	139.N	139.HN	139.CA	139.HA	139.CB	139.HB2										
		115.5	8.37	61.6	4.12	62.2	3.98										
140	asp	140.N	140.HN	140.CA	140.HA	140.CB	140.HB2										
		122.4	8.2	57.5	4.41	41.6	2.83										
141	tyr	141.N	141.HN	141.CA	141.CB												
		120.2	8.06	60.7	37.9												
171	ser	171.N	171.HN	171.CA	171.CB												
		113.9	7.68	60.1	64.1												
172	gly	172.N	172.HN	172.CA													
		128.5	8.06	45.8													
175	ala	175.N	175.HN	175.CA	175.CB												
		120.8	8	52.9	18.2												
176	ile	176.N	176.HN	176.CA	176.CB												
		118.1	7.49	62.2	37.9												
177	phe	177.N	177.HN	177.CA													
		118.7	8.06	60.1													
179	ser	179.CA	179.CB														
		59.3	64														
180	gly	180.N	180.HN	180.CA													
		128.8	8.24	45.4													
181	ile	181.N	181.HN	181.CA	181.CB												
		119.7	7.82	61	38.2												
182	ile	182.N	182.HN	182.CA	182.CB												
		125.2	8.18	60.8	37.9												
219	met	219.N	219.HN	219.CA	219.CB												
		119.3	7.98	56.8	32.5												
220	ala	220.N	220.HN	220.CA	220.CB												
		122.5	8.13	53.8	18.1												
221	met	221.N	221.HN	221.CA	221.CB												
		117	8	56.3	32.1												
222	leu	222.N	222.HN	222.CA	222.CB												
		121.8	7.9	56	41.5												
223	val	223.N	223.HN	223.CA	223.CB												
		119.3	7.97	63	32.1												
224	glu	224.N	224.HN	224.CA	224.CB												
		123.1	8.31	57.1	29.7												
225	ser	225.N	225.HN	225.CA	225.CB												
		116.1	8.22	58.8	63.9												

Table 4.1 ^{1}H, ^{15}N, ^{13}C chemical shifts of the H_{abc} domain in the closed conformation of syntaxin 1

226	gln	226.N	226.HN	226.CA	226.CB												
		121.8	8.32	56.1	28.9												
227	gly	227.N	227.HN	227.CA													
		127.8	8.25	45.2													
228	glu	228.N	228.HN	228.CA	228.CB												
		120.2	8.26	56.4	30												
229	met	229.N	229.HN	229.CA	229.CB												
		121.9	8.39	55.5	32.3												
230	ile	230.N	230.HN	230.CA	230.CB												
		126.5	7.66	62.8	39.1												

CHAPTER 5 ARE NEURONAL SNARE PROTEINS CA^{2+} SENSORS?

5.1 Introduction

One important aspect of neurotransmitter release is the tight regulation by Ca^{2+} (Goda and Stevens, 1994; Südhof, 1995). The mechanism of Ca^{2+} dependent exocytosis has been extensively studied (Südhof, 1995). There are two components of release: a fast component (in 20-30 ms time scale) that accounts for >90% of total release, and a slow component (in 200-300 ms time scale) that mediates <10% of total release (Goda *et al.*, 1994).

Through previous chapters, it has been emphasized that the SNAREs play a central role in synaptic vesicle exocytosis (Chen and Scheller, 2001; Rizo *et al.*, 2002) and the formation of the SNARE complex brings the synaptic vesicle and plasma membranes in close proximity and might cause membrane fusion (Hanson et al., 1997). However, formation of the core complex in solution is Ca^{2+} independent (Sollner *et al.*, 1993a). Thus, the linkage between Ca^{2+} triggering and SNARE function is unclear. Several observations have suggested that the SNAREs may act in a late stage in exocytosis, perhaps during the Ca^{2+} triggering step. Mutation or deletion of synaptobrevin or SNAP-25 in *Drosophila* and mice leads to more severe defects in Ca^{2+}-induced fusion than Ca^{2+} independent fusion (Broadie et al., 1995; Deitcher et al., 1998; Quetglas et al., 2000; Schoch et al., 2001; Washbourne et al., 2002), while decreasing the level of synaptobrevin and syntaxin in *Drosophila* reduces the Ca^{2+} cooperativity of neurotransmitter release (Stewart *et al.*, 2000). The blockage of

secretion in PC12 cells caused by specific proteolysis of SNAP-25 at residues R180-I181 by type E botulinum neurotoxin can be rescued by supplying a peptide spanning the C-terminal SNARE motif of SNAP-25. However, the rescue requires the presence of peptide in the Ca^{2+} triggering stage of these assays (Chen et al., 1999). In addition, inhibition of exocytosis by type A botulinum neurotoxin, which cleaves SNAP-25 at Q197-R198, can be partially reversed by increasing the neuronal Ca^{2+} concentration (Banerjee et al., 1996; Gerona et al., 2000).

Recent studies by Neher and coworkers showed that overexpression of a SNAP-25 mutant with a double residue mutation (E170A/Q177A) decreases the Ca^{2+}-cooperativity of secretion in chromaffin cells (Sorensen et al., 2002). These results suggest that two residues of SNAP-25, E170 and Q177, might participate in Ca^{2+} binding during exocytosis. Indeed, the surface of the core complex is decorated with multiple acidic residues that could act as Ca^{2+} ligands (Sutton et al., 1998). However, the potential presence of Ca^{2+} binding sites in the core complex has not been directly tested. The crystal structure of the core complex revealed several bound Sr^{2+} ions, but the relevance of this observation is unclear given the high Sr^{2+} concentrations present in the crystals (70mM; Sutton *et al.*, 1998). In addition, some of the strontium ions were located at the interface between two core complexes or bound electrostatically. More recently, three Ca^{2+}-binding sites were observed in the crystal structure of a truncated SNARE complex, but they occurred at the interface between two complexes (Ernst and Brunger, 2003), and thus, the observed Ca^{2+}-binding sites most likely

arise from the crystallization conditions. Therefore, it is still unclear whether the core complex has intrinsic ability to bind Ca^{2+} and play a direct role in the Ca^{2+} triggering step.

To understand the mechanism of Ca^{2+}-triggered neurotransmitter release, it is very important to clarify the Ca^{2+} binding properties of the core complex. In the present study, I have analyzed whether Ca^{2+} directly binds to the core complex using NMR spectroscopy. The results show that the surface of the core complex contains several low-affinity Ca^{2+} binding sites and most of these sites also bind Mg^{2+} with similar affinity. Hence, it is unlikely that the core complex itself functions as a Ca^{2+} sensor. Since it has been shown that synaptotagmin 1, a Ca^{2+} sensor in neurotransmitter release (Geppert *et al.*, 1994; Bennett, 1999; Fernandez-Chacon *et al.*, 2001), interacts with the SNAREs (Südhof, 2002; Chapman, 2002), we further explored the possibility that the phenotype observed for the mutant SNAP25 (E170A/Q177A) in chromaffin cells (Sorensen et al., 2002) might be due to disruption of synaptotagmin 1/core complex interactions. However, our GST pull-down assays showed that the mutant doesn't affect either Ca^{2+}-dependent or Ca^{2+}-independent interactions between the SNARE complex and synaptotagmin 1. Instead, I found that the E170A/Q177A mutation in SNAP-25 hinders the assembly of SDS-resistant core complexes. In summary, these results indicate that the core complex does not directly participate in Ca^{2+} sensing; however, together with the effect of SNAP25 E170A/Q177A on the Ca^{2+}-dependence of secretion, our data suggest that the assembly of the core complex is tightly coupled with Ca^{2+}-triggering of release.

5.2 Material and Methods

5.2.1 Recombinant Protein Preparation

The expression and purification steps of the SNARE motifs of Syntaxin 1A (residues 191-253), synaptobrevin 2 (residues 29-93) and SNAP-25 (residues 11-82-W and 141-203-W) are essentially the same as described in chapter 2.

The double residue mutation E170A/Q177A was introduced into the wildtype SNAP25 expression vector (a gift from Thomas C Südhof's laboratory) or the wildtype SNC plasmid with in vitro site-directed mutagenesis. The Quikchange^{TM} Site-directed Mutagenesis Kit (Stratagene) provides a simple and fast procedure to generate mutant DNA. Since E170 and Q177 are only six residues apart, one pair of synthetic oligonucleotide primers was designed covering the mutation region with both intended substitutions. The oligonucleotide primers were then extended during a temperature cycle. After the temperature cycling, the product was treated with *Dpn* I to specifically digest the parental DNA template that is methylated or hemimethylated, while leaving the newly synthesized DNA untouched. The resulting product was then transformed into *E. coli* XL1-Blue supercompetent cells to repair the nicks and amplify the DNA. The plasmids encoding the desired mutations were purified with Qiagen Plasmid Miniprep Kit and the mutations were verified by DNA sequencing.

The expression and purification procedures for SNC (Q170A/E177A) are essentially the same as those for wild type SNC (see chapter 2). The GST fusion wild type and mutant

SNAP-25 were expressed in *E.coli* BL21 (DE3), isolated by affinity chromatography on glutathione Sepharose 4B (Amersham Pharmacia Biotech.) and cleaved with thrombin (from bovine plasma, Sigma) with the same protocols as those for SNARE motifs (details described in chapter 2). The proteins were then eluted with 20 mM Tris buffer (pH7.4) and further purified with a Mono Q column (Amersham Pharmacia Biotech.). The purity of the preparation was assessed by SDS-PAGE and Coomassie blue staining.

5.2.2 SNARE Complex Preparation and NMR Spectroscopy

Four wildtype SNARE complexes, where each SNARE motif was individually ^{2}H, ^{15}N labeled, were prepared for Ca^{2+} and Mg^{2+} binding experiments. The procedures of preparing the SNARE complex are the same as those mentioned in chapter 2. The SNARE complex samples were prepared in 20 mM Tris (pH7.5) buffer containing 200 mM NaCl with a protein concentration of 150 *u*M. The mutant SNARE complex containing SNC (E170A/Q177A) with ^{2}H, ^{15}N labeled syntaxin SNARE motif for ^{1}H, ^{15}N TROSY-HSQC experiments was prepared in the same manner and the final mutant complex contained 100 *u*M protein in 20 mM Tris (pH7.5) buffer with 200 mM NaCl. All NMR experiments were performed on Varian INOVA500 or INOVA600 spectrometers at 32 ^{o}C. All NMR data were processed with the program NMRPipe (Delaglio et al., 1995) and analyzed with the program NMRView (Johnson *et al.*, 1994).

5.2.3 GST Pull-down Assay

The GST pull-down assay was performed in collaboration with Jiong Tang in the Südhof laboratory. Recombinant GST-fusion SNAP-25 and E170A/Q177A SNAP-25 proteins (6.25 μg) were immobilized on 10 μl of Glutathione Sepharose beads (Amersham Pharmacia Biotech.) for 3.5h at 4 ^{o}C. After washing the beads once with Buffer A (50 mM Hepes, 100 mM NaCl, 4 mM EGTA. pH 7.2, and 0.1% Triton (X-100), syntaxin (180-264) and synaptobrevin (1-96) were added to form different complexes at 4 ^{o}C for overnight incubation. The molar ratios of syntaxin fragment and synaptobrevin fragment to GST-SNAP25A were 1:2.5:3. Beads were washed twice with binding buffer (50mM Hepes, 100mM NaCl, 4mM EGTA and 0.1% TritonX-100, pH 7.2, with or without 1mM free CaCl2) before adding a recombinant synaptotagmin 1 fragment, which contains the two C_2-domains of synaptotagmin 1 (C_2AB fragment). Binding was carried out at 4 ^{o}C for 2 hours followed by washing beads three times with the same binding buffer. Proteins were then eluted with 40 μl 20 mM EGTA at RT for 10 minutes. Half of the proteins were loaded on SDS-PAGE gel and followed by Coomassie Brilliant Blue staining. All reactions are performed in 200 μl total volume.

5.2.4 Core Complex Assembly Assays

Stoichiometric amounts of purified SyxS, Syb2, SNN and wildtype SNC or mutant SNC (E170A/Q177A) were mixed quickly at room temperature to a final concentration of 10 uM in 20 mM sodium phosphate buffer (pH7.5) containing 150 mM NaCl. Aliquots (10uL) were taken 1 min, 5 min, 20min, and 1 hour after mixing, diluted immediately with SDS sample buffer and frozen for subsequent analysis by SDS-PAGE. The rest of the reaction mixtures

were incubated at 4 ^{o}C overnight, and two 10 ul aliquots were diluted with SDS sample buffer for analysis with and without boiling. All samples were then analyzed by SDS-PAGE followed by Coomassie Brilliant Blue staining. The assembly assays with the full length SNAP-25 were performed with essentially the same procedure, except that the isolated SNARE motifs of SNAP-25 were replaced with the full length wild type SNAP-25 or the mutant SNAP-25 (E170A/Q177A).

5.2.5 Thermal Denaturation

Thermal denaturation curves were recorded on an Aviv model 62DS spectropolarimeter using a 1mm path length cell monitoring the CD absorption at 222 nm. The core complex samples for thermal denaturation were the same samples obtained after overnight assembly as described above. The fraction of unfolded protein at each temperature was calculated by using the formula $(I_{obs} - I_f)/(I_u - I_f)$, where I_{obs} is the observed signal intensity, and I_u and I_f are the signal intensities of the unfolded and folded states, respectively. I_u and I_f were calculated by extrapolation of the linear regions of the unfolding curves.

5.3 Results

5.3.1 Ca^{2+} binding sites of the SNARE complex

The ^{1}H-^{15}N TROSY-HSQC experiment is also a useful tool to analyze Ca^{2+} binding sites in a protein or protein complex (Ubach et al., 1998), in addition to studying protein-protein interaction (see chapter 3). As explained in chapter 3, each cross-peak in a ^{1}H-^{15}N TROSY-

HSQC spectrum corresponds to one NH group for each nonproline residue in a ^{15}N labeled protein. Ca^{2+} has a strong effect on the NH groups that are near the Ca^{2+} binding sites, resulting in either changes of the chemical shifts or broadening of the resonance signal due to chemical exchange (Ubach et al., 1998). Thus, the binding sites can be easily identified according to the cross-peak movement or the decrease of the cross-peak intensity upon adding Ca^{2+}.

To investigate the potential presence of Ca^{2+}-binding sites in the core complex, I prepared four core complex samples where only one of the SNARE motifs was ^{2}H, ^{15}N labeled. The ^{1}H-^{15}N TROSY-HSQC experiments were then used to monitor Ca^{2+} binding to each SNARE motif. Comparing the HSQC spectra of the core complexes in the absence and presence of Ca^{2+}, we observed substantial cross-peak shifts for the SyxS (Figure 5.1a) and SNN SNARE motifs (Figure 5.1c), while the Syb2 SNARE motif exhibited less and smaller changes (Figure 5.1b). There was only one cross-peak that underwent large movement for the SNC helix. However, several cross-peaks broadened beyond detection (Figure 5.1d), presumably because of some slow chemical exchange process induced by Ca^{2+} binding.

The largest chemical shift changes were mapped onto the crystal structure of the core complex. Based on the space arrangement, the changes can be grouped into four regions (Figure 5.2a). Potential Ca^{2+} ligands are illustrated in each region (Figure 5.2b, 5.2c, 5.2d and 5.2e). The abundance of ligands in some of them suggested that they could have more than one binding site. To distinguish different binding sites in each region and obtain the Ca^{2+}

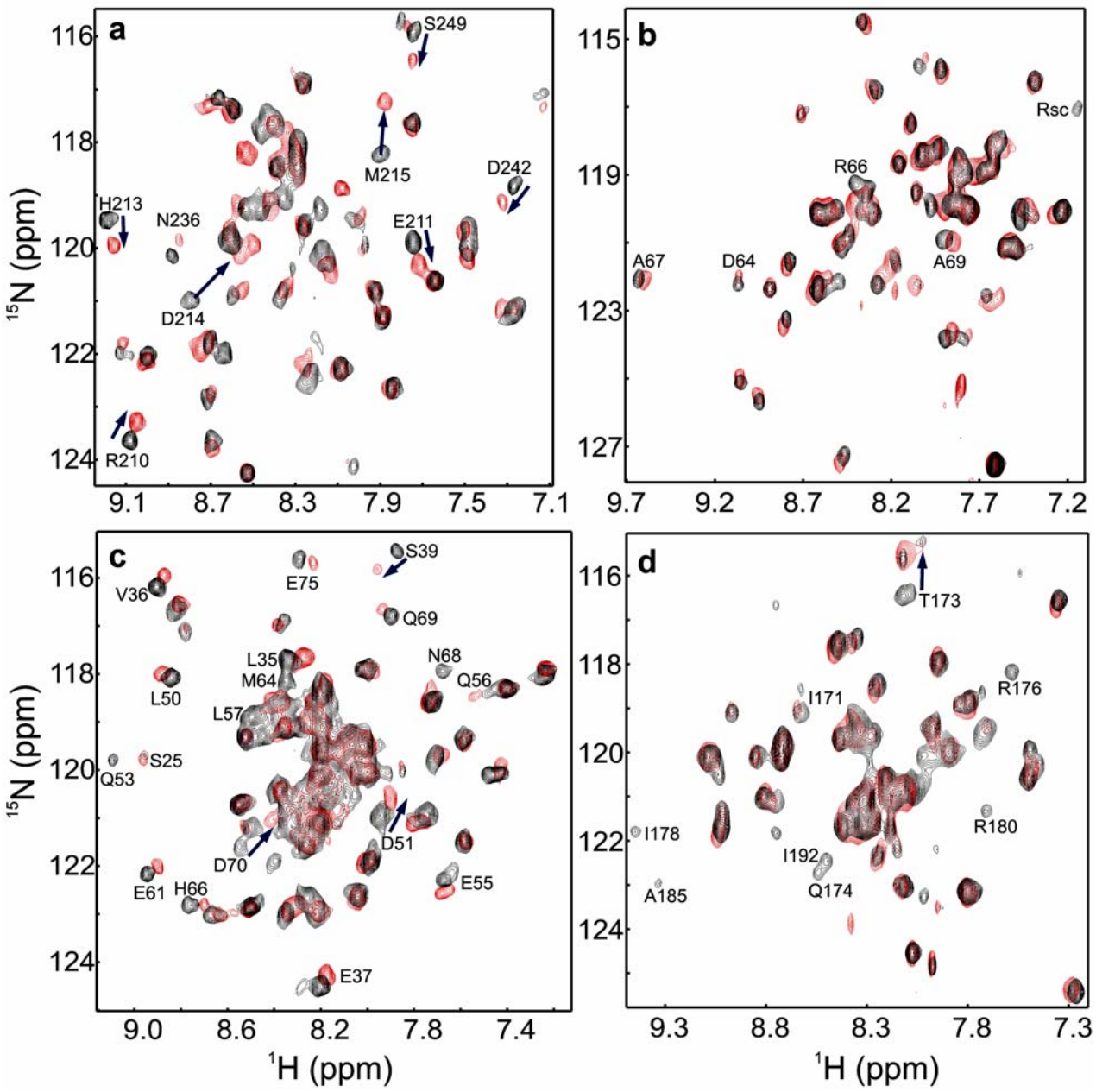
a
S249
M215
D242
H213
N236
E211
D214
R210
b
Rsc
R66
A67
D64
A69
c
S39
E75
V36
Q69
L35
M64
N68
Q56
L50
L57
S25
Q53
D51
D70
E61
H66
E55
E37
d
T173
I171
R176
I178
R180
I192
Q174
A185
15N (ppm)
1H (ppm)

Figure 5.1

Figure 5.1 Ca^{2+}-induced changes in the ^{1}H-^{15}N TROSY-HSQC spectra of the core complex. ^{1}H-^{15}N TROSY-HSQC spectra of the core complex with the SyxS (a), Syb2 (b), SNN (c) and SNC (d) SNARE motifs ^{2}H,^{15}N-labeled in the absence of Ca^{2+} (black contours) and in the presence (red contours) of 20 mM Ca^{2+} (a,c,d) or 30mM Ca^{2+} (b) are shown. The assignments of the cross-peaks with large movements are indicated. Arrows illustrate some of the Ca^{2+}-induced cross-peak shifts. Arginine sidechain NH groups are indicated by 'Rsc'.

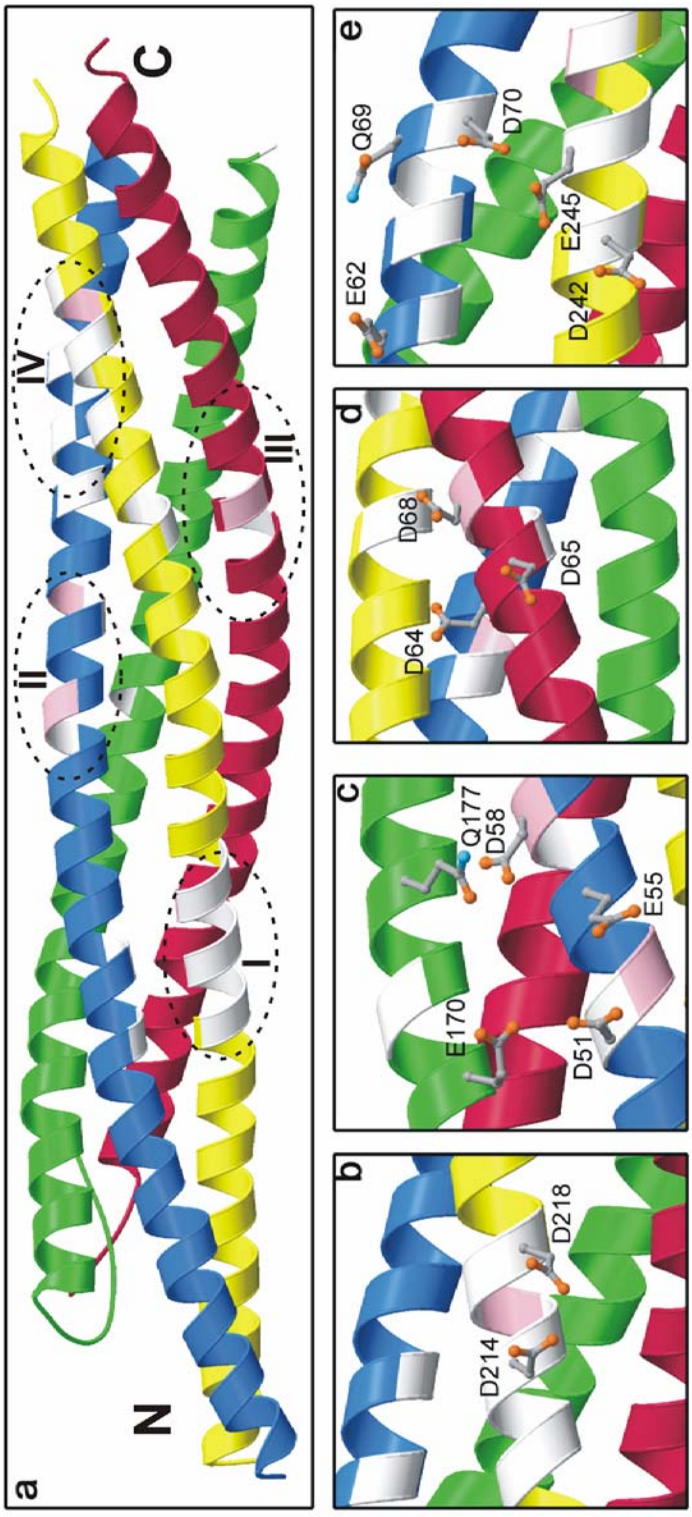
a
N
C
I
II
III
IV
b
D214
D218
c
E170
Q177
D58
D51
E55
d
D64
D68
D65
e
E62
Q69
D70
D242
E245

Figure 5.2

Figure 5.2 Ca^{2+} binding regions in the core complex. (a) Ribbon diagram of the crystal structure of the core complex (Sutton *et al.*, 1998; PDB accession number 1SFC). The color coding is as follows: SyxS, yellow; Syb2, red; SNN, blue; SNC, green. For each helix, residues whose NH group has a Ca^{2+}-induced chemical shift change are colored in white. Residues in the Ca^{2+} binding regions that could not be assigned or could not be monitored due to cross-peak overlap are colored in pink. Four Ca^{2+} binding regions are labeled by dotted circles. (b,c,d,e) Close-ups of each Ca^{2+} binding region showing the potential Ca^{2+} binding ligands. The corresponding side chains are displayed as ball-and-stick models with oxygen atoms in orange and nitrogen atoms in blue. The figure was prepared with the program Molscript (Kraulis, 1991).

binding affinities, I then carried out Ca^{2+} titration experiments monitored by ^{1}H-^{15}N TROSY-based HSQC spectra for each helix except synaptobrevin, for which the Ca^{2+}-induced chemical shift changes couldn't be monitored, because either the movements are too small or the cross-peaks are in the crowded region. The results are summarized in table 5.1 and typical movements of individual cross-peak during the titrations are shown in Figure 5.3. The Ca^{2+} binding regions of the core complex are discussed separately in the following sections.

- *Region I*

The first region locates at the N-terminal part of the core complex, including residues 210-218 of the SyxS SNARE motif and residues 35 and 39 of the SNN SNARE motif. It has been shown that the sidechains of Asp214 and Asp218 of Syx nicely form one Sr^{2+} binding site in the crystal structure of the SNARE complex (Figure 5.1b). Comparing with the other three regions, residues in region I have the largest chemical shift changes upon adding Ca^{2+}. The corresponding cross-peaks moved linearly from the positions of the Ca^{2+} free state to those of the Ca^{2+} bound state, suggesting one Ca^{2+} binds to this region. As an example, Figure 5.3a illustrates the movement of SyxS Met215 HSQC cross-peak, which is mainly in its nitrogen dimension. The dependence of its ^{15}N chemical shift on the Ca^{2+} concentration is plotted and fitted to a standard protein-ligand equilibrium curve with a dissociation-constant (K_D) around 15 mM (Figure 5.3e). Consistently, analyses of all the other residues of Syntaxin 1A in the region I yielded a similar result with an average K_D value of 14 mM (Table 5.1). To summarize, the sidechains of Asp214 and Asp218 of Syntaxin 1 form a weak Ca^{2+} binding site in region I.

- *Region II*

The second region is around the zero-layer, which is a highly conserved polar layer formed by three glutamines and one arginine that are buried in the middle of hydrophobic layers (Figure 5.6; Sutton *et al.*, 1998). Sr^{2+} binds to this region differently in the three independent complexes in the asymmetric unit of the crystals of the isolated SNARE complex. One of the SNARE complexes binds three strontium ions simultaneously with the sidechains of Asp51, Glu52 and Glu55 of SNAP-25. In another SNARE complex, only one Sr^{2+} is bound by the sidechains of Asp58, Glu170 and Gln177 of SNAP-25 and the third SNARE complex doesn't bind strontium at all.

Our NMR study shows that Ca^{2+} binds to the interface between the two helices of SNAP-25 at this region. Potential ligands include Asp51, Glu55 and Asp58 of SNAP-25N and Glu170 and Gln177 of SNAP-25C (Figure 5.2c). The cross-peaks corresponding to the residues in region II moved along a straight line with the increase of Ca^{2+} concentration in the titration experiment, indicating that either the region binds only one Ca^{2+} ion or multiple Ca^{2+} ions bind to this region with similar affinities. The dependence of the chemical shifts of individual residues on the Ca^{2+} concentration can be fit to standard protein-ligand equilibrium curves with a single binding site. Analyses of all the residues in this region yielded very similar dissociation constants with an average K_D of 3.7 mM. Figure 5.3b depicts the evolution of the residue T173 of SNAP-25, which is right in the middle of the cavity, and curve fitting of the data is shown in Figure 5.3f. However, given the abundance of

potential Ca^{2+} ligands in this region we cannot completely rule out the possibility of multiple Ca^{2+} binding sites with very similar affinities.

- *Region III*

Right next to the zero-layer, a third region is mainly formed by three aspartates (Asp64, Asp65 and Asp68) of synaptobrevin. Looking at the geometry of the three aspartate sidechains in the crystal structure of SNARE complex, we can see that they form a relatively small pocket (Figure 5.2d). This site has been found to bind various cations in different crystal forms of the SNARE complex, such as, Sr^{2+} in the SNARE complex (Sutton *et al.*, 1998) and Mg^{2+} in the complexin/SNARE complex (Chen *et al.*, 2002). As described before, the HSQC spectra of synaptobrevin only exhibited minor changes upon adding Ca^{2+}. However, residue N236 and residue A237 of Syntaxin 1A, which point right towards this region, showed large Ca^{2+}-induced changes, suggesting that this site is indeed affected by Ca^{2+} in solution. The binding affinity can be estimated based on the dependence of ^{15}N chemical shift of residue N236 of Syntaxin 1A on the Ca^{2+} concentration (Figure 5.3c and 5.3g), and the affinity is around 8.3 mM.

- *Region IV*

The last region with substantial Ca^{2+}-induced changes contains residues 240-249 of Syntaxin 1A and residues 63-70 in the SNAP-25N. This region is part of the oligomerization interface in the crystal structure of the SNARE complex, and several Sr^{2+} ions have been found to bind to this region between two SNARE complexes. The relevance of these Sr^{2+} binding sites is

unclear given the fact that the core complex does not oligomerize in solution under the conditions of my NMR experiments (Chen *et al.*, 2002). The NMR study shows that Ca^{2+}-induced changes span a big area. Several acidic residues in this region, including Asp242, Glu245 of Syntaxin 1A and Glu62, Gln69 and Asp70 of SNAP-25, may provide ligands for Ca^{2+} binding (Figure 5.2e). Their sidechains are orientated distantly from each other in the crystal structure. The random orientations might be explained by the fact that Glu62, Gln69 and Asp70 of SNAP-25 don't bind Sr^{2+} in the crystal structure. The large cavity and the number of ligands led me to propose that there might be more than one Ca^{2+}-binding site. Indeed, residue Gly63 in SNAP-25 showed a slight nonlinear trajectory (Figure 5.3d); however the curvature is not very obvious because of the small overall movement. Quantitative analysis of the binding affinity yielded quite scattered results (Table 5.1). With the current data, it is hard to rationalize how many Ca^{2+}-binding sites there are in this region and which residues are primarily affected by the same Ca^{2+} binding. Just for estimation, I listed the average K_D values of all the residues in SyxS and SNN separately in Table 5.1. The K_D values suggest these are also low affinity Ca^{2+} binding sites.

In summary, I found several Ca^{2+} binding sites on the surface of the core complex, including one region where mutation of two putative Ca^{2+} ligands (Glu170 and Gln177 of SNAP-25) reduces the Ca^{2+} dependence of neurotransmitter release. However, the low Ca^{2+} binding affinity observed for these sites raises the concern that they may constitute non-specific sites where divalent cations bind electrostatically.

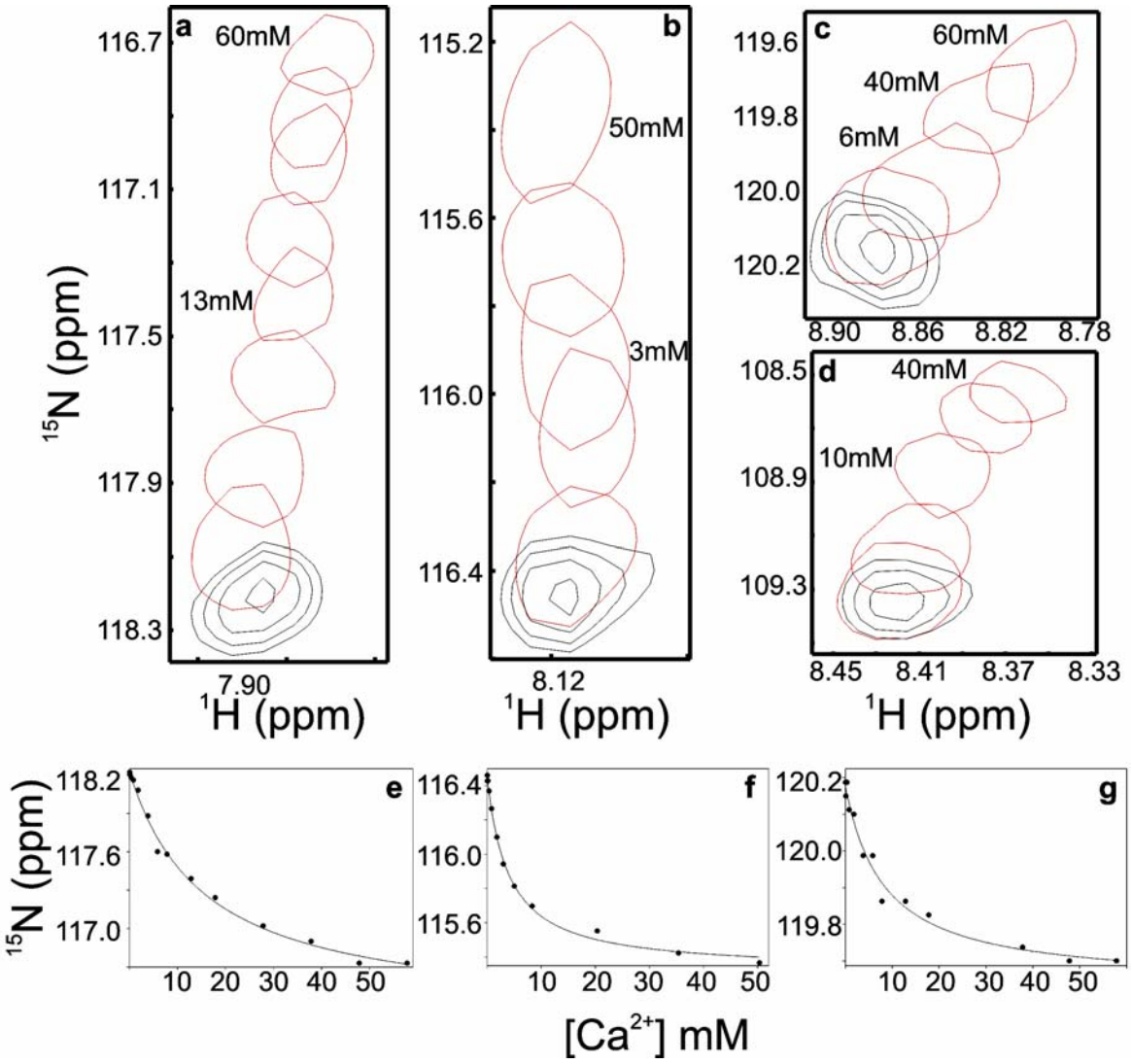
a
60mM
13mM
116.7
117.1
117.5
117.9
118.3
7.90
b
50mM
3mM
115.2
115.6
116.0
116.4
8.12
c
60mM
40mM
6mM
119.6
119.8
120.0
120.2
8.90
8.86
8.82
8.78
d
40mM
10mM
108.5
108.9
109.3
8.45
8.41
8.37
8.33
^{15}N (ppm)
^{1}H (ppm)
e
f
g
118.2
117.6
117.0
116.4
116.0
115.6
120.2
120.0
119.8
10
20
30
40
50
[Ca^{2+}] mM

Figure 5.3

Figure 5.3 Ca^{2+} titrations of the core complex monitored by NMR spectroscopy and analysis of the Ca^{2+} binding affinities. The top panels illustrate the Ca^{2+}-dependent shifts of selected cross-peaks: syntaxin Met215 (a), SNAP-25 Thr173 (b), syntaxin Asn236 (c) and SNAP-25 Gly63 (d). Bottom panels show the Ca^{2+}-dependence of the ^{15}N chemical shifts of Syntaxin Met215 (e), SNAP-25 Thr173 (f) and Syntaxin Asn236 (g). The curves were fitted with the following function

$Y=d0+(df-d0)*(P+X+K-SQRT((P+X+K)^2-4*P*X))/2P$

Where P is the protein concentration, d0 is the chemical shift in the absence of Ca^{2+}, df is the chemical shift upon saturation with Ca^{2+}, K is the dissociation constant, X is the Ca^{2+} concentration, and Y is the observed chemical shift during the Ca^{2+} titration.

Region	Nucleus	Kd(mM)	Average Kd(mM)	Potential Ligands
I	Syx210N	13.2±2.3	14.0±1.4	Syx214, Syx218
	Syx211N	12.4±2.1		
	Syx213N	14.6±2.5		
	Syx214N	13.4±2.5		
	Syx215N	15.5±1.7		
	Syx217N	16.0±2.6		
	Syx218H	12.6±1.8		
II	SNN50H	2.8±0.7	3.7±0.8	SNN51,SNN55,SNN58, SNC170,SNC177
	SNN51N	4.5±1.0		
	SNN55N	4.5±0.8		
	SNN57H	2.9±0.7		
	SNC17N	3.9±0.3		
III	Syx236N	8.3±1.9	8.3±1.9	Syb64,Syb65,Syb68
IV	Syx241H	6.0±1.8	6.8±1.8	Syx242,Syx245, SNN70,SNN62,SNN69
	Syx242N	4.9±1.1		
	Syx245H	5.5±1.0		
	Syx246H	8.2±0.9		
	Syx249N	9.2±1.8		
	SNN66H	7.2±1.8	8.7±2.6	
	SNN70N	7.1±1.7		
	SNN63N	11.7±2.3		

Table 5.1 Dissociation constants of Ca^{2+}-binding sites in the core complex. The table lists the dissociation constants (K_d) for Ca^{2+} binding to different sites of the core complex calculated from the Ca^{2+} dependence of the chemical shifts of individual nuclei of the core complex, as well as the average K_d values obtained for groups of nuclei in the four different regions. For region 4, averages were calculated separately for nuclei from the Syx and SNN SNARE motifs. Syx: syntaxin; Syb: synaptobrevin; SNN: SNAP-25 N-terminal SNARE motif; SNC: SNAP-25 C-terminal SNARE motif.

To study the divalent cation specificity of these sites, I used the same technique to test Mg^{2+} binding to the core complex. The TROSY-HSQC spectra of core complex samples where individual SNARE motifs are ^{2}H, ^{15}N labeled are compared in the absence and presence of Mg^{2+} in Figure 5.4. The cross-peaks corresponding to residues in region IV didn't move even in the presence of 20mM Mg^{2+}, indicating that this region doesn't bind Mg^{2+} (cross-peaks labeled in black in Figure 5.4a and 5.4b). However, Mg^{2+} induced similar chemical shift changes for the residues in regions I-III as those observed in Ca^{2+} binding studies (cross-peaks labeled in blue in Figure 5.4). Although the changes of some cross-peaks are smaller in magnitude, the shifts are in the same direction and the binding affinities for Mg^{2+} are similar as those for Ca^{2+}, indicating that Mg^{2+} and Ca^{2+} bind to these sites in an analogous mode. Thus, we found four regions in the core complex that bind metal ions. Region I, II and III can bind both Mg^{2+} and Ca^{2+} weakly, while region IV, although exhibiting Ca^{2+}-specificity, also binds to Ca^{2+} with low affinity. Given the low affinities and non-specificity of the binding sites, these Ca^{2+} binding regions are unlikely to be physiologically relevant.

These data strongly suggested that the core complex itself is unlikely to be a Ca^{2+} sensor in neurotransmitter release. However, these results don't completely rule out the possibility that the core complex may form part of the Ca^{2+} sensing machinery in neurotransmitter release. From a structure point of view, the core complex assumes an extended structure, which makes it very unlikely to form a full Ca^{2+} coordination site by itself. Core complexes could aggregate to help each other forming integral Ca^{2+} binding sites. However, no overall

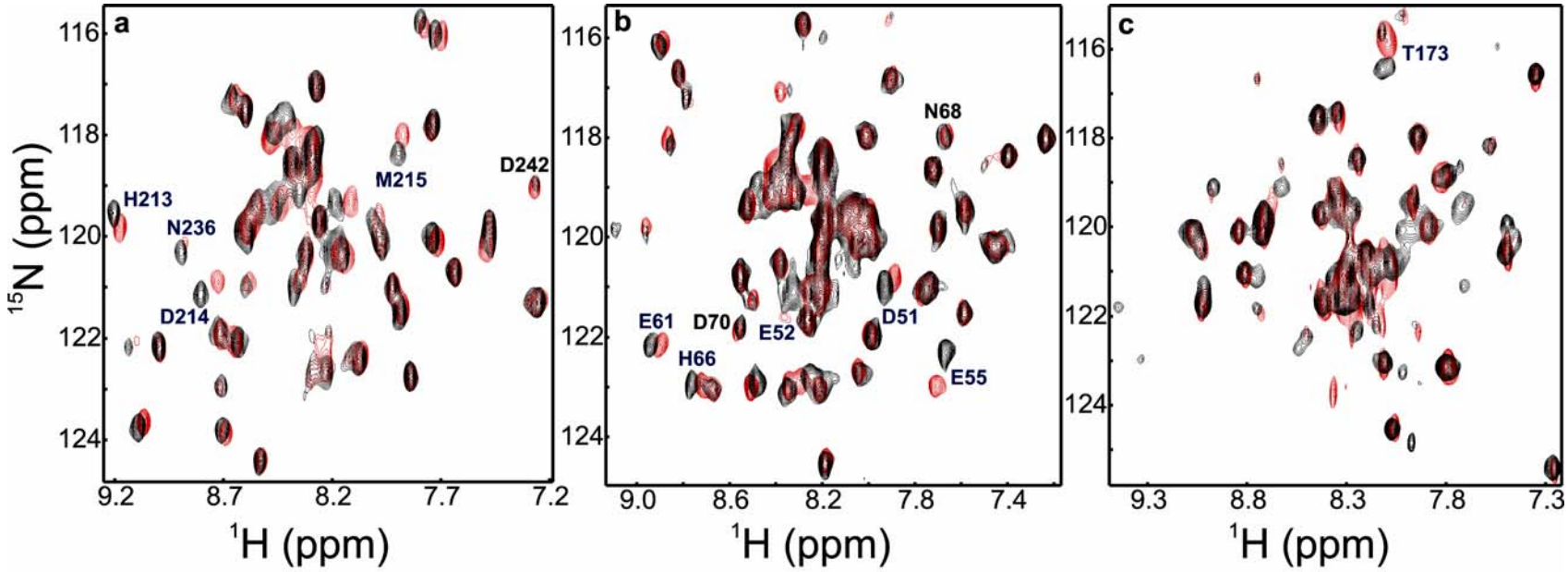

Figure 5.4 Mg^{2+}-induced changes in the ^{1}H-^{15}N TROSY-HSQC spectra of the core complex. ^{1}H-^{15}N TROSY HSQC spectra of the core complex with the SyxS (a), SNN (b) and SNC (c) SNARE motifs ^{2}H,^{15}N-labeled in the absence of Mg^{2+} (black contours) and in the presence (red contours) of 20 mM Mg^{2+} are shown. The assignments of the cross-peaks with large movements are shown in blue. The assignments of the cross-peaks that had significant Ca^{2+}-induced movements, but did not move in the presence of 20mM Mg^{2+}, are shown in black.

cross-peak broadening, an indication of aggregation, was observed in the NMR spectra of the core complex in the presence of Ca^{2+}.

Another possibility arises from the observation that phospholipids dramatically increase the Ca^{2+} affinity of synaptotagmin I, the Ca^{2+} sensor in neurotransmitter release, by completing the coordination spheres of the Ca^{2+} ions (Fernandez-Chacon *et al.*, 2001). Thus, could phospholipids, which play a key role in exocytosis, help the core complex to bind Ca^{2+}? I tested this possibility by monitoring fluorescence resonance energy transfer (FRET) from tryptophan residues in the core complex to dansyl-labeled, phosphatidylserine containing vesicles. However, no FRET was observed between the core complex and the phospholipids either in the absence or presence of Ca^{2+}.

5.3.2 Synaptotagmin Binding is not Affected by the SNAP25 E170A/Q177A Mutation

A previous study by Neher and coworker showed that overexpression of SNAP-25 with a double mutation (E170A/Q177A) in chromaffin cells has a severe effect on the Ca^{2+}-dependent secretion. However, our NMR study showed that region II, where E170 and Q177 of SNAP-25 are potential ligands, is a low affinity and nonspecific Ca^{2+} binding region. Therefore, the phenotype of overexpression of SNAP-25 mutant cannot be explained by the direct Ca^{2+} binding to the core complex.

Ca^{2+}-dependent and Ca^{2+}-independent interactions between the SNAREs and synaptotagmin 1, the main Ca^{2+} sensor that triggers fast neurotransmitter release, have been

reported by several independent studies (Südhof, 2002; Chapman, 2002). Hence, to reconcile the discrepancy between the severe phenotype of the mutant SNAP-25 (E170A/Q177A) in Ca^{2+} dependent exocytosis and the weak Ca^{2+} binding of the core complex, I tested the possibility that residues E170 and Q177 of SNAP-25 might be critical for the interaction between the SNAREs and synaptotagmin 1. In collaboration with Jiong Tang from Dr. Thomas südhof's laboratory, we studied the effect of the SNAP-25 mutation E170A/Q177A on the SNAREs/Synaptotagmin 1 interaction with a GST pull-down experiment. Recombinant GST-fusions of the wild type SNAP-25 and mutant SNAP-25 (E170A/Q177A) were immobilized on glutathione sepharose beads, followed by 2 hours incubation with a recombinant synaptotagmin 1 fragment containing the two C_2-domains (C_2AB fragment) in the presence of different combinations of synaptobrevin SNARE motif, syntaxin SNARE motif and Ca^{2+}. The components that bind to the immobilized SNAP-25 only in the presence of Ca^{2+} can be eluted with EGTA buffer, while those that interact with the SNAP-25 in a Ca^{2+}-independent manner remain on the beads. The EGTA eluate and the beads were analyzed separately by SDS-PAGE (Figure 5.5). As expected, binary complexes of SNAP-25 and syntaxin (180-264) and ternary complexes of SNAP-25, syntaxin (180-264), and synaptobrevin (1-96) were formed, and the interactions among SNAREs are Ca^{2+} independent. The Synaptotagmin 1 C_2AB fragment binds to the wild type SNAP-25 in a Ca^{2+}-dependent manner, while both Ca^{2+}-dependent and Ca^{2+}-independent interactions were found between the synaptotagmin 1 C_2AB fragment and the binary or ternary SNARE complexes. These results are consistent with previous studies (Gerona *et al.*, 2000; Rickman and Davletov, 2003; Shin *et al.*, 2003). The pull down assay with mutant SNAP-25

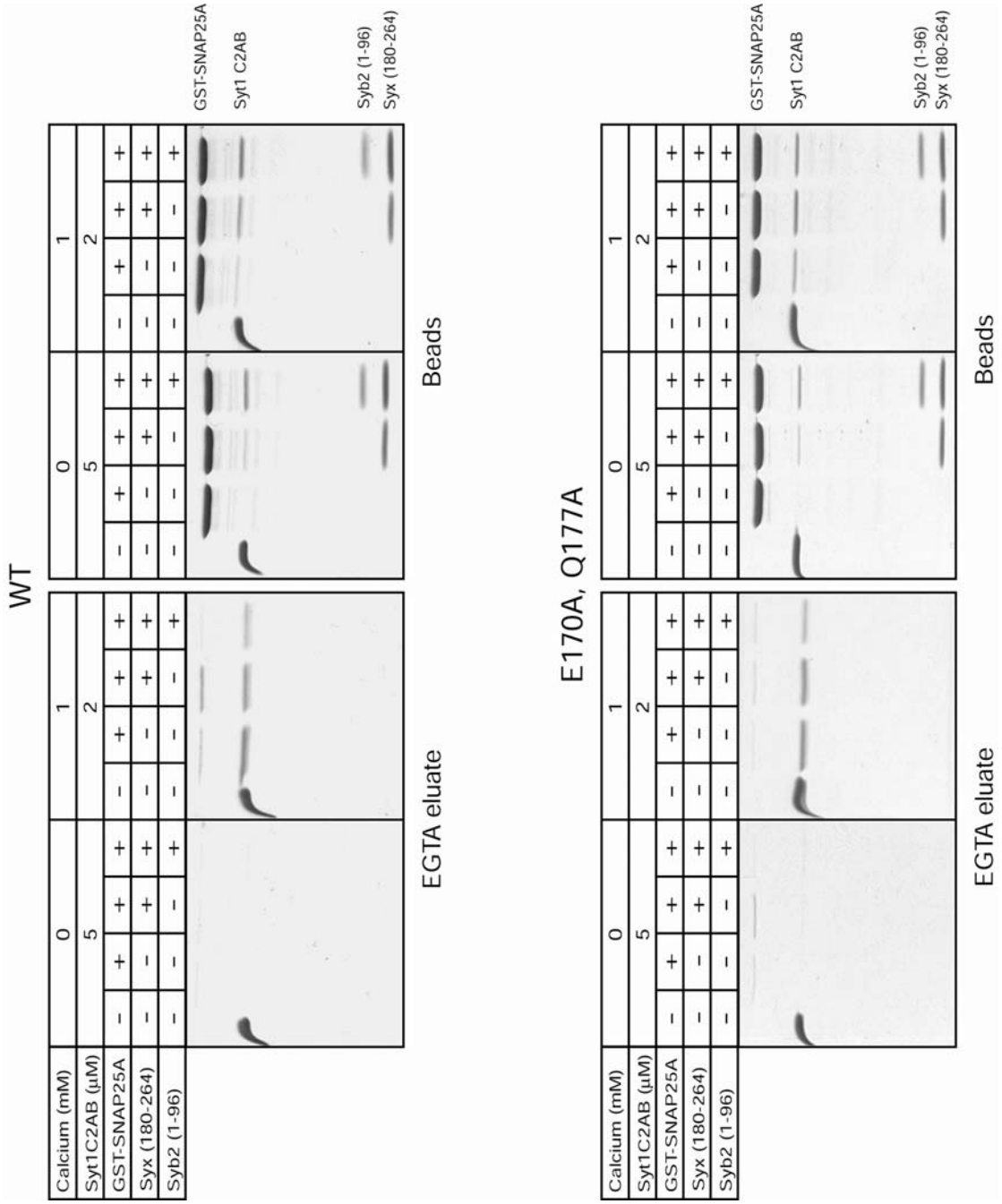
WT
E170A, Q177A
Calcium (mM)
Syt1C2AB (μM)
GST-SNAP25A
Syx (180-264)
Syb2 (1-96)
0
5
1
2
EGTA eluate
Beads
GST-SNAP25A
Syt1 C2AB
Syb2 (1-96)
Syx (180-264)

Figure 5.5

Figure 5.5 The E170A/Q177A SNAP-25 mutation has no effect on SNARE/synaptotagmin 1 interactions. Binding of the synaptotagmin 1 C_2AB-fragment to immobilized WT (top panel) and E170/Q177A mutant GST-SNAP-25 was assayed in the presence or absence of the Syx and Syb SNARE motifs, and Ca^{2+} or EGTA. The components that bind in a Ca^{2+}-dependent manner were eluted with EGTA buffer (left panels) and those that bind independently of Ca^{2+} remained on the beads (right panels). The EGTA eluates and the beads were analyzed by SDS-PAGE and Coomassie blue staining.

(E170A/Q177A) yielded essentially the same results (compare Figure 5.5 top panels and bottom panels). Thus, the E170/Q177 mutation of SNAP-25 does not significantly affect the interaction between SNAREs and synaptotagmin 1 in the presence or absence of Ca^{2+}.

5.3.3 The E170A/Q177A SNAP-25 Mutation Impairs Core Complex Assembly

Taking a close look at the crystal structure of the core complex, we found that residues E170 and Q177 of SNAP-25 are involved in several sidechain interactions (Figure 5.6). Particularly interesting is the observation that residue E170 is hydrogen bonded with the ε-oxygen of SNAP-25 Q174, which is one of the four residues that form the zero-layer. Residue E170 and the residues in the zero-layer are remarkably conserved among the entire SNARE super family, suggesting their functional importance. This observation led us to consider the possibility that the E170A/Q177A mutation in SNAP-25 might affect the assembly of the core complex or its stability.

Taking advantage that the core complex is stable in SDS buffer, I further analyzed the effects of the E170A/Q177A SNAP-25 mutation on the formation of the core complex with SDS-PAGE. I first tested the formation of the core complex after overnight incubation of the four individual SNARE motifs, SyxS, Syb2, SNN and SNC. As depicted in Figure 5.7a (lane 1 and lane 2), the wild type SNARE motifs formed substantial amounts of SDS-resistant minimal core complexes (ca. 30 kDa), which disassembled into the isolated SNARE motifs after boiling. In contrast, much less SDS-resistant complexes formed when I replaced the wild type SNC with mutant SNC (E170A/Q177A). The difference is more clear when

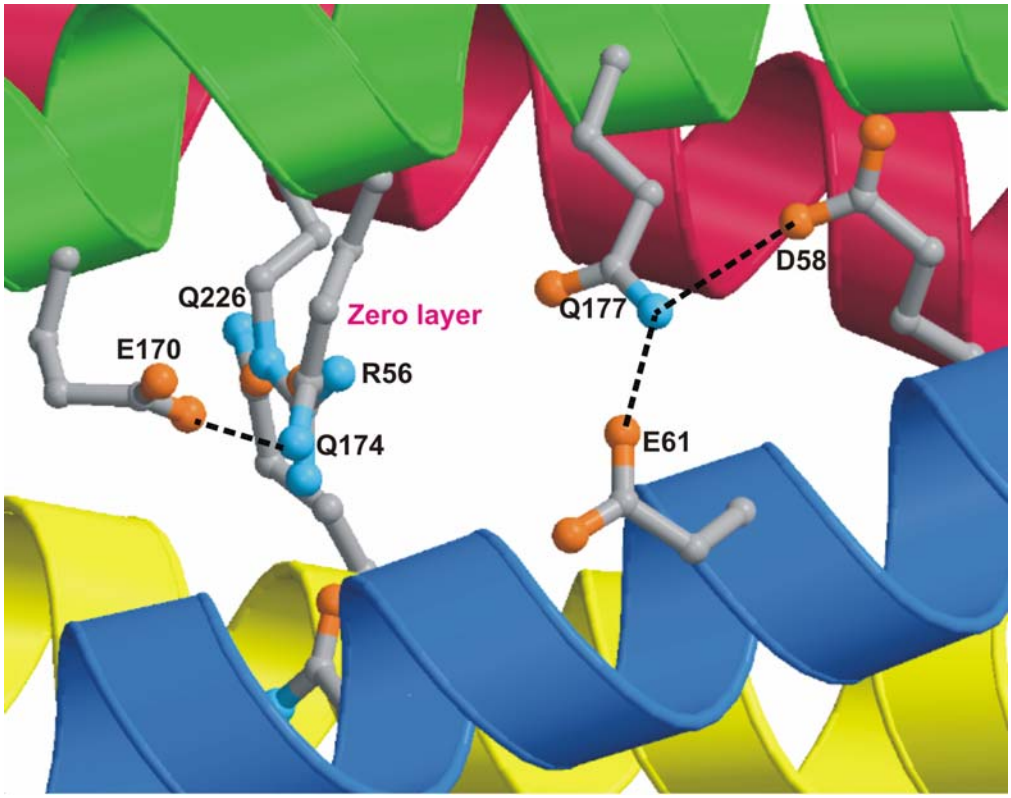

Figure 5.6 The SNAP-25 Glu170 and Gln177 are involved in several side chain interactions within the core complex. A close up of a ribbon diagram of the crystal structure of the core complex (Sutton *et al.*, 1998) is shown. The sidechains of SNAP-25 Glu170 and Glu177, the residues that interact with them, and three of the residues that form the zero-layer are represented in ball-and-stick models (the fourth residue from the polar layer has been omitted for clarity). The color coding for the ribbons is the same as in Figure 5.2. The figure was prepared with the program Molscript (Kraulis, 1991).

comparing the kinetics of the core complex formation during the first hour of incubation. The wild type SNARE motifs form substantial amount of SDS-resistant core complexes after only one minute of incubation, whereas the assembly rate was much slower for the mutant SNC (E170A/Q177A) (Figure 5.7b).

The stability of the assembled core complex with mutant SNC (E170A/Q177A) was characterized with thermal denaturation monitored by circular dichroism (CD). The mutant complexes denatured at only slightly lower temperature than the wild type complexes (89 ^{o}C for the mutant complexes and 91^{o}C for the wild type complexes; Figure 5.8a). On the other hand, to characterize the effects of the E170A/Q177A SNAP-25 mutation on the structure of the core complex, I took a ^{1}H-^{15}N HSQC spectrum of a mutant complex sample assembled with ^{2}H, ^{15}N-labeled syntaxin SNARE motif and non-labeled Syb2, SNN and E170A/Q177A mutant SNC (Figure 5.8b). The overall distribution of the cross-peaks of the mutant complex resembled that of the wild type core complex (Figure 5.1d, black contours). However, numerous additional cross-peaks, some of which were broad and/or of weak intensity, were observed in the ^{1}H-^{15}N HSQC spectrum of the mutant complex. These results suggested that the majority of the mutant complexes assume a structure similar to the wild type core complex, while a small population of the mutant complex has different structures, probably with incorrect alignments of the four SNARE motifs. Therefore, the E170A/Q177A SNAP-25 mutation leads to some degree of structural heterogeneity.

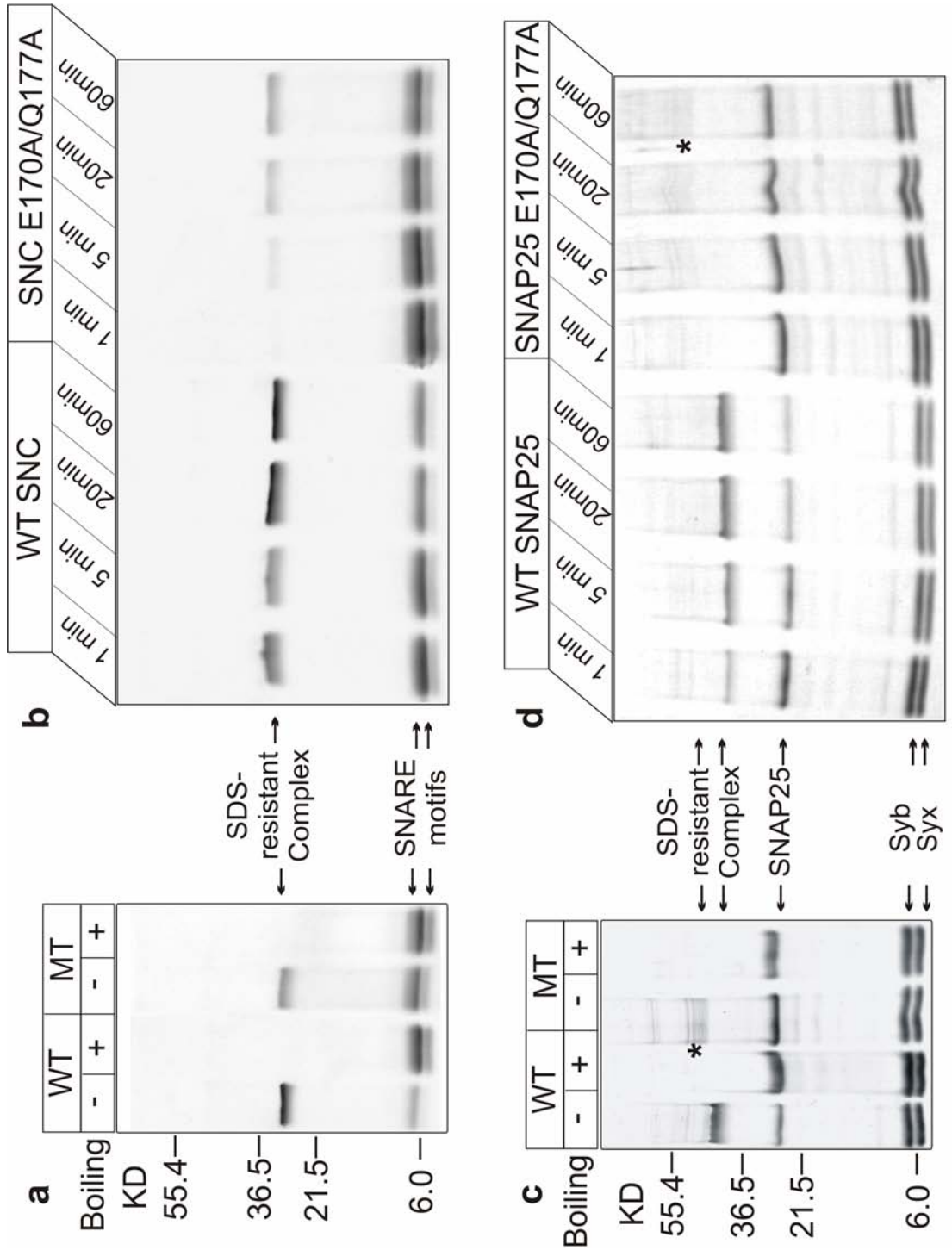
a
Boiling
WT
MT
-
+
-
+
KD
55.4
36.5
21.5
6.0
SDS-resistant Complex
SNARE motifs
b
WT SNC
SNC E170A/Q177A
1 min
5 min
20min
60min
c
d
WT SNAP25
SNAP25 E170A/Q177A
SDS-resistant Complex
SNAP25
Syb
Syx
*

Figure 5.7

Figure 5.7 The E170A/Q177A mutation in SNAP-25 hinders core complex assembly. (a) Wild type (WT) and E170A/Q177A mutant (MT) SNC were incubated with the SNN, SyxS and Syb2 (all SNARE motifs are at 10 μM concentration) overnight at 4°C to allow complexes to form. Complex samples before boiling (lane 2 and 4) and after boiling (lane 1 and 3) were analyzed by SDS-PAGE followed by Coomassie blue staining. (b) Time dependent formation of SDS-resistant complexes between the WT or E170A/Q177A mutant SNC and SNN, SyxS and Syb2. (c,d) Similar experiments as those described in (a) and (b), except that the isolated SNN and SNC SNARE motifs were replaced with wild type or E170A/Q177A mutant full-length SNAP-25. The multiple faint bands corresponding to the mutants SDS-resistant complexes are indicated with an asterisk (*).

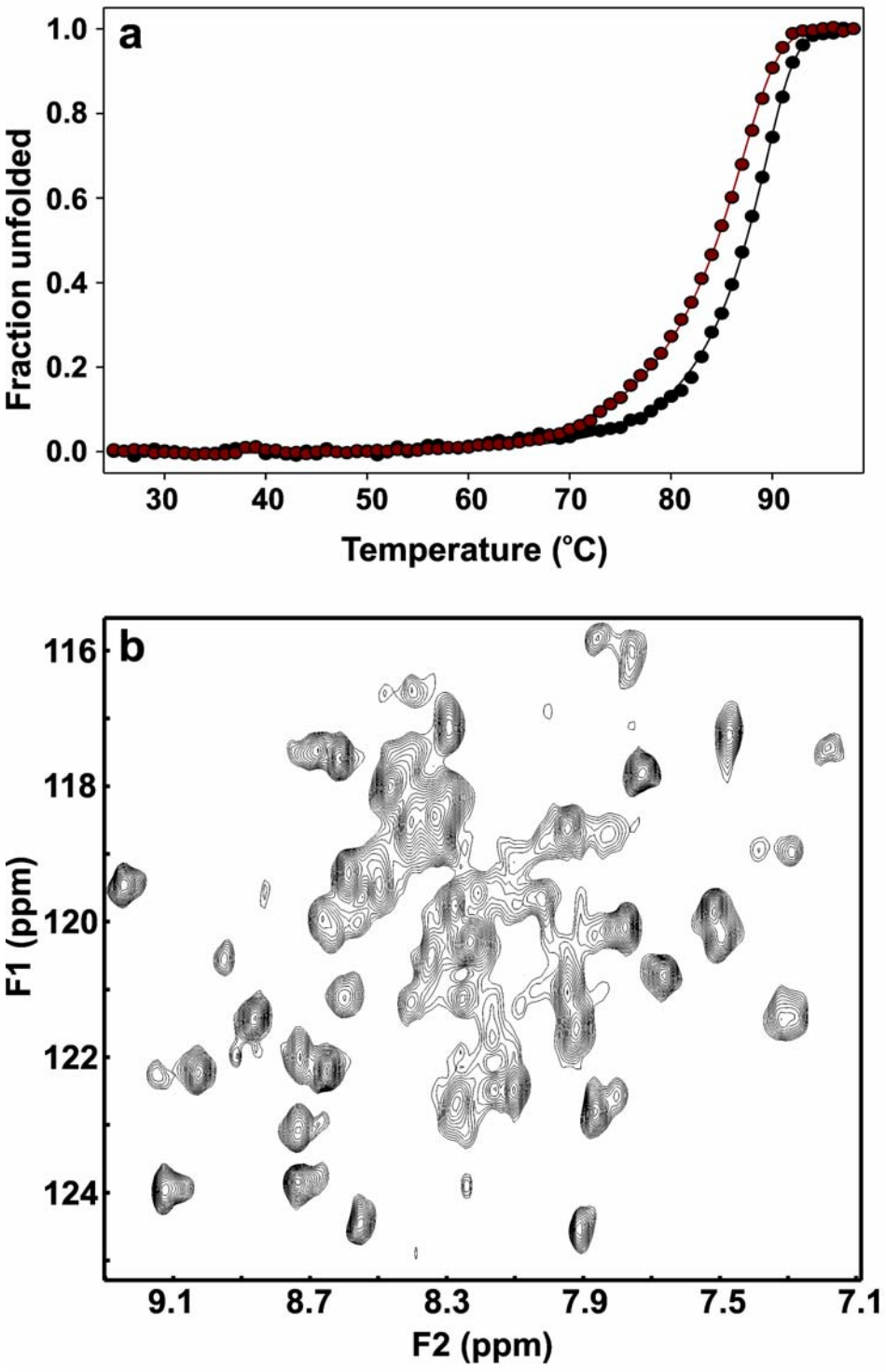
a
Fraction unfolded
1.0
0.8
0.6
0.4
0.2
0.0
30
40
50
60
70
80
90
Temperature (°C)
b
F1 (ppm)
116
118
120
122
124
9.1
8.7
8.3
7.9
7.5
7.1
F2 (ppm)

Figure 5.8

Figure 5.8 Analysis of the E170A/Q177A mutant SNARE complex by thermal denaturation and NMR spectroscopy. (a) Thermal denaturation curves of 3 *u*M wild type core complex (black circles) or the mutant core complex containing SNC (E170A/Q177A) SNARE motif (red circles). Denaturation as a function of temperature was monitored by the decrease in the CD absorbance at 222 nm associated with the loss of helical structure upon disassembly. The curves were normalized after subtracting the linear temperature dependence of the absorbance of the assembled and disassembled states derived from the extremes of the denaturation curves. (b) ^{1}H-^{15}N TROSY-HSQC spectrum of a core complex (100 *u*M) assembled with ^{2}H, ^{15}N-labeled E170A/Q177A mutant SNC and unlabeled SNN, SyxS and Syb2.

In vivo, the two SNARE motifs of SNAP-25 are connected by a linker. Therefore, the mechanism and kinetics of core complex formation might be different when the syntaxin and synaptobrevin SNARE motifs assemble with the full length SNAP-25 instead of the separated SNARE motifs, since the assembly will be a ternary rather than a quaternary reaction. Hence, I also tested the effects of the E170A/Q177A mutation on core complex assembly using the full length SNAP-25. Again, overnight incubation yielded more SDS-resistant core complex for the wild type SNAP-25 than for the SNAP-25 (E170A/Q177A) mutant (Figure 5.7c), and the analysis of the kinetics of core complex formation also revealed a much faster rate for the wild type than for the mutant SNAP-25 (Figure 5.7d).

An intriguing observation is that the complexes containing the E170A/Q177A SNAP-25, indicated by the asterisk (*) at lane 3 in Figure 5.7c and lane 8 in Figure 5.7d, appeared as multiple faint bands on SDS-PAGE with molecular weight higher than that of the wild type core complex (ca. 39 kDa). Thus, the E170A/Q177A mutation of SNAP-25 leads to formation of the heterogeneous SDS-resistant core complexes. Attempts to characterize the nature of this heterogeneity with NMR spectroscopy were hampered by the aggregation of the core complex containing full length SNAP-25. However, thermal denaturation monitored by circular dichroism showed that the melting temperature of the mutant complexes is comparable to that of the wild type complexes (85°C for mutant and 87°C for wild type complexes).

As mentioned before, the minimal core complex with SNC (E170A/Q177A) also exhibited some heterogeneity indicated by the ^{1}H- ^{15}N HSQC spectrum (Figure 5.8b). It is not clear whether the heterogeneity of the SDS-resistant core complex containing the mutant full length SNAP-25 is related to the heterogeneity of the mutant minimal core complex since the latter migrated in SDS-PAGE as a single band (Figure 5.7a and 5.7b). However, in both cases, the mutation E170A/Q177A of SNAP-25 leads to some degree of mis-assembly of the core complex, which might be due to an incorrect register among the four SNARE motifs. The full length SNAP-25 (E170A/Q177A) seems to cause higher percentage of the improperly assembled core complex. It is possible that the presence of both SNAP-25 SNARE motifs in a single molecule might facilitate the formation of misaligned core complexes that are highly stable and difficult to rearrange into the correct conformation. Regardless of the differences observed between the experiments performed with full length SNAP-25 or its separate SNARE motifs, both experiments conclusively showed that the E170A/Q177A mutation has a marked effect on the kinetics and efficiency of core complex assembly.

5.4 Significance and Discussion

The importance of the SNAREs in neurotransmitter release has been well established. However, the precise function of the SNAREs and the exact point when the SNAREs play a role remain under discussion (Weber *et al.*, 1998; Ungermann *et al.*, 1998; Schoch *et al.*, 2001; Rizo *et al.*, 2002). Several recent studies have shown that the SNARE complex may

function at a late step that is close to the Ca^{2+} triggering step of the neurotransmitter release (Broadie *et al.*, 1995; Deitcher *et al.*, 1998; Chen *et al.*, 1999; Gerona *et al.*, 2000; Stewart *et al.*, 2000; Schoch *et al.*, 2001; Washbourne *et al.*, 2002). In addition, the observation that overexpression of SNAP-25 with the double mutation (E170A/Q177A) changed the Ca^{2+}-cooperativity of exocytosis in chromaffin cells suggested that the SNARE complex might actually function in Ca^{2+} sensing (Sorensen *et al.*, 2002). However, it is not clear whether the SNARE complex binds Ca^{2+} directly and this has become a crucial question to understand the SNAREs function, as well as the mechanism of neurotransmitter release. With the help of the backbone resonance assignments of the SNARE complex obtained through my previous studies (see chapter 2), I mapped the Ca^{2+} binding sites of the core complex and estimated the binding affinity for each site with ^{1}H-^{15}N HSQC experiments. Four Ca^{2+} binding regions with clusters of acidic amino acids were found on the surface of the SNARE complex. However, these sites bind Ca^{2+} with low affinity and most of them are not specific for Ca^{2+}. Therefore, these Ca^{2+} binding sites are very unlikely to be physiologically relevant.

To reconcile the discrepancy between the severe effect on Ca^{2+} dependent exocytosis by overexpression the mutant SNAP-25 (E170A/Q177A) and the weak Ca^{2+} binding of the core complex, I also explored the possibility that some auxiliary components may provide ligands, together with the core complex, to generate a full Ca^{2+} binding site and thereby increase the Ca^{2+} binding affinity. Inspired by the observation that phospholipids dramatically increase the Ca^{2+} binding affinity of synaptotagmin 1(Fernandez-Chacon *et al.*, 2001), I tested the effect of phospholipids on Ca^{2+} binding to the core complex. However, no interaction

between the core complex and phospholipids was found in the presence or absence of Ca^{2+}. Another possible mechanism to increase the apparent Ca^{2+} affinity of the core complex could involve cooperative Ca^{2+} binding with another protein such as synaptotagmin 1, which exhibits Ca^{2+}-dependent and independent interactions with the core complex (Südhof, 2002; Chapman, 2002). However, attempts to study the effect of the synaptotagmin 1 on Ca^{2+} binding to the core complex using ^{1}H-^{15}N TROSY-HSQC spectra were hindered by extensive resonance broadening (X.Chen and J. Rizo; unpublished results). Alternatively, our GST pull-down experiments revealed that the mutant SNAP-25 (E170A/Q177A) has no effect on the interaction between Synaptotagmin 1 and the SNARE complexes either in the presence or absence of Ca^{2+} (Figure 5.5). Thus, it is highly unlikely that the severe phenotype of the mutant SNAP-25 (E170A/Q177A) in Ca^{2+} dependent exocytosis arises from direct disruption of Ca^{2+}-dependent or Ca^{2+}-independent interactions between synaptotagmin 1 and the SNAREs. In summary, all the evidences suggest that SNAREs are unlikely to function as direct Ca^{2+} sensors.

The observation that the mutation E170A/Q177A of SNAP-25 hinders core complex assembly is striking given the fact that residues E170 and Q177 are on the surface of the core complex, and thus are not directly involved in the multiple hydrophobic interactions that mediate the formation of the core complex. This finding emphasizes the importance of surface residues for formation of SDS-resistant core complexes. Although the hydrophobic layers almost certainly underlie the high stability of the core complex, it is easy to envision that the large number of hydrophobic residues present in each SNARE motifs may allow the

formation of different four-helix bundles where the helices are aligned with different registers. The existence of the highly conserved hydrophilic residues that form the zero-layer in the middle of the four-helix bundle, together with specific polar interactions on the surface of the complex such as those involving Glu170 and Gln177 of SNAP-25, may be crucial for finding the correct register and/or lock the complex in the correct alignment. Indeed, the E170A/Q177A SNAP-25 mutation not only decreases the efficiency and the rate of formation of SDS-resistant complexes, but also leads to formation of heterogeneous complexes (see the multiple bands in lane 3 of Figure 5.7c and lane 8 of Figure 5.7d), which may correspond to SDS-resistant four-helix bundles with a variety of registers. Note that although less SDS-resistant core complexes were observed for the mutant than for the wild type SNAP-25 (Figure 5.7a and 5.7c), the mutation did not seem to reduce the amount of syntaxin and synaptobrevin bound to SNAP-25 in our GST pull down experiments (Figure 5.5). Thus, the mutant SNAP-25 may still be able to form additional incorrectly registered complexes that are not SDS-resistant.

It is important to note that, in addition to changing the Ca^{2+}-dependence of secretion, overexpression of the E170A/Q177A SNAP-25 mutant in chromaffin cells strongly inhibited Ca^{2+}-dependent exocytosis, particularly the initial fast burst phase (Sorensen *et al.*, 2002). Given the importance of the SNAREs in the neurotransmitter release, the inhibition of exocytosis is thus very likely to arise from the severe impairment of the core complex assembly by the mutation. However, can a defect in core complex assembly explain the decrease in the Ca^{2+}-cooperativity of exocytosis caused by overexpression of the mutant

SNAP25 (E170A/Q177A) in chromaffin cells? The mechanism of the Ca^{2+}-cooperativity of neurotransmitter release is still not well understood. The cooperativity might arise from binding of multiple Ca^{2+} ions to the Ca^{2+} sensor, synaptotagmin 1, since the C_2AB domain of synaptotagmin 1 can bind a total of five Ca^{2+} ions (Ubach *et al.*, 1998; Fernandez *et al.*, 2001), which corresponds well with the Ca^{2+} cooperativity of neurotransmitter release in the calyx of Held (Schneggenburger and Neher, 2000; Bollmann et al., 2000). However, mutagenesis studies showed that some Ca^{2+}-binding sites of synaptotagmin 1 are more critical for release than others (Mackler *et al.*, 2002; Fernandez-Chacon *et al.*, 2002; Robinson *et al.*, 2002). Thus, the cooperativity may also arise from binding of multiple Ca^{2+} ions to several correlated synaptotagmin 1 molecules. Furthermore, additional components, besides synaptotagmin 1, are involved in the regulation of the neurotransmitter release. Hence, the Ca^{2+}-cooperativity might be achieved through a more complicated mechanism, where the assembly of the core complex regulates the process rather than directly affecting Ca^{2+} binding to the sensor. For instance, it has been generally thought that several SNARE complexes (either fully formed or partially assembled) form a ring structure around the site where the vesicle membrane and plasma membrane merge. It is plausible that each synaptotagmin 1 molecule might bind to one SNARE complexes in a Ca^{2+} independent manner and Ca^{2+}-influx triggers the cooperative action of multiple synaptotagmin 1 molecules and core complexes, which subsequently leads to fusion. In this model, a decrease in the number of the core complexes by the E170A/Q177A mutation in SNAP-25 could reduce the number of synaptotagmin 1 molecules that cooperate in triggering release, and consequently lead to a decrease in the Ca^{2+}-cooperativity. Regardless of whether this model

is correct, the decrease in the Ca^{2+}-cooperativity caused by the E170A/Q177A mutation of SNAP-25 (Sorensen *et al.*, 2002), together with the observation that the same mutant has dramatic effects on assembly of the core complex suggests that SNARE function is tightly coupled to Ca^{2+} sensing.

CHAPTER 6 CAN SNARES MEDIATE MEMBRANE FUSION?

6.1 Introduction

6.1.1 Basis for Reconstitution: an Art or a Science

Analysis of genomic sequence data predicts that 30% of the genes of *Homo sapiens*, *Escherichia coli* and *Saccharomyces cerevisae* are encoding integral membrane proteins (Wallin and von, 1998). However, there is considerably less information about the structure and function of membrane proteins compared to our knowledge about soluble proteins. Membrane proteins are naturally embedded in a mosaic lipid bilayer, but the complexity and heterogeneity of the native membrane hinders direct biophysical and biochemical studies and straightforward interpretations of the results. To simplify the systems, reconstitution methods are commonly used to study membrane protein. Reconstitution of a membrane protein basically involves purification of the membrane protein and re-incorporation of the purified protein into artificial membranes, which most often are liposomes with known lipid compositions. To facilitate analyzing the structure and function of the membrane protein, a reconstitution should meet the following criteria:

- The reconstituted proteoliposomes should remain unilamellar.
- The size of the proteoliposomes should be homogeneous.
- The reconstituted proteoliposomes should be stable.
- The proteoliposomes should have low permeability.
- The protein insertion should be homogeneous.

- The incorporated protein should have the correct orientation.

Unfortunately, reconstitution of membrane proteins is not an easy task. The mechanisms of reconstitution are not yet well understood, which makes it difficult to rationalize all the information reported. So far, there does not seem to exist a reconstitution strategy that serves equally well for all membrane proteins. Extensive trial and error is usually needed to establish an appropriate reconstitution method for a particular membrane protein. Hence, reconstitution of membrane proteins has long been considered more like an art than a science.

With a better understanding of the properties of membrane proteins and lipids, together with the lessons learned from systematic research on the reconstitution of membrane proteins, general guidelines and rules for reconstitution are starting to emerge (Rigaud *et al.*, 1995; Rigaud *et al.*, 2003). Four basic strategies have been used to reconstitute membrane proteins into liposomes, including mechanical means, freeze-thawing, organic solvents, and detergents (Figure 6.1). Since most membrane proteins are isolated and purified in the presence of detergents, detergent mediated reconstitution is so far the most frequently used strategy. Detergent mediated reconstitution can be carried out in two distinct schemes (Figure 6.1). The standard scheme is to co-solubilize the membrane protein with phospholipids in order to form an isotropic solution of binary lipid-detergent and ternary lipid-protein-detergent micelles. The detergent is then removed, resulting in progressive formation of

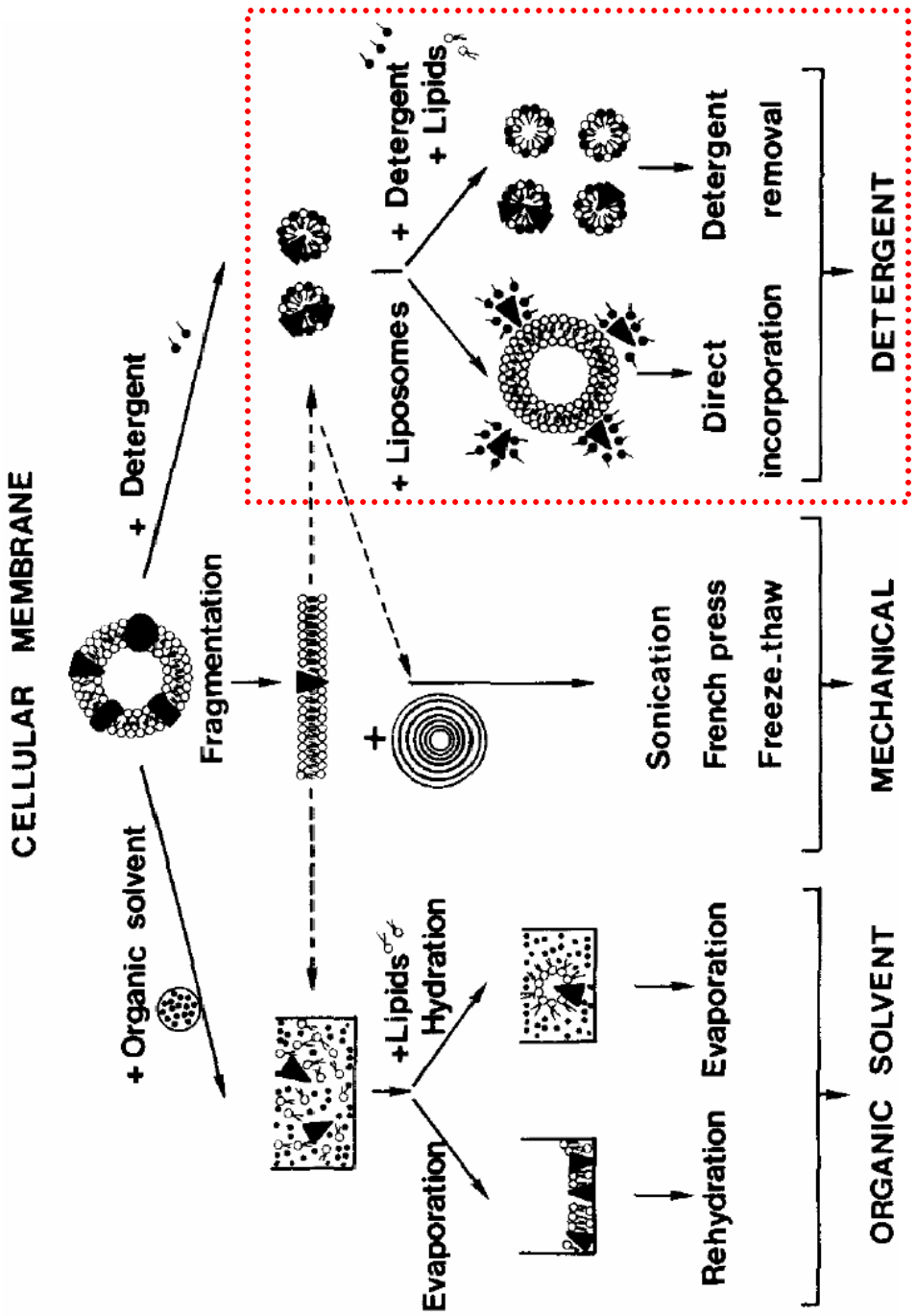
CELLULAR MEMBRANE
+ Organic solvent
+ Detergent
Fragmentation
+ Liposomes
+ Detergent
+ Lipids
Direct
incorporation
Detergent
removal
DETERGENT
+Lipids
Hydration
Evaporation
Sonication
French press
Freeze_thaw
MECHANICAL
Rehydration
Evaporation
ORGANIC SOLVENT

Figure 6.1

Figure 6.1 Strategies that have been used to reconstitute membrane proteins: organic solvent mediated reconstitutions, mechanical methods and detergent mediated reconstitutions. The major procedures starting from isolating membrane proteins to reincorporating into liposomes are illustrated. The detergent mediated reconstitution method, which has been widely used, is encircled by the dotted lines (Rigaud et al., 1995).

proteoliposomes. However, due to the intrinsic heterogeneity of the binary and ternary micelles, proteoliposomes produced by this method are typically inhomogeneous with regards to size and protein insertion (Rigaud *et al.*, 1995). The alternative scheme is to incorporate membrane proteins directly into detergent saturated liposomes, followed by detergent removal. This second method is based on the assumption that the reconstitution process follows the reversed pathway of the detergent-mediated solubilization of liposome, and thus the two processes may share the same intermediate structures (Rigaud *et al.*, 1995).

The detergent mediated solubilization of liposomes has been extensively studied (Lichtenberg *et al.*, 1983; Lichtenberg, 1985; Silvius, 1992). The results of most of these studies have been related to a "three stage model" describing the solubilization process of liposomes by increasing concentration of detergents (Figure 6.2). In stage I, the monomeric detergent and the mole fraction of detergent in the liposomes are increased, but bilayer solubilization does not occur until the liposomes become saturated with detergent. Stage II is basically the transition of the detergent saturated liposomes into phospholipid-detergent micelles. This stage ends when all the liposomes are completely solubilized into mixed micelles. In stage III, the mole fraction of the detergent in the micelles increases with the increase of total detergent concentration. A critical parameter describing the solubilization process is the effective detergent to lipid molar ratio (R_{eff}), defined as:

$$R_{eff}=(D_{total}-D_{water})/[lipid]$$

Where [lipid] and D_{total} are the total lipid and detergent concentrations respectively, and D_{water} is the monomeric detergent concentration. The effective ratios at the onset and total

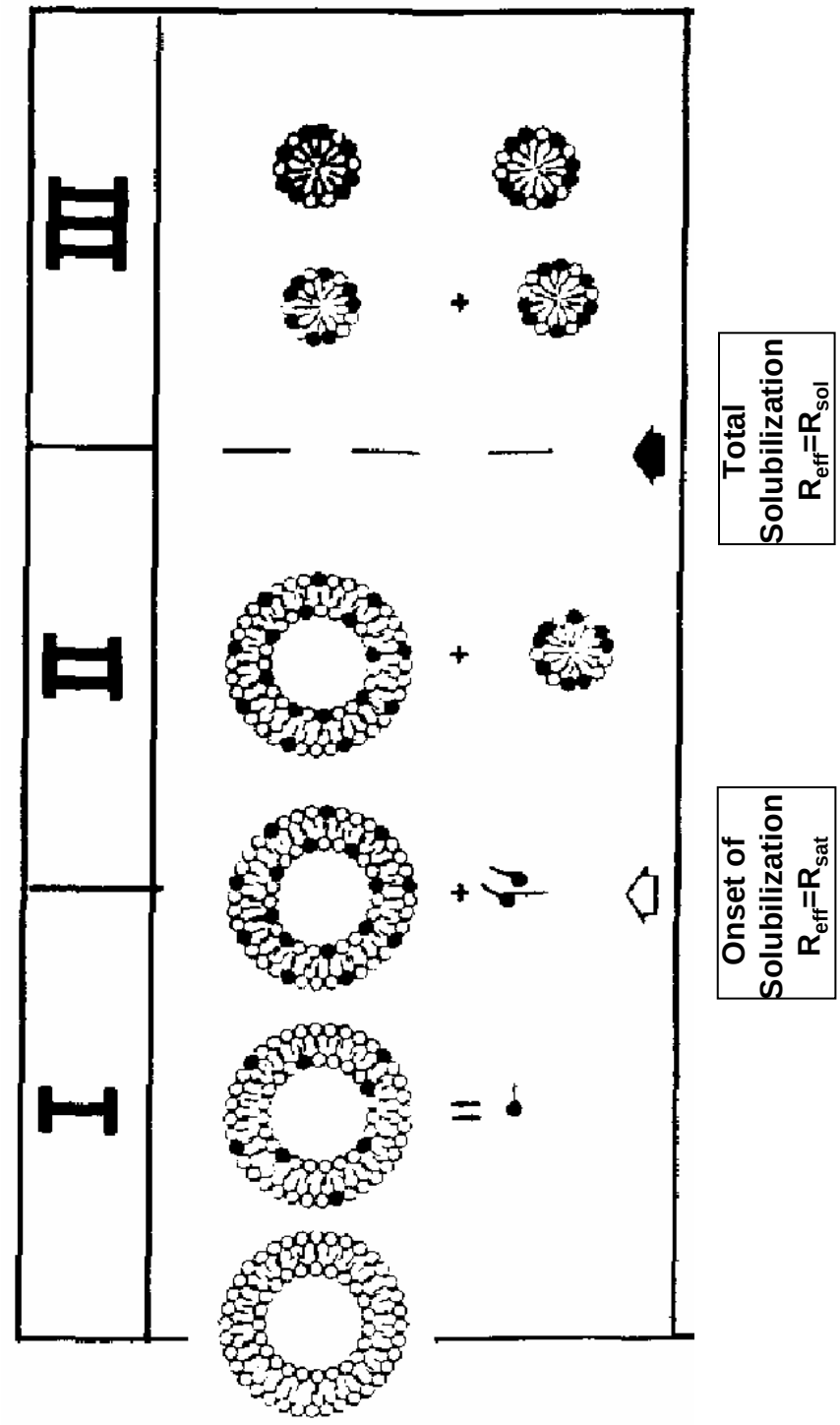
I
II
III
Onset of Solubilization $R_{eff}=R_{sat}$
Total Solubilization $R_{eff}=R_{sol}$

Figure 6.2

Figure 6.2 The three stage model of the detergent mediated solubilization process of liposomes. In stage I, detergent keeps inserting into the liposomes till all the liposomes are saturated by detergent. In stage II, the liposomes start to break down into lipid-detergent micelles. In stage III, all the liposomes have been solubilized into mixed micelles, and the mole detergent fraction of detergent increases with the total detergent concentration. The effective detergent-lipid ratio at onset of solubilization is defined as "R_{sat}", while the effective detergent-lipid ratio at total solubilization of the liposomes is defined as "R_{sol}" (Rigaud et al., 1995).

solubilization are referred to as R_{sat} and R_{sol}, respectively. The R_{sat} and R_{sol} for different detergents have been calculated and the values are summarized in table 6.1 (Rigaud *et al.*, 1995).

Detergent	R_{sat} (mol/mol)	R_{sol} (mol/mol)	D_{water} (mM)
Octyl Glucoside	1.3	2.6	17
Triton X-100	0.64	2.5	0.18
Sodium Cholate	0.3	0.9	2.18

Table 6.1 Parameters describing the solubilization process of liposomes by different detergents. The values were obtained using liposomes prepared with egg phosphatidylcholine-egg phosphatidic acid mixtures (9/1, molar ratio).

As a mirror image of the solubilization process, reconstitution of membrane proteins can be carried out in three distinct steps. First, the preformed liposomes are solubilized with different amounts of detergent throughout the entire range of the lamellar to micellar transition. Second, the purified membrane protein is added to the detergent treated liposomes and incubated until the detergent reaches equilibration. Finally, the detergent is removed and the resulting proteoliposomes are analyzed to select the best detergent concentration for reconstitution. Note that, when the detergent concentration is high enough to completely solubilize the preformed liposome, the reconstitution basically merges with the standard detergent mediated reconstitution scheme described above. This three-step strategy provides

a systematic way to optimize the reconstitution conditions for each individual membrane protein. Indeed, using this strategy, researchers have successfully reconstituted several membrane proteins with multiple transmembrane regions, such as, bacteriorhodopsin, Ca^{2+}-ATPase, F0F1-ATPases, and bacteriorhodopsin-F0F1-ATPases (Paternostre *et al.*, 1988; Rigaud *et al.*, 1988; Richard *et al.*, 1990; Levy *et al.*, 1990a; Levy *et al.*, 1990b; Levy *et al.*, 1990c; Levy *et al.*, 1992; Yu *et al.*, 1993; Hao *et al.*, 1994).

6.1.2 Reconstitution of the SNAREs Involved in Neurotransmitter Release

The neuronal SNAREs include the vesicle membrane protein synaptobrevin and the plasma membrane proteins syntaxin and SNAP-25. The SNAREs emerging from the vesicle and plasma membranes form a very tight complex, the core complex, which brings the two opposing membranes together and therefore might cause fusion. Although there is little doubt that core complex formation is crucial for exocytosis, whether the SNAREs are sufficient for fusion is still under debate. Clearly, reconstituting the vesicle SNAREs (v-SNAREs) and the target membrane SNAREs (t-SNAREs) into separate liposomes and testing for fusion between the two types of liposomes would be the most straightforward way to answer this question. However, this task is not as simple as it sounds. Several attempts to reconstitute the SNAREs have been reported. Surprisingly, some researchers showed that SNAREs alone can execute membrane fusion (Weber *et al.*, 1998; Parlati *et al.*, 1999; Schuette *et al.*, 2004), while in other researcher's hands, the reconstituted SNAREs failed to mediate membrane fusion (Hu *et al.*, 2002; Kweon *et al.*, 2003; Chen *et al.*, 2004). Why did the different reconstitution experiments yield such contradictory results? To clarify the confusion and find

the best way to reconstitute SNARE proteins, below I am going to briefly discuss each reconstitution approach and attempt to explain the discrepancies between the observations made with different experimental systems.

The first experiments were done by Dr. James Rothman and his colleagues (Weber *et al.*, 1998; Parlati *et al.*, 1999). In their assay, spontaneous membrane fusion was observed between the proteoliposomes with t-SNAREs and the proteoliposomes with v-SNAREs. The proteoliposomes were prepared with the standard detergent mediated reconstitution. Briefly, phospholipids were first mixed with protein in the presence of the detergent octyl-β-D-glucopyranoside (OG). Then, the detergent was rapidly diluted to a concentration that is below its critical micellar concentration (CMC), and proteoliposomes formed spontaneously upon the rapid dilution. Residual detergent was removed by extensive dialysis. This reconstitution method usually yields proteoliposomes of different sizes and compositions. An even bigger concern is the use of exceedingly large amount of synaptobrevin to prepare the v-SNARE proteoliposomes (a protein:lipid mol ratio of 1:20 (Weber *et al.*, 1998). For comparison, the synaptobrevin to lipid mol ratio on a native synaptic vesicle is between 1:100 and 1:750 (Jahn and Südhof, 1994; Walch-Solimena *et al.*, 1995). The proteoliposomes loaded with such a large amount of protein may be unstable and prone to artificial fusion. Indeed, in an effort to investigate the effect of synaptotagmin 1 on the “SNARE mediated membrane fusion”, Chapman and his coworkers repeated the same reconstitution experiments performed by Rothman and colleagues except lowering the synaptobrevin concentration to the amount found in native synaptic vesicles (Tucker *et al.*, 2004).

Interestingly, less than half a round of fusion was observed in two hours, whereas more than 5 rounds of fusion were observed in the assay performed by Rothman and colleagues (Parlati *et al.*, 1999). It is important to note that the hallmarks of physiologically relevant fusion, such as content mixing, absence of leakiness and inhibition by inverted cone lipids have never been properly addressed (Rizo *et al.*, 2002). Thus, improvement of the reconstitution method and careful characterization of the proteoliposomes and the fusion reaction are necessary before this assay can yield convincing results.

Jahn and colleagues also reported that substantial amounts of SNARE mediated fusion was observed in their reconstitution assay, where physiological amounts of SNAREs were incorporated in the proteoliposomes (Schuette *et al.*, 2004). The SNAREs were reconstituted with a similar method as that has been used by Rothman and colleagues, except for two differences. First, the detergent that mediated reconstitution was sodium cholate rather than OG. Unlike OG, a non-ionic detergent with CMC of 25mM, cholate is an anionic detergent and its CMC is about 9-15 mM. The second difference lies in the step of detergent removal. Instead of using the method of fast dilution followed by extensive dialysis, the authors removed the detergent by gel-filtration. This technique provides a fast way to remove detergent; however, there are also some problems inherent with this technique, such as incomplete protein incorporation and broader size distribution of proteoliposomes than found by dialysis (Rigaud *et al.*, 1995). It is not clear how these differences in the reconstitution of SNAREs could lead to such a dramatic effect on membrane fusion. It should be noted that

the inhomogeneity of the proteoliposomes and lack of evidence for content mixing and absence of leakiness challenge the physiological relevance of the observed fusion.

In contrast, the reconstitution experiments performed by Davletov and coworkers yielded intriguing results (Hu *et al.*, 2002): the synaptobrevin on synaptic vesicles is unable to form core complexes with either soluble or reconstituted syntaxin/SNAP-25 in the absence of Ca^{2+}. Consequently, no fusion was observed between the synaptic vesicles purified from brains and the t-SNARE proteoliposomes prepared using a similar method as described (Weber *et al.*, 1998). These surprising results were then confirmed by an independent study performed by Shin and colleagues, who provided a structural explanation for the restriction of synaptobrevin by the membrane (Kweon *et al.*, 2003; Chen *et al.*, 2004). In this study, reconstitution was pursued with the second detergent-mediated procedure as discussed above. Briefly, 100 mM preformed large unilamellar vesicles (LUV; ~ 100nm in diameter) were mixed with the purified SNARE proteins in the presence of certain amount of detergent (0.6% OG), which is not enough to totally solubilize the liposomes, but is supposed to keep the SNAREs from aggregating and help the SNAREs insert into the LUVs (Kweon *et al.*, 2003). The detergent was then removed by extensive dialysis. Clearly, the detergent concentration used to assist protein incorporation is critical for the success of this reconstitution. Systematic studies on several membrane proteins revealed that the optimal conditions for octyl-glucoside-mediated reconstitution are usually at the onset of liposome solubilization, that is, $R_{eff}=R_{sat}$ (Rigaud *et al.*, 1995). However, a simple calculation showed that the R_{eff} (~0.03) in Shin's reconstitution experiment is much lower than the R_{sat} for OG

(~1.3; see table 6.1). Unfortunately, it was not explained why such a low R_{eff} was used and the characterization of the proteoliposomes was not shown. Thus, it might be argued that the inability to form the core complex and the failure to mediate fusion by the SNAREs could be due to the improper insertion of the SNARE proteins into the liposomes.

Therefore, whether or not the SNAREs can cause membrane fusion remains an open question. This chapter reports the progress of my ongoing project, which is to set up a reliable reconstitution system to test whether the SNAREs can cause fusion and, in the long run, to eventually dissect the process of neurotransmitter release, clarifying the function of each component involved in this process. Up to now, I have already successfully reconstituted the SNARE proteins, and the reconstitution system has been carefully characterized. However, fairly a small amount of fusion was observed between proteoliposomes containing v- and t-SNAREs according to a standard fluorescence resonance energy transfer assay (Struck *et al.*, 1981).

6.2 Material and Methods

6.2.1 Recombinant Protein Preparation

The construct expressing a GST fusion of full length synaptobrevin 2 (amino acids 1-116; abbreviated Syb) was a gift from Yeon-Kyun Shin's laboratory. The plasmid was transformed into *Escherichia coli* BL21 (DE3) cells for protein expression. The full length synaptobrevin expression and purification procedures were the same as those for the SNARE

motifs (see chapter 2), except that detergents were present in all the purification steps. The detergent containing buffers are listed below.

1. The resuspension buffer, for resuspension of the harvested cells, contained PBS buffer, 2 mM EDTA, 5 mM EGTA, 0.5 mM ABESF, 10 *u*l/ml sigma inhibitor cocktail (Sigma), 0.05% Tween-20, 0.5% n-lauroyl sarcosine, 0.4% Triton X-100, 10 mM β-mercaptoethanol and 1 mM DTT.
2. The wash buffer, which was used to remove unbound proteins and non-specifically bound proteins from glutathione beads, contained PBS buffer, 1 mM DTT and 1% Triton X-100.
3. The thrombin cleavage buffer, which usually contained 50 mM Tris, pH 8.0, 200 mM NaCl and 2.5mM $CaCl_2$, had in addition 1 mM DTT and 0.8% OG.
4. The elution buffer, which was used to elute synaptobrevin from glutathione beads, contained 25 mM Hepes, pH 7.0, 1 mM DTT and 1% OG
5. Buffers for ion exchange chromatography (MonoS colume)

Buffer A: 25 mM Hepes, pH 7.0, 1 mM DTT and 1% OG

Buffer B: 25 mM Hepes, 1M NaCl, pH 7.0, 1 mM DTT and 1% OG

The typical yield according to the UV_{280nm} measurement is 1-2 mg per liter of culture.

Christina Schuette from Reinhard Jahn's laboratory kindly sent me the N-terminally shortened syntaxin construct, His-tagged syntaxin (amino acids 183-288; abbreviated SyxH3; Schuette *et al.*, 2004). This syntaxin fragment contains only the SNARE motif region and transmembrane region of syntaxin. The plasmid was transformed into *Escherichia coli* BL21

(DE3) cells for protein expression. For a routine one liter bacteria culture, 50 ml LB media was inoculated with a single colony from an agar/kanamycin plate and incubated in a shaker at 250 rpm overnight at 37^{o}C. The next day, a proper amount of culture (usually 10-20 ml) was transferred to 1liter LB media to make sure that the starting OD_{600} is around 0.1. All media contained 30 ug/ml kanamycin. The flask was incubated at 37^{o}C and shaken at 250 rpm till OD_{600} reached 0.6-0.8, then 0.5 ml 1M IPTG was added to induce protein expression for 5-6 hours. The cells were harvested by centrifugation at 4000 rpm for 30 min in swing buckets with a rotor JS 4.2 (Model J6-MI centrifuge, Beckman Instruments) and resuspended into 10 ml extraction buffer (100 mM Tris/HCl, pH 7.4, 500 mM NaCl and 8 mM Imidazole) containing 2 mM EDTA, 5 mM EGTA, 0.5 mM ABESF and 10 *u*l/ml sigma inhibitor cocktail (Sigma). To facilitate cell disruption, the cell suspension was frozen with liquid nitrogen and then thawed before protein purification. 10 ml extraction buffer with 10% sodium cholate was added into the cell suspension, followed by 15 min incubation at room temperature. Next, solid urea was added to the cell suspension till the final concentration reached 6M. The mixture was incubated at room temperature for additional 15 min and then passed through the high pressure homogenizer (Model EmulsiFlex-C5, Avestin Inc.) for three times. The cell debris was spun down by centrifugation at 18,000 rpm for 30 min in a JA-20 rotor with the Beckman centrifuge (model J2-21). The supernatant was filtered with 0.45 *u*M syringe filter (Nalgene) and mixed with 1.5 ml slurry of the cleaned nickel-nitrilotriacetic acid (Ni-NTA) agarose (QIAGEN) at 4°C overnight. The following day, unbound proteins and non-specifically bound proteins were removed by washing extensively with washing buffer (50 mM Tris/HCl, pH7.4, 250 mM NaCl, 4 mM Imidazole, and 1.5%

Cholate). The resin was then washed with 3 ml thrombin cleavage buffer (50 mM Tris, pH 8.0, 200 mM NaCl, 2.5mM $CaCl_2$, and 1% OG) for three times. The N-terminal His tag was removed with 5-7 units/ml thrombin (from bovine plasma, sigma) for 4 hours at room temperature. It is very difficult to elute the SyxH3, which tends to stick on the agarose beads. Taking advantage that the syntaxin fragment does not have any tertiary structure (Dulubova *et al.*, 1999), I eluted the protein with 20 mM Tris buffer (pH 7.4) containing 8 M Urea and 1% OG. The SyxH3 was further purified by ion exchange chromatography using a Vivapure Q colume (Vivascience). The Q column was first equilibrated with 20 mM Tris buffer (pH 7.4). Then, the SyxH3 was loaded onto the column followed by extensive washing with low salt buffer to remove urea. Finally, the syntaxin fragment was eluted with 20 mM Tris buffer (pH 7.4) containing 1 M NaCl and 1% OG. The purity of the preparation was assessed by SDS-PAGE and Coomassie blue staining. The typical yield according to the UV_{280nm} measurement is about 1 mg per liter of culture.

The expression and purification steps of the full length SNAP-25 have been described in chapter 5.

6.2.2 Preparation of Liposomes by Extrusion

Two different lipid compositions have been tested for the reconstitution.

1. A commonly used lipid composition for reconstitution (Weber *et al.*, 1998; Parlati *et al.*, 1999; Kweon *et al.*, 2003): POPC (1-palmitoyl, 2-oleoyl phosphatidylcholine) and DOPS (1,2-dioleoyl phosphatidylserine) in an 85:15 mol ratio.

2. A lipid composition more similar to that of synaptic vesicles (Hu *et al.*, 2002): Brain phosphatidylcholine (PC), brain phosphatidylethanolamine (PE), brain phosphatidylserine (PS) and cholesterol in a 48:20:12:20 mol ratio.

All lipids were obtained from Avanti Polar lipids, except cholesterol, which was purchased from Sigma. Typically, 200 *ul* 15mM lipids in chloroform (Avanti Polar Lipids) were mixed thoroughly according to composition 1 or composition 2. For fluorescent donor liposome preparations, 1.5% (mol/mol) NBD-DPPE (N-(7-nitro-2,1,3-benzoxadiazole-4-yl)-1,2-dipalmitoyl-PE) and 1.5% (mol/mol) rhodamine-DPPE (N-(lissamine rhodamine B sulfonyl) 1,2-dipalmitoyl-PE) were included. The lipid mixture in chloroform was evaporated using a nitrogen stream in a hood to form a thin lipid film, which was then thoroughly dried with a vacuum pump for two hours to remove residual organic solvent. The dried lipid film was then hydrated with 200 *ul* reconstitution buffer (25 mM Hepes, 100 mM KCl, pH 7.5, 1.0 mM DTT) with vigorous shaking for 5 minutes, and large multilamellar vesicles (LMV) would form after hydration. To prevent the membranes from fouling and improve the homogeneity of the size distribution of the final suspension, the LMV suspension was disrupted by five times freeze/thaw cycles. The lipid suspension was then forced through a polycarbonate filter with 80 nm pore size for at least twenty-one times. This procedure typically yields large unilamellar vesicles (LUV) with a mean diameter of 100 nm (see Figure 6.3a).

To prepare liposomes containing self-quenched carboxyfluorescein (CF), the dried lipid film was hydrated with 200 *ul* reconstitution buffer containing 70 mM CF. Then the liposomes were prepared with the same procedure as described above. The CF not trapped inside the liposomes was removed by extensive dialysis.

6.2.3 Reconstitution of the SNAREs into the Preformed Liposomes

Typically, 100 *ul* of the preformed liposomes (15mM lipid) and 200 *ul* of the purified SNARE protein or the protein complex were mixed at room temperature. The protein solution contained 1% OG. Thus, the mixture contained 5 mM lipids and 0.66% OG. Under the conditions, R_{eff} is around 1.2, which is very close to R_{sat} for OG (~1.3; see table 6.1). Such reconstitution conditions were chosen based on systematic studies of OG mediated reconstitution (Rigaud *et al.*, 1995). For preparation of the Syb proteoliposomes, the lipid to protein ratio was 250:1 (molar ratio). For preparation of the SyxH3 proteoliposomes, the lipid to protein ratio was 500:1 (molar ratio). For preparation of the SyxH3/SNAP-25 proteoliposomes, the syntaxin fragment and SNAP-25 were pre-mixed on ice for at least 30 min before reconstitution, and the lipid to the SyxH3/SNAP-25 complex ratio was 500:1 (molar ratio). The mixture was kept at room temperature for 30 min under gentle stirring. Then the detergent was removed by a three-step dialysis (in Pierce 100-500 ul Slide-A-Lyzer 10KDa cutoff dialysis cassette) as follows. First, the mixture was dialyzed against 500 ml reconstitution buffer containing 0.5 g Biobeads SM2 beads (Bio-Rad) for one hour at room temperature. Next, the dialysis was continued against 500 ml fresh reconstitution buffer containing 0.5 g Biobeads for two more hours at room temperature. Finally, the sample was

transferred to 1 liter fresh reconstitution buffer containing 1.0 g Biobeads and dialyzed at 4 ^{o}C overnight.

In some instances, a Nycodenz gradient was used to purify the proteoliposomes and check the efficiency of the protein incorporation. 750 *ul* of the proteoliposomes were mixed with an equal volume of 80% Nycodenz in an 11x60 mm ultraclear centrifuge tube (Beckman), and overlaid sequentially with 1 ml of 30 % Nycodenze and 500 *ul* of reconstitution buffer. The gradient was then centrifuged in a SW60Ti rotor (Beckman) at 35,000 rpm for 4 hours at 4 ^{o}C. A clear liposome band appeared at the 0/30% Nycodenz interface after centrifugation. The fractions were collected and Nycodenz was removed by dialysis against reconstitution buffer for 2 hours at 4 ^{o}C. The protein content in each fraction was also analyzed by SDS-PAGE followed by Coomassie Brilliant Blue staining.

6.2.4 Dynamic Light Scattering Tests

Dynamic light scattering (DLS) was performed on a DynaPro dynamic light scattering model 99D instrument (DynaPro International) using 10 sec acquisition time at 37 ^{o}C. The liposomes or the proteoliposomes were diluted 100 times (50 uM lipid) and spun at 13,000 rpm for 10 min with a micro benchtop centrifuge (Fisher Scientific) before subjected to DLS measurement. The laser power was adjusted to keep the intensity between 500,000 counts and 2000,000 counts. The results were then processed with the program Dynamics V6 (DynaPro International). The radii and the size distribution were calculated with the regularization algorithm provided by this software.

6.2.5 Electron Microscopy

For negative staining, the liposomes or the proteoliposome were diluted 100 times (about 50 uM lipids). 4 *ul* of samples were applied to formvar-covered and carbon-coated glow-discharged 300 mesh copper grids for 2 min and stained with 1 % uranyl acetate for 1 min. The grids were examined using a JEOL 1200EX Transmission Electron Microscope operating at 120kV. Electron micrographs were taken with the HR 1k x 1k cooled CCD digital camera.

The liposome or proteoliposome samples for cryo-electron microscopy usually contained about 5 mM lipids. 4 *ul* of samples were applied to cabon-coated glow-discharged holey grids. The grids were blotted and plunged into liquid ethane. Electron microscopy images were obtained with a JEOL-2100F Transmission Electron Microscope at 200kV. Electron micrographs were taken with CCD digital camera with 20 micron defocus.

6.2.6 Bicinchoninic Acid (BCA) Assay to Test Protein Concentration

The protein concentration in each proteoliposome sample was estimated with the BCA protein assay kit (Pierce). A set of standard BSA solutions (0, 5, 25, 50, 125, 250 ug/ml) was prepared freshly. Aliquots (50 *ul*) of each standard or proteoliposome sample were placed into an appropriately labeled glass tube (13x100 mm; Fisher) individually. 1.0 ml of the working reagent (WR: 50 parts of BCA Reagent A with 1 part of BCA Reagent B) was added to each tube and mixed well. All the tubes were then incubated at 60 ^{o}C for 30 min. After incubation, the tubes were cooled to room temperature and the absorbance at 562 nm

(OD_{562}) was measured. The standard curve was generated by plotting the OD_{562} versus the BSA concentration (ug/ml). The protein concentration in each proteoliposome sample was then determined according to the standard curve.

6.2.7 Determination of Total Phospholipids in Liposome Samples

The phospholipid concentration was estimated according to the amount of phosphorus in each sample. The basis of this assay is briefly explained as follows. Liposomes are first digested by perchloric acid. The released inorganic phosphate is then reacted with ammonium molybdate in the presence of a reduction agent (ascorbic acid), forming a complex that gives a strong blue color. Thus, the amount of phosphorus can be determined by colorimetric detection.

The liposome samples containing 1-160 nMoles of phosphorus were placed into the bottom of each glass tube (13x100 mm; Fisher). For a standard curve, 0, 5 *ul*, 10 *ul*, 25 *ul*, 50 *ul*, 75 *ul*, 100 *ul* and 125 *ul* of 1.0 mM K_3PO_4 solution were placed into eight separate glass tubes. 10 *ul* of 2% Ammonium Molybdate was added into each tube and mixed well with the samples or the standards. All the tubes were then heated to 90-100 ^oC until dry. Next, 300 *ul* of 70% perchloric acid was added into each tube, followed by heating at 180 ^oC for about 30 min or until the yellow color disappeared. The tubes were cooled at room temperature and 1.5 ml of 0.4% Ammonium Molybdate was added into each tube and mixed well by vortexing. Then, 0.225 ml of 10% ascorbic acid was added into each tube, and again mixed well by vortexing. The mixtures were then heated for 10 min at 90 ^oC to develop a blue color

and then cooled down to room temperature for 20 min. The absorbance at 820 nm (OD_{820}) was measured and the standard curve was generated by plotting the OD_{820} versus the amount of the phosphorus for each standard K_3PO_4 solution. The concentration of phosphorus in each sample was calculated according to the standard curve. The amount of phospholipids was estimated directly on a molar basis from the amount of phosphorus.

6.2.8 Leakage Assay

The liposomes or proteoliposomes containing a high concentration of carboxyfluorescein (CF) were diluted 40-50 fold (approximately 100 uM lipid). The release of CF from liposomes or proteoliposomes was monitored on a Perkin Elmer LS50-B spectrofluorimeter with a 50 *ul* Quartz fluorometer cuvette (Nova Biotech). The emission spectra from 500 to 550 nm were acquired every 20 min for two hours at 37^{o}C, with an exciting wavelength of 490 nm and a scan speed of 1200 nm/min. To minimize photo-bleaching effect, the lamp was set to auto-off for 10s before each measurement. After 2 hours, 1% OG was added to solubilize the liposomes or the proteoliposomes and the emission spectrum was then recorded as 100 % release of CF.

6.2.9 Protein Orientation Test

10ul of the proteoliposomes were incubated with 4 *ul* of 40 ug/ml chymotrypsin in the presence or absence of detergent (1 ul of 10% OG) at 37 ^{o}C for 1.5 hours and SDS sample buffer were added immediately to stop the reaction. All samples were then analyzed by SDS-PAGE followed by Coomassie Brilliant Blue staining.

6.2.10 Fusion Assay

The proteoliposomes were pre-incubated at 37 ^{o}C before mixing. Typically, 15 *ul* Syb liposomes were mixed with 30 *ul* SyxH3/SNAP-25 liposomes in a 50 *ul* Quartz fluorometer cuvette (Nova Biotech). Fusion was followed by NBD fluorescence increase. The NBD fluorescence was monitored every 10 sec in a Perkin Elmer LS50-B spectrofluorimeter (excitation 460 nm, slit 10 nm; emission 538 nm, slit 15 nm). After 2 hours at 37 ^{o}C, 1% OG was added to solubilize the proteoliposomes, resulting in a dramatic increase of the NBD signal. The final NBD fluorescence was acquired and used as the maximal signal for normalization.

6.2.11 Conversion of Percent of NBD Fluorescence to Rounds of Fusion

To obtain a calibration curve for converting percent of NBD fluorescence into rounds of fusion, a series of liposomes containing different amounts of fluorescent lipids were prepared. Since the efficiency of energy transfer is independent of the surface density of the energy donor (Struck, Biochemistry), all the liposomes contained 1.5% NBD-DPPE, while the percent of the rhodamine-DPPE varied from 0 to 2.5%. The NBD fluorescence of each liposome was recorded in the absence and presence of the detergent (1% OG). The efficiency of energy transfer (E; quenching of the energy donor) was calculated based on the equation (Fung and Stryer, 1978): $E=1-F/F_0$, where F is the NBD fluorescence in the presence of rhodamine and F_0 is the fluorescence in the presence of detergent. The standard curve was generated by plotting the efficiency of energy transfer versus rhodamine concentration.

Taking the effect of protein into account, I prepared a series of syb proteoliposomes containing 1.5%, 0.75% and 0.375% of NBD/rhodamine DPPE. The NBD fluorescence of each proteoliposome was recorded in the absence and presence of the detergent (1% OG) and transfer efficiency was calculated. The relation of the transfer efficiency versus the percentage of NBD/rhodamine DPPE was plotted. The results fit very well with the standard curve obtained with protein free liposomes.

6.3 Results

6.3.1 Characterization of the liposomes and the proteoliposomes

The liposomes were prepared with the commonly used lipid composition (POPC:DOPS=85:15 molar ratio), and then the purified SNARE proteins were incorporated into the liposomes (5 mM) in the presence of 0.66% OG, corresponding to an R_{eff} of about 1.2. After detergent removal by extensive dialysis, the proteoliposomes were analyzed by DLS. The liposomes prepared by extrusion were quite homogeneous, with an average radius of about 45 nm (Figure 6.3a). The Syb proteoliposomes also showed narrow size distribution with slightly increased size (about 50 nm in radius; Figure 6.3b). Reconstitution of the t-SNAREs was performed in two different ways. SyxH3 was first mixed with SNAP-25 in the presence of 1% OG, and then the protein complex was reconstituted into liposomes. The proteoliposomes produced by this method had a narrow size distribution with an average radius of 60 nm (Figure 6.3c). I also tried to reconstitute the SyxH3 first, and add the SNAP-25, a soluble protein, to the SyxH3 proteoliposome afterwards. However, the

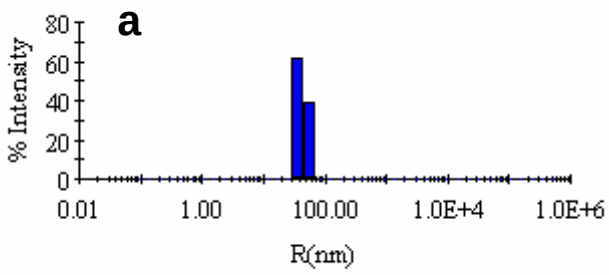

Item	R(nm)	%Pd
Peak	44.5	20.0

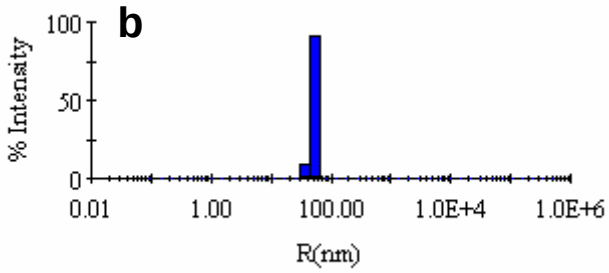

Item	R(nm)	%Pd
Peak	54.0	9.6

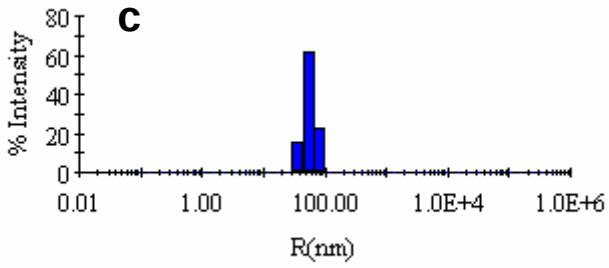

Item	R(nm)	%Pd
Peak	59.1	24.5

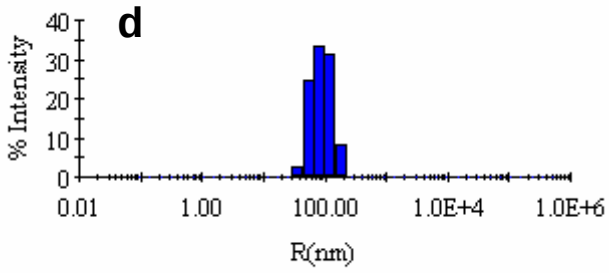

Item	R(nm)	%Pd
Peak	96.0	39.0

Figure 6.3

Figure 6.3 DLS analysis showing the radii and the size distribution of the liposomes and the proteoliposomes prepared with the commonly used lipid composition (lipid composition 1). (a) Protein free liposomes. (b) Proteoliposomes containing Syb. (c) Proteoliposomes containing SyxH3/SNAP-25. (d) Proteoliposomes containing SyxH3. R is the radii and %Pd represents the percentage of polydispersity.

proteoliposomes containing the SyxH3 alone exhibited wide size distribution and the average size became about 100 nm in radius (Figure 6.3d). Thus, in the following studies, the SyxH3 was always reconstituted together with SNAP-25 unless indicated otherwise.

In separated experiments, I prepared the liposomes with a lipid composition similar to that of synaptic vesicles (brain PC : brain PE : brain PS : cholesterol =48:20:12:20, mol ratio; see (Hu *et al.*, 2002)) and reconstituted the SNARE proteins into this type of liposomes. The DLS analysis showed that the radii and the size distribution of the liposomes do not change with the lipid composition (Figure 6.4a). However, unlike the liposomes containing POPC (85%) and DOPS (15%), which become bigger upon protein incorporation (Figure 6.3b, 6.3c and 6.3d), the proteoliposomes with the new lipid composition have similar size as the protein free liposomes (Figure 6.4b and 6.4c), which is probably due to the presence of cholesterol. The proteoliposomes with both lipid compositions have been used for all the following assays and no significant difference was observed. The results shown in the following sections are mostly obtained with the proteoliposomes with lipid composition 2 unless indicated otherwise.

The morphology of the proteoliposomes has also been checked by cryo-electron microscopy. Consistent with the DLS results, the electron micrographs showed that the proteoliposomes have nice round shape with about 100 nm in diameter, although a higher dispersion in size can be observed by EM (Figure 6.5a and 6.5b).

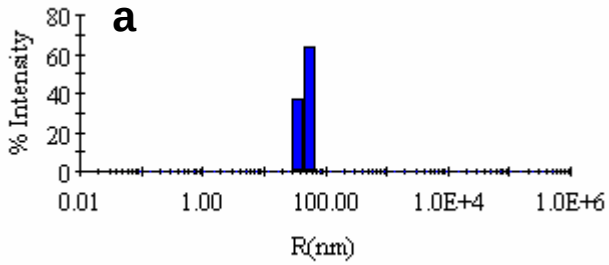

Item	R(nm)	%Pd
Peak	48.9	18.0

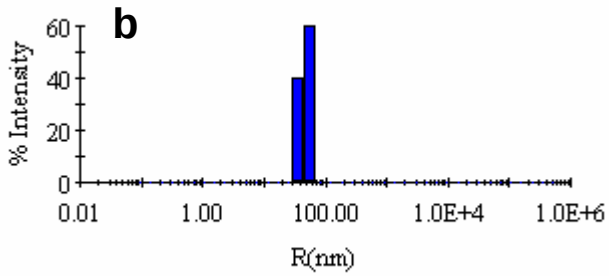

Item	R(nm)	%Pd
Peak	48.3	18.5

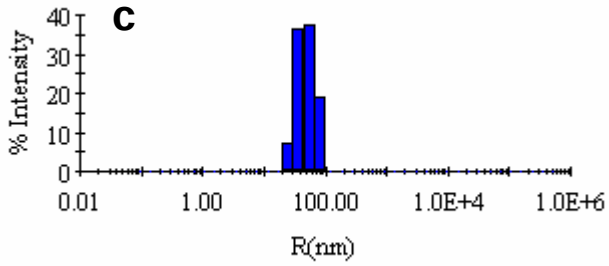

Item	R(nm)	%Pd
Peak	51.9	34.1

Figure 6.4

Figure 6.4 DLS results showing the radii and the size distribution of the liposomes and the proteoliposomes with a lipid composition more similar to that of synaptic vesicles (lipid composition 2). (a) Protein free liposome. (b) Proteoliposomes containing Syb. (c) Proteoliposomes containing SyxH3/SNAP-25. R is the radii and %Pd represents the percentage of polydispersity.

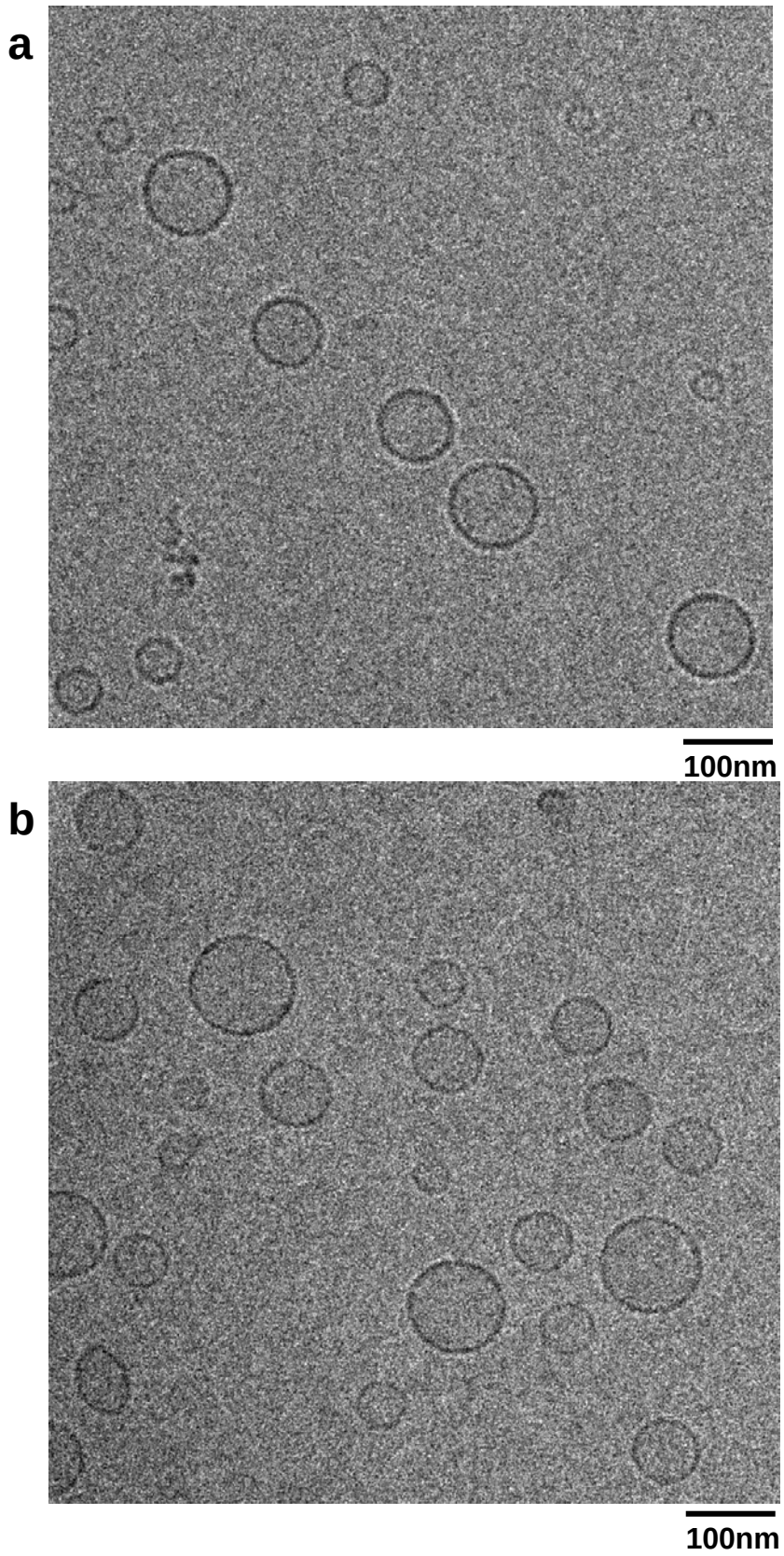

Figure 6.5 Cryo-electron microscopy images of (a) the Syb proteoliposomes and (b) the SyxH3/SNAP-25 proteoliposomes.

To check the efficiency of the protein incorporation, the proteoliposomes were investigated by means of flotation on discontinuous Nycodenz gradients. Liposomes have low density and will float to the top of the gradient at the 0/30% Nycodenz interface, while the protein aggregates have high density and will stay at the bottom of the gradient. Fractions (~200 *ul*) were collected from the top of the gradient and the protein content was analyzed by SDS-PAGE and Coomassie staining (Figure 6.6; lane 1-6). To identify any protein aggregate, the 40% Nycodenz solution (~1.5 ml) at the bottom of the gradient was analyzed by trichloroacetic acid (TCA) precipitation, followed by SDS-PAGE and Coomassie staining (Figure 6.6; lane 7). In the preparations of Syb proteoliposomes, more than 90 % of the protein appeared in fraction 2 and fraction 3, where the liposome band was observed (Note that the fluorescent lipids moved as a pink band in SDS-PAGE). Thus, most of the Syb was incorporated into the liposomes, and practically no Syb aggregate was identified with Coomassie blue staining (Figure 6.6a). However, the incorporation of the SyxH3/SNAP-25 was less efficient and the SyxH3/SNAP-25 aggregates were observed (Figure 6.6b, lane 7). Since only 15 *ul* of each 200 *ul* fraction was loaded to the gel (Figure 6.6b, lane 1-6), while the sample of the protein aggregate was precipitated from 1.5 ml gradient solution (Figure 6.6b, lane 7), the band intensity should not be compared directly. According to a rough estimation, about 80% of the SyxH3/SNAP-25 was incorporated into the liposomes.

The fractions 2 and 3 were combined and the Nycodenz in the sample was removed by dialysis. The total lipid and protein concentration were determined by phosphorus assay and BCA assay respectively. The recovery of phospholipids was about 50%, and lipid to protein

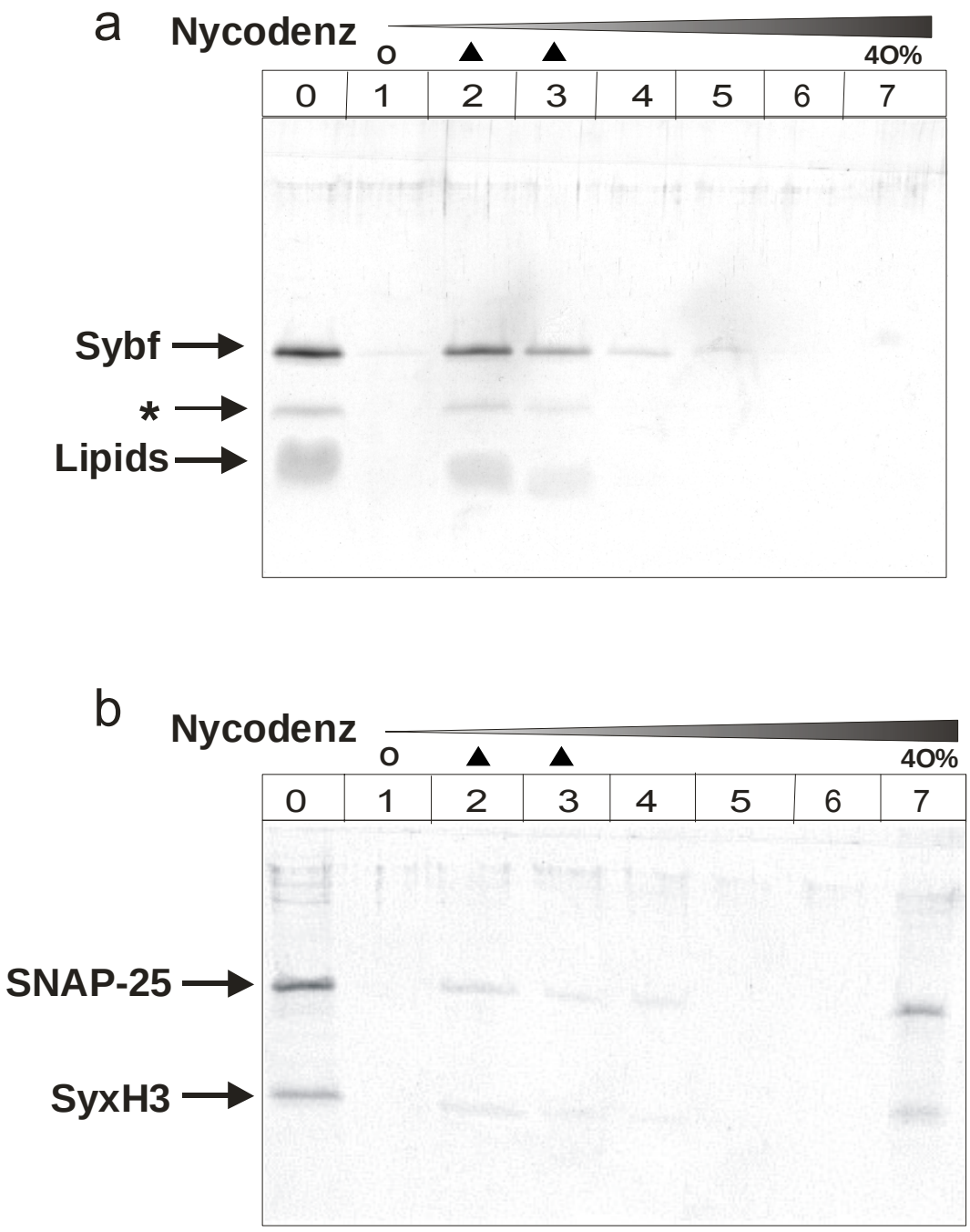
a
Nycodenz
o
40%
0
1
2
3
4
5
6
7
Sybf
*
Lipids
b
Nycodenz
o
40%
0
1
2
3
4
5
6
7
SNAP-25
SyxH3

Figure 6.6

Figure 6.6 Efficiency of the protein incorporation into liposomes. (a) Purification of the Syb proteoliposomes with Nycodenz gradient. (b) Purification of the SyxH3/SNAP-25 proteoliposomes with Nycodenz gradient. (Lane 0) Samples before purification. (Lane 1-6) Fractions (~200 *ul*) were collected from the top of the Nycodenz gradient and the protein content in each fraction was analyzed by SDS-PAGE and Coomassie blue staining. (Lane 7) The rest of the sample at the bottom of the gradient (~1.5 ml) was TCA precipitated and subject to SDS-PAGE analysis and Coomassie blue staining. Black triangles indicate the fractions where a clear liposome band was observed in the centrifuge tubes. The bands labeled by asterisk are N-terminal degradation products of synaptobrevin (Weber et al., 1998). The bands labeled as lipids are the fluorescent lipids, which can be seen as a single pink band in SDS-PAGE.

ratio was about 200:1 (molar ratio) for the Syb proteoliposomes and about 400:1 (molar ratio) for the SyxH3/SNAP-25 proteoliposomes.

The orientation of the reconstituted SNAREs was determined by their accessibility to chymotrpsin digestion (Figure 6.7). After chymotrypsin treatment, there is basically no SyxH3/SNAP-25 detectable by SDS-PAGE and Coomassie blue staining (Figure 6.7, lane 2), indicating that majority of the t-SNAREs were reconstituted with the cytoplasmic domains on the outside. For the Syb proteoliposomes, approximately 20% of the Syb remained intact after the chymotrypsin treatment (Figure 6.7, lane 5), whereas all the Syb in the liposomes, when solubilized by detergent (1% OG), was digested by chymotrypsin under the same condition (Figure 6.7, lane 6). Thus, about 80% of the Syb was oriented with the SNARE motif on the outside of the liposomes.

The proteoliposomes without membrane integrity cannot be used in the assay for content mixing, a hallmark for membrane fusion. More importantly, instability of the proteoliposomes can cause artificial fusion. Therefore, it is of interest to study the leakage of the proteoliposomes. Taking advantage that CF at high concentration (>10 mM) can self-quench, I encapsulated concentrated CF (70 mM) in the liposomes, and the leakage of liposomes was monitored as the enhancement of CF fluorescence intensity. In a two-hour period, very little leakage was detected for either the protein-free liposomes or the proteoliposomes, comparing with the fluorescence intensity after adding detergent to induce 100% release of CF (Figure 6.8). Note that the initial fluorescence intensity is higher in the

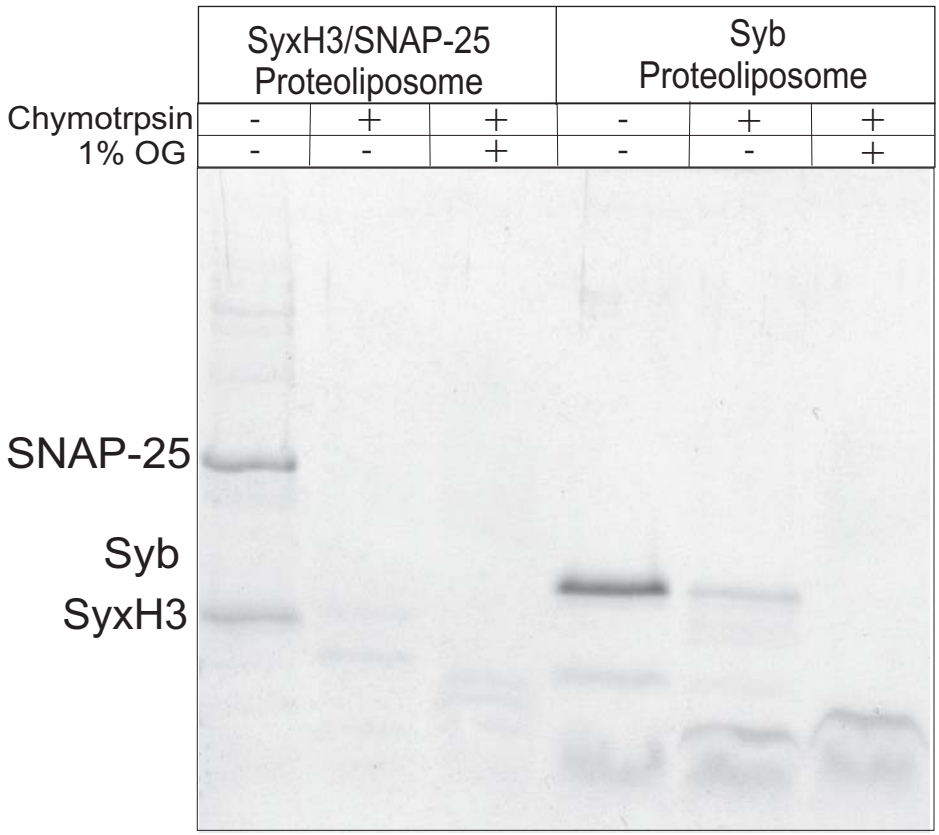

Figure 6.7 Orientation of the SNAREs in proteoliposomes. The SyxH3/SNAP-25 proteoliposomes and the Syb proteoliposomes were treated with Chymotrpsin in the absence or prescence of detergent (1% OG) and analyzed by SDS-PAGE and Coomassie staining.

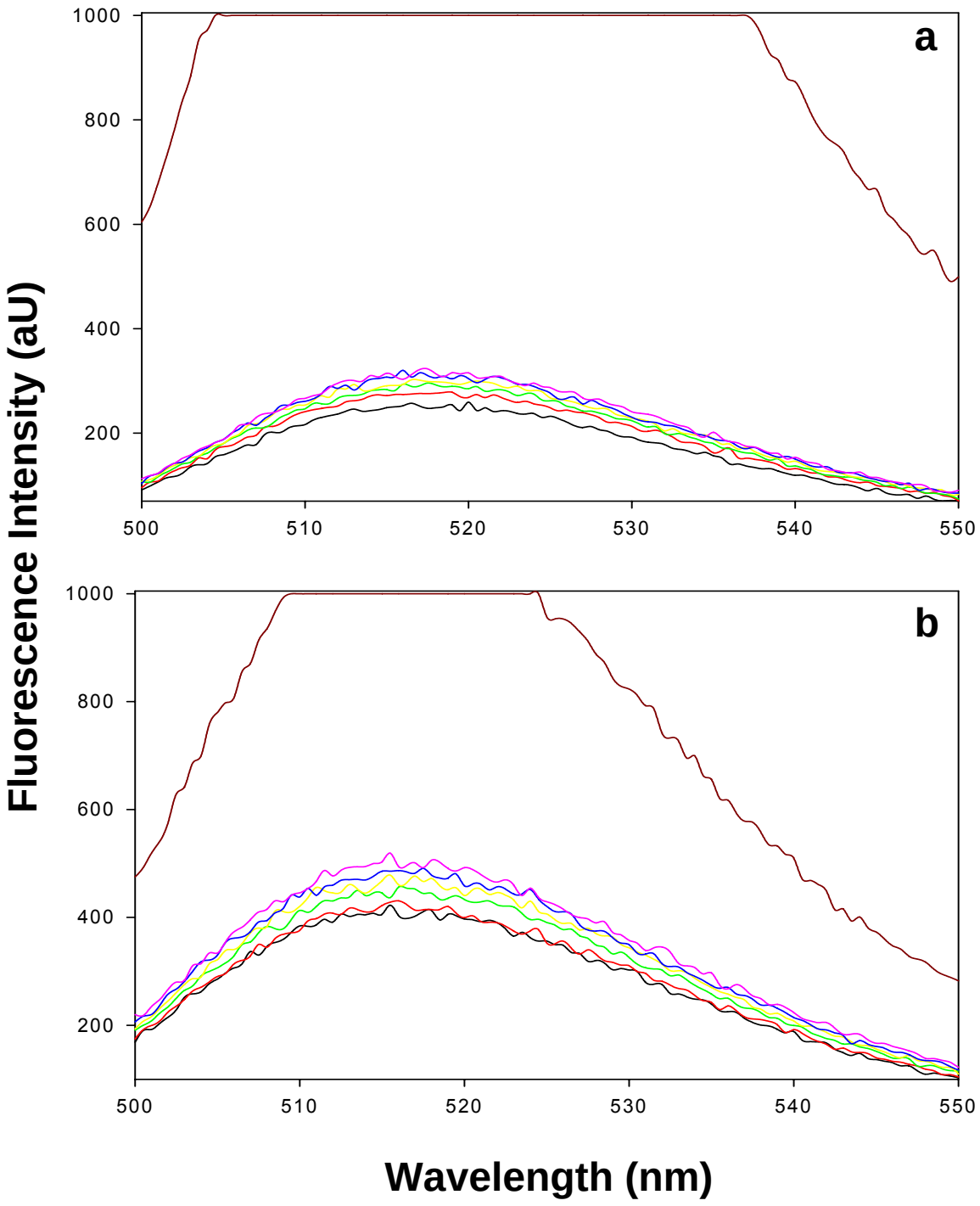
a
b
1000
800
600
400
200
500
510
520
530
540
550
Fluorescence Intensity (aU)
Wavelength (nm)

Figure 6.8

Figure 6.8 Leakage of the liposomes (a) or the Syb proteoliposomes (b) monitored by CF release. The fluorescence of CF was monitored every 20 minutes and the spectra were colored in black, red, green, yellow, blue and pink, sequentially. 1% OG was added to solubilize the liposomes or the proteoliposomes at the end of each experiment to completely release CF incorporated in the liposomes or the proteoliposomes (brown curves).

Syb proteoliposomes probably because some CF leaked out during protein incorporation and lead to less self-quenching and higher background (Figure 6.8b). Indeed, the total CF fluorescence intensity of the Syb proteoliposomes (after adding detergent) was much lower than that of the protein free liposomes. Unfortunately, the fluorescence intensity of 100% released CF for both liposomes and proteoliposomes exceeded the maximum signal of the instrument, so I was not able to normalize the results. However, it is clear that in two-hour period, the same time period that fusion would be measured, the leakage is very little.

In summary, I have successfully reconstituted the SNAREs into liposomes. The proteoliposomes prepared with the current method have homogeneous size distribution. The protein incorporation is highly efficient with correct unidirectional orientation and the proteoliposome is stable enough for the following fusion assays.

6.3.2 Fusion Assay

To test whether the proteoliposomes containing SyxH3/SNAP-25 and the proteoliposomes containing Syb could fuse with each other, I employed a well-characterized lipid mixing assay (Struck *et al.*, 1981). This assay involves fluorescence resonance energy transfer between NBD-DPPE (N-(7-nitro-2,1,3-benzoxadiazole-4-yl)-1,2-dipalmitoyl-PE), the energy donor, and rhodamine-DPPE (N-(lissamine rhodamine B sulfonyl) 1,2-dipalmitoyl-PE), the energy acceptor. When both fluorescent lipids are present in liposomes at appropriate surface densities, the NBD fluorescence will be quenched because of the energy transfer. When these fluorescent “donor” liposomes fuse with other nonfluorescent “acceptor” liposomes, the

surface densities of both fluorescent lipids are reduced, which results in a decrease in quenching and an increase in NBD fluorescence at 538 nm (Figure 6.9).

6.3.2.1 Fusion between the v- and t-SNARE proteoliposomes prepared with the reconstitution method used by Rothman and colleagues

To verify the results reported by Rothman and colleagues (Weber *et al.*, 1998; Parlati *et al.*, 1999), I followed the same protocols as described (Weber *et al.*, 1998) to reconstitute the purified SNAREs. The leakage assay to test stability of the proteoliposomes prepared with this method was hindered by the difficulties to incorporate CF inside the proteoliposomes. However, as discussed before, Rothman and colleagues used exceedingly large amount of synaptobrevin to prepare the v-SNARE proteoliposomes, which thus might be highly unstable. Fusion between the v- and t-SNARE proteoliposomes was also monitored with the lipid mixing assay as described (Weber *et al.*, 1998). Similarly, a substantial amount of lipid mixing was observed (red curve in Figure 6.10), whereas no fusion was observed between the proteoliposomes containing v-SNAREs or t-SNAREs and the protein free liposomes (black curve in Figure 6.10). Thus, these experiments serve as a positive control for both the lipid mixing assay and the SNARE protein fragments that I am using, which are slightly different from the constructs used by Rothman and colleagues. Interestingly, Rothman and colleagues claimed that successful reconstitution of t-SNARE vesicles depended on the use of a preformed complex of syntaxin and SNAP-25 coexpressed in the same bacterial cells (Weber *et al.*, 1998). However, I prepared the SyxH3 and the SNAP-25 from bacterial cells separately, and then mixed them before reconstitution. The similar results from my

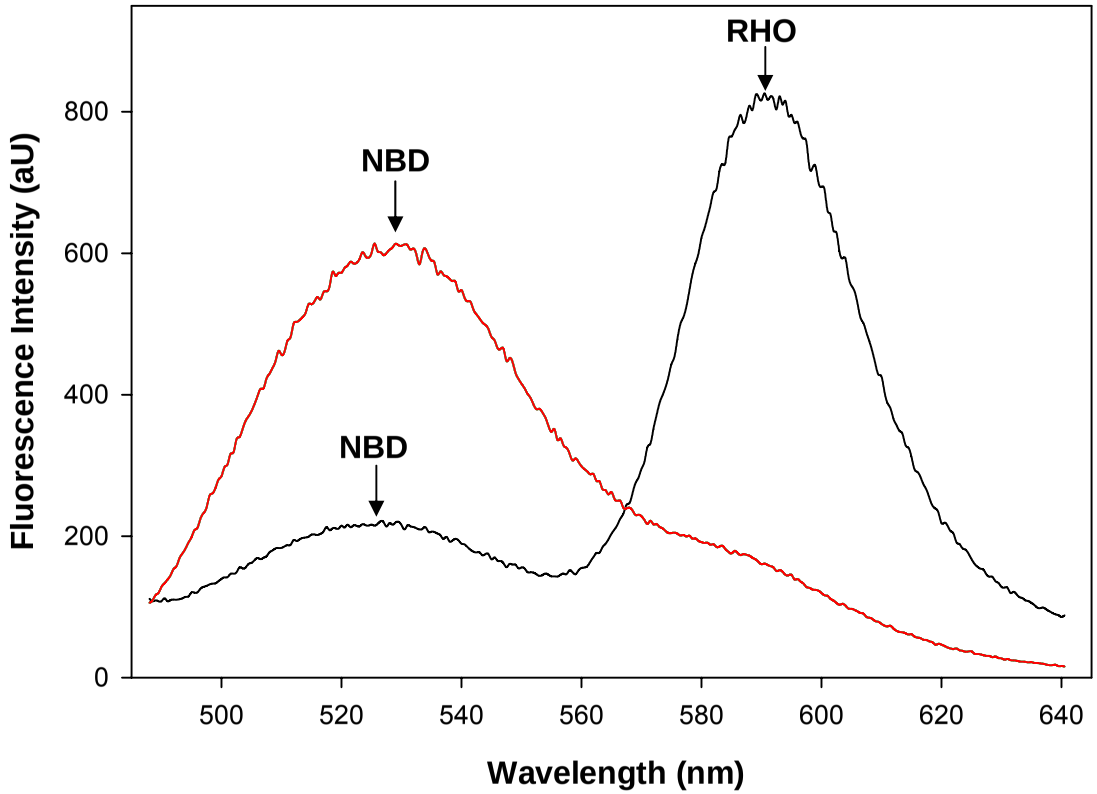

Figure 6.9 Typical fluorescence spectra of the NBD/rhodamine labeled liposomes. Fluorescence spectra of the liposomes containing 1.5% NBD-DPPE and 1.5% rhodamine-DPPE before (black curve) and after (red curve) adding detergent (1% OG). The excitation wavelength was 460nm. Before adding detergent, the NBD signal was quenched by rhodamin (Black curve). After adding detergent, the NBD signal increased dramatically (Red curve). Rhodamine is abbreviated as RHO.

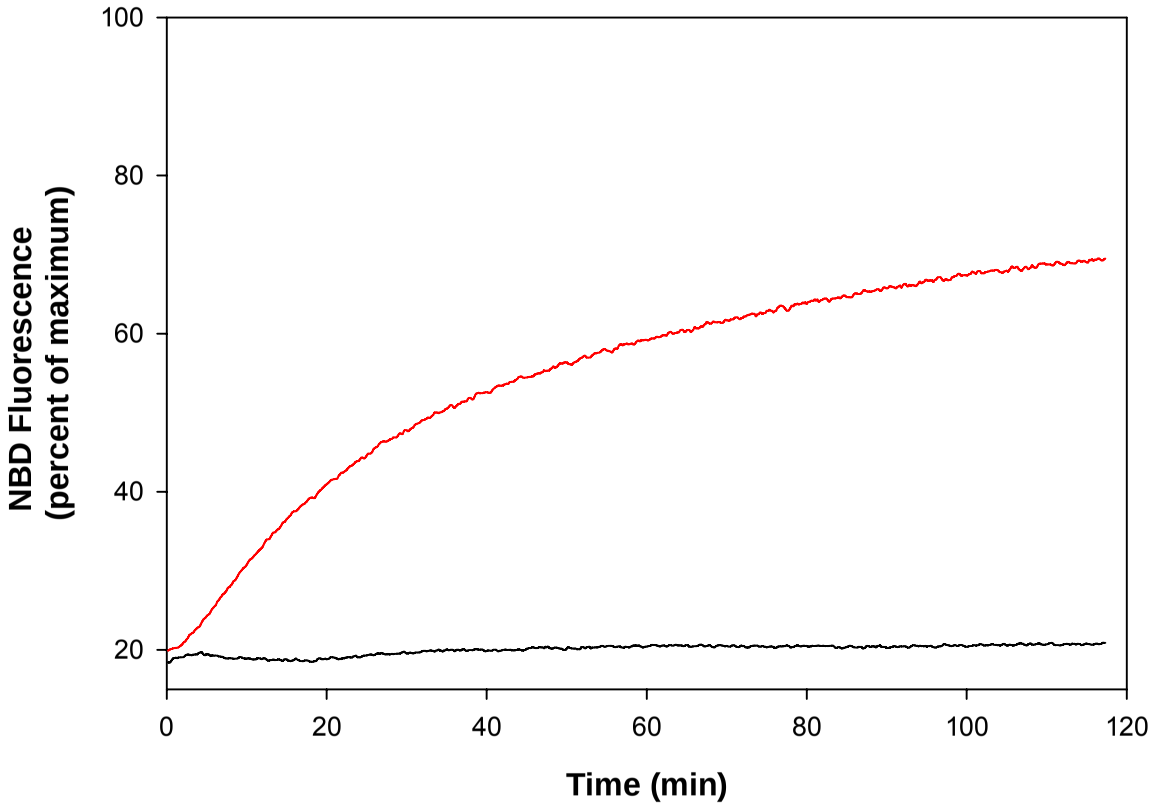

Figure 6.10 Fusion between the v- and t-SNARE proteoliposomes prepared with the reconstitution method described in (Weber *et al.*, 1998). The v-SNARE proteoliposomes containing fluorescent lipids were mixed with non-fluorescent liposomes (black) or t-SNARE proteoliposomes (red). NBD fluorescence was monitored at 538nm and normalized by setting the lowest NBD fluorescence signal to 0% and the maximal signal after adding detergent to 100% fluorescence.

experiment show that the coexpression of the SyxH3 and the SNAP-25 in the same bacterial cells is not necessary.

6.3.2.2 Fusion between the well-characterized v- and t-SNARE proteoliposomes

I then repeated the same lipid mixing assay with the proteoliposomes prepared with the new reconstitution methods and carefully characterized. Very little fusion was observed after two hours at 37^{o}C (red curve in Figure 6.11). Note that the v-SNARE proteoliposomes in this experiment contained 10 fold less synaptobrevin than those prepared with the reconstitution method used by Rothman and colleagues, which may explain the dramatic difference observed in these two experiments. In fact, Chapman and his colleagues also observed much less fusion when they followed the same reconstitution protocols used by Rothman and colleagues, except for lowering the amount of synaptobrevin in the v-SNARE proteoliposomes (Tucker *et al.*, 2004).

To get a better sense of how much fusion has occurred, I calibrated the fusion assay. Since the efficiency of energy transfer is independent of the surface density of the energy donor, NBD-DPPE (Struck *et al.*, 1981), I prepared a series of the liposomes containing 1.5% NBD-DPPE and different percentage of rhodamine-DPPE ranging from 0 to 2.5%. The NBD fluorescence of each liposome was recorded in the absence and presence of the detergent (1% OG). A standard curve of the energy transfer efficiency versus the rhodamine concentration was then generated for further calibration (Figure 6.12). In my reconstitution assay, there are two fold more synaptobrevin molecules in each v-SNARE proteoliposome than the

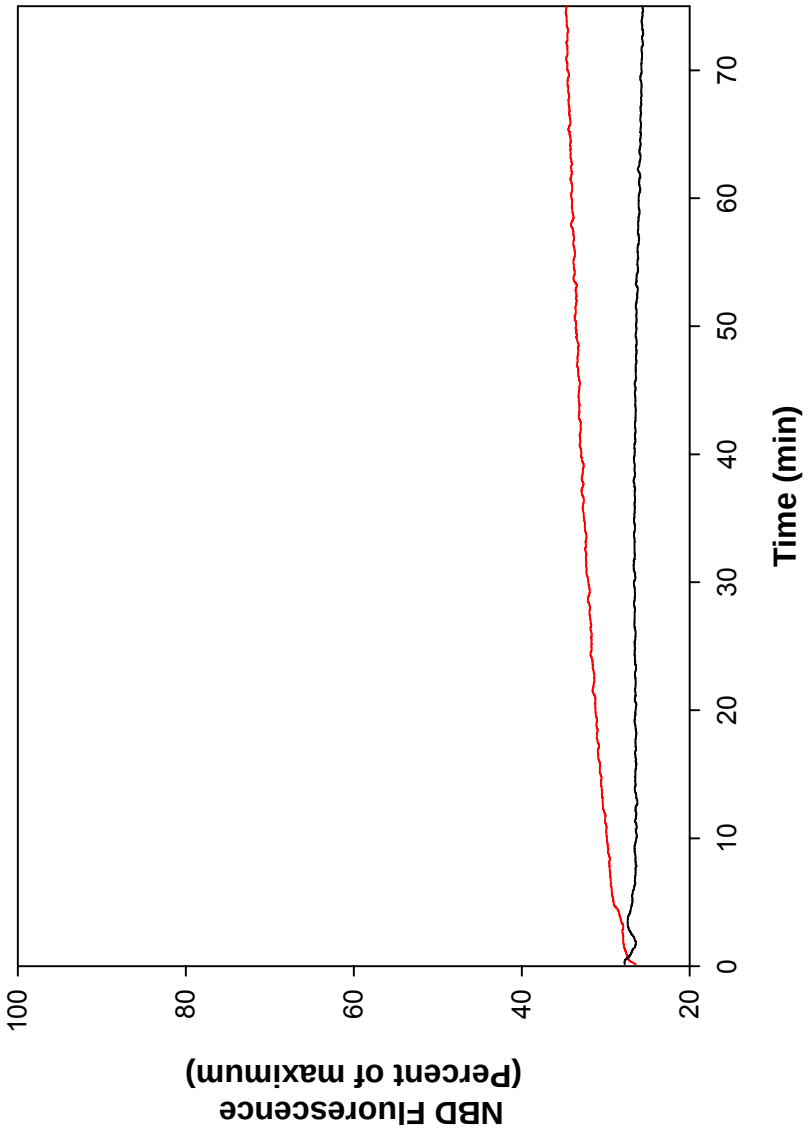

Figure 6.11 Fusion between the well-characterized v- and t-SNARE proteoliposomes. The experimental setting and color coding were the same as those for Figure 6.10.

SyxH3/SNAP-25 molecules in each t-SNARE proteoliposome. To have equal number of v- and t-SNARE proteins, I added 2 fold more t-SNARE proteoliposomes than v-SNARE proteoliposomes in each fusion reaction. Assuming that once a t-SNARE proteoliposome fuses with a v-SNARE proteoliposome all the SyxH3/SNAP-25 molecules would immediately form complexes with the Syb molecules after one round of fusion, only half of the Syb molecules on the liposomes would remain available for the next round of fusion. Therefore, the maximum number of rounds of fusion for the fluorescent donor proteoliposomes (containing v-SNARE) should be two. Based on these arguments, I prepared three Syb proteoliposomes with 1.5%, 0.75% and 0.375% of NBD/rhodamine, corresponding to 0, 1 and 2 rounds of fusion, respectively. Their transfer efficiency versus the percentage of rhodamine fits very well with the standard curve and 2 rounds of fusion lead to a change of transfer efficiency from 80% to 5% (red dots in Figure 6.12). However, the efficiency of energy transfer only changed from 75% to 70% in the fusion reaction performed with the well-characterized proteoliposomes. Estimation based on the standard curve showed that only about 0.17 rounds of fusion occurred. For comparison, the fusion assay using the proteoliposomes prepared with the Rothman's reconstitution methods showed that the efficiency of energy transfer changed from 80% to 30% under the same conditions, which corresponds to about 1.5 rounds of fusion.

6.4 Discussion and Future Direction

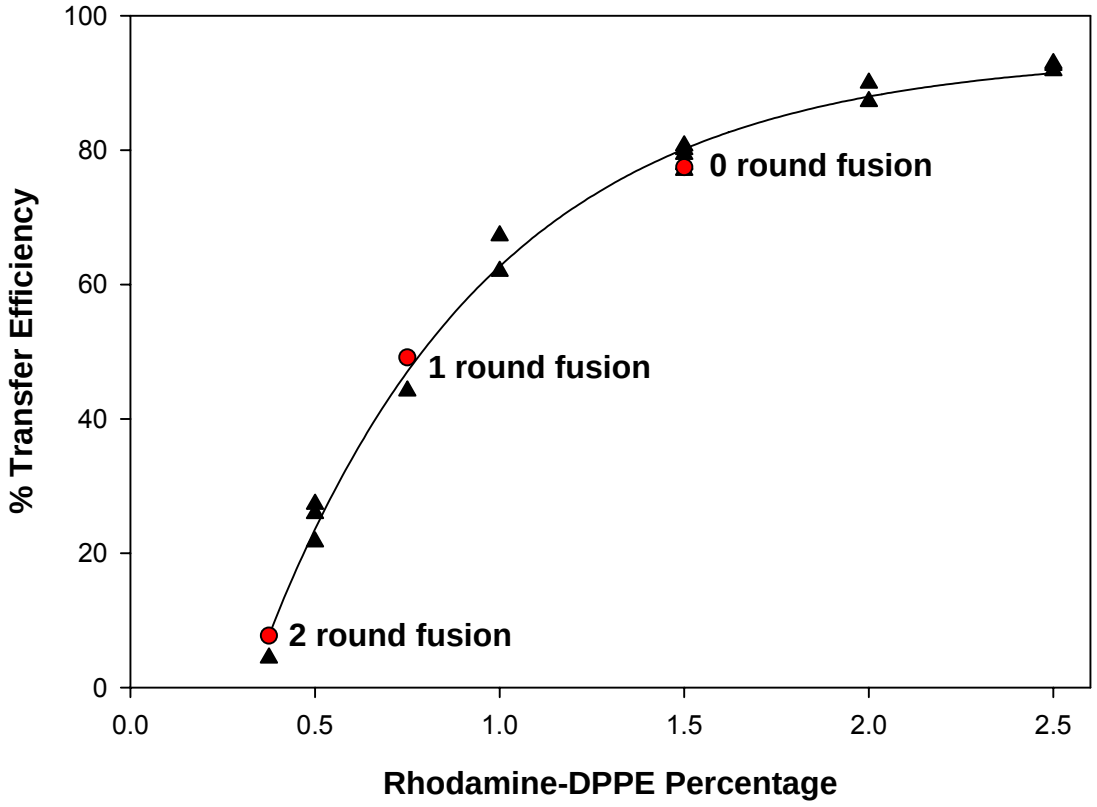

Figure 6.12 Calibration of the fusion assay. Efficiency of energy transfer as a function of the percentage of rhodamine-DPPE in the liposomes (black curve). The amount of NBD-DPPE was kept constant (1.5%), while the amount of rhodamine-DPPE was varied to the indicated concentrations. The results from three independent experiments (black triangles) were fitted to the exponential function ($Y=-64.0507+158.3109\times(1-0.1995^{x})$), where Y is the energy transfer efficiency and x is the percentage of rhodamine-DPPE. The energy transfer efficiencies for the Syb proteoliposomes containing 1.5%, 0.75% and 0.375% of NBD/rhodamine are shown (red dots).

The SNAREs play an important role in neurotransmitter release. However, whether the SNAREs alone can mediate membrane fusion is still under debate. To understand the exact function of the SNAREs, several attempts of reconstitution of membrane fusion with SNAREs in cell-free assay systems have been reported (Weber *et al.*, 1998; Parlati *et al.*, 1999; Hu *et al.*, 2002; Kweon *et al.*, 2003; Schuette *et al.*, 2004; Chen *et al.*, 2004). However, different studies yielded contradictory results (Rizo, 2003). To clarify the confusion, I set up a reconstitution system with well characterized proteoliposomes containing t-SNAREs or v-SNAREs. Interestingly, small amount of fusion was observed between the fluorescent labeled v-SNARE proteoliposomes and the unlabeled t-SNARE proteoliposomes. In addition, some preliminary data show that the observed fusion was caused by small percentage of proteoliposomes which contained large amount of protein. Therefore, SNAREs alone are not sufficient to mediate membrane fusion.

How could we explain the robust lipid-mixing observed between the proteoliposomes prepared with the reconstitution method used by Rothman and colleagues? Imagining that a v-SNARE proteoliposome approaches a t-SNARE proteoliposome, the SNAREs residing at the closest region between two proteoliposomes can form SNARE complexes easily without causing membrane fusion (Figure 6.13a). However, the SNAREs located at the other region of the proteoliposomes would also start to associate through their N-terminal regions (Figure 6.13b). According to a zippering model (Matos *et al.*, 2003), the partially assembled SNARE complexes would zip up towards their C-termini in order to form fully assembled core complexes. Such a process exerts strong forces on the membranes where the SNAREs

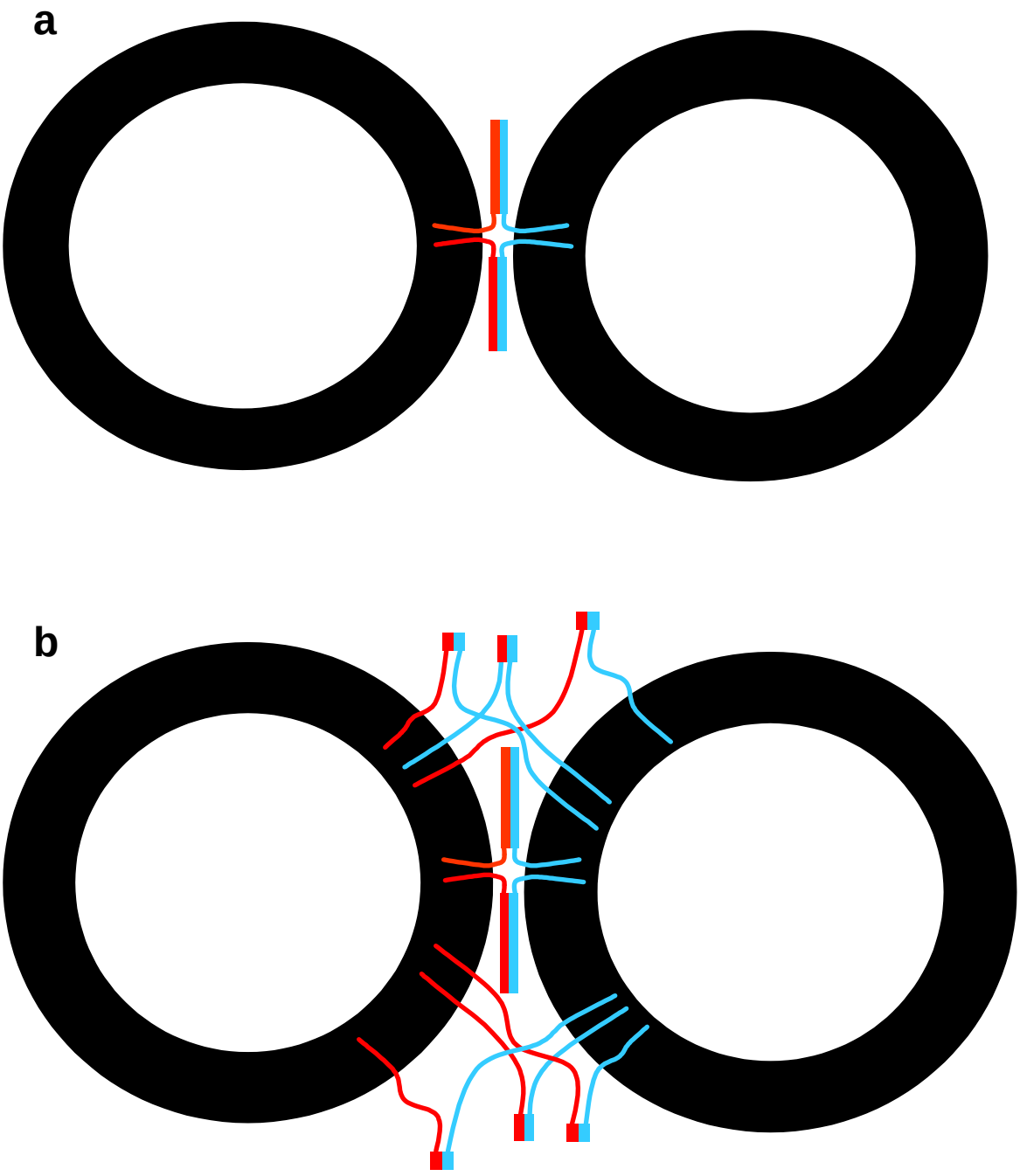
a
b

Figure 6.13 Models illustrating the problem associated with the reconstitution assay performed by Rothman and his colleagues. (a) The formation of the core complex at the closest point between the proteoliposomes containing v- and t-SNAREs. (b) The reconstituted SNAREs located at the other regions of the proteoliposomes can associate through their N-terminal region. The proteoliposomes are pictured as black circles. The v-SNAREs are colored in red and the t-SNAREs are colored in blue.

anchored. If the proteoliposomes were loaded with large amounts of SNAREs (750 copies of synaptobrevin per proteoliposome, see Weber *et al.*, 1998), there could be hundreds of the partially formed SNARE complexes trying to form fully assembled core complexes, which would lead to disordered rupture of membrane, rather than a smooth, physiological membrane fusion. Although the discussion above is just speculation, there are several lines of evidence supporting this idea. For instance, the insertion of a flexible linker (up to 27 residues) between the transmembrane domain and the SNARE motif region of syntaxin or synaptobrevin only moderately affected the "fusion" (McNew *et al.*, 1999). This observation suggested that the lipid-mixing is very unlikely to be caused by the formation of the SNARE complexes at the closest point between the proteoliposomes. In addition, significant leakage accompanying the "fusion" process, as a direct consequence of the disordered membrane rupture, has been observed (Nickel *et al.*, 1999). Unfortunately, the leakage was tested with an oligonucleotide probe, which might be too large for an assessment of leakage (Nickel *et al.*, 1999). More definitive evidence would depend on the results form a leakage assay with appropriate probes, such as carboxyfluorescein.

Although the SNAREs undoubtedly play a crucial role in membrane fusion, there is so far no clear evidence showing that the SNAREs are capable of forming fusion pores or organizing the formation of fusion pores. Hence, other important component(s) is required for smooth, well-organized and tightly regulated fusion. Potential candidates for such roles include several proteins that have been found to be critical for neurotransmitter release, such as munc18-1, munc13-1 and the synaptic vesicle Ca^{2+} sensor synaptotagmin I. With the

carefully characterized reconstitution assay, the function of these additional components can be directly tested.

BIBLIOGRAPHY

1. Almers W and Tse FW (1990) Transmitter release from synapses: does a preassembled fusion pore initiate exocytosis? *Neuron,* **4,** 813-818.

2. Arac D, Murphy T, and Rizo J (2003) Facile detection of protein-protein interactions by one-dimensional NMR spectroscopy. *Biochemistry,* **42,** 2774-2780.

3. Augustine GJ, Burns ME, DeBello WM, Pettit DL, and Schweizer FE (1996) Exocytosis: proteins and perturbations. *Annu Rev Pharmacol Toxicol,* **36,** 659-701.

4. Bai YW, Milne JS, Mayne L, and Englander SW (1993) Primary Structure Effects on Peptide Group Hydrogen-Exchange. *Proteins-Structure Function and Genetics,* **17,** 75-86.

5. Bailey S (1994) The Ccp4 Suite - Programs for Protein Crystallography. *Acta Crystallographica Section D-Biological Crystallography,* **50,** 760-763.

6. Banerjee A, Kowalchyk JA, DasGupta BR, and Martin TFJ (1996) SNAP-25 is required for a late postdocking step in Ca2+-dependent exocytosis. *Journal of Biological Chemistry,* **271,** 20227-20230.

7. Basanez G, Goni FM, and Alonso A (1998) Effect of single chain lipids on phospholipase C-promoted vesicle fusion. A test for the stalk hypothesis of membrane fusion. *Biochemistry,* **37,** 3901-3908.

8. Bennett MK and Scheller RH (1993) The molecular machinery for secretion is conserved from yeast to neurons. *Proc Natl Acad Sci U S A,* **90,** 2559-2563.

9. Bennett MR (1999) The concept of a calcium sensor in transmitter release. *Prog Neurobiol,* **59,** 243-277.

10. Betz A, Okamoto M, Benseler F, and Brose N (1997) Direct interaction of the rat unc-13 homologue Munc13-1 with the N terminus of syntaxin. *J Biol Chem,* **272,** 2520-2526.

11. Blasi J, Chapman ER, Link E, Binz T, Yamasaki S, De Camilli P, Südhof TC, Niemann H, and Jahn R (1993a) Botulinum neurotoxin A selectively cleaves the synaptic protein SNAP-25. *Nature,* **365,** 160-163.

12. Blasi J, Chapman ER, Yamasaki S, Binz T, Niemann H, and Jahn R (1993b) Botulinum neurotoxin C1 blocks neurotransmitter release by means of cleaving HPC-1/syntaxin. *EMBO J,* **12,** 4821-4828.

13. Bollmann JH, Sakmann B, and Borst JG (2000) Calcium sensitivity of glutamate release in a calyx-type terminal. *Science,* **289,** 953-957.

14. Bracher A, Perrakis A, Dresbach T, Betz H, and Weissenhorn W (2000) The X-ray crystal structure of neuronal Sec1 from squid sheds new light on the role of this protein in exocytosis. *Structure Fold Des,* **8,** 685-694.

15. Brenner S (1974) The genetics of Caenorhabditis elegans. *Genetics,* **77,** 71-94.

16. Broadie K, Prokop A, Bellen HJ, O'Kane CJ, Schulze KL, and Sweeney ST (1995) Syntaxin and synaptobrevin function downstream of vesicle docking in Drosophila. *Neuron,* **15,** 663-673.

17. Brose N, Petrenko AG, Südhof TC, and Jahn R (1992) Synaptotagmin: a calcium sensor on the synaptic vesicle surface. *Science,* **256,** 1021-1025.

18. Brunger AT, Adams PD, Clore GM, Delano WL, Gros P, Grosse-Kunstleve RW, Jiang JS, Kuszewski J, Nilges M, Pannu NS, Read RJ, Rice LM, Simonson T, and Warren GL (1998) Crystallography & NMR system: A new software suite for macromolecular structure determination. *Acta Crystallographica Section D-Biological Crystallography,* **54,** 905-921.

19. Carr CM, Grote E, Munson M, Hughson FM, and Novick PJ (1999) Sec1p binds to SNARE complexes and concentrates at sites of secretion. *J Cell Biol,* **146,** 333-344.

20. Chapman ER (2002) Synaptotagmin: A Ca(2+) sensor that triggers exocytosis? *Nat Rev Mol Cell Biol,* **3,** 498-508.

21. Chen X, Tomchick DR, Kovrigin E, Arac D, Machius M, Südhof TC, and Rizo J (2002) Three-dimensional structure of the complexin/SNARE complex. *Neuron,* **33,** 397-409.

22. Chen Y, Xu YB, Zhang F, and Shin YK (2004) Constitutive versus regulated SNARE assembly: a structural basis. *Embo Journal,* **23,** 681-689.

23. Chen YA, Scales SJ, Jagath JR, and Scheller RH (2001) A discontinuous SNAP-25 C-terminal coil supports exocytosis. *J Biol Chem,* **276,** 28503-28508.

24. Chen YA, Scales SJ, Patel SM, Doung YC, and Scheller RH (1999) SNARE complex formation is triggered by Ca2+ and drives membrane fusion. *Cell,* **97,** 165-174.

25. Chen YA and Scheller RH (2001) Snare-mediated membrane fusion. *Nature Reviews Molecular Cell Biology,* **2,** 98-106.

26. Chernomordik L (1996) Non-bilayer lipids and biological fusion intermediates. *Chem Phys Lipids,* **81,** 203-213.

27. Chernomordik L, Kozlov MM, and Zimmerberg J (1995) Lipids in biological membrane fusion. *J Membr Biol,* **146,** 1-14.

28. Clore GM and Gronenborn AM (1994) Multidimensional Heteronuclear Nuclear-Magnetic-Resonance of Proteins. *Nuclear Magnetic Resonance, Pt C,* **239,** 349-363.

29. Clore GM and Gronenborn AM (1998) New methods of structure refinement for macromolecular structure determination by NMR. *Proc Natl Acad Sci U S A,* **95,** 5891-5898.

30. Cornilescu G, Delaglio F, and Bax A (1999) Protein backbone angle restraints from searching a database for chemical shift and sequence homology. *J Biomol NMR,* **13,** 289-302.

31. Davletov BA and Südhof TC (1993) A single C2 domain from synaptotagmin I is sufficient for high affinity Ca2+/phospholipid binding. *J Biol Chem,* **268,** 26386-26390.

32. Deitcher DL, Ueda A, Stewart BA, Burgess RW, Kidokoro Y, and Schwarz TL (1998) Distinct requirements for evoked and spontaneous release of neurotransmitter are revealed by mutations in the Drosophila gene neuronal-synaptobrevin. *J Neurosci,* **18,** 2028-2039.

33. Delaglio F, Grzesiek S, Vuister GW, Zhu G, Pfeifer J, and Bax A (1995) Nmrpipe - A Multidimensional Spectral Processing System Based on Unix Pipes. *Journal of Biomolecular Nmr,* **6,** 277-293.

34. Dulubova I, Sugita S, Hill S, Hosaka M, Fernandez I, Südhof TC, and Rizo J (1999) A conformational switch in syntaxin during exocytosis: role of munc18. *EMBO J,* **18,** 4372-4382.

35. Dulubova I, Yamaguchi T, Arac D, Li H, Huryeva I, Min SW, Rizo J, and Südhof TC (2003) Convergence and divergence in the mechanism of SNARE binding by Sec1/Munc18-like proteins. *Proc Natl Acad Sci U S A,* **100,** 32-37.

36. Eastwood SL and Harrison PJ (2000) Hippocampal synaptic pathology in schizophrenia, bipolar disorder and major depression: a study of complexin mRNAs. *Mol Psychiatry,* **5,** 425-432.

37. Edwardson JM, Wang CT, Gong B, Wyttenbach A, Bai J, Jackson MB, Chapman ER, and Morton AJ (2003) Expression of mutant huntingtin blocks exocytosis in PC12 cells by depletion of complexin II. *J Biol Chem,* **278,** 30849-30853.

38. Englander SW and Hiller R (2001) Dynamics and thermodynamics of hyperthermophilic proteins by hydrogen exchange. *Hyperthermophilic Enzymes, Pt C,* **334,** 342-350.

39. Ernst JA and Brunger AT (2003) High resolution structure, stability, and synaptotagmin binding of a truncated neuronal SNARE complex. *Journal of Biological Chemistry,* **278,** 8630-8636.

40. Farmer BT and Venters RA (1995) Assignment of Side-Chain C-13 Resonances in Perdeuterated Proteins. *Journal of the American Chemical Society,* **117,** 4187-4188.

41. Fasshauer D, Antonin W, Subramaniam V, and Jahn R (2002) SNARE assembly and disassembly exhibit a pronounced hysteresis. *Nat Struct Biol,* **9,** 144-151.

42. Fasshauer D, Bruns D, Shen B, Jahn R, and Brunger AT (1997a) A structural change occurs upon binding of syntaxin to SNAP-25. *J Biol Chem,* **272,** 4582-4590.

43. Fasshauer D, Eliason WK, Brunger AT, and Jahn R (1998a) Identification of a minimal core of the synaptic SNARE complex sufficient for reversible assembly and disassembly. *Biochemistry,* **37,** 10354-10362.

44. Fasshauer D, Otto H, Eliason WK, Jahn R, and Brunger AT (1997b) Structural changes are associated with soluble N-ethylmaleimide-sensitive fusion protein attachment protein receptor complex formation. *J Biol Chem,* **272,** 28036-28041.

45. Fasshauer D, Sutton RB, Brunger AT, and Jahn R (1998b) Conserved structural features of the synaptic fusion complex: SNARE proteins reclassified as Q- and R-SNAREs. *Proc Natl Acad Sci U S A,* **95,** 15781-15786.

46. Fernandez C and Wider G (2003) TROSY in NMR studies of the structure and function of large biological macromolecules. *Curr Opin Struct Biol,* **13,** 570-580.

47. Fernandez I, Arac D, Ubach J, Gerber SH, Shin O, Gao Y, Anderson RG, Südhof TC, and Rizo J (2001) Three-dimensional structure of the synaptotagmin 1 c(2)b-domain. Synaptotagmin 1 as a phospholipid binding machine. *Neuron,* **32,** 1057-1069.

48. Fernandez I, Ubach J, Dulubova I, Zhang X, Südhof TC, and Rizo J (1998) Three-dimensional structure of an evolutionarily conserved N-terminal domain of syntaxin 1A. *Cell,* **94,** 841-849.

49. Fernandez-Chacon R, Konigstorfer A, Gerber SH, Garcia J, Matos MF, Stevens CF, Brose N, Rizo J, Rosenmund C, and Südhof TC (2001) Synaptotagmin I functions as a calcium regulator of release probability. *Nature,* **410,** 41-49.

50. Fernandez-Chacon R, Shin OH, Konigstorfer A, Matos MF, Meyer AC, Garcia J, Gerber SH, Rizo J, Südhof TC, and Rosenmund C (2002) Structure/function analysis of Ca2+ binding to the C2A domain of synaptotagmin 1. *J Neurosci,* **22,** 8438-8446.

51. Ferro-Novick S and Jahn R (1994) Vesicle fusion from yeast to man. *Nature,* **370,** 191-193.

52. Fiebig KM, Rice LM, Pollock E, and Brunger AT (1999) Folding intermediates of SNARE complex assembly. *Nat Struct Biol,* **6,** 117-123.

53. French S and Wilson K (1978) Treatment of Negative Intensity Observations. *Acta Crystallographica Section A,* **34,** 517-525.

54. Fung BK and Stryer L (1978) Surface density determination in membranes by fluorescence energy transfer. *Biochemistry,* **17,** 5241-5248.

55. Garcia EP, Gatti E, Butler M, Burton J, and De Camilli P (1994) A rat brain Sec1 homologue related to Rop and UNC18 interacts with syntaxin. *Proc Natl Acad Sci U S A,* **91,** 2003-2007.

56. Gardner KH and Kay LE (1998) The use of 2H, 13C, 15N multidimensional NMR to study the structure and dynamics of proteins. *Annu Rev Biophys Biomol Struct,* **27,** 357-406.

57. Geppert M, Goda Y, Hammer RE, Li C, Rosahl TW, Stevens CF, and Südhof TC (1994) Synaptotagmin I: a major Ca2+ sensor for transmitter release at a central synapse. *Cell,* **79,** 717-727.

58. Geppert M and Südhof TC (1998) RAB3 and synaptotagmin: The yin and yang of synaptic membrane fusion. *Annual Review of Neuroscience,* **21,** 75-95.

59. Gerona RR, Larsen EC, Kowalchyk JA, and Martin TF (2000) The C terminus of SNAP25 is essential for Ca(2+)-dependent binding of synaptotagmin to SNARE complexes. *J Biol Chem,* **275,** 6328-6336.

60. Goda Y and Stevens CF (1994) Two components of transmitter release at a central synapse. *Proc Natl Acad Sci U S A,* **91,** 12942-12946.

61. Grote E, Carr CM, and Novick PJ (2000) Ordering the final events in yeast exocytosis. *J Cell Biol,* **151,** 439-452.

62. Grzesiek S and Bax A (1993) The Importance of Not Saturating H2O in Protein Nmr - Application to Sensitivity Enhancement and Noe Measurements. *Journal of the American Chemical Society,* **115,** 12593-12594.

63. Hanson PI, Roth R, Morisaki H, Jahn R, and Heuser JE (1997) Structure and conformational changes in NSF and its membrane receptor complexes visualized by quick-freeze/deep-etch electron microscopy. *Cell,* **90,** 523-535.

64. Hao LN, Rigaud JL, and Inesi G (1994) Ca2+/H+ Countertransport and Electrogenicity in Proteoliposomes Containing Erythrocyte Plasma-Membrane Ca-Atpase and Exogenous Lipids. *Journal of Biological Chemistry,* **269,** 14268-14275.

65. Hata Y, Slaughter CA, and Südhof TC (1993) Synaptic vesicle fusion complex contains unc-18 homologue bound to syntaxin. *Nature,* **366,** 347-351.

66. Hayashi T, McMahon H, Yamasaki S, Binz T, Hata Y, Südhof TC, and Niemann H (1994) Synaptic vesicle membrane fusion complex: action of clostridial neurotoxins on assembly. *EMBO J,* **13,** 5051-5061.

67. Helm CA and Israelachvili JN (1993) Forces between phospholipid bilayers and relationship to membrane fusion. *Methods Enzymol,* **220,** 130-143.

68. Hu K, Carroll J, Fedorovich S, Rickman C, Sukhodub A, and Davletov B (2002) Vesicular restriction of synaptobrevin suggests a role for calcium in membrane fusion. *Nature,* **415,** 646-650.

69. Ishizuka T, Saisu H, Odani S, and Abe T (1995) Synaphin: a protein associated with the docking/fusion complex in presynaptic terminals. *Biochem Biophys Res Commun,* **213,** 1107-1114.

70. Israelachvili JN, Marcelja S, and Horn RG (1980) Physical principles of membrane organization. *Q Rev Biophys,* **13,** 121-200.

71. Jahn R and Südhof TC (1994) Synaptic vesicles and exocytosis. *Annu Rev Neurosci,* **17,** 219-246.

72. Jahn R and Südhof TC (1999) Membrane fusion and exocytosis. *Annu Rev Biochem,* **68,** 863-911.

73. Johnson BA and Blevins RA (1994) Nmr View - A Computer-Program for the Visualization and Analysis of Nmr Data. *Journal of Biomolecular Nmr,* **4,** 603-614.

74. Jones TA, Zou JY, Cowan SW, and Kjeldgaard M (1991) Improved Methods for Building Protein Models in Electron-Density Maps and the Location of Errors in These Models. *Acta Crystallographica Section A,* **47,** 110-119.

75. Kim KS, Fuchs JA, and Woodward CK (1993) Hydrogen-Exchange Identifies Native-State Motional Domains Important in Protein-Folding. *Biochemistry,* **32,** 9600-9608.

76. Kuboniwa H, Grzesiek S, Delaglio F, and Bax A (1994) Measurement of HN-H alpha J couplings in calcium-free calmodulin using new 2D and 3D water-flip-back methods. *J Biomol NMR,* **4,** 871-878.

77. Kweon DH, Kim CS, and Shin YK (2003) Regulation of neuronal SNARE assembly by the membrane. *Nature Structural Biology,* **10,** 440-447.

78. Lee J and Lentz BR (1997) Evolution of lipidic structures during model membrane fusion and the relation of this process to cell membrane fusion. *Biochemistry,* **36,** 6251-6259.

79. Lerman JC, Robblee J, Fairman R, and Hughson FM (2000) Structural analysis of the neuronal SNARE protein syntaxin-1A. *Biochemistry,* **39,** 8470-8479.

80. Levy D, Bluzat A, Seigneuret M, and Rigaud JL (1990a) A systematic study of liposome and proteoliposome reconstitution involving Bio-Bead-mediated Triton X-100 removal. *Biochim Biophys Acta,* **1025,** 179-190.

81. Levy D, Gulik A, Bluzat A, and Rigaud JL (1992) Reconstitution of the Sarcoplasmic-Reticulum Ca2+-Atpase - Mechanisms of Membrane-Protein Insertion Into Liposomes During Reconstitution Procedures Involving the Use of Detergents. *Biochimica et Biophysica Acta,* **1107,** 283-298.

82. Levy D, Gulik A, Seigneuret M, and Rigaud JL (1990b) Phospholipid Vesicle Solubilization and Reconstitution by Detergents - Symmetrical Analysis of the 2 Processes Using Octaethylene Glycol Mono-N-Dodecyl Ether. *Biochemistry,* **29,** 9480-9488.

83. Levy D, Seigneuret M, Bluzat A, and Rigaud JL (1990c) Evidence for Proton Countertransport by the Sarcoplasmic-Reticulum Ca-2+-Atpase During Calcium-Transport in Reconstituted Proteoliposomes with Low Ionic Permeability. *Journal of Biological Chemistry,* **265,** 19524-19534.

84. Lichtenberg D (1985) Characterization of the solubilization of lipid bilayers by surfactants. *Biochim Biophys Acta,* **821,** 470-478.

85. Lichtenberg D, Robson RJ, and Dennis EA (1983) Solubilization of phospholipids by detergents. Structural and kinetic aspects. *Biochim Biophys Acta,* **737,** 285-304.

86. Lin RC and Scheller RH (1997) Structural organization of the synaptic exocytosis core complex. *Neuron,* **19,** 1087-1094.

87. Lin RC and Scheller RH (2000) Mechanisms of synaptic vesicle exocytosis. *Annu Rev Cell Dev Biol,* **16,** 19-49.

88. Lindau M and Almers W (1995) Structure and function of fusion pores in exocytosis and ectoplasmic membrane fusion. *Curr Opin Cell Biol,* **7,** 509-517.

89. Link E, Edelmann L, Chou JH, Binz T, Yamasaki S, Eisel U, Baumert M, Südhof TC, Niemann H, and Jahn R (1992) Tetanus toxin action: inhibition of neurotransmitter release linked to synaptobrevin proteolysis. *Biochem Biophys Res Commun,* **189,** 1017-1023.

90. Littleton JT, Stern M, Schulze K, Perin M, and Bellen HJ (1993) Mutational analysis of Drosophila synaptotagmin demonstrates its essential role in Ca(2+)-activated neurotransmitter release. *Cell,* **74,** 1125-1134.

91. Lodish HF (2000). *Molecular cell biology.* W.H. Freeman, New York.

92. Mackler JM, Drummond JA, Loewen CA, Robinson IM, and Reist NE (2002) The C(2)B Ca(2+)-binding motif of synaptotagmin is required for synaptic transmission in vivo. *Nature,* **418,** 340-344.

93. Margittai M, Fasshauer D, Pabst S, Jahn R, and Langen R (2001) Homo- and heterooligomeric SNARE complexes studied by site-directed spin labeling. *J Biol Chem,* **276,** 13169-13177.

94. Markin VS, Kozlov MM, and Borovjagin VL (1984) On the theory of membrane fusion. The stalk mechanism. *Gen Physiol Biophys,* **3,** 361-377.

95. Matos MF, Mukherjee K, Chen XC, Rizo J, and Südhof TC (2003) Evidence for SNARE zippering during Ca2+-triggered exocytosis in PC12 cells. *Neuropharmacology,* **45,** 777-786.

96. Matos MF, Rizo J, and Südhof TC (2000) The relation of protein binding to function: what is the significance of munc18 and synaptotagmin binding to syntaxin 1, and where are the corresponding binding sites? *Eur J Cell Biol,* **79,** 377-382.

97. May AP, Misura KM, Whiteheart SW, and Weis WI (1999) Crystal structure of the amino-terminal domain of N-ethylmaleimide-sensitive fusion protein. *Nat Cell Biol,* **1,** 175-182.

98. McMahon HT, Missler M, Li C, and Südhof TC (1995) Complexins: cytosolic proteins that regulate SNAP receptor function. *Cell,* **83,** 111-119.

99. McNew JA, Weber T, Engelman DM, Sollner TH, and Rothman JE (1999) The length of the flexible SNAREpin juxtamembrane region is a critical determinant of SNARE-dependent fusion. *Mol Cell,* **4,** 415-421.

100. Misura KM, Gonzalez LC, Jr., May AP, Scheller RH, and Weis WI (2001a) Crystal structure and biophysical properties of a complex between the N-terminal SNARE region of SNAP25 and syntaxin 1a. *J Biol Chem,* **276,** 41301-41309.

101. Misura KM, Scheller RH, and Weis WI (2000) Three-dimensional structure of the neuronal-Sec1-syntaxin 1a complex. *Nature,* **404,** 355-362.

102. Misura KM, Scheller RH, and Weis WI (2001b) Self-association of the H3 region of syntaxin 1A. Implications for intermediates in SNARE complex assembly. *J Biol Chem,* **276,** 13273-13282.

103. Monck JR, Oberhauser AF, and Fernandez JM (1995) The exocytotic fusion pore interface: a model of the site of neurotransmitter release. *Mol Membr Biol,* **12,** 151-156.

104. Morton AJ and Edwardson JM (2001) Progressive depletion of complexin II in a transgenic mouse model of Huntington's disease. *J Neurochem,* **76,** 166-172.

105. Munson M, Chen X, Cocina AE, Schultz SM, and Hughson FM (2000) Interactions within the yeast t-SNARE Sso1p that control SNARE complex assembly. *Nat Struct Biol,* **7,** 894-902.

106. Naday I, Ross S, Westbrook EM, and Zentai G (1998) Charge-coupled device fiber optic taper array x-ray detector for protein crystallography. *Optical Engineering,* **37,** 1235-1244.

107. Navaza J (1994) Amore - An Automated Package for Molecular Replacement. *Acta Crystallographica Section A,* **50,** 157-163.

108. Nicholson KL, Munson M, Miller RB, Filip TJ, Fairman R, and Hughson FM (1998) Regulation of SNARE complex assembly by an N-terminal domain of the t-SNARE Sso1p. *Nat Struct Biol,* **5,** 793-802.

109. Nickel W, Weber T, McNew JA, Parlati F, Sollner TH, and Rothman JE (1999) Content mixing and membrane integrity during membrane fusion driven by pairing of isolated v-SNAREs and t-SNAREs. *Proc Natl Acad Sci U S A,* **96,** 12571-12576.

110. Nietlispach D, Clowes RT, Broadhurst RW, Ito Y, Keeler J, Kelly M, Ashurst J, Oschkinat H, Domaille PJ, and Laue ED (1996) An approach to the structure determination of larger proteins using triple resonance NMR experiments in conjunction with random fractional deuteration. *Journal of the American Chemical Society,* **118,** 407-415.

111. Nonet ML, Grundahl K, Meyer BJ, and Rand JB (1993) Synaptic function is impaired but not eliminated in C. elegans mutants lacking synaptotagmin. *Cell,* **73,** 1291-1305.

112. Otwinowski Z and Minor W (1997) Processing of X-ray diffraction data collected in oscillation mode. *Macromolecular Crystallography, Pt A,* **276,** 307-326.

113. Pabst S, Hazzard JW, Antonin W, Südhof TC, Jahn R, Rizo J, and Fasshauer D (2000) Selective interaction of complexin with the neuronal SNARE complex. Determination of the binding regions. *J Biol Chem,* **275,** 19808-19818.

114. Pabst S, Margittai M, Vainius D, Langen R, Jahn R, and Fasshauer D (2002) Rapid and selective binding to the synaptic SNARE complex suggests a modulatory role of complexins in neuroexocytosis. *J Biol Chem,* **277,** 7838-7848.

115. Parlati F, Weber T, McNew JA, Westermann B, Sollner TH, and Rothman JE (1999) Rapid and efficient fusion of phospholipid vesicles by the alpha-helical core of a SNARE complex in the absence of an N-terminal regulatory domain. *Proc Natl Acad Sci U S A,* **96,** 12565-12570.

116. Paternostre MT, Roux M, and Rigaud JL (1988) Mechanisms of Membrane-Protein Insertion Into Liposomes During Reconstitution Procedures Involving the Use of Detergents .1. Solubilization of Large Unilamellar Liposomes (Prepared by Reverse-Phase Evaporation) by Triton X-100, Octyl Glucoside, and Sodium Cholate. *Biochemistry,* **27,** 2668-2677.

117. Pelham HR (1999) SNAREs and the secretory pathway-lessons from yeast. *Exp Cell Res,* **247,** 1-8.

118. Perin MS, Brose N, Jahn R, and Südhof TC (1991a) Domain structure of synaptotagmin (p65). *J Biol Chem,* **266,** 623-629.

119. Perin MS, Fried VA, Mignery GA, Jahn R, and Südhof TC (1990) Phospholipid binding by a synaptic vesicle protein homologous to the regulatory region of protein kinase C. *Nature,* **345,** 260-263.

120. Perin MS, Johnston PA, Ozcelik T, Jahn R, Francke U, and Südhof TC (1991b) Structural and functional conservation of synaptotagmin (p65) in Drosophila and humans. *J Biol Chem,* **266,** 615-622.

121. Pervushin K, Riek R, Wider G, and Wuthrich K (1997) Attenuated T-2 relaxation by mutual cancellation of dipole-dipole coupling and chemical shift anisotropy indicates an avenue to NMR structures of very large biological macromolecules in solution. *Proc Natl acad Sci U S A,* **94,** 12366-12371.

122. Pevsner J, Hsu SC, and Scheller RH (1994) n-Sec1: a neural-specific syntaxin-binding protein. *Proc Natl Acad Sci U S A,* **91,** 1445-1449.

123. Poirier MA, Hao JC, Malkus PN, Chan C, Moore MF, King DS, and Bennett MK (1998a) Protease resistance of syntaxin.SNAP-25.VAMP complexes. Implications for assembly and structure. *J Biol Chem,* **273,** 11370-11377.

124. Poirier MA, Xiao W, Macosko JC, Chan C, Shin YK, and Bennett MK (1998b) The synaptic SNARE complex is a parallel four-stranded helical bundle. *Nat Struct Biol,* **5,** 765-769.

125. Quetglas S, Leveque C, Miquelis R, Sato K, and Seagar M (2000) Ca2+-dependent regulation of synaptic SNARE complex assembly via a calmodulin- and phospholipid-binding domain of synaptobrevin. *Proc Natl acad Sci U S A,* **97,** 9695-9700.

126. Reim K, Mansour M, Varoqueaux F, McMahon HT, Südhof TC, Brose N, and Rosenmund C (2001) Complexins regulate a late step in Ca2+-dependent neurotransmitter release. *Cell,* **104,** 71-81.

127. Richard P, Rigaud JL, and Graber P (1990) Reconstitution of CF0F1 into liposomes using a new reconstitution procedure. *Eur J Biochem,* **193,** 921-925.

128. Rickman C and Davletov B (2003) Mechanism of calcium-independent synaptotagmin binding to target SNAREs. *Journal of Biological Chemistry,* **278,** 5501-5504.

129. Rigaud JL and Levy D (2003) Reconstitution of membrane proteins into liposomes. *Liposomes, Pt B,* **372,** 65-86.

130. Rigaud JL, Paternostre MT, and Bluzat A (1988) Mechanisms of membrane protein insertion into liposomes during reconstitution procedures involving the

use of detergents. 2. Incorporation of the light-driven proton pump bacteriorhodopsin. *Biochemistry*, **27,** 2677-2688.

131. Rigaud JL, Pitard B, and Levy D (1995) Reconstitution of Membrane-Proteins Into Liposomes - Application to Energy-Transducing Membrane-Proteins. *Biochimica et Biophysica Acta-Bioenergetics,* **1231,** 223-246.

132. Rizo J (2003) SNARE function revisited. *Nat Struct Biol,* **10,** 417-419.

133. Rizo J and Südhof TC (2002) Snares and munc18 in synaptic vesicle fusion. *Nat Rev Neurosci,* **3,** 641-653.

134. Robinson IM, Ranjan R, and Schwarz TL (2002) Synaptotagmins I and IV promote transmitter release independently of Ca(2+) binding in the C(2)A domain. *Nature,* **418,** 336-340.

135. Rothman JE (1994) Mechanisms of intracellular protein transport. *Nature,* **372,** 55-63.

136. Sabatini BL and Regehr WG (1999) Timing of synaptic transmission. *Annu Rev Physiol,* **61,** 521-542.

137. Schiavo G, Benfenati F, Poulain B, Rossetto O, Polverino dL, DasGupta BR, and Montecucco C (1992) Tetanus and botulinum-B neurotoxins block neurotransmitter release by proteolytic cleavage of synaptobrevin. *Nature,* **359,** 832-835.

138. Schneggenburger R and Neher E (2000) Intracellular calcium dependence of transmitter release rates at a fast central synapse. *Nature,* **406,** 889-893.

139. Schoch S, Deak F, Konigstorfer A, Mozhayeva M, Sara Y, Südhof TC, and Kavalali ET (2001) SNARE function analyzed in synaptobrevin/VAMP knockout mice. *Science,* **294,** 1117-1122.

140. Schuette CG, Hatsuzawa K, Margittai M, Stein A, Riedel D, Kuster P, Konig M, Seidel C, and Jahn R (2004) Determinants of liposome fusion mediated by synaptic SNARE proteins. *Proc Natl acad Sci U S A,* **101,** 2858-2863.

141. Shao X, Davletov BA, Sutton RB, Südhof TC, and Rizo J (1996) Bipartite Ca2+-binding motif in C2 domains of synaptotagmin and protein kinase C. *Science,* **273,** 248-251.

142. Shao X, Fernandez I, Südhof TC, and Rizo J (1998) Solution structures of the Ca2+-free and Ca2+-bound C2A domain of synaptotagmin I: does Ca2+ induce a conformational change? *Biochemistry,* **37,** 16106-16115.

143. Shao X, Li C, Fernandez I, Zhang X, Südhof TC, and Rizo J (1997) Synaptotagmin-syntaxin interaction: the C2 domain as a Ca2+-dependent electrostatic switch. *Neuron,* **18,** 133-142.

144. Shin OH, Rhee JS, Tang J, Sugita S, Rosenmund C, and Südhof TC (2003) Sr2+ binding to the Ca2+ binding site of the synaptotagmin 1 C2B domain triggers fast exocytosis without stimulating SNARE interactions. *Neuron,* **37,** 99-108.

145. Shin OH, Rizo J, and Südhof TC (2002) Synaptotagmin function in dense core vesicle exocytosis studied in cracked PC12 cells. *Nat Neurosci,* **5,** 649-656.

146. Silvius JR (1992) Solubilization and functional reconstitution of biomembrane components. *Annu Rev Biophys Biomol Struct,* **21,** 323-348.

147. Sollner T, Bennett MK, Whiteheart SW, Scheller RH, and Rothman JE (1993a) A protein assembly-disassembly pathway in vitro that may correspond to sequential steps of synaptic vesicle docking, activation, and fusion. *Cell,* **75,** 409-418.

148. Sollner T, Whiteheart SW, Brunner M, Erdjument-Bromage H, Geromanos S, Tempst P, and Rothman JE (1993b) SNAP receptors implicated in vesicle targeting and fusion. *Nature,* **362,** 318-324.

149. Sollner TH (2003) Regulated exocytosis and SNARE function (Review). *Mol Membr Biol,* **20,** 209-220.

150. Sorensen JB, Matti U, Wei SH, Nehring RB, Voets T, Ashery U, Binz T, Neher E, and Rettig J (2002) The SNARE protein SNAP-25 is linked to fast calcium triggering of exocytosis. *Proc Natl Acad Sci U S A,* **99,** 1627-1632.

151. Stewart BA, Mohtashami M, Trimble WS, and Boulianne GL (2000) SNARE proteins contribute to calcium cooperativity of synaptic transmission. *Proc Natl acad Sci U S A,* **97,** 13955-13960.

152. Struck DK, Hoekstra D, and Pagano RE (1981) Use of resonance energy transfer to monitor membrane fusion. *Biochemistry,* **20,** 4093-4099.

153. Südhof TC (2002) Synaptotagmins: why so many? *J Biol Chem,* **277,** 7629-7632.

154. Südhof TC (1995) The synaptic vesicle cycle: a cascade of protein-protein interactions. *Nature,* **375,** 645-653.

155. Südhof TC, De Camilli P, Niemann H, and Jahn R (1993) Membrane fusion machinery: insights from synaptic proteins. *Cell,* **75,** 1-4.

156. Südhof TC and Rizo J (1996) Synaptotagmins: C2-domain proteins that regulate membrane traffic. *Neuron,* **17,** 379-388.

157. Sutton RB, Davletov BA, Berghuis AM, Südhof TC, and Sprang SR (1995) Structure of the first C2 domain of synaptotagmin I: a novel Ca2+/phospholipid-binding fold. *Cell,* **80,** 929-938.

158. Sutton RB, Fasshauer D, Jahn R, and Brunger AT (1998) Crystal structure of a SNARE complex involved in synaptic exocytosis at 2.4 A resolution. *Nature,* **395,** 347-353.

159. Takahashi S, Yamamoto H, Matsuda Z, Ogawa M, Yagyu K, Taniguchi T, Miyata T, Kaba H, Higuchi T, Okutani F, and . (1995) Identification of two highly homologous presynaptic proteins distinctly localized at the dendritic and somatic synapses. *FEBS Lett,* **368,** 455-460.

160. Tokumaru H, Umayahara K, Pellegrini LL, Ishizuka T, Saisu H, Betz H, Augustine GJ, and Abe T (2001) SNARE complex oligomerization by synaphin/complexin is essential for synaptic vesicle exocytosis. *Cell,* **104,** 421-432.

161. Tucker WC, Weber T, and Chapman ER (2004) Reconstitution of Ca2+-regulated membrane fusion by synaptotagmin and SNAREs. *Science,* **304,** 435-438.

162. Ubach J, Lao Y, Fernandez I, Arac D, Südhof TC, and Rizo J (2001) The C2B domain of synaptotagmin I is a Ca2+-binding module. *Biochemistry,* **40,** 5854-5860.

163. Ubach J, Zhang X, Shao X, Südhof TC, and Rizo J (1998) Ca2+ binding to synaptotagmin: how many Ca2+ ions bind to the tip of a C2-domain? *EMBO J,* **17,** 3921-3930.

164. Ungermann C, Sato K, and Wickner W (1998) Defining the functions of trans-SNARE pairs. *Nature,* **396,** 543-548.

165. Verhage M, Maia AS, Plomp JJ, Brussaard AB, Heeroma JH, Vermeer H, Toonen RF, Hammer RE, van den Berg TK, Missler M, Geuze HJ, and Südhof TC (2000) Synaptic assembly of the brain in the absence of neurotransmitter secretion. *Science,* **287,** 864-869.

166. Voets T, Toonen RF, Brian EC, de Wit H, Moser T, Rettig J, Südhof TC, Neher E, and Verhage M (2001) Munc18-1 promotes large dense-core vesicle docking. *Neuron,* **31,** 581-591.

167. Walch-Solimena C, Blasi J, Edelmann L, Chapman ER, Von Mollard GF, and Jahn R (1995) The t-SNAREs syntaxin 1 and SNAP-25 are present on organelles that participate in synaptic vesicle recycling. *J Cell Biol,* **128,** 637-645.

168. Wallin E and von HG (1998) Genome-wide analysis of integral membrane proteins from eubacterial, archaean, and eukaryotic organisms. *Protein Sci,* **7,** 1029-1038.

169. Washbourne P, Thompson PM, Carta M, Costa ET, Mathews JR, Lopez-Bendito G, Molnar Z, Becher MW, Valenzuela CF, Partridge LD, and Wilson MC (2002) Genetic ablation of the t-SNARE SNAP-25 distinguishes mechanisms of neuroexocytosis. *Nat Neurosci,* **5,** 19-26.

170. Weber T, Zemelman BV, McNew JA, Westermann B, Gmachl M, Parlati F, Sollner TH, and Rothman JE (1998) SNAREpins: minimal machinery for membrane fusion. *Cell,* **92,** 759-772.

171. Wishart DS and Sykes BD (1994) The 13C chemical-shift index: a simple method for the identification of protein secondary structure using 13C chemical-shift data. *J Biomol NMR,* **4,** 171-180.

172. Wu MN, Fergestad T, Lloyd TE, He Y, Broadie K, and Bellen HJ (1999) Syntaxin 1A interacts with multiple exocytic proteins to regulate neurotransmitter release in vivo. *Neuron,* **23,** 593-605.

173. Wu MN, Littleton JT, Bhat MA, Prokop A, and Bellen HJ (1998) ROP, the Drosophila Sec1 homolog, interacts with syntaxin and regulates neurotransmitter release in a dosage-dependent manner. *EMBO J,* **17,** 127-139.

174. Wu MN, Schulze KL, Lloyd TE, and Bellen HJ (2001) The ROP-syntaxin interaction inhibits neurotransmitter release. *Eur J Cell Biol,* **80,** 196-199.

175. Wüthrich K (1986). *NMR of proteins and nucleic acids.* Wiley, New York.

176. Xiao W, Poirier MA, Bennett MK, and Shin YK (2001) The neuronal t-SNARE complex is a parallel four-helix bundle. *Nat Struct Biol,* **8,** 308-311.

177. Xu T, Rammner B, Margittai M, Artalejo AR, Neher E, and Jahn R (1999) Inhibition of SNARE complex assembly differentially affects kinetic components of exocytosis. *Cell,* **99,** 713-722.

178. Yamaguchi T, Dulubova I, Min SW, Chen X, Rizo J, and Südhof TC (2002) Sly1 binds to Golgi and ER syntaxins via a conserved N-terminal peptide motif. *Dev Cell,* **2,** 295-305.

179. Yamazaki T, Lee W, Arrowsmith CH, Muhandiram DR, and Kay LE (1994a) A Suite of Triple-Resonance Nmr Experiments for the Backbone Assignment of N-15, C-13, H-2 Labeled Proteins with High-Sensitivity. *Journal of the American Chemical Society,* **116,** 11655-11666.

180. Yamazaki T, Lee W, Revington M, Mattiello DL, Dahlquist FW, Arrowsmith CH, and Kay LE (1994b) An Hnca Pulse Scheme for the Backbone Assignment of N-15,C-13,H-2-Labeled Proteins - Application to A 37-Kda Trp Repressor Dna Complex. *Journal of the American Chemical Society,* **116,** 6464-6465.

181. Yu X, Carroll S, Rigaud JL, and Inesi G (1993) H+ Countertransport and Electrogenicity of the Sarcoplasmic-Reticulum Ca-2(+) Pump in Reconstituted Proteoliposomes. *Biophysical Journal,* **64,** 1232-1242.

182. Zimmerberg J, Vogel SS, and Chernomordik LV (1993) Mechanisms of membrane fusion. *Annu Rev Biophys Biomol Struct,* **22,** 433-466.

VITAE

Xiaocheng Chen was born in Changzhou, Jiangsu Province, People's Republic of China on January 24, 1977, the daughter of Tiansheng Chen and Lingling Zhao. Both of her parents are engineers. She has a sister, who is currently a Ph.D. candidate at Purdue University, West Lafayette, IN. After completing her work at Changzhou No.1 Middle School, Changzhou, Jiangsu in 1995, she entered Nanjing University at Nanjing, Jiangsu. She received the degree of Bachelor of Science with a major in biochemistry from Nanjing University in June, 1999. Then she continued her graduate study in Nanjing University for one more year. In August 2000, she entered the Graduate School of Biomedical Sciences at the University of Texas Health Science Medical Center at San Antonio, TX. Intrigued by the fantastic research did by Dr. Rizo-Rey and his colleagues, she transferred to the University of Texas Southwestern Medical Center at Dallas and joined Dr. Rizo-Rey's laboratory in January 2001. After four years hard work, she was awarded the degree of Doctor of Philosophy in March 2005 from the Molecular Biophysics Program at the University of Texas Southwestern Medical Center at Dallas. Currently, she is working as a postdoctoral fellow in Dr. Rizo-Rey's laboratory in the University of Texas Southwestern Medical Center.

Permanent Address: 31 Guangcheng Road, Unit A, Room 301,
Changzhou, Jiangsu, China, 213015